Acta Pharmacologica Sinica (2012) 33: 145–147
 1671-4083/12 $32.00
www.nature.com/aps

Editorial

Obesity, a health burden of a global nature

Zhi-yun ZHANG, Ming-wei WANG*

The National Center for Drug Screening and the State Key Laboratory of Drug Research, Shanghai Institute of Materia Medica, Chinese Academy of Sciences, Shanghai 201203, China

Acta Pharmacologica Sinica (2012) 33: 145–147; doi: 10.1038/aps.2011.185

Obesity, the primary health threat in the 21st century, affects the quality of life physiologically, economically and psychologically, irrespective of cultural, financial or ethnic background. Prevalence of obesity has been increasing steadily during the past 30 years worldwide, especially in developed countries. In America, almost one-third of adult population are obese (BMI ≥30 kg/m^2)[1] and healthcare expenditure for obesity had reached nearly 75 billion USD in 2003[2]. A similar picture has been seen in developing countries as well where incidence of obesity is rising at an alarming speed. In China, according to one report, 12.1% and 2.6% of the urban population are either overweight (25 kg/m^2 ≤ BMI ≤30 kg/m^2) or clinically obese (BMI ≥30 kg/m^2)[3]. The situation in children is more disturbing: a 2005 study conducted in northern coastal large cities of China shows that the combined prevalence of obesity had reached 32.5% in boys and 17.6% in girls, respectively[4]. Possible contributing factors may include steady economic growth, lifestyle changes and significantly reduced family size since the late 1970's.

From a medical stand point, obesity contributes to a broad range of health issues, involving type 2 diabetes mellitus, cardiovascular and kidney diseases (see review by Barton), as well as certain cancers, *etc*[5]. It significantly increases mortality, causes physical impairment and psychological stigma, and results in economic burden that is largely unmanageable even in many affluent societies. Therefore, prevention and treatment of obesity are a common challenge with extraordinary urgency to both developed and developing nations, and all-out efforts are required to exploit efficient strategies, from policy to education, from research to industry, and from physicians to patients.

Obesity is generally recognized as disturbances in energy homeostasis between nutrient intake and expenditure. The balance is controlled by the central nervous system (CNS), mainly the neurons located in hypothalamus. They sense nutrient molecules in circulation and peripheral signaling proteins released by organs in order to regulate energy homeostasis[6]. However, the exact molecular mechanisms relative to pathogenesis of obesity remain elusive (see review by Herbst), and may include interaction of different genes (see article by Ke *et al*), environmental factors, life style, social status and even intrauterine or neonatal nutritional states[7]. It is believed that a chronic, low grade inflammation, in response to excess nutrients or energy, in the metabolic tissues is involved in the development of obesity (see review by Gao and Ye). A cascade may exist starting from release of inflammatory cytokines [tumor necrosis factor (TNF)-α, interleukin-1(IL-1)β, CCL2, *etc*] and activation of inflammatory kinases (JNK, IKK, PKR *etc*) by metabolic cells, progressing towards tissue malfunction (*eg* insulin resistance), and eventually linking inflammation to obesity-related diseases, such as type 2 diabetes[8].

While prevention is largely dependent upon change of life style, therapeutic approaches are dominated by medications that result in weight loss, covering both small molecules and peptides aiming at a variety of drug targets (Tables 1 and 2)[9–11]. Of which, sibutramine, phentermine, rimonabant, lorcaserin, contrave, qnexa, liraglutide, tesofensine and velneperit, *etc,* target the CNS and decrease energy intake via reducing appetite or increasing satiety, whereas orlistat and cetilistat interfere with nutrient absorption in the digestive system. Although the pipeline looks prosperous, only one drug (orlistat) is available at present for long-term weight control because sibutramine was withdrawn last year due to an increased cardiovascular risk[12]. Others that were approved for short-term treatment (*eg* phentermine, diethylpropion, benzphetamine and phendimetrazine) all have the limitation of controlled use because of potential drug abuse[13].

With worldwide demands for a "magic bullet" to loose body weight, major pharmaceutical companies are chasing after the multibillion-dollar obesity market even under extremely high risks. In 2010, Sanofi-Avantis decided to discontinue all ongoing clinical trials and to suspend sales of its cannabinoid

* To whom correspondence should be addressed.
E-mail wangmw@mail.shcnc.ac.cn
Received 2011-12-07 Accepted 2011-12-08

Table 1. Anti-obesity drugs approved, rejected, withdrawn or revised by the FDA.

Drug	Company	Mechanism of action	Comments
Anti-obesity drugs presently on the market			
Orlistat	Roche, GSK	Pancreatic lipase inhibitor	Approved for long-term use in 1999
Phentermine	Not available	Adrenaline reuptake inhibitor	Schedule IV drug, approved for short-term use
Diethylpropion	Not available	Norepinephrine/dopamine releasing stimulator	Schedule IV drug, approved for short-term use
Benzphetamine	Pharmacia	Norepinephrine/dopamine releasing stimulator	Schedule III drug, approved for short-term use
Phendimetrazine	Not available	Norepinephrine/dopamine releasing stimulator	Schedule III drug, approved for short-term use
Anti-obesity drugs that await for decisions			
Contrave	Orexigen	Bupropion+naltrexone	The FDA requested data on long-term cardiovascular risk assessment in 2011
Qnexa	Vivus	Phentermine+topiramate	The FDA requested data on teratogenic potential in 2010
Anti-obesity drugs rejected by the FDA			
Rimonabant	Sanofi-Aventis	CB1R antagonist	Not approved in the USA due to its psychiatric side-effects and withdrawn from the European market in 2009 for increased risk of serious psychiatric disorders
Lorcaserin	Arena Pharma	Selective 5-HT_{2C} receptor agonist	Not approved due to concerns over carcinogenicity observed in rats in 2010
Anti-obesity drugs withdrawn from the market			
Fenfluramine and dexfenfluramine	Wyeth-Ayerst	5-HT_{2B} receptor agonist	Withdrawn after reports of valvular heart damage and primary pulmonary hypertension in 1997
Phenylpropanolamine	Not available	Norepinephrine/dopamine releasing stimulator	Withdrawn for increased risk of hemorrhagic stroke in 2000
Sibutramine	Abbott	NA/5-HT reuptake blocker	Withdrawn for increased risk of cardiovascular events in 2010

5-HT, 5-hydroxytryptamine; NA, noradrenaline; CB1R, cannabinoid 1 receptor; FDA, Food and Drug Administration; GSK, GlaxoSmithKline.

Table 2. A glance of new anti-obesity drugs in the pipeline.

Drug	Company	Mechanism of action	Stage
Empatic	Orexigen	Bupropion+zonisamide	Phase III
Pramlintide	Amylin	Leptin analog + amylin analog	Phase III
Cetilistat	Alizyme/Takeda	Pancreatic lipase inhibitor	Phase III
Liraglutide	Novo Nordisk	Long-acting GLP-1 analog	Phase III
Tesofensine	NeuroSearch	NA/DA/5-HT reuptake inhibitor	Phase II
Velneperit	Shinogi	Neuropeptide Y5 receptor antagonist	Phase II
Obinepitide	7TM	PPY3-36 and pancreatic polypeptide analog	Phase II
LY377604	Eli Lilly	β-3 adrenergic receptor agonist	Phase II
ZGN-433	Zafgen	MetAP2 inhibitor	Phase I
PF-04971729	Pfizer	SGLT2 inhibitor	Phase I
PF-04620110	Pfizer	DGAT1 inhibitor	Phase I
GSK 598809	GSK	D3 receptor antagonist	Phase I
GSK 1521498	GSK	μ-opioid receptor antagonist	Phase I

GLP-1, glucagon-like peptide-1; PPY3-36, peptide YY3-36; MetAP2, methionyl aminopeptidase 2; SGLT2, sodium glucose co-transporter type 2; DGAT1, diglyceride acyltransferase.

1 receptor (CB1R) blocker, rimonabant, following the recommendation from the European Medicines Agency in response to serious psychiatric side-effects[14]. Merck and Pfizer wasted no time to cease the development of their versions of CB1R antagonists, taranabant and CP-945598, respectively, making CB1R as a drug target dubious. Thus, a new strategy to discover selective CB1R blockers that predominantly interact with the receptor in the periphery has been debated[14].

Haunted by the withdrawal of sibutramine and the end of CB1R blockers, the developers of anti-obesity drugs experienced further setbacks. Apart from rejecting regulatory approval of Vivus's combination product qnexa and Arena's locaserin[15], the Food and Drug Administration requested a cardiovascular outcome study for another combination therapy, Orexigen's contrave[10]. Obviously, the paramount concern on therapeutics against obesity is safety because it is not a fatal disease and requires long-term management. In comparison with physical exercise and diet control that demand for active participation, the advantage of a safe and efficacious pill is unquestionable albeit it is passive in terms of patient efforts.

The multi-facet actions of the gut hormone, glucagon-like peptide-1 (GLP-1), render it ideal as a target for drug intervention[16]. Encouraged by early success with a GLP-1 mimetic, exenatide, in diabetic weight loss[17], liraglutide, a long-acting GLP-1 analog, was shown to reduce body weight in both animal models of obesity (see article by Hansen *et al*) and human clinical studies[18]. Similar effects in animal models were also seen with a non-peptidic GLP-1 receptor agonist Boc5[19] and one of its analogs (see review by He *et al*).

As demonstrated in the treatment of many other diseases, combination therapy is more effective than a single agent. Of the four such products (qnexa, contrave, empatic and pramlintide), qnexa and contrave were previously approved for other indications. Clinical trials revealed that qnexa (phentermine plus topiramate) and contrave (bupropion plus naltrexone) administration induced a net weight loss of 12.2 kg and 6.2 kg, respectively, compared with a reduction of 4.0 kg or 3.2 kg when phentermine or bupropion was administered alone[10].

Facing such an unprecedented challenge on a global scale, it is far from adequate in terms of novel approaches to obesity management. Clearly, the most important task lies in education that alters social behavior capable of preventing the prevalence of obesity from rising. In this special issue, several topics that relate to obesity etiology, animal models (see review by Nilsson *et al*), therapeutics and clinical implications are covered in order to provide a glance of the latest developments in this important field.

References

1 Wang YF, Beydoun MA, Liang L, Caballero B, Kumanyika SK. Will all Americans become overweight or obese? Estimating the progression and cost of the US obesity epidemic. Obesity 2008; 16: 2323–30.
2 Finkelstein EA, Ruhm CJ, Kosa KM. Economic causes and consequences of obesity. Annu Rev Publ Health 2005; 26: 239–57.
3 Wu YF. Overweight and obesity in China. Br Med J 2006; 333: 362–3.
4 Cheng TO, Ji CY. Prevalence and geographic distribution of childhood obesity in China in 2005. Int J Cardiol 2008; 131: 1–8.
5 Dixon JB. The effect of obesity on health outcomes. Mol Cell Endocrinol 2009; 316: 104–8.
6 Friedman JM. Obesity causes and control of excess body fat. Nature 2009; 459: 340–2.
7 Zhang ZY, Zeng JJ, Kjaergaard M, Guan N, Raun K, Nilsson C, *et al.* Effects of a maternal diet supplemented with chocolate and fructose beverage during gestation and lactation on rat dams and their offspring. Clin Exp Pharmacol Physiol 2011; 38: 613–22.
8 Gregor MF, Hotamisligil GS. Inflammatory mechanisms in obesity. Annu Rev Immunol 2011; 29: 415–45.
9 Tseng YH, Cypess AM, Kahn CR. Cellular bioenergetics as a target for obesity therapy. Nat Rev Drug Discov 2010; 9: 465–81.
10 Powell AG, Apovian CM, Aronne LJ. New drug targets for the treatment of obesity. Clin Pharmacol Ther 2011; 90: 40–51.
11 Caveney E, Caveney BJ, Somaratne R, Turner JR, Gourgiotis L. Pharmaceutical interventions for obesity: a public health perspective. Diabetes Obes Metab 2011; 13: 490–7.
12 Sayburn A. Withdrawal of sibutramine leaves European doctors with just one obesity drug. Br Med J 2010; 340: c477.
13 Bray GA. Drug insight: appetite suppressants. Nat Clin Pract Gastroenterol Hepatol 2005; 2: 89–95.
14 Bifulco M, Pisanti S. End of the line for cannabinoid receptor 1 as an anti-obesity target? An opinion. Nat Rev Drug Discov 2009; 8: 594.
15 Jones D. Suspense builds on anti-obesity rollercoaster ride. Nat Rev Drug Discov 2011; 10: 5–6.
16 Small CJ, Bloom SR. Gut hormones as peripheral anti obesity targets. Curr Drug Targets CNS Neurol Disord 2004; 3: 379–88.
17 DeFronzo RA, Ratner RE, Han J, Kim DD, Fineman MS, Baron AD. Effects of exenatide (exendin-4) on glycemic control and weight over 30 weeks in metformin-treated patients with type 2 diabetes. Diabetes Care 2005; 28: 1092–100.
18 Astrup A, Rossner S, Van Goal L, Rissanen A, Niskanen L, Al Hakim M, *et al.* Effects of liraglutide in the treatment of obesity: a randomised, double-blind, placebo-controlled study. Lancet 2009; 374: 1606–16.
19 He M, Su HR, Gao WW, Johansson SM, Liu Q, Wu XY, *et al.* Reversal of obesity and insulin resistance by a non-peptidic glucagon-like peptide-1 receptor agonist in diet-induced obese mice. PLoS ONE 2010; 5: e14205.

Acta Pharmacologica Sinica (2012) 33: 148–154
 1671-4083/12 $32.00
www.nature.com/aps

Review

A continued saga of Boc5, the first non-peptidic glucagon-like peptide-1 receptor agonist with *in vivo* activities

Min HE[1, 2], Ni GUAN[2], Wei-wei GAO[1], Qing LIU[1, 2], Xiao-yan WU[1], Da-wei MA[3], Da-fang ZHONG[2], Guang-bo GE[4], Chuan LI[2], Xiao-yan CHEN[2], Ling YANG[4], Jia-yu LIAO[1, 5], Ming-wei WANG[1, 2, *]

[1]The National Center for Drug Screening and [2]the State Key Laboratory of Drug Research, Shanghai Institute of Materia Medica, Chinese Academy of Sciences, Shanghai 201203, China; [3]Shanghai Institute of Organic Chemistry, Chinese Academy of Sciences, Shanghai 200032, China; [4]Dalian Institute of Chemical Physics, Chinese Academy of Sciences, Dalian 116023, China; [5]Department of Bioengineering, University of California, Riverside, California, CA 92521, USA

Glucagon-like peptide-1 (GLP-1)-based therapy presents a promising option for treating type 2 diabetes. However, there are several limitations relative to the peptidic GLP-1 mimetics currently on the market or under development. This concern has led to a continued interest in the search for non-peptidic agonists for GLP-1 receptor (GLP-1R). Here, we briefly review the discovery, characterization and current status of a novel class of cyclobutane-derivative-based non-peptidic agonists for GLP-1R, including Boc5 and its newly discovered analogue WB4-24. Although the oral bioavailability of such compounds still poses great challenges, the progress made so far encourages us to identify a truly 'druggable' small molecule agonist for GLP-1R.

Keywords: type 2 diabetes; glucagon-like peptide-1; non-peptidic agonist; Boc5; G-protein coupled receptor

Acta Pharmacologica Sinica (2012) 33: 148–154; doi: 10.1038/aps.2011.169

Introduction

Type 2 diabetes mellitus (T2DM) comprises an array of dysfunctions resulting from a combination of resistance to insulin action and inadequate insulin secretion. It is characterized by hyperglycemia and associated with microvascular, macrovascular and neuropathic complications. T2DM is also linked causally with obesity, which is a global health burden in itself[1]. Unless appropriate action is taken, it is predicted that there will be at least 350 million people in the world with T2DM by the year 2030[2]. This situation is further worsened by the fact that currently available drugs such as insulin, sulfonylureas and thiazolidinediones only have limited efficacy and do not address two major problems, declining β-cell function and associated obesity. Therefore, the quest for novel therapeutics to combat diabetes and related metabolic abnormalities is justifiably intensive.

Glucagon-like peptide-1 (GLP-1)-based therapy presents an alternative and effective approach to treat T2DM[3]. GLP-1 is a gastrointestinal peptide produced by the proglucagon gene in L-cells of the small intestine in response to nutrients. It is thought to exert anti-hyperglycemic effects by stimulating insulin secretion, slowing gastric emptying, inhibiting glucagon release, stimulating β-cell proliferation and differentiation, and improving satiety[4]. GLP-1 appears to be an ideal and complementary approach to T2DM management for several reasons[3]: (i) glucose-dependent release of insulin does not cause hypoglycemia; (ii) suppression of food consumption leads to reduced body weight; and (iii) protection of β-cell mass and function lessens the severity of T2DM. However, a major limitation in extending these advantages to clinical benefits resides in the very short half-life of GLP-1 *in vivo* (approximately 1–2 min)[5]. This is attributed to NH_2-terminal degradation by dipeptidyl peptidase IV (DPP-IV) and renal clearance[6]. Hence, a significant amount of efforts have been made to identify molecules that activate the GLP-1 pathway with improved pharmacokinetic properties.

Current available GLP-1 mimetics encompass two classes of agents[7]: GLP-1R agonists (*eg*, exenatide and liraglutide) that are structurally related to GLP-1 and orally available DPP-IV inhibitors (*eg*, sitagliptin, saxagliptin and vildagliptin) that elevate circulating GLP-1 concentrations via limiting the degradation of endogenous GLP-1. Various human and animal

* To whom correspondence should be addressed.
E-mail wangmw@mail.shcnc.ac.cn
Received 2011-09-08 Accepted 2011-11-12

studies show that these therapeutic agents achieve meaningful reductions in hemoglobin A (1c) (HbA1c) levels without causing significant hypoglycemia. In addition, decreases in body weight have been observed with GLP-1R agonists accompanied by beneficial effects on human cardiac function[8]. While the market outlook for GLP-1 mimetics seems favorable, certain limitations, such as repeated injections required for synthetic peptides and lack of weight loss following treatment with DPP-IV inhibitors, may prevent us from fully capturing the therapeutic potential of GLP-1 mimetics. Orally active, non-peptidic GLP-1R agonists thus remain a promising approach to tackle such challenges.

The GLP-1R belongs to the class B family of G-protein-coupled receptors (GPCRs), consisting of seven membrane spanning domains connected to each other by three extracellular and three intracellular loops. It is widely recognized that GPCRs represent the most important target class for therapeutic intervention[9]. Although there are a numerous examples of class A GPCRs being activated by small molecule agonists, very few non-peptidic ligands have been discovered for class B GPCRs. For instance, only several small molecule GLP-1R agonists with diverse structural features and functional selectivity (orthosteric, allosteric, ago-allosteric, inverse, or partial/full agonists) were reported[10–15]. Among them, substituted cyclobutane Boc5 is the one that has been investigated most systematically both *in vitro* and *in vivo* to date.

Pharmacology

Boc5 was discovered following a high-throughput screening campaign against 48,160 small molecule compounds by use of a luciferase reporter assay in HEK293 cells stably expressing the rat GLP-1R gene linked to cAMP response element. Acute intraperitoneal (ip) and oral administration of Boc5 (0.1, 0.3, 2, and 3 mg) dose-dependently inhibited food intake in normal C57BL/6J mice, an effect that could be blocked by pretreatment with specific GLP-1R antagonist exendin(9–39). Daily injection of Boc5 (2 or 3 mg; 6 weeks) into *db/db* mice reduced HbA1c, improved glucose tolerance and lowered body weight in *db/db* diabetic mice[11]. Encouraged by these initial results, we further characterized the pharmacological properties of Boc5 in both normal and *db/db* mice with emphasis on glycemic control and weight loss. In addition to the beneficial effects on glycemic control, cumulative food intake and body weight, Boc5 was shown to be capable of amplifying glucose-dependent insulin secretion, increasing insulin sensitivity, reducing body fat mass, slowing gastric emptying and inducing satiety at higher doses beyond the therapeutic window[16]. Clearly, the anti-diabetic action exerted by Boc5 truly resembled that of the native peptide and the therapeutic effects could only be seen in diabetic *db/db* mice but not in normal animals, implying a good safety profile (Tables S1 and S2).

Although the *db/db* mouse represents a convenient model of diabetes, it does not fully simulate the pathogenesis of human T2DM and obesity. Therefore, we subsequently explored the therapeutic utility of Boc5 in a mouse model of diet-induced obesity (DIO), commonly used in efficacy assessment of new anti-diabetic agents. Guided by a pilot dose ranging study in male C57BL/6J mice where DIO was completely preventable through intermittent Boc5 administration (Figure S1), we designed and carried out a comprehensive investigation for this indication. Three times a week, not once daily, ip injections of Boc5 (0.3, 3, and 1 mg) for 12 weeks resulted in typical dose-dependent responses in regulating food intake, adiposity, glucose homeostasis and insulin sensitivity[17], similar to that reported previously in *db/db* mice[11, 16]. Of interest is our finding that Boc5 was able of normalizing pancreas β-cell mass and islet size through suppression of compensatory β-cell hyperplasia in DIO mice resistant to insulin actions, accompanied normalization of dyslipidemia, adipocytokines dysregulation, adipocyte malfunction and liver injury[17].

In several *in vitro* (luciferase reporter[11] and binding[11] assays) and short-term *in vivo* (food intake[11], gastric emptying[16] and stimulation of insulin secretion[16]) studies, where GLP-1 or exenatide were used as positive controls, maximally stimulating effects of Boc5 were similar in magnitude to that of the peptides, albeit the latter being approximately 3 to 4 orders of magnitude more potent. Although the action site(s) for the anorectic effect induced by peripheral administration of GLP-1R agonists are not clear, several lines of evidence suggest that the inhibition on food intake caused by exenatide and liraglutide are mediated via activation of GLP-1R expressed on sub-diaphragmatic vagal afferents, as well as in the brain[18]. We do not know at this stage whether Boc5 passes the blood brain barrier, our earlier work demonstrated that Boc5, at a dose of 6 mg elicited conditioned taste aversion (CTA) in C57BL/6J mice[16], implying the involvement of both peripheral and central GLP-1 signaling pathways.

While the anti-diabetic effects of Boc5 were observable by oral[11, 16] and subcutaneous administration (Figure S2), the oral route required significantly higher doses to show efficacy. On the other hand, exogenous Boc5 had been shown to possess a markedly extended duration of action on several biological systems[11, 16, 17]. Hence, additional experiments were conducted to examine the pharmacokinetic properties of Boc5 in Sprague-Dawley (SD) rats and C57BL/6J mice, following a single dose of oral (*po*), ip, or intravenous (iv) administration. Samples were assayed for the prototype drug using HPLC, and mean plasma concentration-time curve and pharmacokinetic parameters were calculated (Figure S3, Table S3). One of the most striking features of the results was that the plasma drug level was hard to measure after a po dose of Boc5 in both rats (20 mg/kg) and mice (250 mg/kg). In contrast, the prototype drug could be readily detected after either ip or iv administration (20 mg/kg for rats and 75 mg/kg for mice). The half-lives ($T_{1/2}$) for Boc5 in rats and mice were 35.4 h and 12.1 h following ip administration, and 41.7 h and 8.71 h following iv administration, respectively; and the bioavailabilities in rats and mice were 71.6% and 51.2%, respectively when injected intraperitoneally (Table S3). Since plasma protein binding was moderate for Boc5 in mice (36.2%±5.5%; Table S4), we presume that the lack of free molecule after oral administra-

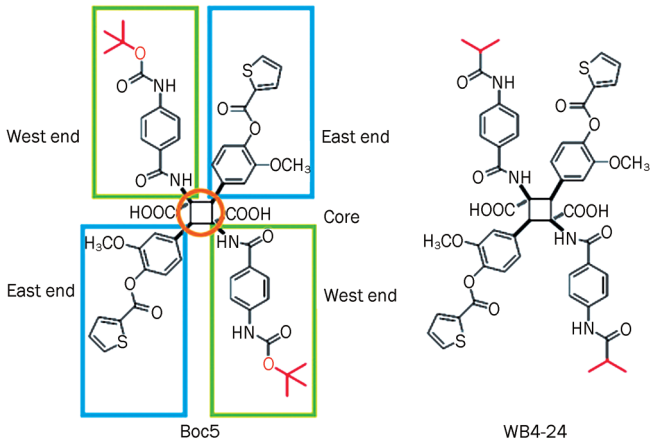

Figure 1. The structures of Boc5 and WB4-24.

tion may have been caused by metabolism in the gut, where the ester bonds at Boc (Figure 1, west end) and thienyl groups (Figure 1, east end) positions were quickly metabolized by esterase on the epithelial lining of the intestine (Figure S4). Further *in vitro* studies revealed that Boc5 was metabolized to 3 metabolites by B-type esterase(s) localized in the microsomal fraction of the mouse liver. These hydrolyzed metabolites (M-1, M-2, and M-3) were identified as dethiophenecarboxyl-Boc5, bisdethiophenecarboxyl-Boc5 and 2-thiophenecarboxylic acid, respectively, by use of UFLC-DAD-ESI-MS, with the help of authentic standard (Figure S4A). Luciferase reporter assay showed that dethiophenecarboxyl-Boc5 (M-1) at concentrations up to 100 μmol/L evoked maximally only 50% of Boc5 response (37% of GLP-1 response) with an estimated EC_{50} value was 16.0 μmol/L, approximately twelve times higher than that of Boc5 (1.3 μmol/L). Both bisdethiophenecarboxyl-Boc5 (M-2) and 2-thiophenecarboxylic acid (M-3) lost agonist activities (Figure S4B). In addition, Boc5 was very stable in hepatic microsomes from mini-pigs (PLM), rats (RLM) and humans (HLM), as well as human intestinal microsomes (HIM); the conventional metabolic enzymes in human including cytochrome P450s (CYPs), UDP-glucuronosyltransferases (UGTs) and esterases were not involved in the metabolism of this novel molecule (data not shown). These data were consistent with relatively long plasma half-lives of Boc5 after non-oral routes of administration.

Improvement

In order to understand the structure-activity relationship of this class of GLP-1R agonists, a series of symmetrical chemistry efforts were made to optimize the core, west and east ends of Boc5 (Figure 1). Among several dozen analogues prepared, WB4-24 demonstrated more potent bioactivities than Boc5 both *in vitro* (GLP-1R binding and cAMP response) and *in vivo* (food intake inhibition)[19]. With these results, we designed and performed an array of experiments using the mouse DIO model described above to characterize this compound. First, we studied the effects of WB4-24 on energy metabolism. As shown in Figures 2A and 2B, intermittent WB4-24 administration (ip, 3 times a week) led to a dose-dependent and significant reduction in body weight over the first 12-week treatment period. The maximal weight losses were approximately 31.8% ($P<0.01$), 13.0% ($P<0.01$) and 8.3% ($P<0.05$) at 3, 1, and 0.3 mg on different time points (4, 6, and 8 weeks, respectively) compared to that of obese controls. In addition, the pace of weight loss in 3 mg WB4-24 treated DIO mice was much faster than that of Boc5, reaching to the lean control level within the first 4 weeks of therapy (Figure 2A). Likewise, subchronic WB4-24 administration dose-dependently inhibited daily food intake, and 3 mg of WB4-24 displayed better potency than Boc5 between weeks 1 and 5 (Figures 2C and 2D).

Next, we investigated the effects of this derivative of Boc5 on blood glucose homeostasis. Glucose tolerance was quantified as the area-under-the-curve integrated from 0~120 min (AUC_{120}) after an intraperitoneal glucose challenge (intraperitoneal glucose tolerance test, IPGTT). Prior to initiating therapy with WB4-24, DIO mice showed impaired glucose tolerance relative to lean control mice ($P<0.01$, Figures 3A and 3F). IPGTTs conducted at 4 and 12 weeks after subchronic WB4-24 ip injections revealed a dose-dependent restoration of glucose tolerance, such that the glucose profile of mice receiving 3 mg of WB4-24 was indistinguishable from that of lean controls at 4 weeks ($P>0.05$, Figures 3B, 3C, and 3F). WB4-24 and Boc5 at 3 mg played similar roles in improving glucose tolerance during the 12-week observation period (Figures 3B and 3C).

Serum satiety hormone concentrations were also measured to study the endocrine status of treated animals. At the end of 12-week treatment, the blood samples were collected from WB4-24-treatd (3 mg), Boc5-treated (3 mg), lean and obese control groups. Fasting satiety hormones including insulin, leptin, active GLP-1 and glucagon levels were analyzed. Compared to lean controls, obese mice had significantly higher serum insulin ($P<0.01$), leptin ($P<0.01$) and glucagon ($P<0.01$) concentrations with the exception of active GLP-1 ($P>0.05$, Figure 4). Such an adaptation of serum satiety hormones in the obese state has been documented previously[20]. Conversely, both WB4-24 and Boc5 treatment significantly reduced the serum insulin ($P<0.01$), leptin ($P<0.01$) and glucagon ($P<0.05$) levels, which was in agreement with the reported studies on peptidic GLP-1R agonists[21]. Suppression of glucagon secretion following subchronic administration of Boc5 and WB4-24 further supports our dogma that this class of molecules truly activates the full spectrum of GLP-1 actions (Table 1).

Of note was our observation that each WB4-24 dose group markedly regained body weight, after a rapid initial fall, even during the treatment course (Figure 2A). This surprising phenomenon prompted us to perform a further study through reintroduction of 3 mg WB4-24 to the same dose group in parallel with both lean and obese controls. Figure 2A shows that 8 weeks after the cessation of WB4-24 administration, mice became obese again with body weight rebound to the pre-treatment level (~40 g); 8-week re-treatment only induced a moderate weight loss (7.5%), approximately one-fourth of that

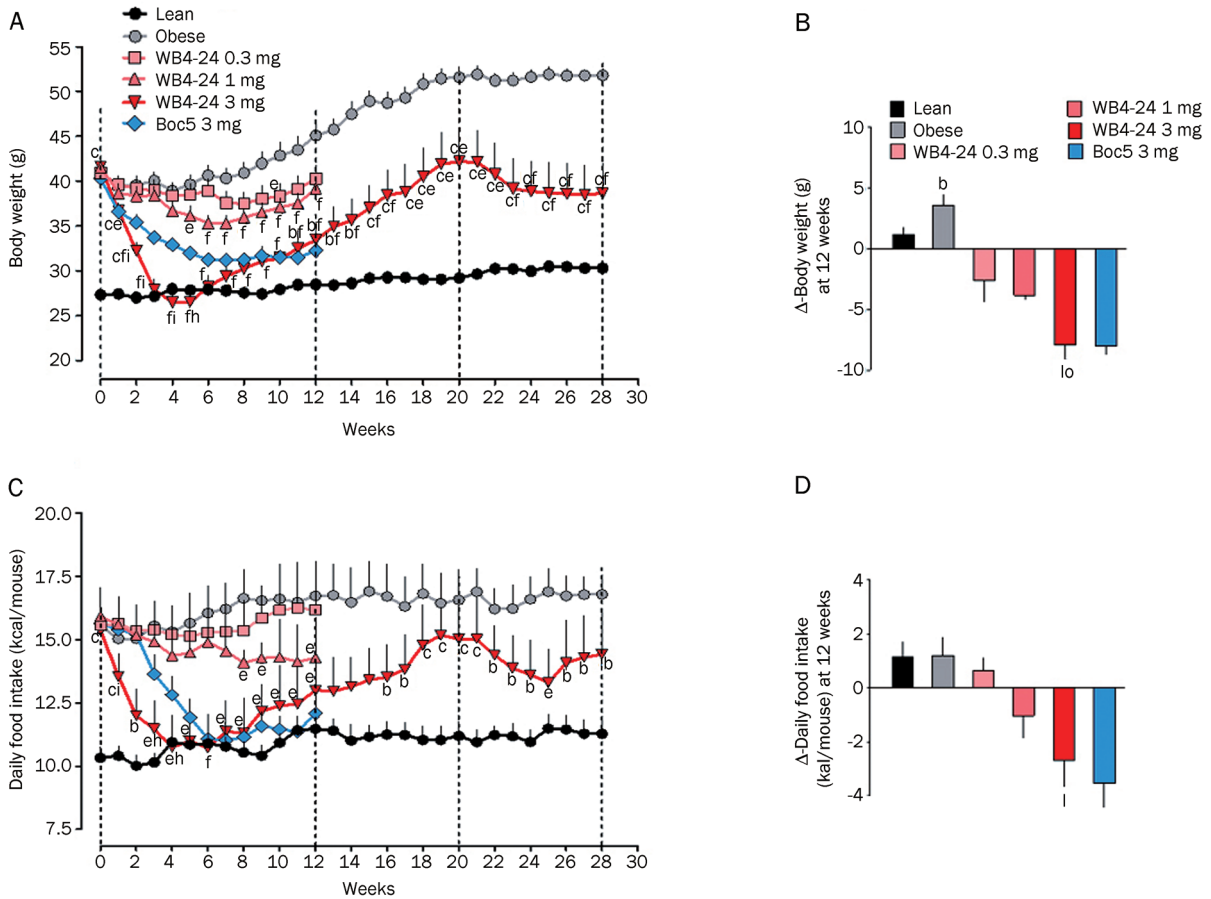

Figure 2. Effects of WB4-24 treatment on body weight and food intake in diet-induced obese (DIO) mice. Animals were maintained on high fat diet (HFD) for 12 weeks and then randomly assigned into 4 treatment groups with matched body weight. They were injected (ip), 3 times a week (Monday, Wednesday and Friday), with 0 (obese control), 0.3, 1, or 3 mg of WB4-24 (1% DMSO, 20% PEG400 in saline, pH 7.4, 0.5 mL) for 12 weeks. To compare the *in vivo* effects of WB4-24 and Boc5, a positive control group treated with 3 mg of Boc5, previously proven to be effective in combating obesity, was presented. A further comparator group of mice consuming standard chow diet (lean control) was used to index responses to normal values. Except for animals in 3 mg WB4-24, obese and lean control groups, all mice were sacrificed at the end of therapy. The remaining mice were kept under observation without therapeutic intervention. An 8-week new treatment regimen (3 mg WB4-24) was introduced two months after the cessation of the initial therapy. Time course of body weight changes (A) and daily food intake (C) over the 28-week investigational period were monitored. The changes of body weight (Δ-body weight, B) and daily food intake (Δ-daily food intake, D) over the first 12-week period were analyzed. Statistical analysis was performed using GraphPad Prism software (GraphPad, San Diego, CA, USA) by one-way analysis of variance (ANOVA), followed by Bonferroni *post hoc* analysis. Values are presented as mean±SEM. n=6–9 per group. $^{b}P<0.05$, $^{c}P<0.01$ compared with lean controls. $^{e}P<0.05$, $^{f}P<0.01$ compared with obese controls. $^{h}P<0.05$, $^{i}P<0.01$ compared with 3 mg Boc5-treated mice. $^{l}P<0.01$ compared with 0.3 mg WB4-24-treated mice. $^{o}P<0.05$ compared with 1 mg WB4-24-treated mice.

Table 1. Comparison of the therapeutic effects of glucagon-like peptide-1 (GLP-1) and Boc5.

Type 2 diabetes mellitus	GLP-1	Boc5
Insulin secretion ↓	Insulin secretion ↑	√
Insulin resistance	Insulin sensitivity ↑	√
β-cell function ↓	β-cell function ↑	√
Hyperglucagonemia	Glucagon secretion ↓	√
Obesity	Body weight ↓, food intake ↓	√
Gastric emptying ↑, –, or ↓	Gastric emptying ↓	√
Hyperlipidaemia	Triglyceride ↓, cholesterol ↓, nonesterified fatty acid ↓	√

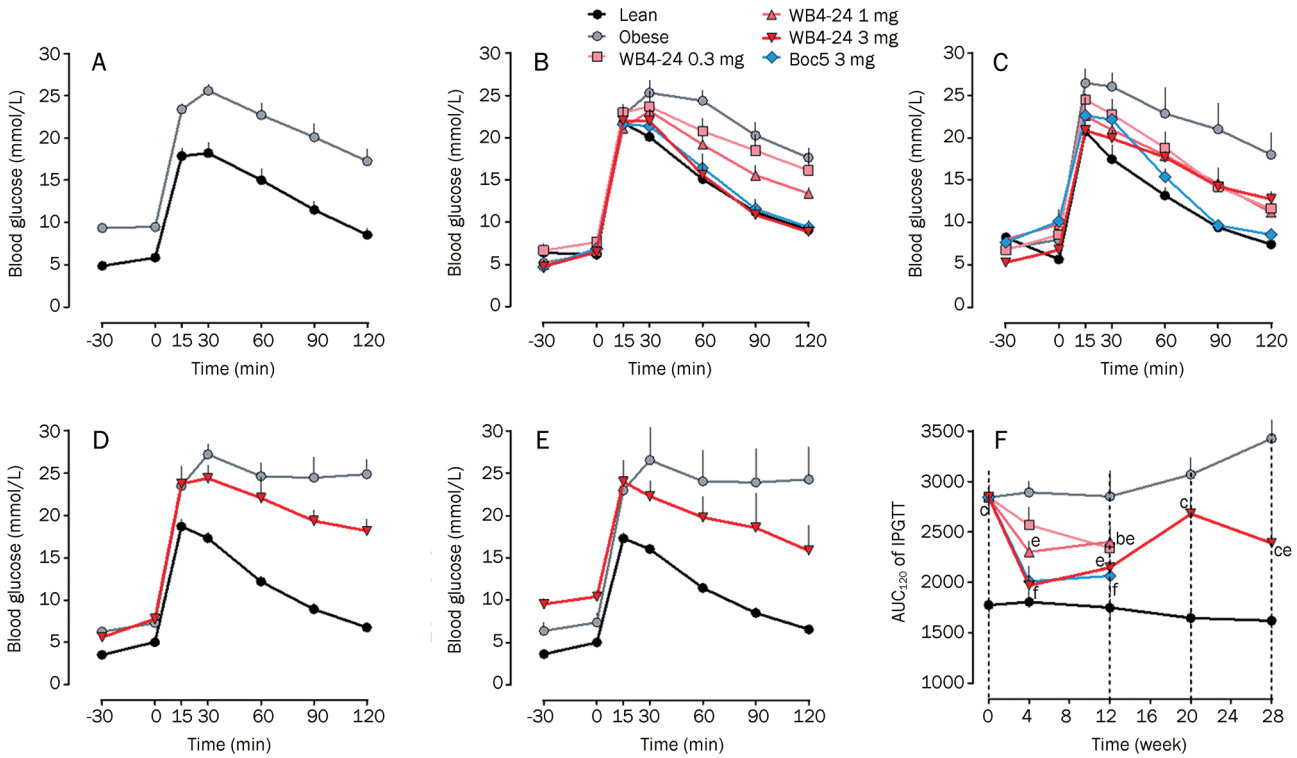

Figure 3. Effects of WB4-24 on glucose homeostasis in DIO mice. The experiments were conducted as described in Figure 1 legend and intraperitoneal glucose tolerance tests (IPGTTs) were carried out at week 0 (A), 4 (B), 12 (C), 20 (D), and 28 (E) after initial treatment with WB4-24. The glucose area-under-curve integrated from 0–120 min (AUC_{120}) was calculated for each mouse (F). Statistical analysis was performed using GraphPad Prism software by one-way analysis of ANOVA, followed by Bonferroni *post hoc* analysis. Values are presented as mean±SEM. n=6–9 per group. $^{b}P<0.05$, $^{c}P<0.01$ compared with lean controls. $^{e}P<0.05$, $^{f}P<0.01$ compared with obese controls.

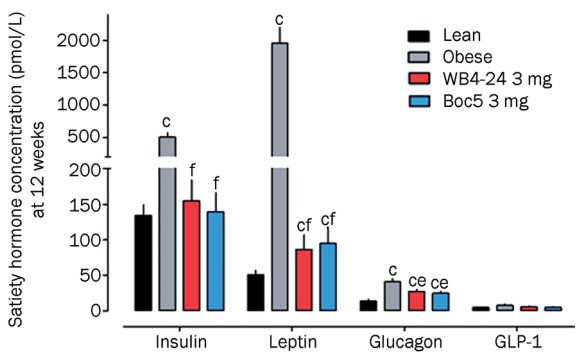

Figure 4. Effects of WB4-24 on serum satiety hormone concentrations in DIO mice. The experiments were conducted as described in Figure 1 legend. At the end of 12-week treatment, blood samples were collected from WB4-24-treated (3 mg), Boc5-treated (3 mg), lean and obese control groups. Fasting satiety hormones including insulin, leptin, active GLP-1 and glucagon levels were analyzed using Luminex 200 system (Luminex, Austin, USA) with the mouse endocrine MILLIPLEX MAP kit supplied by Millipore (Billerica, MA, USA). Statistical analysis was performed using GraphPad Prism software by one-way analysis of ANOVA, followed by Bonferroni *post hoc* analysis. Values are presented as mean±SEM. n=6–9 per group. $^{c}P<0.01$ compared with lean controls; $^{e}P<0.05$, $^{f}P<0.01$ compared with obese controls.

produced by the initial treatment, accompanied by attenuated inhibitory action on food intake (Figure 2C) and failure to restore glucose tolerance to the normal state ($P<0.05$, Figures 3D, 3E, and 3F).

It is possible that such a reduced efficacy may have resulted from potential immunogenicity of cyclobutane derivatives because of their relatively large molecular sizes (>1000). The peptidic GLP-1 mimetic, exenatide, has been shown to elicit specific antibody responses in about 40% of patients[22, 23]. In one study reported at EASD (European Association for the Study of Diabetes) 2010, antibody titers to exenatide reached a peak early in the treatment[24], whereas in another study, 61% of patients developed antibody reactions to exenatide after 26-week treatment, and patients with high antibody titers had smaller HbA1c reductions than those with low titers[25]. This may provide a link between decreased hypoglycemic efficacy and patients with antibodies to exenatide. Therefore, it was prudent to investigate the possibility in the context of repeated treatments with WB4-24 (molecular weight=1074).

Serum samples were subsequently collected from mice that received the 2nd WB4-24 treatment (3 mg) upon completion of dosing and specific antibodies were measured using an ELISA assay developed in-house. Briefly, WB4-24-carrier protein conjugate was prepared according to the 1-ethyl-3-(3-dimethylaminopropyl) carbodiimide hydrochloride (EDC) coupling approach[26]. The molar ratio of WB4-24 to carrier protein (bovine serum albumin, BSA) was approximately 30:1, evaluated by spectroscopy and trinitrobenzene sulfonate

(TNBS) method[27]. A 96-well microtiter plate was coated with 100 μl (2 μg/mL) of the conjugate at 4 °C overnight. The serum samples were serially diluted from 1:50 and added to each well of the blocked (20% normal sheep serum) plate. Bound antibody was then detected by goat anti-mouse Ig-HRP (BD Pharmingen, NJ, USA). Endpoint titers were finally determined at the x-axis intercept of the dilution curve, at two times the absorbance (A_{450}) given by the lean/obese control serum[28]. The results showed that 4 of 6 (67%) WB4-24-treated mice developed WB4-24 antibodies at titers of 23.38, 240.3, 27 and 487.1, respectively, while the titers of other two mice were too low to be measured. This range of anti-WB4-24 antibody titers was similar to that of anti-exenatide antibody (≤125) in humans[29, 30]. Statistical analysis (Figure 5) revealed that antibody titer had a positive correlation with the efficacy in terms of daily food intake in treated DIO mice (r=0.8227; P<0.05). In the cases of body weight and AUC_{120} of IPGTT, the correlations were not statistically significant (P>0.05). Therefore, this observation may be suggestive of the existence of an antibody-mediated neutralizing mechanism, further studies are required to examine whether GLP-1R paralysis (down-regulation or tolerance) caused by continuous exposure to high doses of WB4-24 contributed to the reduced efficacy[31]. Moreover, it is of importance to note that the antibody formation may result in safety issues, immune-related and hypersensitivity reactions in particular, although such adverse events have yet to be unmasked in our hands[32].

Conclusion

Obvious, limited success has been achieved since Boc5 was first reported in 2007 as a full non-peptidic agonist for GLP-1R. Although WB4-24 exhibited more potent bioactivities than Boc5 at the same dose level, its bioavailability and exposure level in the plasma should be, in theory, comparable to Boc5 because both ester and thienyl groups on the east end remain unchanged (Figure 1). Our inability to develop a 'druggable' molecule beyond the current structural class is consistent with the inherent difficulties in discovery of non-peptidic ligands for class B GPCRs. The unique structural architecture and activation mechanism of GPCRs are pivotal factors in this issue. Little secondary structure information is available, and rational drug design has to rely on low homology template modeling of rhodopsin[33]. High resolution crystal structures of GPCRs will certainly expand our understanding of how a ligand gains access to and binds within the receptor binding pocket and finally guide the structure-based drug design[34]. It is encouraging that Underwood[35] recently released the crystal structure of the extracellular domain of GLP-1R showing the molecular details of GLP-1 binding to the receptor extracellular N-terminal domain (ECD), an essential step in the two-domain binding mechanism applicable to class B GPCRs in general. The latest findings of Dezelak and Bavec[36] suggested that the third intracellular loop of GLP-1R worked as competitive substrate for mono-ADP-ribosyltransferase, which reduced mono-ADP-ribosylation of β subunit. This posttranslational modification of third loop of GLP-1R might represent a possible novel mechanism of receptor activity regulation and a potential target in treatment of T2DM. In conjunction with our determination of the crystal structures of Boc5[19] and WB4-24 (unpublished data), these latest developments will support us to characterize the binding site and ligand-mediated conformational changes induced by GLP-1, Boc5 or WB4-24, and to facilitate molecular modeling strategies to discover more potent and 'druggable' small molecule agonists.

Acknowledgements

We are indebted to Jing MA, Jing-kang SHEN, and Cai-hong ZHOU for valuable discussions, and to Dale E MAIS for critical review of this manuscript. This work was supported in part by grants from the Ministry of Science and Technology of China (2009ZX09302-001 and 2012ZX093004011), the Chinese Academy of Sciences (KSCX1-YW-02-2 and KSCX2-YW-R-17), Shanghai Science and Technology Development Fund (074319114, 08DZ2291300, and 09DZ2291200), the K C Wong Education Foundation and the CAS-Novo Nordisk Research Fund.

Author contribution

Ming-wei WANG, Da-wei MA, Da-fang ZHONG, Chuan LI, and Ling YANG designed the research; Min HE, Ni GUAN,

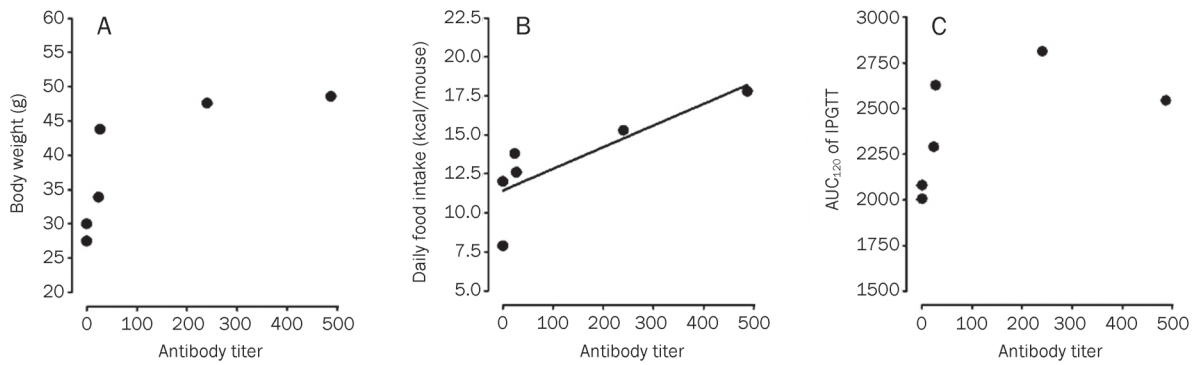

Figure 5. Correlation between plasma antibody titers and therapeutic efficacy in DIO mice treated with WB4-24. WB4-24 antibody titers had no statistically significant correlation with body weight (r=0.7758, P=0.698, n=6; A) or AUC_{120} of IPGTT (r=0.5627, P=0.245, n=6; C). The line in column B represents the positive correlation between WB4-24 antibody titers and daily food intake (r=0.8227, P=0.0444, n=6). Statistical analysis was performed using GraphPad Prism software by Pearson's correlation analysis.

Wei-wei GAO, Guang-bo GE, Qing LIU, Xiao-yan WU, and Xiao-yan CHEN performed the experiments; Ming-wei WANG, Da-fang ZHONG, Guang-bo GE, Chuan LI, and Ling YANG analyzed the data; and Min HE and Ming-wei WANG wrote the paper.

References

1 Report of the expert committee on the diagnosis and classification of diabetes mellitus. Diabetes Care 2003; 26 Suppl 1: S5–20.
2 Screening for Type 2 Diabetes. Report of a World Health Organization and International Diabetes Federation meeting. 2003. Available from: http://www.who.int/diabetes/publications/en/screening_mnc03.pdf
3 Gallwitz B. Glucagon-like peptide-1-based therapies for the treatment of type 2 diabetes mellitus. Treat Endocrinol 2005; 4: 361–70.
4 Meier JJ, Nauck MA. The potential role of glucagon-like peptide 1 in diabetes. Curr Opin Investig Drugs 2004; 5: 402–10.
5 Baggio LL, Drucker DJ. Biology of incretins: GLP-1 and GIP. Gastroenterology 2007; 132: 2131–57.
6 Drucker DJ. Minireview: the glucagon-like peptides. Endocrinology 2001; 142: 521–7.
7 Drab SR. Incretin-based therapies for type 2 diabetes mellitus: current status and future prospects. Pharmacotherapy 2010; 30: 609–24.
8 Grieve DJ, Cassidy RS, Green BD. Emerging cardiovascular actions of the incretin hormone glucagon-like peptide-1: potential therapeutic benefits beyond glycaemic control? Br J Clin Pharmacol 2009; 57: 1340–51.
9 Eglen RM. GPCRs revisited: new insights lead to novel drugs. Pharmaceuticals 2011; 4: 244–72.
10 Knudsen LB, Kiel D, Teng M, Behrens C, Bhumralkar D, Kodra JT, *et al*. Small-molecule agonists for the glucagon-like peptide 1 receptor. Proc Natl Acad Sci U S A 2007; 104: 937–42.
11 Chen D, Liao J, Li N, Zhou C, Liu Q, Wang G, *et al*. A nonpeptidic agonist of glucagon-like peptide 1 receptors with efficacy in diabetic *db/db* mice. Proc Natl Acad Sci U S A 2007; 104: 943–8.
12 Gong YD. A novel 3-(8-Chloro-6-(trifluoromethyl)imidazo[1,2-a] pyridine-2-yl)phenyl acetate skeleton and pharmacophore model as glucagon-like peptide 1 receptor agonists. Bull Korean Chem Soc 2010; 31: 3760–4.
13 Sloop KW, Willard FS, Brenner MB, Ficorilli J, Valasek K, Showalter AD, *et al*. Novel small molecule glucagon-like peptide-1 receptor agonist stimulates insulin secretion in rodents and from human islets. Diabetes 2010; 59: 3099–107.
14 Wang MW, Liu Q, Zhou CH. Non-peptidic glucagon-like peptide-1 receptor agonists: aftermath of a serendipitous discovery. Acta Pharmacol Sin 2010; 31: 1026–30.
15 Liao JY, Hong YF, Wang Y, Von geldern TW, Zhang KE. Phenylalanine derivatives and their use as non-peptide GLP-1 receptor modulators. WO Patent 2011094890. 2011; August 11.
16 Su H, He M, Li H, Liu Q, Wang J, Wang Y, *et al*. Boc5, a non-peptidic glucagon-like peptide-1 receptor agonist, invokes sustained glycemic control and weight loss in diabetic mice. PLoS ONE 2008; 3: e2892.
17 He M, Su H, Gao W, Johansson SM, Liu Q, Wu X, *et al*. Reversal of obesity and insulin resistance by a non-peptidic glucagon-like peptide-1 receptor agonist in diet-induced obese mice. PLoS ONE 2010; 5: e14205.
18 Kanoski SE, Fortin SM, Arnold M, Grill HJ, Hayes MR. Peripheral and central GLP-1 receptor populations mediate the anorectic effects of peripherally administered GLP-1 receptor agonists, liraglutide and exendin-4. Endocrinology 2011; 152: 3103–12.
19 Liu Q, Li N, Yuan YY, Lu HL, Wu XY, Zhou CH, *et al*. Cyclobutane derivatives as novel non-peptidic small molecule agonists of glucagon-like peptide-1 receptor. J Med Chem 2011. Doi: 10.1021/jm201150j.
20 Parnell JA. Differential secretion of satiety hormones with progression of obesity in JCR:LA-corpulent rats. Obesity 2008; 16: 736–42.
21 Toft-Nielson M, Madsbad S, Holst JJ. The effect of glucagon-like peptide 1 (GLP-1) on glucose elimination in healthy subjects depends on the pancreatic glucoregulatory hormones. Diabetes 1996; 45: 552–6.
22 Buse JB, Henry RR, Han J, Kim DD, Fineman MS, Baron AD. Effects of exenatide (exendin-4) on glycemic control over 30 weeks in sulfonylurea-treated patients with type 2 diabetes. Diabetes Care 2004; 27: 2628–35.
23 DeFronzo RA, Ratner RE, Han J, Kim DD, Fineman MS, Baron AD. Effects of exenatide (exendin-4) on glycemic control and weight over 30 weeks in metformin-treated patients with type 2 diabetes. Diabetes Care 2005; 28: 1092–100.
24 Fineman M. Antibodies to exenatide did not cross-react with human GLP-1 or glucagon or alter the efficacy or safety of exenatide. Diabetologia 2010; 53: S342.
25 Buse JB. The incidence of antibody formation and the levels of antibodies are lower with liraglutide than exenatide in a head-to-head comparison. Diabetologia 2010; 53: S341.
26 Hermanson GT. Preparation of hapten-carrier immunogen conjugates. In: Hermanson GT, editor. Bioconjugate Techniques. New York: Academic Press; 2008. p 745–82.
27 Singh KV, Kaur J, Varshney GC, Raje M, Suri CR. Synthesis and characterization of hapten-protein conjugates for antibody production against small molecules. Bioconjugate Chem 2004; 15: 168–73.
28 Hutchings CL, Gilbert SC, Hill AV, Moore AC. Novel protein and poxvirus-based vaccine combinations for simultaneous induction of humoral and cell-mediated immunity. J Immunol 2005; 175: 599–606.
29 Kendall DM, Riddle MC, Rosenstock J, Zhuang D, Kim DD, Fineman MS, *et al*. Effects of exenatide (exendin-4) on glycemic control over 30 weeks in patients with type 2 diabetes treated with metformin and a sulfonylurea. Diabetes Care 2005; 28: 1083–91.
30 Zinman B, Hoogwerf BJ, Duran Garcia S, Milton DR, Giaconia JM, Kim DD, *et al*. The effect of adding exenatide to a thiazolidinedione in suboptimally controlled type 2 diabetes: a randomized trial. Ann Intern Med 2007; 146: 477–85.
31 Reidelberger RD, Haver AC, Apenteng BA, Anders KL, Steenson SM. Effects of exendin-4 alone and with peptide YY(3–36) on food intake and body weight in diet-induced obese rats. Obesity 2011; 19: 121–7.
32 Faludi P, Brodows R, Burger J, Ivanyi T, Braun DK. The effect of exenatide re-exposure on safety and efficacy. Peptides 2009; 30: 1771–4.
33 Stenkamp RE, Teller DC, Palczewski K. Crystal structure of rhodopsin: a G-protein-coupled receptor. ChemBioChem 2002; 3: 963–7.
34 Cherezov V, Rosenbaum DM, Hanson MA, Rasmussen SG, Thian FS, Kobilka TS, *et al*. High-resolution crystal structure of an engineered human beta2-adrenergic G protein-coupled receptor. Science 2007; 318: 1258–65.
35 Underwood CR, Garibay P, Knudsen LB, Hastrup S, Peters GH, Rudolph R, *et al*. Crystal structure of glucagon-like peptide-1 in complex with the extracellular domain of the glucagon-like peptide-1 receptor. J Biol Chem 2010; 285: 723–30.
36 Dezelak M, Bavec A. Third intracellular loop of glucagon like-peptide-1 receptor is coupled with endogenous mono-ADP-ribosyltransferase — novel type of receptor regulation? Eur J Pharmacol 2011; 666: 35–42.

Acta Pharmacologica Sinica (2012) 33: 155–172

www.nature.com/aps

Review

Rare adipose disorders (RADs) masquerading as obesity

Karen L HERBST

Department of Medicine, University of California, San Diego and Veteran's Affairs San Diego Healthcare System, USA

Rare adipose disorders (RADs) including multiple symmetric lipomatosis (MSL), lipedema and Dercum's disease (DD) may be misdiagnosed as obesity. Lifestyle changes, such as reduced caloric intake and increased physical activity are standard care for obesity. Although lifestyle changes and bariatric surgery work effectively for the obesity component of RADs, these treatments do not routinely reduce the abnormal subcutaneous adipose tissue (SAT) of RADs. RAD SAT likely results from the growth of a brown stem cell population with secondary lymphatic dysfunction in MSL, or by primary vascular and lymphatic dysfunction in lipedema and DD. People with RADs do not lose SAT from caloric limitation and increased energy expenditure alone. In order to improve recognition of RADs apart from obesity, the diagnostic criteria, histology and pathophysiology of RADs are presented and contrasted to familial partial lipodystrophies, acquired partial lipodystrophies and obesity with which they may be confused. Treatment recommendations focus on evidence-based data and include lymphatic decongestive therapy, medications and supplements that support loss of RAD SAT. Associated RAD conditions including depression, anxiety and pain will improve as healthcare providers learn to identify and adopt alternative treatment regimens for the abnormal SAT component of RADs. Effective dietary and exercise regimens are needed in RAD populations to improve quality of life and construct advanced treatment regimens for future generations.

Keywords: adiposis dolorosa; Dercum's disease; lipedema; multiple symmetric lipomatosis; familial multiple lipomatosis; familial partial lipodystrophy; lymph; lymphatics

Acta Pharmacologica Sinica (2012) 33: 155–172; doi: 10.1038/aps.2011.153

Introduction

Lifestyle-induced obesity in children and adults has reached epidemic proportions worldwide. In the United States (US), a third of adults aged 20 years and over are overweight, a third are obese, and over five percent are extremely obese[1]. The National Health and Nutrition Examination Survey and Pediatric Nutrition Surveillance System reported a tripling of the prevalence of obesity among US school-age children and adolescents over the past three decades[2]. Numerous published studies validate the weight loss efficacy of lifestyle changes that include decreased amounts and types of food, and improved exercise regimens. Medications used for the treatment of obesity are severely limited[3, 4]. Bariatric surgery has been exceptional in its ability to induce weight loss and resolve the co-morbidities of obesity, though complications rates can be high[5], many people are still obese by body mass index (BMI) after Roux-en-Y gastric bypass (RYGB)[6], and weight regain occurs[7, 8].

This review aims to demonstrate lymphatic dysfunction as a component of rare adipose disorders (RADs) that increases the amount and alters the location of subcutaneous adipose tissue (SAT) while resisting fat loss after lifestyle changes or bariatric surgery. Lipodystrophies are also discussed as they may be confused with rare adipose disorders (RADs).

* To whom correspondence should be addressed.
E-mail karen.herbst@va.gov
Received 2011-08-31 Accepted 2011-10-12

Non-lifestyle causes of obesity

Lipodystrophies

Lipodystrophies or fat redistribution syndromes involve a primary lack or loss of SAT; however, increased SAT in other areas can be confused with lifestyle-induced obesity. Human immunodeficiency virus (HIV)-associated lipodystrophy, is well-known, but familial partial lipodystrophies are rare and therefore less well known, and can go undiagnosed for years or are never recognized. Acquired partial lipodystrophy, also rare, with a progressive and symmetrical lipoatrophy of SAT starting from the face and spreading to the upper part of the body, sparing the legs, can be confused with the RAD, lipedema, due to a disproportion between upper and lower body SAT (see below).

Acquired lipodystrophies

Human immunodeficiency virus (HIV)-associated lipodystrophy

HIV-and highly active antiretroviral treatment (HAART)-associated lipodystrophy includes loss of SAT from the face,

buttocks, arms, and legs. In men with lipodystrophy, SAT can be increased on the abdomen and chest (gynecomastia), and a dorsocervical fat pad or "buffalo hump" is common[9, 10]. The SAT in the dorsocervical fat pad is thought to be identical to the SAT in multiple symmetric lipomatosis (MSL), one of the RADs (see below). Upper body fat, including parotid hypertrophy, circumferential enlargement of the neck and a dorsocervical fat pad are associated with insulin resistance in HIV+ men[11–13] as is intermuscular fat and SAT on the legs in HIV+ women[14]. Large breasts are part of HIV lipodystrophy in Black women and other non-Caucasian ethnicities[15]. Women with HIV may also develop increased SAT on the upper part of the arm out of context with the usual lipoatrophy in this area in HIV+ men suggesting an estrogen and/or progesterone component to location of the SAT. This upper arm SAT looks visually similar to the SAT in women with the RAD, MSL (see below and Figure 1). In addition to excision of excess SAT as treatment for lipodystrophy[16], tesamorelin, a synthetic analogue of human growth hormone-releasing hormone, is FDA-approved for the reduction of excess visceral adipose tissue in HIV-infected patients with lipodystrophy. Visceral adipose tissue was reduced up to 18% during active use of tesamorelin[17]. The glucagon-like peptide-1 agonist, exenetide, also improved the HIV- and treatment-induced obesity through weight loss in a single case[18].

Acquired partial lipodystrophy (APL; BARRAQUER-SIMONS syndrome)

Acquired partial lipodystrophy is characterized by a regional loss of SAT primarily in children and adolescents starting at the face and extending to the waist, sparing the legs; in fact SAT may be increased on the legs[19]. Because of the higher amount of SAT in the legs compared to the upper body, APL could be confused with the RAD, lipedema (Figure 2). In lipedema, there is increased fat on the legs but the fat of the upper body is normal or increased (see below). APL is thought to be autoimmune occurring after a febrile (viral) illness[20] with

Figure 2. Acquired partial lipodystrophy and lipedema. A, a 37 year old woman with acquired partial lipodystrophy. C3 level<16.1 mg/dL (normal range: 90-180) and C4 level 23.11 mg/dL (normal range: 10-40). Note the loss of SAT from the upper body to the waist but obesity of the hips and legs (photo by Dr Alper GURLEK). B, a woman with lipedema stage II and a previous history of obesity with a 100 kg weight loss; note redundant skin on arms and abdomen from weight loss of non-RAD fat; note also lipedema in legs.

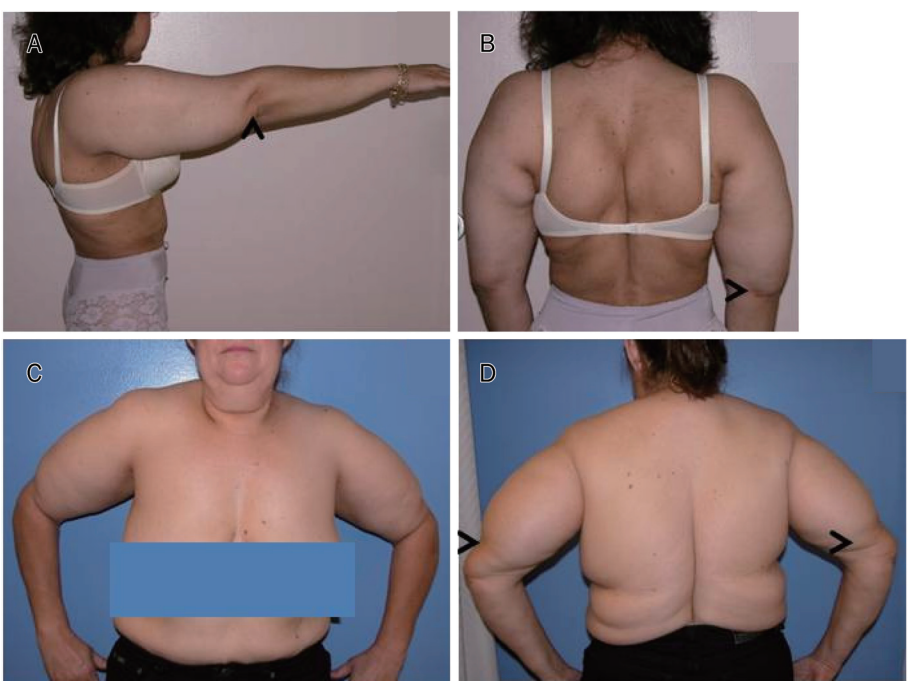

Figure 1. Multiple symmetric lipomatosis with or without HIV infection. A and B, non-HIV-related MSL Type II; note increased upper arm size and increased fat on back. Not shown is increased fat in the labia majora. C and D, increased arm and back fat, respectively in HIV-and HAART-induced MSL Type II. Arrows point to end of MSL fat on the upper arm. Normal labia majora (not shown).

low levels of complement factor 3 (C3) and the presence of a circulating autoantibody called complement 3-nephritic factor. Treatment with the thiazolidinedione, rosiglitazone, improved levels of C3 and increased SAT in a participant with APL[21].

Familial partial lipodystrophies (FPLD)

FPLD Type 1: FPLD1, also known as Köbberling lipodystrophy, is a lesser known partial lipodystrophy primarily found in women causing a lipodystrophy of the arms, legs, and sometimes breasts, with an increase in fat on the abdomen and remainder of the trunk[22]. The prevalence of FPLD1 and any genetic mutation remains unknown. There are no blood or urine biomarkers for FPLD1. FPLD1 may go unrecognized if the practitioner does not recognize the lipodystrophy; finding a ledge where SAT ends on the buttocks can help in the diagnosis. Diabetes and hypertriglyceridemia are highly prevalent in FPLD1 while acanthosis nigricans is minimal. Treatment is restricted to usual care of obesity-associated co-morbidities, although, RYGBP should be considered as it improved weight and co-morbidities in a case of FPLD1[23].

FPLD Type 2: The best studied FPLD is Type 2 (FPLD2), also known as Dunnigan lipodystrophy. In FPLD2, SAT is lost around the time of puberty from the legs, arms, buttocks, abdomen and chest; areas of remaining SAT deposits are on the back, face and chin, giving a Cushingoid appearance; fat is increased in the labia majora in women[24]; this finding also occurs in women with MSL (Figure 1). Mutations in the lamin A and C gene, LMNA, cause FPLD2[25]. People with FPLD2 have all the co-morbidities associated with obesity. Leptin levels can be very low in lipodystrophies and leptin treatment has shown benefit but remains investigational[26]. RYGB has also shown benefit in reducing the co-morbidities associated with FPLD2[27].

FPLD Type 3: Mutations in the peroxisome proliferator-activated receptor gamma (PPARG) gene can cause partial lipodystrophy with abdominal obesity[28] known as FPLD3[29]; people with FPLD3 may look very similar to FPLD2. Treatment with thiazolidinediones may be useful in people with PPARG gene mutations[30] and other cases of FPLD without identified gene mutations[31].

Additional lipodystrophies and single cases of additional types of FPLD have been well reviewed[19].

RADs

Multiple Symmetric Lipomatosis (Madelung's disease/syndrome; Launois Bensaude syndrome)

Multiple symmetric lipomatosis (MSL) is a rare syndrome (Table 1) originally described in 1846[32], characterized by the painless, symmetrical accumulation of abnormal tumor-like SAT. The first systematic treatise was by the German surgeon Dr Otto Madelung who collected 30 cases and reported an additional 3 cases in 1888 under the name "Fetthals" or fat neck[33], but the French Physicians Drs Pierre-Emile LAUNOIS and Raoul BENSAUDE gave prominence to and caused recognition of MSL by publishing a detailed account of 65 cases in 1898[34]. There are many synonyms for MSL including benign symmetric lipomatosis but this disorder is anything but benign, arguing against its use. Over 300 adult cases are reported in the literature with an age range of 20–71 years. The early literature on MSL was dominated by research on alcoholic men with a reported incidence of 1/25 000 in the Italian population[35]. Non-alcoholics and women are also affected[36–38]; two cases have been reported in children[39, 40].

Table 1. Identifying codes or numbers for SAT Disorders.

Code or number	SAT disorder		
	MSL	DD	Lipedema
OMIM	151800	103200	614103
Listed by NORD	Yes	Yes	No
NLM MESH ID	D008069	D000274	NA*
ICD-9/10	272.8/E88.8	NA/E88.2	NA
Alternative ICD-9/10	NA	338.4/G89.4 Chronic pain syndrome	457.1/189.0 Lymphedema, not elsewhere classified
Orphanet number	2398	36397	77243

ICD=International Classification of Diseases; MESH=medical subject headings; NLM=national Library of Medicine; NORD=National Organization of Rare Disease; OMIM=Online Mendelian Inheritance in Man®; *Application for a MESH code submitted

Diagnosis

Identification of MSL is by history and clinical exam. There are no blood or urine biomarkers for MSL and the gene(s) remains unknown in a majority of cases. Individuals with MSL have increased SAT, either as discrete non-encapsulated lipomas or as a confluent increase in SAT in a symmetrical distribution on the neck, the back, the chest, the upper arms, or on the thighs; MSL usually spares the distal limbs[41] but not in many women with MSL where the altered fat may be global[42] (Figure 3). Because the appearance and location of SAT in MSL can vary, MSL has been divided into three types:

Clinical types of MSL[37, 43]

Type I, head and/or neck with extension down the back, or only on the back: In rare cases, MSL SAT can invade the lingual muscles of the tongue[44, 45], or the vocal cords and compress the recurrent laryngeal nerve causing hoarseness[46], or increase periorbital fat[47]. Tracheal or esophageal compression and the superior vena cava syndrome can be found in 15%–20% of patients[48]. The presence of a dorsocervical fat pad (buffalo hump) can be found both in MSL[41, 49, 50] and HIV-associated lipodystrophy[9, 10, 51, 52]; it has been proposed that the fat in these two disorders arises from brown adipose tissue located in that area[53].

Type II body: Includes the shoulder girdle, the upper arms, the thorax, the back, the abdomen and upper buttocks. In one case, fat grew around the testicles in the scrotum and was contiguous with MSL tissue in the perineum and the root of the penis[54]. Also rare is growth of the MSL fat on the hands[55].

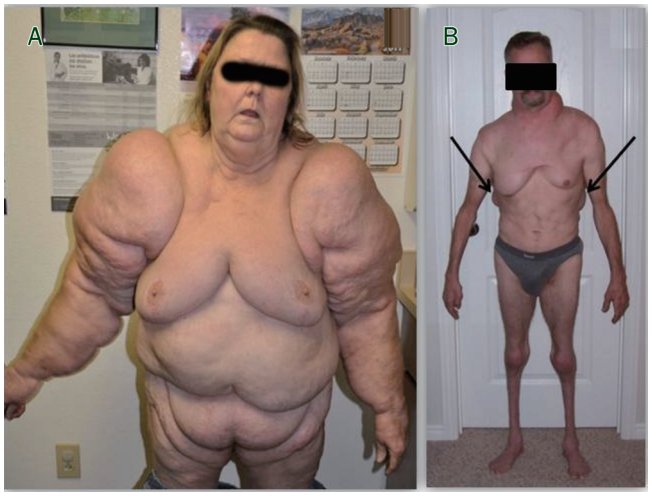

Figure 3. Whole body MSL and MSL-associated lipodystrophy. While MSL is noted to spare the forearms (see text), the entire body can be clearly affected. A, 60 year old woman with a history of alcohol dependence with global MSL SAT; note prevalent SAT on the forearms (photo by Dr Andy COREN). This type of MSL may be easily confused with global obesity or lipedema stage III. B, 50 year old man with MSL Types I and II with associated muscle and normal fat atrophy (also note the increased back MSL SAT; arrows); this type of MSL may be confused with partial lipodystrophy.

Many individuals have a combination of Types II and III. While the MSL fat grows, normal fat and muscle can undergo wasting which can be confused with a partial lipodystrophy (Figure 3).

Type III, thigh (female type): Rarest type. MSL type III is clinically similar to and may be instead, the RAD, lipedema (see below). Women tend to have Type II and III MSL with widespread altered SAT[41].

MSL inheritance

MSL is thought to be inherited through mitochondrial mutations in a few familial cases including multiple deletions of mitochondrial DNA, and the myoclonus epilepsy and ragged-red fibers (MERRF) tRNA(Lys) A>G(8344) mutation[56, 57]. Klopstock *et al* found mitochondrial mutations in only 2 of 12 patients studied[50]. Chalk *et al* found no mitochondrial pathology or mutations in four siblings with MSL with a pattern favoring autosomal recessive[58]. The phenotype of MSL may require a combined effect of alcohol (or other insult) and a currently unknown genetic mutation.

Histology of MSL fat

Individual fat cells have been described as smaller than normal[38, 49, 59] or normal sized[38]. MSL SAT is thought to be derived from brown adipose tissue (BAT) or as white adipose tissue (WAT) that transdifferentiates into BAT[49, 60, 61]. Ultrastructurally, brown adipocytes have numerous large mitochondria packed with cristae. Under light microscopy, brown adipocytes have cytoplasmic lipids arranged as numerous small droplets (multilocularity), while white adipocytes have cytoplasmic lipids arranged in a unique vacuole (unilocularity). In BAT, the metabolic reactions of mitochondria are uncoupled from ATP synthesis by uncoupling protein (UCP)-1 so that energy produced is released as heat[62]. Infants and even adolescents have a substantial amount of BAT, especially between the shoulder blades. BAT persists throughout adulthood in the perirenal, omental, mesenteric, pericardial, intercostal, axillary, cervical, and interscapular fat, embedded within WAT[63, 64] with an approximated ratio of 1 brown adipocyte for every 200 white adipocytes[65, 66].

By light microscopy, adipocytes in MSL SAT are monovacuolar[67, 68] or multivacuolar[69]. By electron microscopy of long-term primary cultures from the stromal vascular fraction (SVF), containing stem and immune cells, cells were polymorphic with thin microfilaments suggestive of elevated metabolic activity[69], were multivacuolar, and had large mitochondria packed with cristae suggesting a more BAT phenotype in MSL[60, 68].

Physiology of MSL SAT

MSL SAT may arise from a stem cell population either destined to form BAT, or WAT that transdifferentiates to BAT; in either case, UCP-1 levels help track BAT features. SAT cells from subjects with MSL express UCP-1 suggesting its origin as BAT[61, 70], but this is not substantiated in all cases[71]. Adrenergic receptors (AR) that respond to sympathetic input, such as the three subtypes of β-AR, β_1-, β_2- and β_3-, promote lipolysis and energy expenditure. Cells isolated from the MSL SVF did not increase UCP-1 in response to noradrenaline even though MSL cells express all three β-AR[61]. Resting energy expenditure (REE) may be expected to be higher in MSL with BAT; indeed REE when normalized to fat free mass was mildly higher in MSL subjects than normal, suggestive of energy uncoupling and heat generation[72], however, REE in other subjects with MSL was within normal limits[38]. In MSL cell culture, catecholamines did not increase lipolysis, expression of inducible nitric oxide synthase (iNOS) or PPARγ coactivator-1α (PGC-1α), a coregulator of nuclear receptors that control metabolic pathways in BAT[61, 73–75]. Two other groups found a normally reactive adenylate cyclase system and a normal number of a- and β-adrenergic receptors in MSL SAT[76, 77]. Cytokine and adipokine levels in MSL are also mixed[37, 61]. While the multilocularity of MSL SAT is suggestive of BAT, more data in a larger number of subjects of well characterized participants are needed to substantiate the cell type of origin and functionality of pathways.

The increase in MSL fat is extensive and deforming, compressing tissue structures and vessels. Early, MSL SAT is watery but later becomes fibrotic and scars easily[78]. Similarly in obesity, excess fat physically impedes lymph collection and flow, protein-rich lymphatic fluid collects in SAT, resulting in lymphedema and tissue hypoxia[79]. SAT also grows in the presence of lymphedema[80]. Further accumulation of fluid in the setting of decreased oxygen tension leads to fibrosis[81]. Interestingly, ischemia activates the growth of adipose-

derived progenitor cells[82]. Congestion of lymph nodes by other means, such as lymphoma in the neck, induces fat growth similar to MSL[83]. Increased volumes of SAT in MSL, like obesity, may therefore be sufficient to externally compress vasculature and lymphatics inducing further growth of SAT as seen in other localized fat collections[84]. Impedance of lymph flow into lymph collectors is a local effect and does not affect flow in larger lymph trunks, therefore the role of lymphoscintigraphy in MSL is questionable[85].

Conditions associated with MSL

Alcohol-induced liver disease is common in MSL. Hyperlipidemia, hyperuricemia, hypothyroidism, and diabetes mellitus have been reported but are not consistent amongst those affected[86, 87]. People with MSL I or II should be tested for sleep apnea[87]. Cancerous transformation of the SAT is uncommon; development of myxoid liposarcoma was reported in one case[88]. Slowly progressive axonal sensory and autonomic peripheral neuropathies have been reported to occur after the development of MSL fat and impairment of autonomic function has been suggested as a cause of sudden death[86, 89]. The neuropathology is a distal axonal demyelination different from that associated with alcohol intake[58, 86, 90]; this impairment seems to be prevalently parasympathetic[48, 91]. In a ten year follow-up, ~10% of 31 patients died from sudden death due to autonomic neuropathy[36]. Surgical placement of a cardiac pacemaker may be needed.

MSL treatment recommendations

Primary recommendations

1) Alcohol abstinence: Abstinence from alcohol may arrest further progression of the MSL SAT but does not cause regression of the SAT deformities[92].

2) Lymphatic decongestive therapy (LDT): Includes manual lymphatic drainage (MLD), wrapping of the limbs, compression garments, exercise such as pool therapy and other non-impact exercise (so as to avoid lactic acid accumulation in tissue due to poor lymph flow), dietary recommendations, and skin care. Manual lymphatic drainage works well to reduce MSL SAT before fibrosis[93].

3) Surgery: Surgical resection and liposuction provide the only means of dramatically decreasing the MSL SAT[94–97]. In a majority of cases of MSL Type II and III, resection or liposuction of the lipomatosis is considered cosmetic and insurance companies are reluctant to cover this procedure[98]. Unfortunately, the fat usually penetrates and surrounds deeper structures such as muscle and bone, making total excision of the abnormal tissue difficult[92]; the lipomatosis can, therefore, recur after liposuction or excision[87, 99, 100]; in three of eleven patients in one series[101].

Additional considerations for MSL treatment

4) β_2-Adrenergic Agonist: After demonstrating an intact lipolytic response of the MSL fat to catecholamines, an oral β_2-AR specific drug, salbutamol, 15 mg per day in divided doses, reversed the rapid accumulation of the MSL fat and increased REE in a man with MSL, but was effective only during active use[102].

5) Fibric acid: A man with MSL Type II with a past history of hypertriglyceridemia was treated with fenofibrate 200mg daily. The circumference of his abdomen decreased 119 cm (46.9 in) to 108 cm (42.7 in) within a year. Fibric acids are PPARα agonists. Activation of the PPARα receptor may suppress expression of proteins involved in the architecture of BAT, thereby maintaining BAT in a quiescent state[103].

6) Growth hormone: Growth hormone (GH) treatment has been suggested in the community of individuals with MSL as a treatment option (personal communication) but GH levels were normal in one subject with MSL during a glucose tolerance test[49] and in three other subjects[104] suggesting a normal GH axis. Testing for GH deficiency should be undertaken and replacement considered only for those deficient in this hormone.

7) Lifestyle: Lifestyle improvements provide no resolution of the MSL SAT[105].

8) Local SAT injections: Corticosteroid injections have been suggested as treatment for lipomatosis such as MSL SAT[106] but there are a number of cases demonstrating the development of lipomatosis after steroid use[107, 108]. Local injection with thyroxine[107], enoxaparin[109], deoxycholate[110], and phosphatidylcholine[78] have also been proposed for treatment of lipomas but the latter require multiple injections and use of thyroxine injections in the presence of autonomic dysfunction would be dangerous. In addition, the extent of the SAT in MSL does not allow for single site injections, limiting these treatments to lipomas.

Lipedema (lipoedema; lipalgia; adiposis dolorosa; lipomatosis dolorosa of the legs; lipohypertrophy dolorosa; painful column leg)

Lipedema is generally unknown to medical providers, is easily confused as obesity, does not have a MESH term in the National Library of Medicine, and does not have an International Classification of Diseases (ICD) code; it does have an Online Mendelian Inheritance in Man code, and is recognized by Orphanet (a European website providing information about orphan drugs and rare diseases (Table 1). Drs Allen and Hines Jr from the Mayo clinic labeled this condition as lipedema in 1940[111]. Outside the US, lipedema is known as "lipoedema", meaning edema of the fat. This disorder is likely very common but underdiagnosed.

Diagnosis

The diagnosis of lipedema is made clinically by history, visual inspection and physical exam as extensive deposition of SAT between the iliac crest and the malleoli and approximately 30% of the time, on the arm[42]. When the fat is palpated, it will be tender and feel like round peas in a plastic bag or a "beanie baby"[111, 112]. Larger nodules, lumps, lipomas or angiolipomas may also be found in the SAT. There are no blood or urine biomarkers for lipedema and the gene(s) is unknown. The skin and SAT is thicker in lipedema compared

to healthy controls and muscle mass is not edematous as it is in lymphedema[113]. The skin is also less elastic and striae are common in lipedema.

In 1951, Wold, Hines and Allen analyzed 119 cases and provided the diagnostic criteria for lipedema[114]:

1) Almost exclusive occurrence in women developing by the third decade of life. Prevalence within the population remains grossly under diagnosed[115]. According to an epidemiologic study by Földi E and Földi M[116], lipedema affects 11% of the female population. At least seven cases have been reported in men with testosterone or GH deficiency, or liver disease[114, 115, 117].

2) Bilateral and symmetrical nature with minimal involvement of the feet, resulting in an ''inverse shouldering'' or ''bracelet" effect at the ankle

3) Minimal pitting edema (non-pitting edema is present)

4) Pain, tenderness, and easy bruising

5) Persistent enlargement despite elevation of the extremities or weight loss

6) Increased vascular fragility; easy bruising

Often women note that the lipedema appears or is exacerbated at the time of puberty, pregnancy[118] or menopause suggesting an estrogen component; that few men have this condition except those with hypogonadism or hyperestrogenemia supports this hypothesis.

There are five types of lipedema[119]

Type I: Pelvis, buttocks and hips (saddle bag phenomenon)

Type II: Buttocks to knees, with formation of folds of fat around the inner side of the knee

Type III: Buttocks to ankles

Type IV: Arms

Type V: Lower leg

There may be a mixture of lipedema types in one person, for example Type II and IV. Only the arms may be affected in 3% of lipedema cases (Type IV)[42]. The importance of knowing the different lipedema types is to improve recognition, and identification of differences *ie*, all people with lipedema do not look alike; treatment is similar amongst the types. In addition to types of lipedema, the lipedema progresses through stages; the progression varies greatly amongst those affected and there is no data suggesting everyone need progress through all stages.

There are three stages of lipedema (Figure 4)[112, 120]

Stage 1: Normal skin surface with enlarged hypodermis

Stage 2: Uneven skin with indentations in the fat[121]; larger mounds of tissue grow as unencapsulated masses, lipomas and angiolipomas

Stage 3: Large extrusions of tissue causing deformations especially on the thighs and around the knees

Stage 4: Lipedema with lymphedema (lipolymphedema)

Progression to lipolymphedema can develop during stage II-III. The description and representative pictures of Type III MSL[41] are that of lipedema stage II[38]; no study has formerly differentiated these two SAT disorders. Synonyms for lipedema also include adiposis dolorosa, which is another name for the RAD, Dercum's disease (see below). However, according to Cornely, the trunk, hands and feet are not involved in lipedema "Thus, lipedema differs clearly from Dercum's disease"[122]. As lipedema progresses to lipolymphedema, the hands, feet, trunk and head develop excess SAT making this statement incorrect. Because lymphatic dysfunction is a part of Dercum's disease and many early cases of Dercum's disease are visually and descriptively lipedema (see below), the two SAT disorders are at a minimum, in the same spectrum. Lipedema may also be confused with APL, however, in APL there is a lack of SAT on the face and upper body while in lipedema, SAT is normal or increased in these areas (Figure 1).

Inheritance of lipedema

Inheritance has been noted up to 60% of people with lipedema[118, 123, 124] but is likely higher due to under diagnosis. In six families over three generations with lipedema, the inheritance pattern was autosomal dominant with incomplete

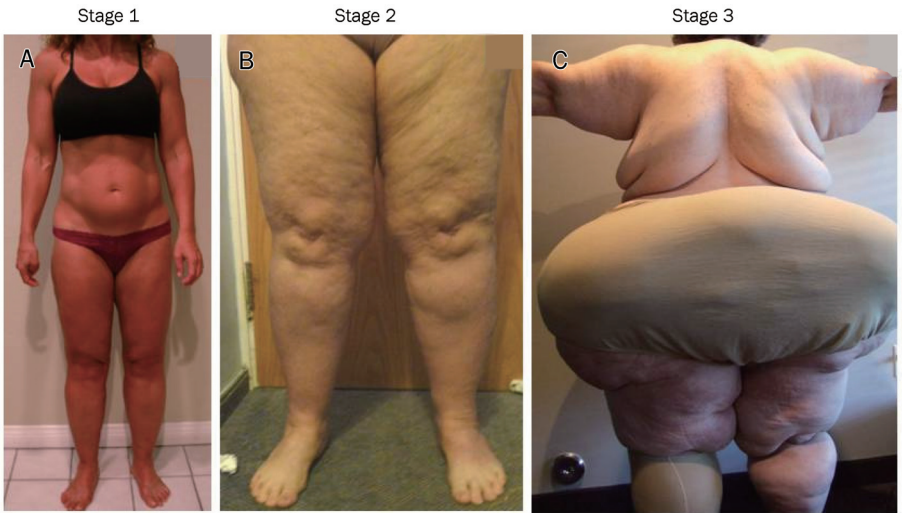

Figure 4. The three stages of lipedema. A, Stage I with little alteration of the skin surface. B, In stage 2, the surface of the skin takes on the appearance of a mattress with lipomas in the fat. C, In stage III lipedema, there are much larger fat extrusions.

penetrance[115].

Histology of lipedema SAT

The gross description of the fat in lipedema is similar to that of MSL with "free fluid fat" in biopsy specimens[125]. Histological exam is not unlike that found for cellulite with dilation of subdermal blood capillaries, perivascular cells, fibrosis of arterioles, fibrosis and dilation of venules, and hypertrophy and hyperplasia of adipocytes[126, 127]. Histochemical studies show adipocytes death and stem cell regeneration[128]. There are also increased numbers of blood vessels especially capillaries and prominent venules[116]. Large clusters of macrophages are found around multiple fat cells (not isolated crown-like structures[129]), surrounding blood vessels and forming oil cysts in lipedema SAT[116, 130]; macrophages may also be a prominent component of cellulite[131]. The histology of lipedema SAT can also appear as normal[125].

Physiology of lipedema SAT

The elasticity of the skin and fascia is decreased in lipedema[132] which in Stage III may progress to abnormally clumped elastic fibers or pseudoxanthoma[133]. The skin loses its role as an abutment for the skeletal muscle venous pump and the increased compliance of the SAT results in an increase in capillary compliance[116, 124]. The permeable capillaries release excess protein-rich fluid into the interstitium along with blood[42, 116, 134, 135]. The veno-arteriolar reflex in lipedema is also absent so that under orthostatic conditions (standing), there is limited vasoconstriction and increased net filtration driving edema[116]. Early on, lymphatic transport increases to accommodate the increased fluid flux from the capillaries[136, 137]. During this time, visualization of lymphatic vessels on a gross level by lymphoscintigraphy is normal[138, 139]. As lipedema progresses, microaneurysms appear in the lymphatics in the skin[139, 140] which eventually leak[125, 136]. It is during this time that hypertrophy and hyperplasia of fat cells accelerates[138] further altering the microlymphatic architecture and increasing venous congestion. The resultant edema increases hydrostatic pressure in the tissue and pain[123, 141].

As an example of what happens in SAT when lymph leaks, mutation of prospero homeoboxprotein 1, encoded by the PROX1 gene, causes leakage from lymphatics and resultant obesity in heterozygote mice[142]. Lymph placed on adipocytes in culture also induces robust growth; in essence, "lymph makes you fat"[143]. Although PROX1 mutations are not known to be associated with lipedema, it is clear that fat grows in response to lymph[80]. Eventually, the microlymphatics may become obliterated in lipedema[144] leading to backflow and an overall dynamic insufficiency of the lymphatic system[42]. The increased tissue pressure and lymphatic vessel leakage lead to the development of lipolymphedema[136, 145, 146]. While lymphedema does not usually develop with cellulite in women, the pathophysiology of cellulite development is similar to that in lipedema, and LDT (see treatments below) improves the cosmetic appearance of cellulite[147, 148]. Lipedema may therefore be an extreme form of cellulite.

Conditions associated with lipedema

Depression and anxiety are very common in people with lipedema for many reasons including the lengthy time to diagnosis, repeated counseling on diet and exercise by the healthcare community when neither is particularly effective and because of the massive and sometimes rapid body metamorphosis over a lifetime. In one clinic, women with lipedema were found to be more depressed than patients with paralysis[112]. Painful SAT is a chronic problem in lipedema[111, 114]. The excess tissue fluid weakens nearby structures leading to the development of joint pains; with progression of lipedema, arthritis develops[149]. Capillary fragility, ecchymosis, hematomas and venous varicosities are common[150]. The Kaposi-Stemmer sign is negative in lipedema (the skin cannot be pinched as a fold by the fingers) until the development of lipolymphedema. Idiopathic edema (IE) is similar to lipedema by description and has been identified in women with lipedema[116, 134]. Other changes in skin include dryness, fungal infections, cellulitis, and slow wound healing. Free fatty acids may be different in both blood and the lipedema SAT[125].

Lipedema treatments recommendations

Primary recommendations

1) Lymphatic Decongestive therapy (LDT) is the standard of care for lipedema. Includes manual lymphatic drainage (MLD), wrapping of the limbs, compression garments, movement therapy, dietary recommendations, and skin care. LDT has been shown to improve skin elasticity, restore the veno-arteriolar reflex, increase pre-lymph drainage and lymph transport in lymphatic vessels[116, 151], and reduce capillary fragility in lipedema[152]. Intermittent pneumatic compression may not improve limb size over MLD alone[153] but may be effective alone when MLD is not available[154]. Compression is most effective when tissue edema is present[155] as in its absence, it has little effect[156]. That compression was effective in lipedema was noted by Hines in a woman with lipedema whose fat and edema were absent under the area covered by her "high-topped shoes"[157].

2) Exercise: Aqua lymphatic therapy (pool hydrotherapy) significantly reduces limb volume in lymphedema[158]. In addition to improving strength and bone mineral density, whole body vibration (WBV) improves peripheral circulation[159, 160] and increases lymph flow, raising the threshold level for edema formation in the legs[161]. During WBV, the user simply stands (or stretches/exercises) on a platform for 10-15 min. making this a very accessible exercise modality.

3) Pain Control: Must be individually optimized; liposuction improves pain (see below).

4) Psychological support: Many women with lipedema are left on their own to find their diagnosis, convince their healthcare providers about lipedema and then seek treatment, all complicated by depression, anxiety and eating disorders; counseling and support during treatment are necessary when any of these are present[116]. Counseling reduces anxiety by 50% in people with secondary lymphedema[162].

5) Surgery: Liposuction works effectively for lipedema to

reduce SAT and pain[122, 163, 164]. In patients who have lipolymphedema, it may be prudent to undergo lymphoscintigraphy to confirm the absence of large lymph vessel damage before pursuing liposuction[116]. Bariatric surgery is ineffective in uncomplicated lipedema (without obesity or lymphedema)[165, 166] but effective in lipedema and lymphedema associated with obesity as long as LDT is performed before and after bariatric surgery[167].

Additional considerations for lipedema treatment

6) Beta-adrenergic agonist: Modeling treatment after capillary leak syndrome, terbutaline sulfate, 5 mg five times daily, and theophylline, 200 mg twice daily, were given to a woman with lipedema (called lymphedema in the paper) and after 10 months a weight loss of 20 kg was noted. Cessation or lowering the medication allowed weight regain[168].

7) Corticosteroids: Corticosteroids produce a fast reduction in swelling and pain but increase the risk of infection, capillary fragility and SAT growth. A series of corticosteroid joint injections is usually well-tolerated without exacerbation of lipedema.

8) Diuretics: Diuretics can quickly deplete lymphedema fluid but concentrate protein in edematous tissue promoting fibrosclerosis[169]. Use of diuretics in lipedema before lymphedema may result in the development of pseudo Barrter's syndrome characterized by hypokalemic-hypochloremic alkalosis, hyperactivity of the renin-angiotensin-aldosterone system and elevation of atrial natriuretic peptide[116, 170].

9) Flavonoids: Daflon is a flavonoid that has been used to treat lymphedema[171-173]; it may be expensive and is unlikely available by prescription. Other flavonoids such as those for venous disease[174] have not been formerly tested in lipedema participants. The International Society of Lymphology does not endorse the use of flavonoids as a substitute for LDT.

10) Lifestyle: Obesity can occur along with lipedema especially in Stage III when the lipedema limits movement, but can also occur when movement is limited by pain in earlier stages; lifestyle improvements should always be considered but are not the cause of lipedema[175]. Lipedema SAT is unaffected by caloric restriction alone[175].

11) Selenium: Sodium selenite (selenium) has proven effective for reduction of secondary lymphedema[169, 176–181]. The US National Research Council has defined the individual maximum safe dietary intake for selenium as 600 μg daily and the no adverse effect level as 800 μg daily.

12) Shock wave therapy: One report suggests that shock wave therapy functions similarly to LDT in reducing oxidative stress of the tissues and in smoothing the dermis and hypodermis[182] which may be useful as part of a treatment plan and when lymphatics are still functioning.

Dercum's disease (adiposis dolorosa; Morbus Dercums)

Dercum's disease (DD) was recognized in 1892 as a clinical entity called "adiposis dolorosa", meaning painful fatty deposits, when Dr Francis X DERCUM from the University of Pennsylvania published on three cases[183]. This sentinel publication was preceded by a report of a single case in 1888[184] and followed by the published autopsy of that case[185]. Numerous case studies, case series and descriptions of DD have been published with such a wide variety of locations for the fatty deposits, including misdiagnoses of obvious cases of lipedema, familial multiple lipomatosis and MSL[186] that, unless one is an expert in SAT disorders, it would be difficult to diagnose this often misunderstood syndrome. DD is currently considered to be a rare disorder (Table 1).

Diagnosis

Diagnosis of DD is made by history and physical exam. Dercum's disease occurs primarily in women with a ratio of females to males of 5-7:1[186–188]; the average age of development in one series was 35 years[188] but it has been reported to develop in children[188–191] and in adults up to age 80 years[186]. One in a 1,000 are affected in Sweden[187]. Many cases of peri- or post-menopausal women with DD have been reported suggesting a hormonal component to the development of DD[192]. In addition to painful SAT, there are many other signs and symptoms associated with DD so a lengthy review of systems is helpful (Table 2).

There are three types of DD[187, 193]:

Type I, juxta-articular (around the joint): Painful folds or nodular fat on the inside of the knees and/or on the hips; in rare cases only evident in the upper-arm fat (similar to Type IV lipedema).

Type II, diffuse, generalized type: Widespread pain from fatty tissue found anywhere from head to the soles of the feet.

Type III, nodular type: Intense pain in and around multiple "lipomas", sometimes in the absence of obesity.

Interestingly, the painful lumps of fat first noticed around joints in DD Type 1 occur in locations of lymph nodes, for example around the knee (popliteal nodes), the elbow (cubit nodes), hips and thighs (inguinal nodes), upper arm (axillary nodes) and supraclavicular. As Dr Kling reported in 112 cases of Type I DD, "Juxta-articular adiposis dolorosa is regarded as the initial and intermediate stage of generalized adiposis dolorosa"[194]. Dercum's disease Type I is therefore, the first stage of DD, and Type II a stage with more widespread dysfunction. Type I DD around the knees is visually consistent with Type IV and Type II lipedema Stages 2–3.

Type III DD is likely a variant of familial multiple lipomatosis (FML) in which men present mainly with lipomas and/or angiolipomas predominating on the lower and upper arms, the lower trunk and thighs and women present with lipomas, angiolipomas and obesity[188, 195]. Angiolipomas can be found in up to 30% of people with DD[188, 196]. The lipomas are generally not painful in FML except if they are growing or traumatized frequently, however, they are painful in DD Type 3. In a DD family, family members may have lipomas without pain[195]. Even if a person with FML has non-painful lipomas, at some point in time a lipoma can become painful, followed by generalized pain in all lipomas. Pack and Ariel[197] described this as lipoma dolorosa, distinct from DD. It is

unclear why the authors make this distinction as others ascribe the same pathological process to both FML and DD Type III, with pain in the latter due to "local conditions"[198]. The "local conditions" may be increased tissue tension from fluid accumulation. In two cases of DD Type III, pain was relieved after local hemorrhage[186]. The underlying pathophysiology of DD needs to be elucidated to further differentiate or group the three types of DD.

DD inheritance: Thought to be autosomal domin-ant[188, 195, 199, 200]. In two families, females were more affected than males suggesting a sex-specific influence on the expression of the DD phenotype[195].

Histology of DD

Some of the unilocular adipocytes are extremely large in DD SAT compared to weight matched controls[187]. Dr Dercum and others found an infiltration of nerves (neuritis)[185, 201] but this has not been substantiated. Increased connective tissue around nerves, blood vessels and as thickened septae has been noted[185, 202, 203]. Perivascular cells[203], giant cells[204], and granulomas suggestive of a foreign body reaction are apparent in some areas[205]. The histology of DD SAT can also appear normal[194, 206–209].

Physiology of DD

The physiology of DD is unknown and many etiologies have been advanced. These include thyroid dysfunction[185], pituitary dysfunction, polyglandular disease, infection, neuritis, alcohol, trauma, a defect in the synthesis of long chain fatty acids[205], lower resting energy expenditure[202], and altered responses to norepinephrine and insulin.[210] Ballet may have been closest to the actual etiology when he stated that it is a "chronic intoxication of endogenous origin"[211]. The evidence currently points to an underlying vascular and lymphatic dysfunction in DD Types I/ II similar to lipedema (Birgher Fagher, personal communication) for the following reasons:

1) Vascular dysfunction as hematemesis[212, 213], epistaxis[213, 214], hemaochezia[212], heavy menses[215, 216], varicose veins[194], and altered vasoconstrictor responses[217] is common in both lipedema and DD. Perivascular infiltration of immune cells have been found in DD tissue[218] suggesting damage to or repair of blood vessels, and brain vasculitis in DD has been reported[219].

2) LDT has been reported to be beneficial in DD[220] as in lipedema.

3) Multiple lipomas can develop in lipedema as in DD[221].

4) Fibrosis secondary to lymphedema[222] is common in lipedema[112] and DD[202].

5) In the presence of lymphatic and vascular dysfunction in lipedema, the fat is painful[112], similar to DD.

6) In the German literature, lipedema is known as adiposis dolorosa, another name for DD[118].

7) Original descriptions of DD match descriptions of lipedema. For example, Spiller described a woman with painful fat as follows: "The obesity was marked over the thighs, calves, abdomen, nates (buttocks), and back. It was also very great in the arms, less marked in the forearms, and absent in the feet and hands"[223]. Dr Collins noted that "The fatty accumulations have not been noticed in the hands, face or feet, and frequently the contrast between the feet which preserve their normal outline and contour and the legs, when the latter are involved, is most striking"[214]. These cases are similar to lipedema in terms of the pattern of painful fat (less likely early on in the hands, feet, face, and forearms) and the latter case describes well the distinct "bracelet" of fat seen at the base of the leg above the foot that is classic in lipedema[112]. The published photographs of the columnar legs with the cuff of fat above the foot, or the mass of tender fat inferomedial to the knee, and the enlarged upper arms in DD are consistent with lipedema[112, 183, 184, 224, 225].

8) The nodular "beans in a bag" feel of the fat in lipedema is the same as in DD Types 1 and 2[188, 226].

9) Dr Dercum described DD as a disorder of the "haemolymph system"[227] though the importance of these structures in humans is unclear. Hemolymph nodes are structures resembling a lymph node, but which can have blood in the sinuses; erythrocytes enter the hemolymph nodes through afferent lymphatics[228]. There are few reports on the function of hemolymph glands in humans.

10) Dr Mills reported "In one case studied carefully with Dr Dercum, there was a general disease of the lymphatic system"[229].

The data suggest that the vascular and lymph system are dysfunctional in both lipedema and DD, that pre-lymph remains in the tissue longer, inducing fat growth and the characteristic beans in a bag feel to the fat. In both lipedema and DD there is a hereditary component[195, 199]. Also in both cases, estrogen and/or progesterone likely play a role resulting in the predominance of women with lipedema and/or DD; lipedema is known to occur with the onset puberty and pregnancy, and DD with menopause, both times of changing hormone levels. In DD, a more widespread insult to the vascular and lymphatic system may occur compared to lipedema. Many of the early reported cases of DD had syphilis[213, 216, 230], well known to affect the lymph nodes, consumed alcohol[214, 231] which acutely increases mesenteric lymphatic pumping but decreases lymphatic myogenic tone[232], or had antecedent trauma which may have affected lymphatic function[207, 213, 233]. Many patients with DD Type I or II noticed their first painful area of fat after a viral flu, severe pneumonia or trauma[188, 213, 234]. Data are needed on lymphatic function in DD to confirm these hypotheses.

Conditions associated with DD

In addition to the two cardinal symptoms of fatty deposits and pain proposed by Dercum[184], Vitaut added the third cardinal symptom of DD, asthenia (abnormal physical weakness or lack of energy)[193]. Accessory symptoms in DD are found in the psychiatric, motor, sensory and sympathetic nervous systems[186] as well as the pulmonary, endocrine, gastrointestinal and rheumatological systems[187, 188, 235] (Table 2).

Thyroid dysfunction has been suggested as one etiology of

Table 2. Cardial and accessory signs and symptoms of Dercum's disease with checkbox.

Cardial Signs/Symptoms	Details	√
Fat deposits	Nodules (lipomas) in fat ranging in size from rice grains to a fist or larger	
Pain in fat deposits for at least 3 months	Pain exacerbated by stress, strenuous exercise, trauma, changes in weather, or other; pain can be spontaneous or on palpation; may wax and wane or move around	
Fatigue (asthenia)	Exacerbated by activities of daily living or exercise	
≥2 accessory symptoms		
Cognitive change(s)	Memory difficulties; difficulty forming thoughts; "brain fog"	
Weight gain	Difficult to lose fatty deposits with lifestyle changes	
Vascular involvement	Visible vascularity near lipomas; telangiectasias; multiple cherry angiomas, multiple petechiae; easy bruising; flushing; hematuria of unknown etiology; heavy or prolonged menstrual bleeding; epistaxis	
SAT edema	Non-pitting	
Gastrointestinal complaints	Gastroesophageal reflux disease, irritable bowel syndrome, bloating, abdominal pain, early satiety	
Joint pain and/or stiffness	Increased in areas of fat deposits	
Muscle pain/stiffness	Especially on awakening or the day after physical activity	
Shortness of breath	In the presence of normal oxygen saturation or as part of the need for oxygen supplementation	
Tachycardia	Varies from palpitations to supraventricular tachycardia requiring beta-blockade	

DD. While a few cases of DD benefited from thyroid treatment[216, 236] many cases of DD failed to improve[192, 215, 230, 237, 238] and DD generally continues to progress during adequate thyroid replacement[188]. Others have suggested multiple endocrine dysfunction as a cause for DD[201] (reviewed[186]) but ACTH and pituitary extract did not improve signs and symptoms associated with DD[192, 239] and hormone testing was normal in other cases[210, 240]. If hypercholesterolemia is present, severe and generalized vascular disease may be found[241].

DD treatment recommendations

Primary recommendations

1) Exercise: Similar to lipedema. Supporting the use of WBV as exercise in DD, WBV slowed the acquisition of fat in female rats[242] and improved pain and fatigue in women with fibromyalgia[243].

2) LDT: LDT[220] and "massage"[225] are known to be beneficial for DD Types I and II; recommendations are similar to lipedema (see above).

3) Pain control: Must be individually optimized; only published or important anecdotal reports are included here:

(a) Chemotherapy: A patient with DD had improved pain and growth of DD SAT slowed on methotrexate combined with infliximab[244]. One case had resolution of her lipomas and pain with paclitaxel and carboplatin (unpublished); once the paclitaxel was discontinued because of neuropathy, the pain and lumps returned.

(b) Cyclic Variations in Adaptive Conditioning (CVAC™): A novel therapy that reduces tissue fluid by variable patterning of different atmospheric pressures around a person sitting in an altitude simulator. Peri-corporal pressure patterns vary from sea level to four sequential altitude levels: 3200 m (10.5K ft), 4419 m (14.5K ft), 5638 m (18.5K ft), and 6858 m (22.5K ft). This 'body conditioning' reduced fluid and pain in 10 DD participants[245] and improved VO_2max in healthy men[246].

(c) Lidocaine: Intravenous (IV) lidocaine has been used with some success to treat the intractable pain associated with DD[217, 247–253]. Many individuals with DD obtain good local pain relief using lidocaine patches, cream, gel or EMLA[248, 254].

(d) Mexilitene: Mexilitene (an antiarrhythmic drug) has been used for the effective treatment of pain in DD[196].

(e) Pregabalin: LDT combined with pregabalin (an anticonvulsant drug used for neuropathic pain) has been used to treat the pain associated with DD[220].

4) Psychological support: See lipedema (above).

5) Surgery: Liposuction is one of the accepted methods of treatment for DD[196, 255–257] resulting in decreased pain[258, 259]. When asked specifically about liposuction in a series of 110 patients, 83 respondents (75.5%) reported having had liposuction; of these, 50.6% reported that the painful fat depots grew back[188]. Surgical resection and liposuction should be preceded by LDT and compression to support all vasculature and decrease the risk of seroma and hematoma formation. DD may be one reason why RYGBP without LDT failed to result in weight loss in a published case[260].

Additional recommendations

6) Aminoacetic acid (glycine) and prostigmine: In three women with DD, a diet consisting of 70 grams protein, 70 grams of fat and 100 grams carbohydrate or 1500 calories/day (specifics unavailable), 10 grams glycine and 45 mg prostigmine daily improved weight loss and energy[261]. If glycine binding in the central nervous system is antagonized, feeding in rats increased[262]; glycine may therefore be an appetite suppressant while prostigmine improves asthenia.

7) Corticosteroids (oral): Cortisone treatment has been shown to help with pain but with none of the other features of DD[263]; cortisone treatment can also induce DD[264]. A series of corticosteroid joint injections is usually well-tolerated without exacerbation of symptoms and signs in DD.

8) Hormonal testing: Testing for thyroid function and assessing a complete panel of pituitary hormones at least once after diagnosis of DD and when symptoms change is prudent so as not to miss accompanying hormonal dysfunction, which should be treated with usual methods. Adipose tissue is a very hormonally responsive tissue[265], so estrogen, progesterone and testosterone levels should be monitored regularly on any replacement regimen so as to regulate high and low levels and avoid wide fluctuations.

9) Lifestyle: While obesity is prominent in DD, the DD SAT is resistant to loss with lifestyle changes[261, 266] while normal SAT as part of obesity can be lost[261].

10) Oxygen therapy: Many people with DD feel short of breath[188]. This can progress on to the need for continuous oxygen therapy. It is unclear why the shortness of breath occurs but it is likely a combination of increased interstitial fluid moving cells away from their oxygen source and a weakened diaphragm. Pulmonary function testing should be performed on everyone with DD that has shortness of breath even if it serves simply as a baseline for future changes or symptoms. Similar to MSL, if a patient has increased thickened fat around the chest or neuropathy, DD patients with shortness of breath and/or edema should be evaluated for thoracic outlet syndrome, sleep apnea and/or autonomic dysfunction.

Co-morbidities associated with obesity in DD are treated as usual.

Conclusions

Obesity is very common and in the limited time allotted to patient care, it may be easy to misdiagnose a patient with a lipodystrophy or a RAD disorder as having simple obesity, and prescribe lifestyle changes only. The widespread increase in abnormal SAT in MSL, DD or lipedema Type II or III can easily masquerade as global obesity (Table 3). The loss of normal fat and muscle in MSL or the disproportion of fat in lipedema can also be confused with lipodystrophy; lipedema Type I is usually overlooked. Lifestyle changes and bariatric surgery work effectively for the obesity component of FPLD and RADs but not for the abnormal SAT tissue in RADs. The RAD SAT likely results from the growth of a brown stem cell population that secondarily compresses lymphatics and vessels (in MSL) or a primarily vascular and lymphatic dysfunction with secondary growth of SAT (in lipedema and DD), neither of which respond well to caloric limitation. Academic testing of various dietary regimens, mechanical treatments, surgery, medications, and supplements is needed for RADs. Understanding the genomics of the RADs is also important to help differentiate lipedema, MSL and DD especially in women where the three disorders can look so much alike, and to assess for RADs in obesity. Improved recognition of RADs may also prove that lipedema and DD are not RADs at all but common disorders and that understanding the underlying pathophysiology of RADs may improve our understanding of refractory obesity. Lymphatic drainage methods used for RADs should be considered in resistant obesity cases or before bariatric surgery, low to very low calorie diets or other methods that induce rapid weight loss requiring optimal lymphatic function.

Acknowledgements

This study received research support from the UCSD NIDDK Diabetes and Endocrinology Research Center Grant P30 DK063491 and the UCSD General Clinical Research Center by Public Health Grant 5M01RR000827. This paper is dedicated to people with RADs and to Birgher Fagher, MD, who died in April of 2011.

Conflicts of interest

This study was approved by the University of California, San

Table 3. Comparison of RAD characteristics.

Characteristic	MSL	RADs DD	Lipedema
Abnormal SAT location	Upper*	Global	Legs±Arms
Diet-resistant SAT	Yes	Yes	Yes
Lipomas	Common in males	Common	Large nodular fat masses
Time of SAT change	Adult	Child to adult	Puberty; by third decade
Painful SAT	Not usually	Yes	Yes
Sex predominance	Male	Female	Female
Lymphatic dysfunction	Secondary	Primary	Primary
Look-alike conditions	Obesity; HIV lipodystrophy	Obesity; FML	Obesity; APL
Associated conditions	Neuropathy	Autoimmune; diabetes	Lymphedema
Population frequency	Rare	Likely common	Likely common
Inheritance pattern	Autosomal dominant or recessive	Autosomal dominant; sex-specific influence	Autosomal dominant; incomplete penetrance
Known gene	tRNALys mutations uncommon	None	None
Known biomarkers	No	No	No
Alcohol association	Yes	No	No

* Can be global especially in women; APL=acquired partial lipodystrophy; FML=familial multiple lipomatosis; RAD=rare adipose disorder; SAT=subcutaneous adipose tissue

Diego Human Research Protection Program and the Research and Development Committee at the Veterans Affairs San Diego Healthcare System. All subjects described herein completed an informed consent process prior to enrollment.

References

1 Ogden CL, Carroll MD. Prevalence of overweight, obesity, and extreme obesity among adults: united states, trends 1960–1962 through 2007–2008. http://www.cdc.gov/nchs/fastats/overwt.htm.
2 Orsi CM, Hale DE, Lynch JL. Pediatric obesity epidemiology. Curr Opin Endocrinol Diabetes Obes 2011; 18: 14–22.
3 James WP, Caterson ID, Coutinho W, Finer N, Van Gaal LF, Maggioni AP, *et al*. Effect of sibutramine on cardiovascular outcomes in overweight and obese subjects. N Engl J Med 2010; 363: 905–17.
4 Sam AH, Salem V, Ghatei MA. Rimonabant: From RIO to Ban. J Obes 2011; 2011: 432607.
5 Bobowicz M, Lehmann A, Orlowski M, Lech P, Michalik M. Preliminary outcomes 1 year after laparoscopic sleeve gastrectomy based on bariatric analysis and reporting outcome system (BAROS). Obes Surg 2011: 15.
6 Butner KL, Nickols-Richardson SM, Clark SF, Ramp WK, Herbert WG. A review of weight loss following Roux-en-Y gastric bypass vs restrictive bariatric surgery: impact on adiponectin and insulin. Obes Surg 2010; 20: 559–68.
7 Ray JB, Ray S. Safety, efficacy, and durability of laparoscopic adjustable gastric banding in a single surgeon U.S. community practice. Surg Obes Relat Dis 2011; 7: 140–4.
8 D'Hondt M, Vanneste S, Pottel H, Devriendt D, Van Rooy F, Vansteenkiste F. Laparoscopic sleeve gastrectomy as a single-stage procedure for the treatment of morbid obesity and the resulting quality of life, resolution of comorbidities, food tolerance, and 6-year weight loss. Surg Endosc 2011; 25: 2498–504.
9 Engelson ES. HIV lipodystrophy diagnosis and management. Body composition and metabolic alterations: diagnosis and management. AIDS Read 2003; 13: S10–14.
10 Lo JC, Mulligan K, Tai VW, Algren H, Schambelan M. "Buffalo hump" in men with HIV-1 infection. Lancet 1998; 351: 867–70.
11 Grunfeld C, Rimland D, Gibert CL, Powderly WG, Sidney S, Shlipak MG, *et al*. Association of upper trunk and visceral adipose tissue volume with insulin resistance in control and HIV-infected subjects in the FRAM study. J Acquir Immune Defic Syndr 2007; 46: 283–90.
12 Mallon PW, Wand H, Law M, Miller J, Cooper DA, Carr A. Buffalo hump seen in HIV-associated lipodystrophy is associated with hyperinsulinemia but not dyslipidemia. J Acquir Immune Defic Syndr 2005; 38: 156–62.
13 Tierney EP, Hanke CW. "Bullfrog neck," a unique morphologic trait in HIV lipodystrophy: case series and review of the literature. Arch Dermatol 1279; 146: 1279–82.
14 Albu JB, Kenya S, He Q, Wainwright M, Berk ES, Heshka S, *et al*. Independent associations of insulin resistance with high whole-body intermuscular and low leg subcutaneous adipose tissue distribution in obese HIV-infected women. Am J Clin Nutr 2007; 86: 100–6.
15 Andany N, Raboud JM, Walmsley S, Diong C, Rourke SB, Rueda S, *et al*. Ethnicity and gender differences in lipodystrophy of HIV-positive individuals taking antiretroviral therapy in Ontario, Canada. HIV Clin Trials 2011; 12: 89–103.
16 Abrams H, Herbst KL. Novel liposuction techniques for the treatment of HIV-associated dorsocervical fat pad and parotid hypertrophy. In: Serdev N, ed. Advanced techniques in liposuction and fat transfer. Vol In press. Rijeka, Croatia: InTech; 2011.
17 Falutz J, Potvin D, Mamputu JC, Assaad H, Zoltowska M, Michaud SE, *et al*. Effects of tesamorelin, a growth hormone-releasing factor, in HIV-infected patients with abdominal fat accumulation: a randomized placebo-controlled trial with a safety extension. J Acquir Immune Defic Syndr 2011; 53: 311–22.
18 Oriot P, Hermans MP, Selvais P, Buysschaert M, de la Tribonniere X. Exenatide improves weight loss insulin sensitivity and beta-cell function following administration to a type 2 diabetic HIV patient on antiretroviral therapy. Ann Endocrinol 1016; 72: 244–6.
19 Garg A. Lipodystrophies: genetic and acquired body fat disorders. J Clin Endocrinol Metab 2011; 96: 3313–25.
20 Kurugol Z, Ulger Z, Berk O, Tugral O. Acquired partial lipodystrophy associated with varicella. Turk J Pediatr 2009; 51: 617–20.
21 Walker UA, Kirschfink M, Peter HH. Improvement of acquired partial lipodystrophy with rosiglitazone despite ongoing complement activation. Rheumatology 2003; 42: 393–4.
22 Herbst KL, Tannock LR, Deeb SS, Purnell JQ, Brunzell JD, Chait A. Kobberling type of familial partial lipodystrophy: an underrecognized syndrome. Diabetes Care 2003; 26: 1819–24.
23 Utzschneider KM, Trence DL. Effectiveness of gastric bypass surgery in a patient with familial partial lipodystrophy. Diabetes Care 2006; 29: 1380–2.
24 Donadille B, Lascols O, Capeau J, Vigouroux C. Etiological investigations in apparent type 2 diabetes: when to search for lamin A/C mutations? Diabetes Metab 2005; 31: 527–32.
25 Decaudain A, Vantyghem MC, Guerci B, Hécart AC, Auclair M, Reznik Y, *et al*. New metabolic phenotypes in laminopathies: LMNA mutations in patients with severe metabolic syndrome. J Clin Endocrinol Metab 2007; 92: 4835–44.
26 Chong AY, Lupsa BC, Cochran EK, Gorden P. Efficacy of leptin therapy in the different forms of human lipodystrophy. Diabetologia 2009; 53: 27–35.
27 McGrath NM, Krishna G. Gastric bypass for insulin resistance due to lipodystrophy. Obes Surg 2006; 16: 1542–4.
28 Ludtke A, Buettner J, Wu W, Muchir A, Schroeter A, Zinn-Justin S, *et al*. Peroxisome proliferator-activated receptor-gamma C190S mutation causes partial lipodystrophy. J Clin Endocrinol Metab 2007; 92: 2248–55.
29 Jeninga EH, van Beekum O, van Dijk AD, Hamers N, Hendriks-Stegeman BI, Bonvin AM, *et al*. Impaired peroxisome proliferator-activated receptor gamma function through mutation of a conserved salt bridge (R425C) in familial partial lipodystrophy. Mol Endocrinol 2007; 21: 1049–65.
30 Ludtke A, Buettner J, Schmidt HH, Worman HJ. New PPARG mutation leads to lipodystrophy and loss of protein function that is partially restored by a synthetic ligand. J Med Genet 2007; 44: e88.
31 Iwanishi M, Ebihara K, Kusakabe T, Chen W, Ito J, Masuzaki H, *et al*. Clinical characteristics and efficacy of pioglitazone in a Japanese diabetic patient with an unusual type of familial partial lipodystrophy. Metabolism 2009; 58: 1681–7.
32 Brodie B. Lectures illustrative of various subjects in pathology and surgery. London, Longman; 1846.
33 Madelung O. Uber den Fetthals. Langenbecks Archiv Klin Chirurg 1888; 37: 106.
34 Lanois P, F FB. L'ade´nolipomatose symmetrique. Bull Soc me´d Hop Paris 1898; 1: 289.
35 Enzi G, Biondetti PR, Fiore D, Mazzoleni F. Computed tomography of deep fat masses in multiple symmetrical lipomatosis. Radiology 1982; 144: 121–4.
36 Enzi G, Busetto L, Ceschin E, Coin A, Digito M, Pigozzo S. Multiple symmetric lipomatosis: clinical aspects and outcome in a long-term

longitudinal study. Int J Obes Relat Metab Disord 2002; 26: 253–61.
37 Harsch IA, Michaeli P, Hahn EG, Ficker JH, Konturek PC. Launois-Bensaude syndrome in a female with type 2 diabetes. Med Sci Monit 2003; 9: CS5–8.
38 Nielsen S, Levine J, Clay R, Jensen MD. Adipose tissue metabolism in benign symmetric lipomatosis. J Clin Endocrinol Metab 2001; 86: 2717–20.
39 Kratz C, Lenard HG, Ruzicka T, Gartner J. Multiple symmetric lipomatosis: an unusual cause of childhood obesity and mental retardation. Eur J Paediatr Neurol 2000; 4: 63–7.
40 Nounla J, Rolle U, Grafe G, Kraling K. Benign symmetric lipomatosis with myelomeningocele in an adolescent: an uncommon association-case report. J Pediatr Surg 2001; 36: E13.
41 Busetto L, Strater D, Enzi G, Coin A, Sergi G, Inelmen EM, *et al*. Differential clinical expression of multiple symmetric lipomatosis in men and women. Int J Obes Relat Metab Disord 2003; 27: 1419–22.
42 Herpertz U. Das lipödem. Lymphologie 1995; 19: 1–11.
43 Donhauser G, Vieluf D, Ruzicka T, Braun-Falco O. Benign symmetric Launois-Bensaude type III lipomatosis and Bureau-Barriere syndrome. Hautarzt 1991; 42: 311–4.
44 Ettl T, Gaumann A, Ehrenberg R, Reichert TE, Driemel O. Encapsulated lipomas of the tongue in benign symmetric lipomatosis. J Dtsch Dermatol Ges 2009; 7: 441–4.
45 Lopez-Ceres A, Aguilar-Lizarralde Y, Villalobos Sanchez A, Prieto Sanchez E, Valiente Alvarez A. Benign symmetric lipomatosis of the tongue in Madelung's disease. J Craniomaxillofac Surg 2006; 34: 489–93.
46 Birnholz JC, Macmillan AS Jr. Advanced laryngeal compression due to diffuse, symmetric lipomatosis (Madelung's disease). Br J Radiol 1973; 46: 245–9.
47 Laure B, Sury F, Tayeb T, Corre P, Goga D. Launois-Bensaude syndrome involving the orbits. J Craniomaxillofac Surg 2011; 39: 21–3.
48 Enzi G. Multiple symmetric lipomatosis: an updated clinical report. Medicine (Baltimore) 1984; 63: 56–64.
49 Kodish ME, Alsever RN, Block MB. Benign symmetric lipomatosis: functional sympathetic denervation of adipose tissue and possible hypertrophy of brown fat. Metabolism 1974; 23: 937–45.
50 Klopstock T, Naumann M, Seibel P, Shalke B, Reiners K, Reichmann H. Mitochondrial DNA mutations in multiple symmetric lipomatosis. Mol Cell Biochem 1997; 174: 271–5.
51 Carr A, Miller J, Law M, Cooper DA. A syndrome of lipoatrophy, lactic acidaemia and liver dysfunction associated with HIV nucleoside analogue therapy: contribution to protease inhibitor-related lipodystrophy syndrome. AIDS 2000; 14: F25–32.
52 Heath KV, Hogg RS, Chan KJ, Harris M, Montessori V, O'Shaughnessy MV, *et al*. Lipodystrophy-associated morphological, cholesterol and triglyceride abnormalities in a population-based HIV/AIDS treatment database. AIDS 2001; 15: 231–9.
53 Urso R, Gentile M. Are 'buffalo hump' syndrome, Madelung's disease and multiple symmetrical lipomatosis variants of the same dysmetabolism? Aids 2001; 15: 290–1.
54 Poggi G, Moro G, Teragni C, Delmonte A, Saini G, Bernardo G. Scrotal involvement in Madelung disease: clinical, ultrasound and MR findings. Abdom Imaging 2006; 31: 503–5.
55 Yamamoto K, Ichimiya M, Hamamoto Y, Muto M. Benign symmetrical lipomatosis of the hands. J Dermatol 2000; 27: 748–9.
56 Klopstock T, Naumann M, Schalke B, Bischof F, Seibel P, Kottlors M, *et al*. Multiple symmetric lipomatosis: abnormalities in complex IV and multiple deletions in mitochondrial DNA. Neurology 1994; 44: 862–6.
57 Berkovic SF, Andermann F, Shoubridge EA, Carpenter S, Robitaille Y, Andermann E, *et al*. Mitochondrial dysfunction in multiple symmetrical lipomatosis. Ann Neurol 1991; 29: 566–9.
58 Chalk CH, Mills KR, Jacobs JM, Donaghy M. Familial multiple symmetric lipomatosis with peripheral neuropathy. Neurology 1990; 40: 1246–50.
59 Enzi G, Favaretto L, Martini S, Fellin R, Baritussio A, Baggio G, *et al*. Metabolic abnormalities in multiple symmetric lipomatosis: elevated lipoprotein lipase activity in adipose tissue with hyper-alphalipoproteinemia. J Lipid Res 1983; 24: 566–74.
60 Zancanaro C, Sbarbati A, Morroni M, Carraro R, Cigolini M, Enzi G, *et al*. Multiple symmetric lipomatosis. Ultrastructural investigation of the tissue and preadipocytes in primary culture. Lab Invest 1990; 63: 253–8.
61 Nisoli E, Regianini L, Briscini L, *et al*. Multiple symmetric lipomatosis may be the consequence of defective noradrenergic modulation of proliferation and differentiation of brown fat cells. J Pathol 2002; 198: 378–87.
62 Rial E, Nicholls DG. The mitochondrial uncoupling protein from guinea-pig brown adipose tissue. Synchronous increase in structural and functional parameters during cold-adaptation. Biochem J 1984; 222: 685–93.
63 Hany T, Gharehpapagh E, Kamel E, Buck A, Himms-Hagen J, von Schulthess G. Brown adipose tissue: a factor to consider in symmetrical tracer uptake in the neck and upper chest region. Eur J Nuclear Med Mol Imaging 2002; 29: 1393–8.
64 Seemayer TA, Knaack J, Wang NS, Ahmed MN. On the ultrastructure of hibernoma. Cancer 1975; 36: 1785–93.
65 Krief S, Lonnqvist F, Raimbault S, Baude B, Van Spronsen A, Arner P, *et al*. Tissue distribution of beta 3-adrenergic receptor mRNA in man. J Clin Invest 1993; 91: 344–9.
66 Oberkofler H, Dallinger G, Liu YM, Hell E, Krempler F, Patsch W. Uncoupling protein gene: quantification of expression levels in adipose tissues of obese and non-obese humans. J Lipid Res 1997; 38: 2125–33.
67 Morelli F, De Benedetto A, Toto P, Tulli A, Feliciani C. Alcoholism as a trigger of multiple symmetric lipomatosis? J Eur Acad Dermatol Venereol 2003; 17: 367–9.
68 Dwells AR, Plans AB, Sarasura JG. Cervical Lipomatosis. Manual de Cirugia Plastica. Vol 39: Sociedad de Espanola de Cirugia; 2000.
69 Cinti S, Enzi G, Cigolini M, Bosello O. Ultrastructural features of cultured mature adipocyte precursors from adipose tissue in multiple symmetric lipomatosis. Ultrastruct Pathol 1983; 5: 145–52.
70 Vila MR, Gamez J, Solano A, Playán A, Schwartz S, Santorelli FM, *et al*. Uncoupling protein-1 mRNA expression in lipomas from patients bearing pathogenic mitochondrial DNA mutations. Biochem Biophys Res Commun 2000; 278: 800–2.
71 Kazumi T, Ricquier D, Maeda T, Masuda T, Hozumi T, Ishida Y, *et al*. Failure to detect brown adipose tissue uncoupling protein mRNA in benign symmetric lipomatosis (Madelung's disease). Endocr J 1994; 41: 315–8.
72 Coin A, Sergi G, Enzi G, Busetto L, Pigozzo S, Lupoli L, *et al*. Total and regional body composition and energy expenditure in multiple symmetric lipomatosis. Clin Nutr 2005; 24: 367–74.
73 Dorigo P, Prosdocimi M, Carpenedo F, Caparrotta L, Tessari F, Enzi G. Multiple symmetric lipomatosis. A defect in adrenergic stimulated lipolysis II. Pharmacol Res Commun 1980; 12: 625–38.
74 Enzi G, Inelmen EM, Baritussio A, Dorigo P, Prosdocimi M, Mazzoleni F. Multiple symmetric lipomatosis: a defect in adrenergic-stimulated lipolysis. J Clin Invest 1977; 60: 1221–9.
75 Desai KS, Zinman B, Steiner G. Multiple symmetric lipomatosis

(Launois-Bensaude syndrome) - adipose tissue insensitivity to cyclic AMP. J Clin Endocrinol Metab 1979; 49: 307–9.
76 Kather H, Schroder F. Adrenergic regulation of fat-cell lipolysis in multiple symmetric lipomatosis. Eur J Clin Invest 1982; 12: 471–4.
77 Pecquery R, Malagrida L, Giudicelli Y. Adipocyte adenylate cyclase and alpha- and beta-adrenergic receptors in one case of multiple symmetric lipomatosis. Biomedicine 1980; 33: 64–6.
78 Bechara FG, Sand M, Sand D, Rotterdam S, Stücker M, Altmeyer P, *et al*. Lipolysis of lipomas in patients with familial multiple lipomatosis: an ultrasonography-controlled trial. J Cutan Med Surg 2006; 10: 155–9.
79 Mogilevskii IL, Osmolovskaia NN, Deputovich SA. Microcirculatory disorders of the arm in post-mastectomy edema. Sov Med 1989: 15–20.
80 Brorson H, Ohlin K, Olsson G, Svensson B, Svensson H. Controlled compression and liposuction treatment for lower extremity lymphedema. Lymphology 2008; 41: 52–63.
81 Garcia Hidalgo L. Dermatological complications of obesity. Am J Clin Dermatol 2002; 3: 497–506.
82 Suga H, Eto H, Aoi N, Kato H, Araki J, Doi K, *et al*. Adipose tissue remodeling under ischemia: death of adipocytes and activation of stem/progenitor cells. Plast Reconstr Surg 2010; 126: 1911–23.
83 Becker ST, Wiltfang J, Klapper W, Repp R, Sinis N, Warnke PH. Massive swelling of the cervical region: an uncommon manifestation of B cell chronic lymphocytic leukemia. Oral Maxillofac Surg 2008; 12: 205–8.
84 Dwyer TM, Mizelle HL, Cockrell K, Buhner P. Renal sinus lipomatosis and body composition in hypertensive, obese rabbits. Int J Obes Relat Metab Disord 1995; 19: 869–74.
85 Vasileiou AM, Bull R, Kitou D, Alexiadou K, Garvie NJ, Coppack SW. Oedema in obesity; role of structural lymphatic abnormalities. Int J Obes (London) 2011; 35: 1247–50.
86. Pollock M, Nicholson GI, Nukada H, Cameron S, Frankish P. Neuropathy in multiple symmetric lipomatosis. Madelung's disease. Brain 1988; 111: 1157–71.
87 Chen XM, Li WY, Ni DF, Wei BJ, Xu CX, Gao ZQ, *et al*. Diagnosis and treatment of Madelung's disease. Zhonghua Er Bi Yan Hou Tou Jing Wai Ke Za Zhi 2006; 41: 524–7.
88 Tizian C, Berger A, Vykoupil KF. Malignant degeneration in Madelung's disease (benign lipomatosis of the neck): case report. Br J Plast Surg 1983; 36: 187–9.
89 Taylor LM, Beahrs OH, Fontana RS. Benign symmetric lipomatosis. Proc Staff Meet Mayo Clin 1961; 36: 96–100.
90 Uglesic V, Knezevic P, Milic M, Jokic D, Kosutic D. Madelung syndrome (benign lipomatosis): clinical course and treatment. Scand J Plast Reconstr Surg Hand Surg 2004; 38: 240–3.
91 Fedele D, Bellavere F, Bosello G, Cardone C, Girardello L, Ferri M, *et al*. Impairment of cardiovascular autonomic reflexes in multiple symmetric lipomatosis. J Auton Nerv Syst 1984; 11: 181–8.
92 Lee HW, Kim TH, Cho JW, Ryu BY, Kim HK, Choi CS. Multiple symmetric lipomatosis: Korean experience. Dermatol Surg 2003; 29: 235–40.
93 Foldi M, Foldi E. Benign symmetric lipomatosis. In: Foldi M, Foldi E, Strossenreyther R, S K, eds. Földi's textbook of lymphology Germany: Elsevier, Urban & Fischer Verlag; 2007; p 430–31.
94 Guilemany JM, Romero E, Blanch JL. An aesthetic deformity: Madelung's disease. Acta Otolaryngol 2005; 125: 328–30.
95 Gonzalez-Garcia R, Rodriguez-Campo FJ, Sastre-Perez J, Munoz-Guerra MF. Benign symmetric lipomatosis (Madelung's disease): case reports and current management. Aesthetic Plast Surg 2004; 28: 108–12; discussion 113.
96 Verhelle NA, Nizet JL, Van den Hof B, Guelinckx P, Heymans O. Liposuction in benign symmetric lipomatosis: sense or senseless? Aesthetic Plast Surg 2003; 27: 319–21.
97 Martinez-Escribano JA, Gonzalez R, Quecedo E, Febrer I. Efficacy of lipectomy and liposuction in the treatment of multiple symmetric lipomatosis. Int J Dermatol 1999; 38: 551–4.
98 Faga A, Valdatta LA, Thione A, Buoro M. Ultrasound assisted liposuction for the palliative treatment of Madelung's disease: a case report. Aesthetic Plast Surg 2001; 25: 181–3.
99 Horl C, Biemer E. Benign symmetrical lipomatosis. Lipectomy and liposuction in the treatment of Madelung disease. Handchir Mikrochir Plast Chir 1992; 24: 93–6.
100 Smith PD, Stadelmann WK, Wassermann RJ, Kearney RE. Benign symmetric lipomatosis (Madelung's disease). Ann Plast Surg 1998; 41: 671–3.
101 Constantinidis J, Steinhart H, Zenk J, Bohlender J, Iro H. Surgical therapy of Madelung's disease in the head and neck area. HNO 2003; 51: 216–20.
102 Leung NW, Gaer J, Beggs D, Kark AE, Holloway B, Peters TJ. Multiple symmetric lipomatosis (Launois-Bensaude syndrome): effect of oral salbutamol. Clin Endocrinol (Oxf) 1987; 27: 601–6.
103 Zeitler H, Ulrich-Merzenich G, Richter DF, Vetter H, Walger P. Multiple benign symmetric lipomatosis — a differential diagnosis of obesity. Is there a rationale for fibrate treatment? Obes Surg 2008; 18: 1354–6.
104 Mirouze J, Orsetti A, Vidal F. Application of 2 radioimmunological methods for the determination of growth hormone. Application to various dysmorphic syndromes. Ann Endocrinol (Paris) 1970; 31: 237–46.
105 Harsch IA, Wiedmann R, Bergmann T, Hahn EG, Wiest GH. Unspecified gain of weight? Internist (Berl) 2005; 46: 1265–9.
106 Botwin KP, Sakalkale DP. Epidural steroid injections in the treatment of symptomatic lumbar spinal stenosis associated with epidural lipomatosis. Am J Phys Med Rehabil 2004; 83: 926–30.
107 McCullen GM, Spurling GR, Webster JS. Epidural lipomatosis complicating lumbar steroid injections. J Spinal Disord 1999; 12: 526–9.
108 Taille C, Fartoukh M, Houel R, Kobeiter H, Remy P, Lemaire F. Spontaneous hemomediastinum complicating steroid-induced mediastinal lipomatosis. Chest 2001; 120: 311–3.
109 Fischer M, Wohlrab J, Taube KM, Marsch WC. Intralesional injection of enoxaparin in benign symmetrical lipomatosis: an alternative to surgery? Br J Dermatol 2001; 144: 629–30.
110 Rotunda AM, Ablon G, Kolodney MS. Lipomas treated with subcutaneous deoxycholate injections. J Am Acad Dermatol 2005; 53: 973–8.
111 Allen EV, Hines EAJ. Lipedema of the legs:A syndrome characterised by fat legs and orthostatic edema. Proc Staff Meet Mayo Clin 1940; 15: 184–7.
112 Fife CE, Maus EA, Carter MJ. Lipedema: a frequently misdiagnosed and misunderstood fatty deposition syndrome. Adv Skin Wound Care 2010; 23: 81–92; 93–84.
113 Dimakakos PB, Stefanopoulos T, Antoniades P, Antoniou A, Gouliamos A, Rizos D. MRI and ultrasonographic findings in the investigation of lymphedema and lipedema. Int Surg 1997; 82: 411–6.
114 Wold LE, Hines EA Jr, Allen EV. Lipedema of the legs; a syndrome characterized by fat legs and edema. Ann Intern Med 1951; 34: 1243–50.
115 Child AH, Gordon KD, Sharpe P, Brice G, Ostergaard P, Jeffery S, *et al*. Lipedema: an inherited condition. Am J Med Genet A 2010; 152A: 970–6.

116 Foldi E, Foldi M. Lipedema. In: Foldi M, Foldi E, eds. Foldi's Textbook of Lymphology. Munich (Germany): Elsevier GmbH; 2006. p417–27.
117 Chen SG, Hsu SD, Chen TM, Wang HJ. Painful fat syndrome in a male patient. Br J Plast Surg 2004; 57: 282–6.
118 Schmeller W, Meier-Vollrath I. Lipödem-aktuelles zu einem weitgehend unbekannter Krankheitsbild. Aktuelle Dermatologie 2007; 33: 1–10.
119 Meier-Vollrath I, Schneider W, Schmeller W. Das Lipodem: neue Möglichkeiten der Therapie. Schweiz Med Forum 2007; 7: 150–5.
120 Meier-Vollrath I, Schmeller W. Lipoedema — current status, new perspectives. J Dtsch Dermatol Ges 2004; 2: 181–6.
121 Pascucci A, Lynch PJ. Lipedema with multiple lipomas. Dermatol Online J 16(9): 4.
122 Cornely ME. Lipedema and Lymphatic Edema. In: Shiffman MA, Di Giuseppe A, eds. Liposuction. Berlin Heidelberg: Springer; 2006: 10–4.
123 Greer KE. Lipedema of the legs. Cutis 1974; 14: 98.
124 Földi E, Földi M. Das Lipödem. In: Földi M, Földi E, Kubik S, eds. Lehrbuch der Lymphologie für Mediziner, Masseure und Physiotherapeuten. Munich: Elsevier, Urban & Fischer; 2005; p 443–53.
125 Stallworth JM, Hennigar GR, Jonsson HT Jr, Rodriguez O. The chronically swollen painful extremity. A detailed study for possible etiological factors. JAMA 1974; 228: 1656–9.
126 Curri SB, Merlen JF. Microvascular disorders of adipose tissue. J Mal Vasc 1986; 11: 303–9.
127 Merlen JF, Curri SB, Sarteel AM. Cellulitis, a conjunctive microvascular disease. Phlebologie 1979; 32: 279–82.
128 Suga H, Araki J, Aoi N, Kato H, Higashino T, Yoshimura K. Adipose tissue remodeling in lipedema: adipocyte death and concurrent regeneration. J Cutan Pathol 2009; 3: 3.
129 Cinti S, Mitchell G, Barbatelli G, Murano I, Ceresi E, Faloia E, *et al*. Adipocyte death defines macrophage localization and function in adipose tissue of obese mice and humans. J Lipid Res 2005; 46: 2347–55.
130 Kaiserling E. Morphological changes in lymphedema and tumors. In: Foldi M, Foldi E, eds. Foldi's Textboof of Lymphology. Munich (Germany): Elsevier, GmbH; 2006: 322–90.
131 Kligman AM. Cellulite: facts and fiction. J Geriatric Dermatol 1997; 5: 136–9.
132 Jagtman BA, Kuiper JP, Brakkee AJ. Measurements of skin elasticity in patients with lipedema of the Moncorps "rusticanus" type. Phlebologie 1984; 37: 315–9.
133 Taylor NE, Foster WC, Wick MR, Patterson JW. Tumefactive lipedema with pseudoxanthoma elasticum-like microscopic changes. J Cutan Pathol 2004; 31: 205–9.
134 Szolnoky G. Chapter 17: Differential Diagnosis - Lipedema. In: Lee BB, Bergan J, Rockson SG, eds. Lymphedema: A Concise Compendium of Theory and Practice. London: Springer-Verlag; 2011. p125–35.
135 Wienert V, Leeman S. Lipedema. Hautarzt 1991; 42: 484–6.
136 Partsch H, Stoberl C, Urbanek A, Wenzel-Hora BI. Clinical use of indirect lymphography in different forms of leg edema. Lymphology 1988; 21: 152–60.
137 Tiedjen KU, Schultz-Ehrenburg U. Isotopenlymphographische Befunde beim Lipödem. In: Holzmann H, Altmeyer P, Hör G, eds. Dermatologie und Nuklearmedizin. Berlin: Springer-Verlag; 1985. p432–438.
138 van Geest AJ, Esten SCAM, Cambier J-PRA, *et al*. Lymphatic disturbances in lipedema. Phlebologie 2003; 32: 138–42.
139 Amann-Vesti BR, Franzeck UK, Bollinger A. Microlymphatic aneurysms in patients with lipedema. Lymphology 2001; 34: 170–175.
140 Bollinger A, Amann-Vesti BR. Fluorescence microlymphography: diagnostic potential in lymphedema and basis for the measurement of lymphatic pressure and flow velocity. Lymphology 2007; 40: 52–62.
141 Harwood CA, Bull RH, Evans J, Mortimer PS. Lymphatic and venous function in lipoedema. Br J Dermatol 1996; 134: 1–6.
142 Harvey NL, Srinivasan RS, Dillard ME, Johnson NC, Witte MH, Boyd K, *et al*. Lymphatic vascular defects promoted by Prox1 haploinsufficiency cause adult-onset obesity. Nat Genet 2005; 37: 1072–81.
143 Schneider M, Conway EM, Carmeliet P. Lymph makes you fat. Nat Genet 2005; 37: 1023–4.
144 Bollinger A. Microlymphatics of human skin. Int J Microcirc Clin Exp 1993; 12: 1–15.
145 Brautigam P, Foldi E, Schaiper I, Krause T, Vanscheidt W, Moser E. Analysis of lymphatic drainage in various forms of leg edema using two compartment lymphoscinctigraphy. Lymphology 1998; 31: 43–55.
146 Bilancini S, Lucchi M, Tucci S, Eleuteri P. Functional lymphatic alterations in patients suffering from lipedema. Angiology 1995; 46: 333–9.
147 de Godoy JM, de Godoy Mde F. Treatment of cellulite based on the hypothesis of a novel physiopathology. Clin Cosmet Investig Dermatol 4: 55–9.
148 Bayrakci Tunay V, Akbayrak T, Bakar Y, Kayihan H, Ergun N. Effects of mechanical massage, manual lymphatic drainage and connective tissue manipulation techniques on fat mass in women with cellulite. J Eur Acad Dermatol Venereol 2009; 24: 138–42.
149 Wenczl E, Daroczy J. Lipedema, a barely known disease: diagnosis, associated diseases and therapy. Orv Hetil 2008; 149: 2121–7.
150 Tsukanov Iu T, Tsukanov A. Syndrome of lower limb volume enlargement in varicosity: causes and medical approaches. Angiol Sosud Khir 2007; 13: 85–91.
151 Tan IC, Maus EA, Rasmussen JC, Marshall MV, Adams KE, Fife CE, *et al*. Assessment of lymphatic contractile function after manual lymphatic drainage using near-infrared fluorescence imaging. Arch Phys Med Rehabil 1992: 756–764 e751.
152 Szolnoky G, Nagy N, Kovacs RK, Dósa-Rácz E, Szabó A, Bársony K, *et al*. Complex decongestive physiotherapy decreases capillary fragility in lipedema. Lymphology 2008; 41: 161–6.
153 Szolnoky G, Borsos B, Barsony K, Balogh M, Kemeny L. Complete decongestive physiotherapy with and without pneumatic compression for treatment of lipedema: a pilot study. Lymphology 2008; 41: 40–4.
154 Adams KE, Rasmussen JC, Darne C, Tan IC, Aldrich MB, Marshall MV, *et al*. Direct evidence of lymphatic function improvement after advanced pneumatic compression device treatment of lymphedema. Biomed Opt Express 2010; 1: 114–25.
155 Beninson J, Edelglass JW. Lipedema — the non-lymphatic masquerader. Angiology 1984; 35: 506–10.
156 Bauke J. Kritische Gegenüberstellung der verschiedenen behandlungsmethoden der adipositas. Med Welt 1983; 34: 201–3.
157 Hines EA Jr. Lipedema and physiologic edema. Proc Staff Meet Mayo Clin 1952; 27: 7–9.
158 Tidhar D, Katz-Leurer M. Aqua lymphatic therapy in women who suffer from breast cancer treatment-related lymphedema: a randomized controlled study. Support Care Cancer 2009; 18: 383–92.
159 Lohman EB 3rd, Petrofsky JS, Maloney-Hinds C, Betts-Schwab H,

Thorpe D. The effect of whole body vibration on lower extremity skin blood flow in normal subjects. Med Sci Monit 2007; 13: CR71–76.
160 Kerschan-Schindl K, Grampp S, Henk C, Resch H, Preisinger E, Fialka-Moser V, *et al*. Whole-body vibration exercise leads to alterations in muscle blood volume. Clin Physiol 2001; 21: 377–82.
161 Stewart JM, Karman C, Montgomery LD, McLeod KJ. Plantar vibration improves leg fluid flow in perimenopausal women. Am J Physiol Regul Integr Comp Physiol 2005; 288: R623–629.
162 Gulias S, Nieto S. Psychological assistaqnce and its importance in the medical treatment of lymphedema. J Soc Phlebol Lymphol 2007; 2: 179–87.
163 Schmeller W, Meier-Vollrath I. Tumescent liposuction: a new and successful therapy for lipedema. J Cutan Med Surg 2006; 10: 7–10.
164 Warren AG, Janz BA, Borud LJ, Slavin SA. Evaluation and management of the fat leg syndrome. Plast Reconstr Surg 2007; 119: 9e–15e.
165 Ray C. Caring for the Bariatric Patient with lymphedema and obesity. Bariatrics Today 2004: 48–50.
166 Foldi E, Foldi M. Lipedema. In: Foldi M, Foldi E, Kubik S, eds. Foldi's Textbook of Lymphology. Munich (Germany): Elsevier GmbH; 2006. p 417–427.
167 Williams A. Amy's Butterfly Journey: Living My Life with Lymphedema and Obesity. Obesity Help 2004: 43–4.
168 Moore JC, Ballas ZK. A novel therapy for lymphedema. Arch Intern Med 2009; 169: 201–2.
169 Bruns F, Micke O, Bremer M. Current status of selenium and other treatments for secondary lymphedema. J Supportive Oncol 2003; 1: 121–30.
170 Sasaki H, Okumura M, Kawasaki T, Kangawa K, Matsuo H. Indomethacin and atrial natriuretic peptide in Pseudo-Bartter's syndrome. N Engl J Med 1987; 316: 167.
171 Pecking AP, Fevrier B, Wargon C, Pillion G. Efficacy of Daflon 500 mg in the treatment of lymphedema (secondary to conventional therapy of breast cancer). Angiology 1997; 48: 93–8.
172 Pecking AP. Evaluation by lymphoscintigraphy of the effect of a micronized flavonoid fraction (Daflon 500 mg) in the treatment of upper limb lymphedema. Int Angiol 1995; 14: 39–43.
173 Casley-Smith JR, Casley-Smith JR. The effects of diosmin (a benzopyrone) upon some high-protein oedemas: lung contusion, and burn and lymphoedema of rat legs. Agents Actions 1985; 17: 14–20.
174 Suter A, Bommer S, Rechner J. Treatment of patients with venous insufficiency with fresh plant horse chestnut seed extract: a review of 5 clinical studies. Adv Ther 2006; 23: 179–90.
175 Cornely ME. Lipedema and Lymphatic Edema. In: Shiffman MA, Di Giuseppe A, eds. Liposuction Principles and Practice. Berlin Heidelberg: Springer; 2006.
176 Conley SM, Bruhn RL, Morgan PV, Stamer WD. Selenium's effects on MMP-2 and TIMP-1 secretion by human trabecular meshwork cells. Invest Ophthalmol Vis Sci 2004; 45: 473–9.
177 Obenheimer H, Jankowiak P, Berlemann K, Hermann V, Diethelm A. Clinical and biological effects of selenium in edema. Paper presented at: Proceedings of the International Symposium: Lymphedema — New Perspectives in Research and Treatment. 1976; Zaragossa, Spain.
178 Schrauzer GN. Selenium in the therapy of chronic lymphedema—mechanistic perspectives and practical applications. Z Lymphol 1997; 21: 16–9.
179 Micke O, Bruns F, Schäfer U, Kisters K, Hesselmann S, Willich N. Selenium in the treatment of acute and chronic lymphedema. Trace Elements and Electrolytes 2000; 17: 206–9.
180 Horvathova M, Jahnova E, Gazdik F. Effect of selenium supplementation in asthmatic subjects on the expression of endothelial cell adhesion molecules in culture. Biol Trace Elem Res 1999; 69: 15–26.
181 Kiremidjian-Schumacher L, Roy M, Glickman R, Schneider K, Rothstein S, Cooper J, *et al*. Selenium and immunocompetence in patients with head and neck cancer. Biol Trace Elem Res 2000; 73: 97–111.
182 Siems W, Grune T, Voss P, Brenke R. Anti-fibrosclerotic effects of shock wave therapy in lipedema and cellulite. Biofactors 2005; 24: 275–82.
183 Dercum FX. Three cases of a hitherto unclassified affection resembling in its grosser aspects obesity, but associated with special nervous symptoms - adiposis dolorosa. Am J Med Sci 1892; civ: 521.
184 Dercum FX. A subcutaneous connective-tissue dystrophy of the arms and back, associated with symptoms resembling myxoedema. Univ Med Magazine Philadelphia 1888: 140–50.
185 Dercum FX. Autopsy in a case of adiposis dolorosa, with microscopical examination. J Nerv Ment Dis 1900;XXVII(8):419–29.
186 Lyon IP. Adiposis and lipomatosis: Considered in reference to their constitutional relations and symptomatology. Arch Int Med 1910; VI: 28–120.
187 Brorson H, Fagher B. Dercum's disease. Fatty tissue rheumatism caused by immune defense reaction? Lakartidningen 1996; 93: 1430; 1433–6.
188 Herbst KL, Asare-Bediako S. Adiposis Dolorosa is More than Painful Fat. The Endocrinologist 2007; 17: 326–44.
189 Walser WC. Adiposis dolorosa in an infant. Boston Med Surg J 1910; CLXII: 906–7.
190 Bruning H, Walter FK. Zur frage der Adipositas dolorosa (Dercumshe Krankheit) in Kindersalter. Ztscyhr f Kinderh 1919; 24: 183.
191 Loening K, Fuss S. Schildrusenveranderungen bei Adipositas dolorosa. Verhandl d Cong f inn Med 1906: 222.
192 Steiger WA, Litvin H, Lasche EM, Durant TM. Adiposis dolorsa (Dercum's disease). N Engl J Med 1952; 247: 393–6.
193 Vitaut L. Maladie de Dercum (adiposis dolorosa). Loire med St Etienne 1901; 20: 254.
194 Kling DH. Juxta-articular adiposis dolorosa, its significance and relation to Dercum's disease and osteo-arthritis. J Arch Surg 1937; 34: 599–630.
195 Lynch HT, Harlan WL. Hereditary factors in adiposis dolorosa (Dercum's disease). Am J Hum Genet 1963; 15: 184–90.
196 Steiner J, Schiltz K, Heidenreich F, Weissenborn K. Lipomatosis dolorosa — a frequently overlooked disease picture. Nervenarzt 2002; 73: 183–7.
197 Pack GT, Ariel IM. Tumors of the soft somatic tissues: a clinical treatise. New York: Hoeber-Harper; 1958.
198 Thimm P. Adipositas dolorosa und schmerzende symmetrische. Lipome Montash f prakt Dermatol 1903; xxxvi: 282.
199 Campen R, Mankin H, Louis DN, Hirano M, Maccollin M. Familial occurrence of adiposis dolorosa. J Am Acad Dermatol 2001; 44: 132–6.
200 Cantu JM, Ruiz-Barquin E, Jimenez M, Castillo L, Macotela-Ruiz E. Autosomal dominant inheritance in adiposis dolorosa (Dercum's disease). Humangenetik 1973; 18: 89–91.
201 Winkelman NW, Eckel JL. Adiposis dolorosa (Dercum's disease) a clinicopathologic study. J Am Med Assoc 1925; 85: 1935–9.
202 Herbst KL, Coviello AD, Chang A, Boyle DL. Lipomatosis-associated inflammation and excess collagen may contribute to lower relative resting energy expenditure in women with adiposis dolorosa. Int J Obes (Lond) 2009; 33: 1031–8.

203 Kirpilä J, Ripatti N. Adipositas dolorosa juxtaarticularis (Dercum's disease) och dess behandling [in Swedish]. Nord Med 1958; 59: 358–60.
204 Hovesen E. Adiposis dolorosa (Dercum's syndrome). Nord Med 1953; 50: 971.
205 Blomstrand R, Juhlin L, Nordenstam H, Ohlsson R, Werner B, Engstrom J. Adiposis dolorosa associated with defects of lipid metabolism. Acta Derm Venereol 1971; 51: 243–50.
206 Page IH. Chemiache Untersuchungen bel der Dercumschen Krankheit. Virchow Arch Path Anat 1930; 279: 262.
207 Mella BA. Adiposis dolorosa. Univ Michigan Med Center J 1967; 33: 79–81.
208 Held JL, Andrew JA, Kohn SR. Surgical amelioration of Dercum's disease: a report and review. J Dermatol Surg Oncol 1989; 15: 1294–6.
209 Campen RB, Sang CN, Duncan LM. Case records of the Massachusetts General Hospital. Case 25-2006. A 41-year-old woman with painful subcutaneous nodules. N Engl J Med 2006; 355: 714–22.
210 Pimenta WP, Paula FJ, Dick-de-Paula I, Piccinato CE, Monteiro CM, Brandão-Neto J, *et al*. Hormonal and metabolic study of a case of adiposis dolorosa (Dercum's disease). Braz J Med Biol Res 1992; 25: 889–93.
211 Ballet G. L'adipose, douloureuse (maladie de Dercum). Presse méd Par 1903; i: 285–8.
212 Price GE. Adiposis dolorosa: a clinical and pathological study, with the report of two cases with necropsy. Am J Med Sci 1909; 137: 705–14.
213 Eshner AA. A case of adiposis dolorosa. J Am Med Assoc 1898; XXXI: 1156–60.
214 Collins J. Adiposis dolorosa. In: Dercum FX, ed. Textbook of Nervous Diseases. Lea Brothers & Co; 1895. p 898–200.
215 Alger EM. Clinical memoranda: A case of adiposis dolorosa. Med News (1882-1905) 1901; 78: 91–2.
216 Frankenheimer JB. Adiposis dolorosa. J Am Med Assoc 1908; L: 1012–3.
217 Skagen K, Petersen P, Kastrup J, Norgaard T. The regulation of subcutaneous blood flow in patient with Dercum's disease. Acta Derm Venereol 1986; 66: 337–9.
218 Falta W. Endocrine diseases. In: Meyers MK, ed. 2 ed. Philadelphia: Blakiston's Son & Co; 1916: 575.
219 Moi L, Canu C, Pirari P, Mura MN, Piludu G, Del Giacco GS. Dercum's disease: a case report. Ann Ital Med Int 2005; 20: 187–91.
220 Lange U, Oelzner P, Uhlemann C. Dercum's disease (Lipomatosis dolorosa): successful therapy with pregabalin and manual lymphatic drainage and a current overview. Rheumatol Int 2008; 29: 17–22.
221 Pascucci A, Lynch PJ. Lipedema with multiple lipomas. Dermatol Online J 2010; 16: 4.
222 Rockson SG. The unique biology of lymphatic edema. Lymphat Res Biol 2009; 7: 97–100.
223 Spiller WG. Clinical Memoranda: Report of three cases of adiposis dolorosa. Med News 1898: 268–70.
224 Eisman J, Swezey RL. Juxta-articular adiposis dolorosa: what is it? Report of 2 cases. Ann Rheum Dis 1979; 38: 479–82.
225 White WH. A case of adiposis dolorosa. Br Med J 1899; 2: 1533–4.
226 Burr CW. A case of adiposis dolorosa with necropsy. J Nervous Mental Disease 1900; XXVII: 519–25.
227 Dercum FX, McCarthy DJ. Autopsy in a case of adiposis dolorosa. Am J Med Sci 1902; (124): 994.
228 Abu-Hijleh MF, Scothorne RJ. Studies on haemolymph nodes. IV. Comparison of the route of entry of carbon particles into parathymic nodes after intravenous and intraperitoneal injection. J Anat 1996; 188: 565–73.
229 Mills CK. A case of adeno lipomatosis: With some remarks on the differential diagnosis of the affectation from adiposis dolorosa and other diseases. J Nervous Mental Disease 1918; 36: 106–8.
230 Stolkind E. Cases of adiposis dolorosa (Dercum's disease). Proc Royal Soc Med 1923; 16 (Clinical Section): 45–7.
231 Hammond JA. An instance of adiposis dolorosa in two sisters. Br Med J 1904; 2: 121.
232 Souza-Smith FM, Kurtz KM, Molina PE, Breslin JW. Adaptation of mesenteric collecting lymphatic pump function following acute alcohol intoxication. Microcirculation 2010; 17: 514–24.
233 Dercum FX. Note on a case of adiposis dolorosa in which there was present also spasticity and contracture involving the extremities. J Nervous Mental Disease 1918; 36: 159–62.
234 Price GE, Bird JT. Adiposis dolorosa: A report of a case with increased sugar tolerance and epileptiform convulsions. J Am Med Association 1925; 84: 247–8.
235 Wortham NC, Tomlinson IP. Dercum's disease. Skinmed 2005; 4: 157-162; quiz 163–4.
236 Bergeron PN. A case of adiposis dolorosa with involvement of the large nerve trunks. J Nerv Mental Disease 1918; 36: 159.
237 Kirpila J, Ripatti N. Adiposis dolorosa juxta-articularis: Dercum's disease & its therapy. Nordisk medicin March 1958; 59: 358–60.
238 Taylor EW, Luce DS. A case of adiposis dolorosa. Boston Medical and Surgical Journal; CLIV: 187–90.
239 Myers B. Case of adiposis dolorosa. Proceedings of the Royal Society of Med 1923; 16 (Clinical Section): 12–3.
240 Palmer ED. Dercum's disease: adiposis dolorosa. Am Fam Physician 1981; 24: 155–7.
241 Szypula I, Kotulska A, Szopa M, Pieczyrak R, Kucharz EJ. Adiposis dolorosa with hypercholesterolemia and premature severe generalized atherosclerosis. Wiad Lek 2009; 62: 64–65.
242 Maddalozzo GF, Iwaniec UT, Turner RT, Rosen CJ, Widrick JJ. Whole-body vibration slows the acquisition of fat in mature female rats. Int J Obes (Lond) 2008; 32: 1348–54.
243 Alentorn-Geli E, Padilla J, Moras G, Lazaro Haro C, Fernandez-Sola J. Six weeks of whole-body vibration exercise improves pain and fatigue in women with fibromyalgia. J Altern Complement Med 2008; 14: 975–81.
244 Singal A, Janiga J, Bossenbroek N, Lim H. Dercum's disease (adiposis dolorosa): a report of improvement with infliximab and methotrexate. J Eur Acad Dermatol Venereol 2007; 21: 717.
245 Herbst KL, Rutledge T. Pilot study: rapidly cycling hypobaric pressure improves pain after 5 days in adiposis dolorosa. J Pain Res 2010; 3: 147–53.
246 Hetzler RK, Sargent RW, Kimura IK, *et al*. The effect of a cyclic variable altitude conditioning program on arterial oxygen saturation acclimation. Paper presented at: 53rd Annual Meeting, American College of Sporte Med, 2006; Denver, CO.
247 Juhlin L. Long-standing pain relief of adiposis dolorosa (Dercum's disease) after intravenous infusion of lidocaine. J Am Acad Dermatol 1986; 15: 383–5.
248 Desai MJ, Siriki R, Wang D. Treatment of pain in Dercum's disease with Lidoderm (lidocaine 5% patch): a case report. Pain Med 2008; 9: 1224–6.
249 Petersen P, Kastrup J. Dercum's disease (adiposis dolorosa). Treatment of the severe pain with intravenous lidocaine. Pain 1987; 28: 77–80.
250 Devillers AC, Oranje AP. Treatment of pain in adiposis dolorosa (Dercum's disease) with intravenous lidocaine: a case report with a

10-year follow-up. Clin Exp Dermatol 1999; 24: 240–1.
251 Atkinson RL. Intravenous lidocaine for the treatment of intractable pain of adiposis dolorosa. Int J Obes 1982; 6: 351–7.
252 Taniguchi A, Okuda H, Mishima Y, Nagata I, Oseko F, Hara M, *et al*. A case of adiposis dolorosa: lipid metabolism and hormone secretion. Int J Obes 1986; 10: 277–81.
253 Iwane T, Maruyama M, Matsuki M, Ito Y, Shimoji K. Management of intractable pain in adiposis dolorosa with intravenous administration of lidocaine. Anesth Analg 1976; 55: 257–9.
254 Reggiani M, Errani A, Staffa M, Schianchi S. Is EMLA effective in Dercum's disease? Acta Derm Venereol 1996; 76: 170–1.
255 Berntorp E, Berntorp K, Brorson H, Frick K. Liposuction in Dercum's disease: impact on haemostatic factors associated with cardiovascular disease and insulin sensitivity. J Intern Med 1998; 243: 197–201.
256 DeFranzo AJ, Hall JH Jr, Herring SM. Adiposis dolorosa (Dercum's disease): liposuction as an effective form of treatment. Plast Reconstr Surg 1990; 85: 289–92.
257 Brorson H, Aberg M, Fagher B. Liposuction in adiposis dolorosa (morbus Dercum) — an effective therapy. Ugeskr Laeger 1992; 154: 1914–5.
258 Wollina U, Goldman A, Heinig B. Microcannular tumescent liposuction in advanced lipedema and Dercum's disease. G Ital Dermatol Venereol 2010; 145: 151–9.
259 Hansson E, Svensson H, Brorson H. Liposuction may reduce pain in Dercum's disease (adiposis dolorosa). Pain Med 2011; 12: 942–52.
260 Tsang C, Aggarwal R, Bonanomi G. Dercum's disease as a cause of weight loss failure after gastric bypass surgery. Surg Obes Relat Dis 2011; 7: 243–5.
261 Wohl MG, Pastor N. Adipositas dolorosa (Dercum's disease). JAMA 1938; 110: 1261–4.
262 Sorrels TL, Bostock E. Induction of feeding by 7-chlorokynurenic acid, a strychnine-insensitive glycine binding site antagonist. Brain Res 1992; 572: 265–8.
263 Spota BB, Brage D. Cortisona Y Enfermedad de Dercum. Dia med B Air 1952; 24: 1930.
264 Greenbaum SS, Varga J. Corticosteroid-induced juxta-articular adiposis dolorosa. Arch Dermatol 1991; 127: 231–3.
265 Rebuffe-Scrive M, Lonnroth P, Marin P, Wesslau C, Bjorntorp P, Smith U. Regional adipose tissue metabolism in men and postmenopausal women. Int J Obes 1987; 11: 347–55.
266 de Médicis Sajous CE. The Internal secretions and the principles of medicine. Vol 1. 9th ed. Philadelphia: FA Davis Co; 1920.

Acta Pharmacologica Sinica (2012) 33: 173–181
 1671-4083/12 $32.00
www.nature.com/aps

Review

Laboratory animals as surrogate models of human obesity

Cecilia NILSSON[1], Kirsten RAUN[1], Fei-fei YAN[2], Marianne O LARSEN[2], Mads TANG-CHRISTENSEN[1, *]

[1]*Diabetes Research Unit, Novo Nordisk A/S and* [2]*Diabetes Research China, Beijing Novo Nordisk Pharmaceuticals Sci & Tech Co Ltd, Beijing 100020, China*

Obesity and obesity-related metabolic diseases represent a growing socioeconomic problem throughout the world. Great emphasis has been put on establishing treatments for this condition, including pharmacological intervention. However, there are many obstacles and pitfalls in the development process from pre-clinical research to the pharmacy counter, and there is no certainty that what has been observed pre-clinically will translate into an improvement in human health. Hence, it is important to test potential new drugs in a valid translational model early in their development. In the current mini-review, a number of monogenetic and polygenic models of obesity will be discussed in view of their translational character.

Keywords: obesity; animal models; sibutramine; liraglutide; KK-A^y mice; ob/ob mice; Zucker rat; diet-induced obesity models

Acta Pharmacologica Sinica (2012) 33: 173–181; doi: 10.1038/aps.2011.203

Introduction

As the prevalence of obesity is rising along with its socioeconomic consequences, the quest to find new treatments or a cure is also increasing (http://www.who.int/mediacentre/factsheets/fs311/en/). Pharmaceutical treatment is one avenue that has been pursued, but currently there are only a limited number of compounds on the market because many have failed or been withdrawn because of side effects. Given that the development process from initial idea to marketed product typically requires more than 10 years and the attrition rate is notably high, it is important that the models used, whether *in vitro* or *in vivo*, are good surrogates for human obesity. Depending on the target in question, there are a number of models that can be applied. In the following pages, we will review the most widely used animal models in obesity research. We have categorized the different models into groups; rodent models are divided into monogenetic, polygenetic, and selectively bred diet-induced obesity (DIO) models, and finally we discuss the DIO pig model. To demonstrate the translational potential of the selected models, we have chosen two different model compound families that have been tested in human cohorts — sibutramine and liraglutide or other glucagon-like peptide-1 (GLP)-1 analogues[1, 2]. Sibutramine is a serotonin and norepinephrine re-uptake inhibitor that was developed for the treatment of obesity and has been on the market for the past 9 years, although in most markets it has been withdrawn because of undesirable side effects [3]. Liraglutide is a GLP-1 analogue currently in phase 3 clinical development for severe obesity after demonstrating positive results in phase 2 trials[2]. By choosing the best suited animal model for a particular study, it is possible to make a qualified assessment as to whether target X and/or compound Y will have an impact in clinical practice at a much earlier point.

* To whom correspondence should be addressed.
E-mail MDTC@novonordisk.com
Received 2011-11-17 Accepted 2011-12-21

Monogenic models

KK-A^y mice

The inbred mouse strain KK was established in Japan and is a mouse model with peripheral insulin sensitivity and glucose intolerance[4]. Insulin resistance in the KK mouse is followed by moderate obesity[5, 6]. The occurrence of diabetes and obesity in KK mice is considered of polygenic origin. However, when the Agouti (A^y) mutation is introduced into the KK strain, the resulting KK-A^y mouse exhibits a more pronounced course of diabetes[7, 8]. The A^y gene is ubiquitously expressed in the KK-A^y mouse, and the agouti protein is thought to act as a melanocortin 4 receptor antagonist, thereby inhibiting the signals from alpha-melanocyte stimulating hormone (α-MSH) and affecting the regulation of energy balance[9, 10]. Thus, KK-A^y can be considered a mouse with a monogenic defect but in a polygenic background that results in a predisposition for obesity.

The body weight of KK-A^y mice usually reaches approxi-

mately 45 g at two months of age, which is characterized as moderate obesity. The body weight stabilizes by 4–5 months of age at approximately 50–60 g, with fat composing approximately 33% of the total body weight. Because obesity is partially caused by hyperphagia, food restriction seems effective in reversing obesity. The diabetes phenotype of KK-A^y mice exhibits as hyperglycemia, hyperinsulinemia, and glucose intolerance, although hyperglycemia declines after 1 year of age. In addition, an elevated pituitary growth hormone level in combination with glycosuria caused by glomerular lesions is often observed in this animal model[11–13].

The development of obesity and diabetes in KK-A^y mice has similarities to the development of human obesity and diabetes, and the strain has also been used in the early development of new experimental therapies. For instance, sibutramine has been tested in KK-A^y mice. Sibutramine acts to suppress calori intake and increase energy expenditure. Weight loss after sibutramine treatment has been shown in both humans and rodents[14, 15]. In KK-A^y mice, sibutramine treatment leads to a reduction in food intake; however, the sensitivity to sibutramine was less pronounced than in wild-type mice[16]. The weight-reducing properties of GLP-1 analogues have not, to the best of our knowledge, been tested in KK-A^y mice. However, exendin-4, a GLP-1 receptor agonist, increases insulin secretion and reduces glucose levels in KK-Ay mice[17, 18].

Ob/ob mouse as a model in obesity research

The *ob/ob* mouse is a monogenic model of obesity and diabetes due to a lack of leptin production. This mouse has been studied in many respects and is a commonly used model in obesity and diabetes research. The *db/db* mouse, which in many aspects resembles the *ob/ob* mouse, carries mutations in the leptin receptor and is usually found on the C57BLKS/J background[19]. This mouse is a model of more severe hyperglycemia and diabetes and will not be discussed in the present review.

The *ob/ob* phenotype was first discovered in mice in the Jackson Laboratory in 1949[20] and was crossed back to the C57Bl/6J background. The background of the metabolic phenotype was investigated by parabiosis studies with *ob/ob* mice and normal mice, which showed that the *ob/ob* mice exhibited reduced food intake and body weight to become phenotypically normal and led to the proposal that *ob/ob* mice lack a humoral satiety factor but still maintain sensitivity to this factor[21]. Based on these observations, considerable effort was put into finding this factor, which led to the positional cloning of leptin in 1994[22]. Furthermore, leptin was shown to be expressed in adipocytes, displayed increased levels in the obese and was reduced by starvation. Leptin mRNA is highly expressed in *ob/ob* mice, but the protein is not found in the plasma of these mice[23].

The *ob/ob* mutation in the C57Bl/6J background results in a phenotype with marked obesity, hyperinsulinemia, insulin resistance and relatively mild hyperglycemia. In contrast, the *ob/ob* mutation on the C57BKS background gives rise to the same phenotype as seen in *db/db* mice with the C57BKS background[24]. The identity of the genetic differences contributing to the different phenotypes is not well understood, but this observation underlines the importance of the background strain when considering mouse models of obesity and diabetes. Several colonies of *ob/ob* mice exist worldwide, each showing variations of the phenotype associated with the *ob/ob* mutation [25].

Obesity is the first observable phenotypic characteristic of the *ob/ob* mouse, whereas insulin resistance and hyperglycemia follow the development of obesity. Apart from increased energy intake, even on a chow diet, obesity is further increased in *ob/o*b mice because of a defect in thermogenesis in brown adipose tissue and therefore a larger deposition of ingested energy as fat[26, 27]. Furthermore, lipogenesis, especially hepatic, is enhanced in *ob/ob* mice, which also adds to the disposition for an obese phenotype[28].

Islet function has been extensively studied in the *ob/ob* mouse, displaying a large capacity for islet growth that results in hyperplasia and a large capacity for insulin secretion[29]. Based on these characteristics, the *ob/ob* mouse has been widely used for studies on insulin secretion in the prediabetic state and as a model of beta-cell stress and proliferation. For more detailed reviews of the phenotypic characteristics of the *ob/ob* mouse, see Lindström[30] and Chua *et al*[31].

Treatment with recombinant leptin in *ob/ob* mice results in an acute reduction of food intake and increase in glucose turnover with increased glucose uptake in brown adipose tissue and the brain, whereas chronic treatment dose-dependently reduces food intake and body weight and also results in an improvement in insulin sensitivity[32–34]. In humans with leptin deficiency, recombinant leptin administration has been shown to have the same profound effects on food intake and body weight as seen in *ob/ob* mice[35]. However, most obese humans do not have leptin deficiency; instead, they have hyperleptinemia and leptin resistance and thus generally do not respond with weight loss during recombinant leptin treatment. This finding underlines the fact that although the *ob/ob* mouse is indeed a valuable and useful animal model of obesity, it does not reflect the complete background of obesity in humans based on its monogenic cause of obesity and will therefore not always be predictive of the effects of pharmaceutical treatments in humans.

Treatment with sibutramine for 6 weeks in 6 week old *ob/ob* mice has been shown to reduce weight gain by 12%, but not to induce weight loss [36]. Because *ob/ob* mice are still growing at 6 weeks of age and thus do not have a stable body weight, it is not surprising that they did not lose weight in this study. However, this observation underlines the importance of choosing a model with a stable body weight if weight loss is the desired outcome of a study. Sibutramine treatment did not have a significant effect on food intake, but it did stop the increase in plasma nonesterified fatty acids (NEFA). Furthermore, the compound induced a decrease in plasma insulin and improved insulin sensitivity compared to vehicle-treated animals[36]. Treatment with sibutramine in humans usually results in a weight loss of approximately 8% and beneficial

effects on NEFA levels[1]. An acute study in *ob/ob* mice showed a dose-dependent reduction of food intake and body weight in this model during the first day after receiving liraglutide. However, 2 weeks of treatment with liraglutide at a dose of 100 μg/kg BID did not show significant effects on body weight in ob/ob mice, although effects on blood glucose levels were seen in this model[37].

Similarly, 2 weeks of exendin-4 treatment in *ob/ob* mice did not significantly affect body weight or food intake[38]. As was seen with sibutramine, another study with exendin-4 (10 or 20 μg/kg BID for 8 weeks) showed a dose-dependent reduction (20%–40%) of weight gain in the *ob/ob* model[39]. One explanation for the lack of effect on body weight in the study by Irvin *et al* could be that exendin-4 was only given once daily. Conversely, the study by Ding *et al* demonstrated an effect of a lower daily amount of exenatide, a synthetic form of exendin-4, indicating that other factors, such as the strain of *ob/ob* mice, could also contribute to the different results.

The lack of a consistent effect on body weight after GLP-1 receptor agonist treatment is in contrast to the robust weight loss that has been seen in humans after treatment with these compounds[40, 41], as well as to other animal models that are not monogenetic in origin.

The Zucker rat

The Zucker rat is a commonly used obese rat model. In 1961, it was discovered by TF ZUCKER and LM ZUCKER that an autosomal recessive mutation in the fatty gene (*fa*) resulted in the obesity seen in the Zucker rat. The homozygotes for the mutation (*fa/fa*) develop early onset obesity because of a defective leptin receptor[42]. The Zucker obese rat is hyperphagic and has reduced energy expenditure, leading to development of pronounced obesity at an early stage in life[43]. Under normal conditions, leptin produced from adipose tissue signals acts via the leptin receptor to reduce food intake. In the obese Zucker rat, this regulatory path is nonfunctional, and despite high levels of circulating leptin, the rats remain hyperphagic. Other orexigenic peptides, such as neuropeptide Y, galanin, orexin and melanin concentrating hormone (MCH), are also upregulated in the Zucker rat[44]. There is a preferential deposition of lipids in adipose tissue, and by 14 weeks of age, the Zucker rat has a fat percentage of 40%[45, 46]. Zucker rats develop insulin resistance in addition to obesity, but glycemic levels remain normal, and they do not develop overt diabetes[47]. In this aspect, the Zucker rat shares similarities with a large portion of the obese human population, the group who are both obese and insulin resistant but are not diabetic. The Zucker rat is therefore considered a good animal model for this metabolic syndrome.

The effect of sibutramine on food intake has also been examined in the Zucker rat. It was found that in lean Zucker rats, which are not homozygous for the *fa* mutation, sibutramine resulted in a significant reduction in food intake compared to the vehicle. In obese Zucker rats, this effect was totally absent at the dose tested (10 mg/kg)[16]. This finding is not in accordance with the effects of sibutramine seen in human clinical studies[1]. Thus, even if the obese Zucker rat is an animal model with several similarities to human obesity and metabolic syndrome, a discrepancy exists with respect to the pharmacological effect of sibutramine. For another class of pharmacological agents, the GLP-1 receptor agonists, the obese Zucker rat has been shown to be more predictive of the human situation with respect to regulation of appetite and body weight. Subchronic treatment of the obese Zucker rat with exendin-4 led to decreased fat deposition, reduced appetite and a reduction in weight gain[48]. Similarly, in humans, treatment with GLP-1 analogues leads to appetite reduction and weight loss[40, 41].

In a colony of outbred Zucker rats, a mutation rendering the diabetic rat was detected, which led to the development of the substrain Zucker Diabetic Fatty (ZDF) rat. Males more frequently show the diabetic phenotype than do the females. The females can develop diabetes if fed a high fat diet. However, the rate of diabetes development in males also depends on the diet[49]. The ZDF rat, especially the male, is widely used as an animal model for studies of anti-diabetic and anti-obesity drugs[50]. For example, liraglutide markedly attenuated the progress of diabetes in ZDF rats. Blood glucose was significantly reduced, and plasma insulin was 2–3-fold higher during a normal 24-h feeding period compared to vehicle-only treatment. Judged by pair feeding, approximately 53% of the anti-hyperglycemic effect was mediated by a reduction of food intake.

Polygenic models

Diet-induced obese rats and mice

Monogenic animal models of obesity are useful because the obesity and adiposity they develop is often severe, resulting in a distinct phenotype. Having a distinct phenotype might be of importance for certain aspects of obesity research. Furthermore, for pharmacological treatment, a clear phenotype with a large window for drugs to exert their effects is considered beneficial.

However, a common argument against the monogenic models in general and the monogenic models deficient in the leptin system in particular is that they are not representative of the human pathogenesis of obesity. Notably few cases of human obesity can be accounted for mutations in leptin or the leptin receptor[51]. The diet-induced obese (DIO) rat and mouse offer more human-like models, where the obesity is based on several factors, including an excess intake of calories. However, diet-induced obesity in rodents can be obtained by different means; there is a large variation both with respect to the content of the diet used, as well as the strain used.

In mice, C57Bl6/J is generally considered an obesity-prone strain in which pronounced weight gain, as well as hyperinsulinemia and sometimes also hyperglycemia is seen. This strain is also the most commonly used mouse strain for diet-induced obesity. A/J mice, on the other hand, are considered obesity resistant[52]. For a more elaborate examination of the obesity propensity of different mice strains, see the work by West *et al*[53,54]. There are also rat strains that are considered resistant

to high fat diet-induced obesity, such as S5B/PI and Lou/C, whereas others develop diet-induced obesity, such as Wistar, Sprague-Dawley, Long Evans and Osborne Mendel rats[55]. Thus, it is clear that the genetic background is of major importance for the body weight response to a high-fat diet.

The modern diet, especially in West, contains high levels of fat and carbohydrates such as fructose and sucrose. Different predefined mouse and rat diets for obesity induction can vary in the percentage of calories from fat and carbohydrates, as well as the source of fat or carbohydrates, all of which can result in minor differences in phenotypes.

For a diet containing 42% of the energy as fat, the source of fat (lard, olive oil, coconut oil or fish oil) has been shown to result in differential effects on body weight gain and glucose homeostasis in male Wistar rats[56]. The authors showed that the most pronounced manifestations of obesity and insulin resistance are seen when the fat source is lard (which contains comparable quantities of saturated fat and monounsaturated fat) or olive oil (monounsaturated fat) compared to coconut oil, fish oil or a chow diet. The relatively beneficial effect of fish oil (polyunsaturated fatty acids) on lipid and glucose homeostasis compared to other fat sources has been shown previously[57–59]. However, the observation that coconut oil, which contains saturated fatty acids, is less deleterious than lard and olive oil has not been corroborated in the literature. There are actually studies suggesting that diets containing more saturated fat are obesogenic and prone to inducing insulin resistance[60, 61]. It has been suggested that the response of the major hypothalamic neuropeptides regulating energy balance varies depending on the type of fat in the diet[60].

A diet high in fat and carbohydrates, either from fructose or sucrose, closely mimics the human diet. A high-fat and high-sucrose diet has been reported to result in a similar effect on body weight, abdominal fat, hyperinsulinemia and hyperglycemia as a high-fat-only diet in mice[52, 62]. In recent years, the role of fructose in the development of adiposity and metabolic syndrome has received significant attention[63]. In rodents, a high-fat and high-fructose diet has been shown to result in metabolic syndrome with obesity and changed body composition[64, 65]. In a study by Shapiro *et al*, it was shown that feeding SD rat with fructose caused leptin resistance, which led to an exacerbated weight gain when also given a high-fat diet, suggesting that fructose increases the propensity for obesity development[66].

Commonly used diets when inducing obesity are the 45% and 60% kcal energy from fat diet (D12451 and D12492, Research Diet), where the fat source is soybean oil and lard, and the difference between the two diets is the lard content. The pharmacological treatment of DIO rodents with anti-obesity agents, such as sibutramine and liraglutide, has been shown to have effects comparable to those reported in humans. Sibutramine reduces food intake, but there are conflicting data as to whether sibutramine has an effect on energy expenditure[67]. In DIO rats, sibutramine has also been shown to reduce body weight compared to placebo (9%) because of a reduction in food intake. This reduction was accompanied by a reduction in body fat[2]. A similar effect with a reduction in food intake and body weight for the GLP1 receptor agonists liraglutide and exendin-4 has also been established in DIO rats fed the 60% HF diet from Research Diet[68]. Also, in DIO mice fed a diet containing 45% calories from fat, liraglutide reduces energy intake and body fat[69]. Thus, diet-induced obese rodents can be considered a valid animal model that reflects the effects seen in humans during pharmacological treatment that affects appetite and thereby reduces body weight. With respect to the effect on obesity of agents that reduce body weight, the diet used is not of crucial importance as long as proper obesity is induced by the diet of choice. However, the extent to which the different diets are comparable with respect to the secondary outcomes of obesity medications, such as plasma lipids and glucose tolerance, needs to be further explored.

Cafeteria diet-induced obesity

Obesity in rats can also be induced with less standardized and predefined diets, such as the Cafeteria Diet, which means that the animals have a choice of various palatable energy-dense food items as an alternative to standard chow[70, 71]. The advantage to this approach is that the diet is palatable and the propensity to overeat is larger than that for a standardized, predefined high-fat diet. Furthermore, it is more similar to the human diet situation. However, the diet is criticized for being difficult to standardize with respect to nutritional content, and the animals might experience deficiencies in proteins or essential vitamins[72]. The model has not been as widely used for the development of obesity treatment as the DIO rat described above. At Novo Nordisk, we have employed a Cafeteria Diet DIO rat model in which the rats were fed chow *ad libitum* and were offered up to 20 g of candy per day. The candy was provided on a rotational basis and included chocolate biscuits, other kinds of chocolate and grape sugar to maximize the interest in the candy and to tempt the rat to eat more. Seventy-five percent of the calories were provided by candy intake because the DIO rat preferred candy over chow. This preference led to a 15%–20% higher weight gain in DIO rats than in chow-fed rats, which was attributable to an increase in fat mass[73]. Treatment with liraglutide, but not with vildagliptin, resulted in a significant reduction in body weight. Liraglutide, but not vildagliptin, reduced the total caloric intake. Interestingly, it also seemed to change food preference because a preferential reduction in candy intake and a relative increase in chow intake were seen after liraglutide treatment in candy-fed rats[73].

DIO-DR

Three decades ago, Dr Levin and co-workers refined the DIO model by selectively breeding Sprague Dawley (SD) rats for obesity[74]. Dr Levin took 100 normal SPD rats and subjected them to a high-fat diet (60% calories from fat). After several weeks on the diet, the animals could be divided into the following three groups: a low, middle and high BW group. Thereafter, the researchers mated rats that had increased their

body weight by a small or large amount in subsequent generations until total segregation was achieved, and the researchers started an out-breeding program. The individual groups were named diet resistant (DR) or obesity prone (DIO)[74]. The advantage of this process was that it was clear from the pup stage they could be absolutely sure that the pups from the DIO group would gain more weight and pups from the DR group would gain less weight when exposed to a high-fat diet. The increase in BW was predominantly caused by a general increase in fat mass and, to a much lesser extent, muscle mass, making the DIO rat a true diet-induced obese rat and not simply a "large" rat. Over approximately the past decade, Dr Levin, academic colleagues, and the biotech and pharmaceutical industry throughout the world have applied this model in target discovery and also as an important benchmark model[75–77]. The obesity in the DIO rat is not caused by a single gene but rather is truly polygenetic in nature. After 14–16 weeks on a high-fat diet (60% calories from fat, provided by Research diet) the metabolic parameters of the DIO rats reflect the altered diet with an increase in TG, insulin and lipids, which mirrors the human condition known as metabolic syndrome, making this model truly translational[75]. The model has shown its value already, as all approved drugs that have a marked effect on BW in humans have been shown to have a similar effect in the DIO rat. Sibutramine *po* for 3 weeks leads to a weight reduction of approximately 10%–13% of basal weight in this model, which is slightly more than what has been seen in clinical experiments. With respect to liraglutide, the weight loss in rats is approximately 10%, which is slightly more (12%)[75] than has been seen in 1-year liraglutide trials performed by Dr Astrup[2].

UCD-T2DM rat

One of the drawbacks of the DIO rodent models is that they develop hyperinsulinemia but not always hyperglycemia, thereby making them good models for obesity but not necessarily for type 2 diabetes. Havel and co-workers[78] have developed a polygenic rat model with adult-onset obesity, insulin resistance and late onset type 2 diabetes that maintains leptin signaling without dietary intervention. The model originates from crossing obese, insulin-resistant SD rats with lean ZDF rats.

Thus, the model is a cross between a model employing obesity and insulin resistance but with β-cells robust enough not to develop diabetes and a model with a β-cell defect that does not develop diabetes when insulin sensitivity is normal. By the F7 generation, it appeared that all animals were homozygous for the β-cell defect[79], and both sexes develop diabetes at 183±10 and 286±17 days of age, respectively (the incidence is 91.9% for males and 42.6% for females). The body weight and caloric intake are significantly higher for the UC Davis type 2 diabetes mellitus rat [UCD (University of California Davis)-T2DM] than the lean SD rat. The increased obesity and hyperphagia precede the onset of diabetes, and after the onset of diabetes, a slow loss of body weight is seen. Furthermore, early body weight has a significant influence on the age of onset of diabetes, which is consistent with the reported increased risk for T2DM with obesity. The UCD-T2DM rat is well suited for studies of pharmacological prevention of T2DM. Liraglutide has been tested for its ability to reduce body weight, as well as to prevent or delay the onset of diabetes in UCD-T2DM rats (0.2 mg/kg)[80]. This study included a group that was weight matched to the liraglutide group. This group was restricted to a food intake of 9% less energy/kg body weight than the animals that received liraglutide. The requirement of a 9% reduction in energy intake as compared to treatment with liraglutide to obtain similar weight suggests a beneficial component of liraglutide treatment on energy expenditure. The energy intake after liraglutide treatment was significantly reduced compared to vehicle-treated animals. Both liraglutide treatment and food restriction significantly delayed the onset of diabetes in the UCD-T2DM rat. However, liraglutide markedly lowered fasted plasma insulin compared to food-restricted rats, suggesting that improved insulin sensitivity was not caused by the effect on body weight alone. The large effect on the delay of the onset of diabetes after food restriction suggests that part of the beneficial effects of liraglutide is mediated via a reduction in energy intake and body weight. Furthermore, despite having a similar body weight, the liraglutide-treated animals had an even more pronounced reduction in body adiposity than did weight-matched animals.
NZO and NoncNZO mouse

The New Zealand obese (NZO) mouse is a polygenic model that develops hyperphagia and juvenile onset obesity, even when fed a low fat diet. Both subcutaneous and visceral fat is accumulated. Furthermore, the mouse develops type 2 diabetes, although at varying frequencies depending on substrain and gender[81, 82].

The NZO mice have been crossed with the nonobese nondiabetic (NON) mouse, which has impaired glucose tolerance and impaired β-cell insulin secretion capacity but still do not develop overt diabetes. The NONcNZO10/LtJ strain is a result of several crossings between NZO and NON mice. Both female and male NONcNZO10/LTJ mice develop obesity, but only males develop type 2 diabetes[83]. The disease inheritance of NONcNZO10/LtJ reflects the complex inheritance pattern of human obesity.

The NZO mice and the NONcNZO10/LtJ mice have primarily been used for pharmacogenetic studies. However, there are reports of pharmacology studies. For example, it has been shown that a β_3-adrenergic receptor agonist (CL316, 243) lowers body weight in these mice while increasing food intake and suppressing the development of diabetes in the mice[84]. Furthermore, rosiglitazone treatment leads to a body weight increase in NONcNZO/LtJ mice and in humans[84, 85]. The utility of the two models in pharmacological obesity studies as well as their predictivity in humans remains to be verified.

Tallyho mouse

The Tallyho mouse is also a model with moderate obesity and male-derived hyperglycemia with a polygenic origin[86]. A recent publication suggests that increased food intake, not

reduced energy expenditure, is the reason for the obesity in Tallyho mice as compared to C57BL6/J mice. When pair fed with C57Bl6/J mice, the Tallyho mice have the same rate of weight gain as the C57Bl6/J mice. Furthermore, the authors show that Tallyho mice have hypothalamic leptin resistance and upregulation of NPY mRNA levels[87]. There are, to the best of our knowledge, no publications in which Tallyho mice have been used in the pharmacological treatment of obesity; therefore, their utility and predictivity for human obesity treatment is unclear.

DIO minipigs

The obese Göttingen minipig is a relatively novel model; therefore, there are few reports on its metabolic status, as well as limited reports of pharmacological intervention studies.

Adult Göttingen minipigs have a body weight of 30 to 35 kg, and food restriction is necessary to maintain a lean phenotype. When fed *ad libitum* with normal pig chow, females have a food intake that is more than double that of the age-specific norms for this breed based on a restricted diet[88]. This increased food intake leads to massive obesity, and by 18 months of age, the pigs are two to three times the weight of animals fed restricted amounts of fat with percentage close to 50% because of their hyperphagic behavior. Thus, without food restriction, this model seems to have a normal development toward severe obesity. The hyperphagic element of this obesity seems similar to the food cravings observed in severely overweight humans, in contrast to the polygenic DIO rodent model, which shows moderate obesity and body fat. The degree of obesity measured by body weight, as well as excess body fat seen in the DIO pig model, closely resembles human obesity. However, one should be aware that the model is not well characterized, and although the obese minipigs become insulin resistant, similar to obese humans, they do not develop type 2 diabetes. Also, this model is resource intensive with respect to space, time and the quantity of compounds needed for studies.

In a pharmacological intervention study[89] with liraglutide, the effect on body weight loss was of the same magnitude as has been shown in human clinical obesity studies with this compound[2]. Six female Göttingen minipigs (Ellegaard Göttingen Minipigs, Dalmose, Denmark) aged approximately 18 months of age and with a mean body weight of 90.3±6.0 kg at the beginning of the study were used in this experiment. The minipigs had been fed *ad libitum* since weaning and this continued throughout the study.

Food intake was monitored continuously throughout the study, and body weight was determined twice weekly using a standard large-animal scale. In this three-period experiment (baseline, treatment and posttreatment follow-up), each animal was used as its own control. Liraglutide profoundly affected food intake with an overall reduction of 60% for the 7-week treatment period without any signs of desensitization. This approach meant that food intake came close to the level required for maintenance of normal body weight in these pigs. Food intake returned to pre-treatment levels within 4 days of termination of liraglutide treatment and, although variable, remained within the pre-treatment range for the remainder of the study. The effect on body weight was a reduction of 4.3±1.2 kg compared to a 7.0±1.0 kg weight gain during the 7 week pre- and post-treatment periods. The DIO Göttingen minipig model seems to resemble human obesity and also responds to a similar degree to obesity intervention treatment with liraglutide.

Conclusion

As described, there are a number of valid surrogate animal models of human obesity that can be utilized in the discovery and developmental process. An overview of the different models in this review is found in Table 1. That these models have translational character is evident from the data we have presented on sibutramine and liraglutide, although the number of models described is far from exhaustive. However, the human obesity phenotype is, for the majority of people, caused by the interplay between a long list of genes and the environment; therefore, the laboratory animal model that best reflects this is polygenetic dietary-induced models. The monogenetic models do have a role in terms of teasing out the mechanism and mode of action of these diseases, but the best surrogate models are the DIO. Over the past few years, a number of models using dietary manipulations (high-fructose/high-carbohydrate) have emerged, but they are left out of the current

Table 1. An overview of the different models of obesity.

	KK-A^y	*Ob/ob*	Zucker	DIO or Cafeteria diet or DIO DR	UCD-T2M	DIO minipig
Cause of disease	Monogenic (A^y) and polygenic (KK)	Monogenic	Monogenic	Induced and polygenic	Polygenic	Induced
Obesity	Yes	Yes	Yes	Yes	Yes	Yes
Hyperphagia	Yes	Yes	Yes	No	Yes	Yes
Hyperinsulinemia	Yes	Yes	Yes	Yes	Yes	Yes
Glucose intolerance	Yes	Yes	Yes	Yes	Yes	?
Hyperglycemia	Yes	Mild	No	No	Yes	No
Weight reducing effect of sibutramine	Marginal	Marginal	No	Yes	?	?
Weight reducing effect of GLP1 analogues	?	None or marginal	Yes	Yes	Marginal	Yes

review because further testing is required to validate these models. It is likely that these models will potentially lead to a model that is even more predictive of the human disease, leaving us with a more optimized tool that will potentially reduce the path to market and will eliminate the necessity of a number of animal studies.

Acknowledgements

The authors thank Senior Scientist Lotte Bjerre KNUDSEN for helpful discussion of the manuscript and Annette THYDE for excellent administrative and technical assistance.

References

1 Padwal RS, Jajumdar SR. Drug treatments for obesity; orlistat sibutramine and rimonabant. Lancet 2007; 369: 71–7.
2 Astrup A, Rössner S, Van Gaal L, Rissanen A, Niskanen L, Al Hakim M, *et al*. Effects of liraglutide in the treatment of obesity: a randomised, double-blind, placebo-controlled study. Lancet 2009; 374: 1606–16.
3 Finer N. Executive steering committee of the sibutramine cardiovascular outcome trial. Withdrawal of sibutramine. Editorial is judgement in advance of the facts. BMJ 2010; 340: C1346.
4 Kondo K, Nozawa K, Tomira T, Ezaki K. Inbred strains resulting from Japanese mice. Bull Exp Anim 1957; 6: 107–12.
5 Igel M, Taylor BA, Phillips SJ, Becker W, Herberg L, Joost HG. Hyperleptinemia and leptin receptor variant Asp600Asn in the obese, hyperinsulinemic KK mouse strain. J Mol Endocrinol 1998; 21: 337–45.
6 Ikeda H. KK mouse. Diabetes Res Clin Practice 1994; 24: S313–S316.
7 Nishimura. Breeding of mice strains for diabetes mellitus. Exp Animals 1969; 18: 147–57.
8 Iwatsuka H, Shino A, Suzuoki Z. General survey of diabetic features of yellow KK mice. Endocrinology 1970; 17: 23–35.
9 Klebig ML, Wilkinson JE, Geisler JG. Ectopic expression of the agouti gene in transgenic mice causes obesity, features of type II diabetes, and yellow fur. Proc Natl Acad Sci U S A 1995; 92: 4728–32.
10 Stütz AM, Morrison CD, Argyropoulus G. The agouti-related protein and its role in energy homeostasis. Peptides 2005; 26: 1771–81.
11 Bray GA, York DA. Genetically transmitted obesity in rodents. Physiol Rev 1971; 51: 598–646.
12 Butler L, Gerritsen GC. A comparison of the modes of inheritance of diabetes in the Chinese hamster and the KK mouse. Diabetologia 1970; 6: 163–7.
13 Butler L. The inheritance of glucosuria in the KK and AY mouse. Can J Genet Cytol 1972; 14: 265–9.
14 Stock MJ. Sibutramine: a review of the pharmacology of a novel anti-obesity agent. Int J Obes Relat Metab Disord 1997; 21 Suppl 1: S25–9.
15 Bray GA, Greenway FL. Current and potential drugs for treatment of obesity. Endocr Rev 1999; 20: 805–75.
16 Matsumoto K, Iijima H. Sibutramine sensitivity assay revealed a unique phenotype of bombesin BB3 receptor-deficient mice. Eur J Pharmacol 2003; 473: 41–6.
17 Song GM, Huan Y, Sun SJ, Chen YT, Liu Q, Shen ZF. Biological activity of EXf, a peptide analogue of exendin-4. Eur J Pharmacol 2010; 628: 261–7.
18 Thorens B, Porret A, Buhler L, Deng SP, Morel P, Widman C. Cloning and functional expression of the GLP-1 receptor: demonstration that exendin-4 is an agonist and exendin 3 (9–39) is an antagonist of the receptor. Diabetes 1993; 42: 1678–82
19 Hummel KP, Dickie MM, Coleman DL. Diabetes, a new mutation in the mouse. Science 1966; 153: 1127–8.
20 Ingalls, AM, Dickie MM, Coleman DL. Obese, a new mutation in the house mouse. J Heredity 1950; 41: 317–8.
21 Coleman DL. Effects of parabiosis of obese with diabetes and normal mice. Diabetologia 1973; 9: 294–8.
22 Zhang Y, Proenca R, Maffei M, Barone M, Leopold L, Friedman JM. Positional cloning of the mouse obese gene and its human homologue. Nature 1994; 372: 425–31.
23 Frederich RC, Lollmann B, Hamann A, Napolitano-Rosen A, Kahn BB, Lowell BB, *et al*. Expression of ob mRNA and its encoded protein in rodents, impact of nutrition and obesity. J Clin Invest 1995; 96: 1658–63.
24 Coleman DL, Hummel KP. Obese gene in the mouse. Diabetologia 1973; 9: 287–93.
25 Herberg L, Coleman DL. Laboratory animals exhibiting obesity and diabetes syndromes. Metabolism 1977; 26: 59–99.
26 Trayhurn P, Jones PM, McGuckin MM, Goodbody AE. Effects of overfeeding on energy balance and brown fat thermogenesis in obese (*ob/ob*) mice. Nature 1982; 295: 323–5.
27 Hogan S, Himms-Hagen J. Abnormal brown adipose tissue in obese (*ob/ob*) mice: response to acclimation to cold. Am J Physiol 1980; 239: E301–E309.
28 Memon RA, Fuller J, Moser AH, Smith PJ, Grunfeld C, Feingold KR. Regulation of putative fatty acid transporters and Acyl-CoA synthetase in liver and adipose tissue in *ob/*ob mice. Diabetes 1999; 48: 121–7.
29 Lindström P. β-Cell function in obese-hyperglycemic mice [*ob/ob* Mice] in the islets of Langerhans, advances in experimental medicine and biology, ed: Islam MS, 2010 654: 463-477, DOI 10.1007/978-90-481-3271-3_20
30 Lindström P. The physiology of obese-hyperglycemic mice [*ob/ob* Mice]. TheScientificWorldJOURNAL 2007; 7: 666–85.
31 Chua S, Herberg L, Leiter EH. Obesity/diabetes in mice with mutations in leptin or leptin receptor genes. In Shafrir E (ed). Animal models of Diabetes Frontiers in Research. London: Boca Raton, Fla. CRC; 2007. p 61–102.
32 Burcelin R, Kamohara S, Li J, Tannenbaum GS, Charron MJ, Friedman JM. Acute intravenous leptin infusion increases glucose turnover but not skeletal muscle glucose uptake in *ob/ob* mice. Diabetes 1999; 48: 1264–9.
33 Pelleymounter MA, Cullen MJ, Baker MB, Hecht R, Winters D, Boone T, *et al*. Effects of the obese gene product on body weight regulation in *ob/ob* mice. Science 1995; 269: 540–3.
34 Weigle DS, Bukowski TR, Foster DC, Holderman S, Kramer JM , Lasser G, *et al*. Recombinant *ob* protein reduces feeding and body weight in the *ob/ob* mouse. J Clin Invest 1995; 96: 2065–70.
35 Farooqi IS, Matarese G, Lord GM, Keogh JM, Lawrence E, Agwu C, *et al*. Beneficial effects of leptin on obesity, T cell hyporesponsiveness and neuroendocrine/metabolic dysfunction of human congenital leptin deficiency. J Clin Invest 2002; 110: 1093–103.
36 Day C, Bailey CJ. Effect of the antiobesity agent sibutramine in obese-diabetic *ob/ob* mice. Int J Obes Relat Metab Disord 1998; 22: 619–23.
37 Rolin B, Larsen MO, Gotfredsen CF, Deacon CF, Carr RD, Wilken M, *et al*. The long-acting GLP-1 derivative NN2211 ameliorates glycemia and increases beta-cell mass in diabetic mice. Am J Physiol Endocrinol Metab 2002; 283: E745–52.
38 Irwin N, McClean PL, Cassidy RS, O'harte FP, Green BD, Gault VA, *et al*. Comparison of the anti-diabetic effects of GIP- and GLP-1-receptor activation in obese diabetic (*ob/ob*) mice: studies with DPP IV resistant N-AcGIP and exendin(1–39)amide. Diabetes Metab Res Rev 2007; 23: 572–9.

39 Ding X, Saxena NK, Lin S, Gupta NA, Anania FA. Exendin-4, a glucagon-like protein-1 (GLP-1) receptor agonist, reverses hepatic steatosis in *ob/ob* mice. Hepatology 2006; 43: 173–81. Erratum in: Hepatology 2006; 44: 515.
40 Vergès B, Bonnard C, Renard E. Beyond glucose lowering: Glucagon-like peptide-1 receptor agonists, body weight and the cardiovascular system. Diabetes Metab 2011. Doi : 10.1016/j.diabet.2011.07.001.
41 Bode B. Liraglutide: a review of the first once-daily GLP-1 receptor agonist. Am J Manag Care 2011; 17: S59–70.
42 Phillips MS, Liu Q, Hammond HA, Dugan V, Hey PJ, Caskey CJ, *et al*. Leptin receptor missense mutation in the fatty Zucker rat. Nat Genet 1996; 13: 18–9.
43 White BD, Martin RJ. Evidence for a central mechanism of obesity in the Zucker rat: role of neuropeptide Y and leptin. Proc Soc Exp Biol Med 1997; 214: 222–32.
44 Artiñano AA, Castro MM. Experimental rat models to study the metabolic syndrome. Br J Nutr 2009; 102: 1246–53.
45 Zucker TF, Zucker LM. Hereditary obesity in the rat associated with high serum fat and cholesterol. Proc Soc Exp Biol Med 1962; 110: 165–71.
46 Zucker LM, Antoniades HN. Insulin and obesity in the Zucker genetically obese rat "fatty". Endocrinology 1972; 90: 1320–30.
47 Bray GA. The Zucker-fatty rat: a review. Fed Proc 1977; 36: 148–53.
48 Szayna M, Doyle ME, Betkey JA, Holloway HW, Spencer RGS, Greig NH, *et al*. Exendin-4 decelerates food intake, weight gain, and fat deposition in Zucker rats. Endocrinology 2000; 141: 1936–41.
49 Corsetti JP, Sparks JD, Peterson RG, Smith RL, Sparks CE. Effect of dietary fat on the development of non-insulin dependent diabetes mellitus in obese Zucker diabetic fatty male and female rats. Atherosclerosis 2000; 148: 231–41.
50 Clark JB, Palmer CJ, Shaw WN. The diabetic Zucker fatty rat. Proc Soc Exp Biol Med 1983; 173: 68–75.
51 Farooqi IS, Jebb SA, Langmack G, Lawrence E, Cheetham CH, Prentice AM, *et al*. Effects of recombinant leptin therapy in a child with congenital leptin deficiency. N Eng J Med 1999; 341: 879–84.
52 Surwit RS, Feinglos MN, Rodin J, Sutherland A, Petro AE, Opara EC, *et al*. Differential effects of fat and sucrose on the development of obesity and diabetes C57BL/6J and A/J mice. Metabolism 1995; 44: 645–51.
53 West DB, Boozer CN, Moody DL, Atkinson RL. Dietary obesity in nine inbred mouse strains. Am J Physiol 1992; 262: R1025–R1032.
54 West DB, Waguespack J, McCollister S. Dietary obesity in the mouse: interaction of strain with diet composition. Am J Physiol 1995; 268: R658–R665.
55 Schemmel R, Mickelsen O, Motawi K. Conversion of dietary to body energy in rats as affected by strain, sex and ration. J Nutr 1972; 102: 1187–97.
56 Buettner R, Parhofer KG, Woenckhaus M, Wrede CE, Kunz-Schughart LA, Scholmerich J, *et al*. Defining high-fat-diet rat models: metabolic and molecular effects of different fat types. J Mol Endocrinol 2006; 36: 485–501.
57 Huang XF, Xin X, McLennan P, Storlien L. Role of fat amount and type in ameliorating diet-induced obesity: insights at the level of hypothalamic arcuate nucleus leptin receptor, neuropeptide Y and pro-opiomelanocortin mRNA expression. Diabetes Obes Metab 2004; 6: 35–44.
58 Storlien LH, Higgins JA, Thomas TC, Brown MA, Wang HQ, Huang XF, *et al*. Diet composition and insulin action in animal models. Br J Nutr 2000; 83 Suppl 1: S85–S90.
59 Delarue J, LeFoll C, Corporeau C, Lucas D. N-3 long chain polyunsaturated fatty acids: a nutritional tool to prevent insulin resistance associated to type 2 diabetes and obesity? Reprod Nutr Dev 2004; 44: 289–99.
60 Wang H, Storlien LH, Huang XF. Effects of dietary fat types on body fatness, leptin, and ARC leptin receptor, NPY, and AgRP mRNA expression. Am J Physiol Endocrinol Metab 2002; 282: E1352–E1359.
61 Storlien LH, Jenkins AB, Chisholm DJ, Pascoe WS, Khouri S, Kraegen EW. Influence of dietary fat composition on development of insulin resistance in rats. Relationship to muscle triglyceride and omega-3 fatty acids in muscle phospholipid. Diabetes 1991; 40: 280–9.
62 Sato-Mito N, Suzui M, Yoshino H, Kaburagi T, Sato K. Long term effects of high fat and sucrose diets on obesity and lymphocyte proliferation in mice. J Nutr Health Aging 2009; 13: 602–6.
63 Bray GA. Soft drink consumption and obesity: it is all about fructose. Curr Opin Lipidol 2010; 21: 51–7.
64 Wada T, Kenmochi H, Miyashita Y, Sasaki M, Ojima M, Sasahara M, *et al*. Spironolactone improves glucose and lipid metabolism by ameliorating hepatic steatosis and inflammation and suppressing enhanced gluconeogenesis induced by high-fat and high-fructose diet. Endocrinology 2010; 151: 2040–9.
65 Couturier K, Batandier C, Awada M, Hininger-Favier I, Canini F, Anderson RA, *et al*. Cinnamon improves insulin sensitivity and alters the body composition in an animal model of the metabolic syndrome. Arch Biochem Biophys 2010; 501: 158–61.
66 Shapiro A, Mu W, Roncal C, Cheng KY, Johnson RJ, Scarpace PJ. Fructose-induced leptin resistance exacerbates weight gain in response to subsequent high-fat feeding. Am J Physiol Regul Integr Comp Physiol 2008; 295: R1370–R1375.
67 Sharma B, Henderson DC. Sibutramine: current status as an anti-obesity drug and its future perspectives. Expert Opin Pharmacother 2008; 9: 2161–73.
68 Hayes MR, Kanoski SE, Alhadeff AL, Grill HJ. Comparative effects of the long-acting GLP-1 receptor ligands, liraglutide and exendin-4, on food intake and body weight suppression in rats. Obesity 2011; 19: 1342–9.
69 Porter DW, Kerr BD, Flatt PR, Holscher C, Gault VA. Four weeks administration of liraglutide improves memory and learning as well as glycaemic control in mice with high fat dietary-induced obesity and insulin resistance. Diabetes Obes Metab 2010; 12: 891–9.
70 Sclafani A, Springer D. Dietary obesity in adult rats: similarities to hypothalamic and human obesity syndromes. Physiol Behav 1976; 17: 461–71.
71 Rothwell NJ, Stock MJ. The cafeteria diet as a tool for studies of thermogenesis. J Nutrition 1988; 118: 925–8
72 Moore BJ. The cafeteria diet–an inappropriate tool for studies of thermogenesis. J Nutr 1987; 117: 227–31.
73 Raun K, von Voss P, Gotfredsen CF, Golozoubova V, Rolin B, Knudsen LB. Liraglutide, a long-acting glucagon-like peptide-1 analog, reduces body weight and food intake in obese candy-fed rats, whereas a dipeptidyl peptidase-IV inhibitor, vildagliptin, does not. Diabetes 2007; 56: 8–15.
74 Levin BE, Hogan S, Sullivan AC. Initiation and perpetuation of obesity and obesity resistance in rats. Am J Physsiol 1989; 256: R766–771.
75 Madsen AN, Hansen G, Paulsen SJ, Lykkegaard K, Tang-Christensen M, Hansen HS, *et al*. Long-term characterization of the diet-induced obese and diet-resistant rat model: a polygenentic rat model mimicking the human obesity syndrome. J Endocrinol 2010; 206: 287–96.
76 Levin BE, Keesey RE. Defense of differing weight set points in diet induced obese and resistant rats. Am J Physiol 1998; 274: R412–9.
77 Levin BE, Dunn-Meynell AA, Balkan B, Keesey RE. Selective breeding for diet-induced obesity and resistance in Spraque Dawley rats. Am J

Physiol 1997; 273; R725–R730.

78 Cummings BP, Digitale EK, Stanhope KL, Graham JL, Baskin DG, Reed BJ, Sweet IR, Griffen SC, Havel PJ. Development and characterization of a novel rat model of type 2 diabetes mellitus: the UC Davis type 2 diabetes mellitus UCD-T2DM rat. Am J Physiol Regul Integr Comp Physiol 2008; 295: R1782–93.

79 Cummings BP, Digitale EK, Stanhope KL, Graham JL, Baskin DG, Reed BJ, *et al*. Development and characterization of a novel rat model of type 2 diabetes mellitus: the UC Davis type 2 diabetes mellitus UCD-T2DM rat. Am J Physiol Regul Integr Comp Physiol 2008; 295: R1782–93.

80 Cummings BP, Stanhope KL, Graham JL, Baskin DG, Griffen SC, Nilsson C, *et al*. Chronic administration of the glucagon-like peptide-1 analog, liraglutide, delays the onset of diabetes and lowers triglycerides in UCD-T2DM rats. Diabetes 2010; 59: 2653–61.

81 Bielschowsky M, Bielschowsky M. A new strain of mice with hereditary obesity. Proc Univ Otago Med School 1953; 31: 29–3.

82 Leiter EH, Reifsnyder PC. Differential levels of diabetogenic stress in two new mouse models of obesity and type 2 diabetes. Diabetes 2004; 53 Suppl 1: S4-11.

83 Cho YR, Kim HJ, Park SY, Ko HJ, Hong EG, Higashimori T, *et al*. Hyperglycemia, maturity-onset obesity, and insulin resistance in NONcNZO10/LtJ males, a new mouse model of type 2 diabetes. Am J Physiol Endocrinol Metab 2007; 293: E327–E336.

84 Koza RA, Flurkey K, Graunke DM, Braun C, Pan HJ, Reifsnyder PC, *et al*. Contributions of dysregulated energy metabolism to type 2 diabetes development in NZO/H1Lt mice with polygenic obesity. Metabolism 2004; 53: 799–808.

85 Pan HJ, Reifsnyder P, Vance DE, Xiao Q, Leiter EH. Pharmacogenetic analysis of rosiglitazone-induced hepatosteatosis in new mouse models of type 2 diabetes. Diabetes 2005; 54: 1854–62.

86 Kim JH, Sen S, Avery CS, Simpson E, Chandler P, Nishina PM, *et al*. Genetic analysis of a new mouse model for non-insulin-dependent diabetes. Genomics 2001; 74: 273–86.

87 Rhee SD, Sung YY, Lee YS, Kim JY, Jung WH, Kim MJ, *et al*. Obesity of TallyHO/JngJ mouse is due to increased food intake with early development of leptin resistance. Exp Clin Endocrinol Diabetes 2011; 119: 243–51.

88 Bollen PJ, Madsen LW, Meyer O, Ritskes-Hoitinga J. Growth differences of male and female Göttingen minipigs during *ad libitum* feeding: a pilot study. Lab Animal 2005; 39: 80–93.

89 Raun K, von Voss P, Knudsen LB. Liraglutide, a once-daily human glucagon-like peptide-1 analog, minimizes food intake in severely obese minipigs. Obesity 2007; 15: 1710–6.

Acta Pharmacologica Sinica (2012) 33: 182–188
 1671-4083/12 $32.00
www.nature.com/aps

Review

Why do anti-inflammatory therapies fail to improve insulin sensitivity?

Zhan-guo GAO, Jian-ping YE*

Antioxidant and Gene Regulation Lab, Pennington Biomedical Research Center, Louisiana State University System, Baton Rouge, LA 70808 , USA

Chronic inflammation occurs in obese conditions in both humans and animals. It also contributes to the pathogenesis of type 2 diabetes (T2D) through insulin resistance, a status in which the body loses its ability to respond to insulin. Inflammation impairs insulin signaling through the functional inhibition of IRS-1 and PPARγ. Insulin sensitizers (such as rosiglitazone and pioglitazone) inhibit inflammation while improving insulin sensitivity. Therefore, anti-inflammatory agents have been suggested as a treatment strategy for insulin resistance. This strategy has been tested in laboratory studies and clinical trials for more than 10 years; however, no significant progress has been made in any of the model systems. This status has led us to re-evaluate the biological significance of chronic inflammation in obesity. Recent studies have consistently asserted that obesity-associated inflammation helps to maintain insulin sensitivity. Inflammation stimulates local adipose tissue remodeling and promotes systemic energy expenditure. We propose that these beneficial activities of inflammation provide an underlying mechanism for the failure of anti-inflammatory therapy in the treatment of insulin resistance. Current literature will be reviewed in this article to present evidence that supports this viewpoint.

Keywords: inflammation; insulin resistance; type 2 diabetes; insulin sensitizer; obesity

Acta Pharmacologica Sinica (2012) 33: 182–188; doi: 10.1038/aps.2011.131; published online 31 Oct 2011

Introduction

For about two decades, it has been known that inflammation contributes to obesity-associated insulin resistance. Inflammatory cytokines (*eg*, TNF-alpha, IL-1, and IL-6) have been shown to induce insulin resistance in multiple organs (fat, muscle and liver). TNF-α elevation was found in adipose tissue of obese mice in 1993[1]. That study provided the first evidence of the role of chronic inflammation during obesity and its association with insulin resistance in an animal model. Macrophages in adipose tissue are the major source of inflammatory cytokines in obesity[2, 3]. Recent studies from multiple groups, including ours, consistently suggest that adipose tissue hypoxia is a root of chronic inflammation in obesity[4]. Hypoxia is likely the result of a reduction in blood flow to adipose tissue, which is supported by some studies in humans and animals[5–7].

In addition to adipose tissue hypoxia, metabolites of fatty acids and glucose, including diacylglyceride (DAG), ceramide, and reactive oxygen species, also contribute to the chronic inflammation in obesity. They activate the inflammatory response in several ways. They can directly interact with signaling kinases (PKCs, JNKs, and IKKs) in cells[8]; the lipids can also signal through cell membrane receptors for lipids, such as TLR4, CD36, or GPR[8–13]. Fat or glucose oxygenation in the mitochondria can also generate reactive oxygen species (ROS), which can then induce activation of the inflammatory kinases (JNK and IKK) in the cytoplasm. The lipids also induce endoplasmic reticulum (ER) stress to activate JNK and IKK[14, 15]. In obesity, these signaling pathways are activated as a result of the surplus calories and involved in the pathogenesis of chronic inflammation.

Chronic inflammation and insulin resistance

At the molecular level, inflammation induces insulin resistance by targeting IRS-1 and PPARγ.

Inflammation and IRS-1 (insulin receptor substrate 1)

In cellular models of insulin resistance, the pro-inflammatory cytokine, TNF-α, is widely used to induce insulin resistance. The data from these cellular studies suggest that TNF-α is a major risk factor for insulin resistance in obesity and other chronic diseases[1, 16, 17]. TNF-α inhibits insulin signaling by serine phosphorylation of IRS-1, which leads to the dissociation of IRS-1 from the insulin receptor and causes degradation of IRS-1 protein[17–19]. In the insulin signaling pathway, IRS-1

* To whom correspondence should be addressed.
E-mail yej@pbrc.edu
Received 2011-08-01 Accepted 2011-09-06

undergoes tyrosine in response to insulin stimulation, which leads to activation of the insulin signaling pathway, downstream PI3K/Akt activation, and Glut4 translocation to the cell membrane for glucose uptake. TNF-α induces insulin resistance by IRS-1 serine phosphorylation through the activation of several serine kinases, including JNK[20, 21], IKK[22], ERK[23–25], PKC[26–28], Akt[28, 29], GSK-3[30–32], IRAK[33], and mTOR[34, 35]. In a recent study, we showed that IKK2 (IKKβ) inhibits IRS-1 function through the activation of S6K, which directly phosphorylates IRS-1 at multiple sites (such as S312/307 and S270/265) in TNF-α-treated cells[22, 36]. Serine phosphorylation induces IRS-1 degradation and serves as a negative feedback signal to impair insulin action[35].

Inflammation inhibits PPARγ function

The IKKβ/NF-κB (nuclear factor kappa B) pathway is a dominant inflammatory signaling pathway. The pathway has been under active investigation in the obesity field after IKKβ was found to induce insulin resistance in obese mice[37]. The serine kinase IKK has three major isoforms, including IKKα (IKK1), IKKβ (IKK2), and IKKγ, which requires IKKβ for NF-κB activation[38]. In obesity, IKKβ is activated by several intracellular signals, such as ROS, ER stress, DAG, and ceramide. IKKβ is also activated by extracellular stimuli, including TNF-α, IL-1, fatty acids[11] and hypoxia[39]. IKKβ induces NF-κB activation by phosphorylation of the Inhibitor of Kappa B alpha (IκBα)[40].

NF-κB is a ubiquitous transcription factor that is formed by two subunits of the Rel family, which includes seven members, p65 (RelA), p50 (NF-κB1), c-Rel, RelB, p100, p105, p52[41]. These members form a homodimer or heterodimer that regulates gene transcription. In most cases, NF-κB is a heterodimer of p65 and p50. P65 contains the transactivation domain and mediates the transcriptional activity of NF-κB. P50 inhibits the transcriptional activity of p65[42], and the NF-κB activity is enhanced in p50 knockout mice[43]. NF-κB inhibits PPARγ function through the competition for transcriptional coactivators or the exchange of corepressors with PPARγ[44]. This process is responsible for inhibiting PPAR-target genes, such as CAP and IRS-2. Our study shows that IKK promotes the activity of HDAC3 in the nuclear corepressor complex. IKK induces nuclear translocation of HDAC3 from the cytoplasm. In the cytosol, HDAC3 associates with IκBα, and the degradation of IκBα promotes HDAC3 translocation into the nucleus. The PPARγ inactivation leads to suppression of IRS-2 expression, a signaling molecule in insulin signaling pathways for Glut4 translocation.

Free fatty acids and insulin resistance

Elevated plasma free fatty acids (FFAs) induce insulin resistance in obese and diabetic subjects[45]. It was known as early as 1983 that lipid infusion caused insulin resistance[46, 47]. To examine the mechanism by which FFAs induced insulin resistance *in vivo*, rats were tested in a hyperinsulinemic-euglycemic clamp after a 5-h infusion of lipids/heparin, which raises plasma FFA concentrations[47]. FFAs resulted in an approximate 35% reduction in insulin sensitivity, indicated by the glucose infusion rate ($P<0.05$ *vs* control), and a 25% reduction in glucose transport activity, as assessed by 2-[1,2-^{3}H]deoxyglucose uptake *in vivo* ($P<0.05$ *vs* control). PKCθ is a major kinase involved in FFA-induced insulin resistance[48]. According to the Randle glucose-fatty acid cycle, the preferential oxidation of free fatty acids over glucose plays a major role in the pathogenesis of insulin sensitivity[49]. Local accumulation of fat metabolites, such as ceramides, diacylglycerol or acyl-CoA, inside skeletal muscle and liver may activate a serine kinase cascade, leading to defects in insulin signaling and glucose transport[50].

Inflammation and energy metabolism

Inflammation is associated with increased energy expenditure in patients with chronic kidney disease[51], cachexia[52], inflammatory bowel disease[53] and Crohn's disease[54]. NF-κB activity can promote energy expenditure, as supported by documents on energy expenditure in cachexia[55, 56] and infection. However, the role of NF-κB in energy expenditure was not tested in transgenic models. To this end, we have investigated energy metabolism in transgenic mice with elevated NF-κB activity. The transcriptional activity of NF-κB is enhanced either by over-expression of NF-κB p65 in the fat tissue, or inactivation of NF-κB p50 by global gene knockout[57, 58]. In these two models, inflammatory cytokines (TNF-α and IL-6) were elevated in the blood, and energy expenditure was increased both during the day and at night[57, 58]. Expression of TNF-α and IL-1 mRNA was increased in adipose tissue and macrophages. These cytokines are positively associated with energy expenditure in the body[56]. In transgenic mice with deficiencies in these cytokines or their receptors, energy accumulation is enhanced and energy expenditure is reduced. This positive energy balance has been reported in transgenic mice deficient in TNF-α[59], IL-1[60], or IL-6[61].

The above literature suggests that energy accumulation induces chronic inflammation. Inflammation may promote energy expenditure in a feedback manner to counteract an energy surplus[62]. Inflammation may act in the peripheral organs/tissues, as well as in the central nervous system, to regulate energy balance. In the peripheral tissues, inflammation induces fat mobilization and oxidation to promote energy expenditure. In the central nervous system, inflammation can inhibit food intake and activate neurons for energy expenditure, while inhibition of inflammation leads to fat accumulation[62].

Anti-inflammation therapies for insulin resistance

In clinical trials, high-dose salicylate was used to inhibit inflammation by targeting IKK/NF-κB[37, 63–65]. Salicylate reduces blood glucose by inhibiting IKK/NF-κB, as seen decades ago in patients with diabetes[64–66]. More studies demonstrated that high-doses of aspirin (~7.0 g/d) improved multiple metabolic measures in patients with T2D, including substantial reductions in fasting and postprandial glucose, triglycerides and FFAs. These changes were associated with reduced hepatic glucose production and improvements in

insulin-stimulated glucose disposal, assessed during hyperinsulinemic-euglycemic clamping[63–65, 67]. Aspirin inhibits the activity of multiple kinases induced by TNF-α, such as JNK, IKK, Akt, and mTOR. It may enhance insulin sensitivity by protecting the IRS proteins from serine phosphorylation[68]. However, the therapeutic value of high-dose aspirin is limited by its side effects, including gastrointestinal irritation and high risk of bleeding.

Statins, a class of anti-inflammatory drugs, have been shown to downregulate the transcriptional activity of NF-κB, AP-1, and HIF-1α[65, 69], with coordinated reductions in the expression of prothrombotic and inflammatory cytokines. Randomized clinical trials have demonstrated that statins reduces CRP, multiple cytokines, and inflammatory markers in the body. Even with modest anti-inflammatory properties, statins do not appear to enhance insulin resistance or significantly improve glycemia[70]. A recent review published in JAMA suggests that statin therapy is associated with excess risk for diabetes mellitus. The researchers analyzed five earlier trials, involving 32 752 patients, to test the effect of the drug dose. Those getting intensive treatment were 12 percent more likely to have diabetes[71], which translates into a 20 percent increase in developing diabetes in the high-dose statin users compared to those who do not take the drugs.

Glucocorticoids are the most effective anti-inflammatory drugs used to treat inflammatory diseases. Dexamethasone is a potent synthetic member of the glucocorticoid class of steroid drugs. In a clinical study, the effect of dexamethasone on insulin-stimulated glucose disposal was investigated with a double-blind, placebo-controlled, cross-over trial comparing insulin sensitivity (measured by the euglycemic hyperinsulinemic clamp) in young healthy males allocated the placebo or 1 mg dexamethasone twice daily for 6 d, each in random order. Six days of dexamethasone therapy was associated with a 30% decrease in insulin sensitivity[72, 73]. This indicates that strong inhibition of inflammation may block the beneficial effects of inflammation on insulin sensitivity.

Interleukin-1β induces inflammation in islets of patients with type 2 diabetes[74]. The interleukin-1–receptor antagonist, a naturally occurring competitive inhibitor of interleukin-1[75], protects human beta cells from glucose-induced functional impairment and apoptosis[76]. The expression of the interleukin-1-receptor antagonist is reduced in pancreatic islets of patients with type 2 diabetes mellitus. High glucose induces the production of interleukin-1β in human pancreatic beta cells, leading to impaired insulin secretion, decreased cell proliferation, and enhanced apoptosis. In this double-blind, parallel-group trial involving 70 patients with type 2 diabetes[74], 34 patients were randomly assigned to receive 100 mg of anakinra (a recombinant human interleukin-1-receptor antagonist) subcutaneously once daily for 13 weeks. In the control group, 36 patients received placebo. All patients underwent an oral glucose-tolerance test. At the end of the study, the two study groups exhibited no difference in insulin resistance, insulin-regulated gene expression in skeletal muscle, serum adipokine levels, and the body-mass index. However, the therapy did improve blood glucose levels. The authors conclude that the improvement is from enhanced pancreatic β-cell function. This study indicates that inhibition of IL-1β improves glucose metabolism, independent of insulin sensitivity.

TNF-α expression is elevated in the adipose tissue of obese rodents and humans. In animal studies, administration of exogenous TNF-α induced insulin resistance, whereas neutralization of TNF-α improved insulin sensitivity. TNF-α knockout mice were used to examine the role of TNF-α in obesity-associated insulin resistance[77]. The KO mice were compared with WT mice in lean and obese (induced by gold-thioglucose [GTG]-injection) conditions at 13, 19, and 28 weeks of age. In the lean condition, the KO mice exhibited a 14% reduction in body weight at 28 weeks of age. The epididymal fat pad was decreased by 25% in weight, relative to those of the wild-type littermate controls. Fasting glucose was reduced slightly by 10%, but the glucose response in an oral glucose tolerance test (OGTT) was not affected. In the obese condition, the body weight was identical between the KO and WT mice. Glucose levels were significantly increased in both groups during the OGTT. This indicates that the absence of TNF-α is not sufficient to protect mice from insulin resistance in obese conditions[77]. Some animal studies[78] and several clinical trials using TNF antagonism have thus far failed to improve insulin sensitivity[79–83]. These facts suggest that there are many unknowns in the relationship of obesity-associated inflammation and insulin resistance.

The role of IL-6 in the pathogenesis of obesity and insulin resistance is controversial. IL-6 knockout (KO) mice were compared with WT littermate mice in lean or obese conditions. IL-6 KO mice displayed obesity, hepatosteatosis, liver inflammation and insulin resistance when compared with the lean condition on a standard chow diet[84]. Overexpression of IL-6 was also used to test insulin resistance in mice. In the study, IL-6 overexpression was generated in skeletal muscle, and the IL-6 protein levels were increased in the circulation. The mice lost both body weight and body fat in response to IL-6 in this model, even though their food intake remained unchanged[85]. These observations suggest that IL-6 increases energy expenditure. In the IL-6 mice, insulin levels were elevated, and hypoglycemia was observed[85]. In another study, Sadagurski *et al* demonstrated that a high level of IL-6 in the circulation reduces obesity and improves metabolic homeostasis *in vivo*[86].

The role of the anti-inflammatory cytokine IL-10 has been studied in the pathogenesis of obesity and insulin resistance[87]. IL-10 is a critical cytokine of M2 (type 2) macrophages. A recent study has identified the roles of M1 (pro-inflammatory) and M2 (anti-inflammatory) macrophages in the regulation of insulin sensitivity[88]. An increase in M2 macrophages and a decrease in M1 macrophages within the adipose tissue are associated with enhanced insulin sensitivity. In another study, the hematopoietic-cell-restricted deletion of IL-10 in mice was used to study the relationship between IL-10 and insulin resistance[89]. The mice were assessed for insulin sensitivity in an insulin tolerance test in lean (chow diet) and obese (high fat diet) conditions. The results show that deletion of IL-10 from

the hematopoietic system does not have an effect on insulin resistance[89]. Other studies suggest that IL-10 cannot improve insulin sensitivity in diet-induced obese mice or humans[90, 91].

New potential drug candidates for insulin resistance

The antidiabetic drug thiazolidinedione (TZD) restores insulin action by activating PPARγ, thus lowering the levels of FFAs in the blood. Activation of PPARγ improves insulin sensitivity in rodents and humans through a combination of metabolic actions, including partitioning of lipid stores and regulating metabolic and inflammatory mediators, termed adipokines[92]. However, TZD-based medicines for insulin sensitization have many side effects: troglitazone (Rezulin) was associated with massive hepatic necrosis; rosiglitazone (Avandia) and muraglitazone, with increased cardiovascular events; and now, pioglitazone has been associated with bladder cancer[93]. These adverse events suggest that the thiazolidinedione-based drugs may not be safe in the long-run. It is necessary to discover a new class of drug to treat insulin resistance.

Recent studies indicate that histone deacetylase (HDAC) inhibitors may be a new class of drug candidates for insulin sensitization. HDACs are key enzymes in regulating gene expression. Protein acetylation is one type of epigenetic regulation of gene expression. Acetylation is controlled by histone acetyltransferases (HATs) and histone deacetylases (HDACs). Histone acetylation by HATs opens the chromatin structure to activate gene transcription, while histone deacetylases (HDACs) repress gene expression. HDACs are divided into three classes: class I HDACs (1, 2, 3, 8, 11), class II HDACs (4, 5, 6, 7, 9, 10)[94] and class III HDACs (SIRT1-7)[95]. Inhibition of histone deacetylase activity has been reported as a new approach to treat diabetes mellitus[96–98]. In our study, supplementation of histone deacetylase inhibitors, butyrate or Trichostatin A, prevented high-fat diet-induced obesity and improved insulin sensitivity in mice. HDAC inhibition promoted energy expenditure, and reduced blood glucose and triglyceride levels in mice[98]. HDAC inhibits insulin resistance on a molecular level by the following means: a) reducing the lipid toxicity[44, 99–102]; b) reducing chronic systemic inflammation[103–108]; c) promoting beta-cell development, proliferation, differentiation and function[97]; and d) promoting energy expenditure[98, 109]. Based on their multiple beneficial effects, HDAC inhibitors may represent a novel drug in the treatment of insulin resistance. However, clinical trials are needed to test this concept.

Conclusions

Type 2 diabetes is one of the major diseases associated with obesity. It is known that obesity promotes type 2 diabetes through insulin resistance, a state in which bodies lose their responsiveness to insulin. Many studies confirm that inflammation and free fatty acids (FFAs) are major pathogenic factors for insulin resistance in obese conditions. The most effective therapy for insulin resistance is to reduce both FFA and inflammation. Diminishing inflammation by anti-inflammatory drugs does not significantly improve insulin sensitivity in animal models or in clinical trials because inflammation is beneficial in regulating energy metabolism. Inhibiting this beneficial activity is likely to cause the failure of anti-inflammatory drugs in treating insulin resistance. Current literature consistently reports that fatty acids remain a therapeutic target in the treatment of insulin resistance. As an insulin sensitization-drug, TZD reduces both FFA and inflammation in the body. However, TZDs have many side effects such as obesity, heart attacks, and bladder cancer. HDAC inhibitors may be a new class of drug for treating insulin resistance by promoting energy expenditure and preventing obesity.

Acknowledgements

This work is partially supported by NIH grants DK068036 and DK085495 to Jian-ping YE and an NIH COBRE grant (2P20RR021945) and ADA grant (1-09-JF-17) to Zhan-guo GAO.

References

1 Hotamisligil GS, Shargill NS, Spiegelman BM. Adipose expression of tumor necrosis factor-alpha: direct role in obesity-linked insulin resistance. Science 1993; 259: 87–91.
2 Xu H, Barnes GT, Yang Q, Tan G, Yang D, Chou CJ, *et al*. Chronic inflammation in fat plays a crucial role in the development of obesity-related insulin resistance. J Clin Invest 2003; 112: 1821–30.
3 Weisberg SP, McCann D, Desai M, Rosenbaum M, Leibel RL, Ferrante AW Jr. Obesity is associated with macrophage accumulation in adipose tissue. J Clin Invest 2003; 112: 1796–808.
4 Ye J, Gao Z, Yin J, He Q. Hypoxia is a potential risk factor for chronic inflammation and adiponectin reduction in adipose tissue of ob/ob and dietary obese mice. Am J Physiol Endocrinol Metab 2007; 293: E1118–28.
5 Larsen OA, Lassen NA, Quaade F. Blood flow through human adipose tissue determined with radioactive xenon. Acta Physiol Scand 1966; 66: 337–45.
6 Crandall DL, Goldstein BM, Huggins F, Cervoni P. Adipocyte blood flow: influence of age, anatomic location, and dietary manipulation. Am J Physiol 1984; 247: R46–51.
7 West DB, Prinz WA, Francendese AA, Greenwood MR. Adipocyte blood flow is decreased in obese Zucker rats. Am J Physiol 1987; 253: R228–33.
8 Brose N, Rosenmund C. Move over protein kinase C, you've got company: alternative cellular effectors of diacylglycerol and phorbol esters. J Cell Sci 2002; 115: 4399–411.
9 Costanzi S, Neumann S, Gershengorn MC. Seven transmembrane-spanning receptors for free fatty acids as therapeutic targets for diabetes mellitus: pharmacological, phylogenetic, and drug discovery aspects. J Biol Chem 2008; 283: 16269–73.
10 Aldhahi W, Hamdy O. Adipokines, inflammation, and the endothelium in diabetes. Curr Diab Rep 2003; 3: 293–8.
11 Lee JY, Ye J, Gao Z, Youn HS, Lee WH, Zhao L, *et al*. Reciprocal modulation of Toll-like receptor-4 signaling pathways involving MyD88 and phosphatidylinositol 3-kinase/AKT by saturated and polyunsaturated fatty acids. J Biol Chem 2003; 278: 37041–51.
12 Weigert C, Brodbeck K, Staiger H, Kausch C, Machicao F, Häring HU, *et al*. Palmitate, but not unsaturated fatty acids, induces the expression of interleukin-6 in human myotubes through proteasome-dependent activation of nuclear factor-kappaB. J Biol Chem 2004; 279: 23942–52.

13 Gao Z, Zhang X, Zuberi A, Hwang D, Quon MJ, Lefevre M, *et al*. Inhibition of insulin sensitivity by free fatty acids requires activation of multiple serine kinases in 3T3-L1 adipocytes. Mol Endocrinol 2004; 18: 2024–34.
14 Nakamura T, Furuhashi M, Li P, Cao H, Tuncman G, Sonenberg N, *et al*. Double-stranded RNA-dependent protein kinase links pathogen sensing with stress and metabolic homeostasis. Cell 2010; 140: 338–48.
15 Ozcan U, Cao Q, Yilmaz E, Lee AH, Iwakoshi NN, Ozdelen E, *et al*. Endoplasmic reticulum stress links obesity, insulin action, and type 2 diabetes. Science 2004; 306: 457–61.
16 Hotamisligil GS, Arner P, Caro JF, Atkinson RL, Spiegelman BM. Increased adipose tissue expression of tumor necrosis factor-alpha in human obesity and insulin resistance. J Clin Invest 1995; 95: 2409–15.
17 Hotamisligil GS, Peraldi P, Budavari A, Ellis R, White MF, Spiegelman BM. IRS-1-mediated inhibition of insulin receptor tyrosine kinase activity in TNF-alpha- and obesity-induced insulin resistance. Science 1996; 271: 665–8.
18 Hotamisligil GS. The role of TNFalpha and TNF receptors in obesity and insulin resistance. J Intern Med 1999; 245: 621–5.
19 Peraldi P, Hotamisligil GS, Buurman WA, White MF, Spiegelman BM. Tumor necrosis factor (TNF)-alpha inhibits insulin signaling through stimulation of the p55 TNF receptor and activation of sphingomyelinase. J Biol Chem 1996; 271: 13018–22.
20 Aguirre V, Uchida T, Yenush L, Davis R, White MF. The c-Jun NH(2)-terminal kinase promotes insulin resistance during association with insulin receptor substrate-1 and phosphorylation of Ser(307). J Biol Chem 2000; 275: 9047–54.
21 Chitturi S, Farrell GC. Etiopathogenesis of nonalcoholic steatohepatitis. Semin Liver Dis 2001; 21: 27–41.
22 Gao Z, Hwang D, Bataille F, Lefevre M, York D, Quon MJ, *et al*. Serine phosphorylation of insulin receptor substrate 1 by inhibitor kappa B kinase complex. J Biol Chem 2002; 277: 48115–21.
23 De Fea K, Roth RA, Modulation of insulin receptor substrate-1 tyrosine phosphorylation and function by mitogen-activated protein kinase. J Biol Chem 1997; 272: 31400–6.
24 Engelman JA, Berg AH, Lewis RY, Lisanti MP, Scherer PE. Tumor necrosis factor alpha-mediated insulin resistance, but not dedifferentiation, is abrogated by MEK1/2 inhibitors in 3T3-L1 adipocytes. Mol Endocrinol 2000; 14: 1557–69.
25 Rui L, Aguirre V, Kim JK, Shulman GI, Lee A, Corbould A, *et al*. Insulin/IGF-1 and TNF-alpha stimulate phosphorylation of IRS-1 at inhibitory Ser307 via distinct pathways. J Clin Invest 2001; 107: 181–9.
26 De Fea K, Roth RA. Protein kinase C modulation of insulin receptor substrate-1 tyrosine phosphorylation requires serine 612. Biochemistry, 1997; 36: 12939–47.
27 Li Y, Soos TJ, Li X, Wu J, Degennaro M, Sun X, *et al*. Protein kinase C Theta inhibits insulin signaling by phosphorylating IRS1 at Ser(1101). J Biol Chem 2004; 279: 45304–7.
28 Ravichandran LV, Esposito DL, Chen J, Quon MJ. Protein kinase C-zeta phosphorylates insulin receptor substrate-1 and impairs its ability to activate phosphatidylinositol 3-kinase in response to insulin. J Biol Chem 2001; 276: 3543–9.
29 Paz K, Liu YF, Shorer H, Hemi R, LeRoith D, Quan M, *et al*. Phosphorylation of insulin receptor substrate-1 (IRS-1) by protein kinase B positively regulates IRS-1 function. J Biol Chem 1999; 274: 28816–22.
30 Eldar-Finkelman H, Krebs EG. Phosphorylation of insulin receptor substrate 1 by glycogen synthase kinase 3 impairs insulin action. Proc Natl Acad Sci U S A 1997; 94: 9660–4.
31 Ilouz R, Kowalsman N, Eisenstein M, Eldar-Finkelman H. Identification of novel glycogen synthase kinase-3beta substrate-interacting residues suggests a common mechanism for substrate recognition. J Biol Chem 2006; 281: 30621–30.
32 Liberman Z, Eldar-Finkelman H. Serine 332 phosphorylation of insulin receptor substrate-1 by glycogen synthase kinase-3 attenuates insulin signaling. J Biol Chem 2005; 280: 4422–8.
33 Kim JA, Yeh DC, Ver M, Li Y, Carranza A, Conrads TP, *et al*. Phosphorylation of Ser24 in the pleckstrin homology domain of insulin receptor substrate-1 by Mouse Pelle-like kinase/interleukin-1 receptor-associated kinase: cross-talk between inflammatory signaling and insulin signaling that may contribute to insulin resistance. J Biol Chem 2005; 280: 23173–83.
34 Ozes ON, Akca H, Mayo LD, Gustin JA, Maehama T, Dixon JE, *et al*. A phosphatidylinositol 3-kinase/Akt/mTOR pathway mediates and PTEN antagonizes tumor necrosis factor inhibition of insulin signaling through insulin receptor substrate-1. Proc Natl Acad Sci U S A 2001; 98: 4640–5.
35 Haruta T, Uno T, Kawahara J, Takano A, Egawa K, Sharma PM, *et al*. A rapamycin-sensitive pathway down-regulates insulin signaling via phosphorylation and proteasomal degradation of insulin receptor substrate-1. Mol Endocrinol 2000; 14: 783–94.
36 Zhang J, Gao Z, Yin J, Quon MJ, Ye J. S6K directly phosphorylates IRS-1 on Ser-270 to promote insulin resistance in response to TNF-(alpha) signaling through IKK2. J Biol Chem 2008; 283: 35375–82.
37 Arkan MC, Hevener AL, Greten FR, Maeda S, Li ZW, Long JM, *et al*. IKK-beta links inflammation to obesity-induced insulin resistance. Nat Med 2005; 11: 191–8.
38 Karin M, Ben-Neriah Y. Phosphorylation meets ubiquitination: the control of NF-[kappa]B activity. Annu Rev Immunol 2000; 18: 621–63.
39 Cummins EP, Berra E, Comerford KM, Ginouves A, Fitzgerald KT, Seeballuck F, et al. Prolyl hydroxylase-1 negatively regulates IkappaB kinase-beta, giving insight into hypoxia-induced NFkappaB activity. Proc Natl Acad Sci U S A 2006; 103: 18154–9.
40 Hacker H, Karin M. Regulation and function of IKK and IKK-related kinases. Sci STKE 2006; 2006: re13.
41 Baeuerle PA, Henkel T. Function and activation of NF-kappa B in the immune system. Annu Rev Immunol 1994; 12: 141–79.
42 Schmitz ML, Baeuerle PA. The p65 subunit is responsible for the strong transcription activating potential of NF-kappa B. EMBO J 1991; 10: 3805–17.
43 Bohuslav J, Kravchenko VV, Parry GC, Erlich JH, Gerondakis S, Mackman N, *et al*. Regulation of an essential innate immune response by the p50 subunit of NF-kappaB. J Clin Invest 1998; 102: 1645–52.
44 Gao Z, He Q, Peng B, Chiao PJ, Ye J. Regulation of nuclear translocation of HDAC3 by IkappaBalpha is required for tumor necrosis factor inhibition of peroxisome proliferator-activated receptor gamma function. J Biol Chem 2006; 281: 4540–7.
45 Boden G. Free fatty acids (FFA), a link between obesity and insulin resistance. Front Biosci 1998; 3: d169–75.
46 Ferrannini E, Barrett EJ, Bevilacqua S, DeFronzo RA. Effect of fatty acids on glucose production and utilization in man. J Clin Invest 1983; 72: 1737–47.
47 Griffin ME, Marcucci MJ, Cline GW, Bell K, Barucci N, Lee D, *et al*. Free fatty acid-induced insulin resistance is associated with activation of protein kinase C theta and alterations in the insulin signaling cascade. Diabetes 1999; 48: 1270–4.
48 Schmitz-Peiffer C, Oakes ND, Browne CL, Kraegen EW, Biden TJ.

Reversal of chronic alterations of skeletal muscle protein kinase C from fat-fed rats by BRL-49653. Am J Physiol 1997; 273: E915–21.
49 Delarue J, Magnan C. Free fatty acids and insulin resistance. Curr Opin Clin Nutr Metab Care 2007; 10: 142–8.
50 Thompson AL, Cooney GJ. Acyl-CoA inhibition of hexokinase in rat and human skeletal muscle is a potential mechanism of lipid-induced insulin resistance. Diabetes 2000; 49: 1761–5.
51 Utaka S, Avesani CM, Draibe SA, Kamimura MA, Andreoni S, Cuppari L. Inflammation is associated with increased energy expenditure in patients with chronic kidney disease. Am J Clin Nutr 2005; 82: 801–5.
52 Moldawer LL, Georgieff M, Lundholm K. Interleukin 1, tumour necrosis factor-alpha (cachectin) and the pathogenesis of cancer cachexia. Clin Physiol 1987; 7: 263–74.
53 Barot LR, Rombeau JL, Steinberg JJ, Crosby LO, Feurer ID, Mullen JL. Energy expenditure in patients with inflammatory bowel disease. Arch Surg 1981; 116: 460–2.
54 Chan AT, Fleming CR, O'Fallon WM, Huizenga KA. Estimated versus measured basal energy requirements in patients with Crohn's disease. Gastroenterology 1986; 91: 75–8.
55 Strasser F. Appraisal of current and experimental approaches to the treatment of cachexia. Curr Opin Support Palliat Care 2007; 1: 312–6.
56 Tisdale MJ. Biology of cachexia. J Natl Cancer Inst 1997; 89: 1763–73.
57 Tang T, Zhang J, Yin J, Staszkiewicz J, Gawronska-Kozak B, Jung DY, *et al*. Uncoupling of inflammation and insulin resistance by NF-kappaB in transgenic mice through elevated energy expenditure. J Biol Chem 2010; 285: 4637–44.
58 Gao Z, Yin J, Zhang J, He Q, McGuinness OP, Ye J. Inactivation of NF-kappaB p50 leads to insulin sensitization in liver through post-translational inhibition of p70S6K. J Biol Chem 2009; 284: 18368–76.
59 Pamir N, McMillen TS, Kaiyala KJ, Schwartz MW, LeBoeuf RC. Receptors for tumor necrosis factor-alpha play a protective role against obesity and alter adipose tissue macrophage status. Endocrinology 2009; 150: 4124–34.
60 Chida D, Osaka T, Hashimoto O, Iwakura Y. Combined interleukin-6 and interleukin-1 deficiency causes obesity in young mice. Diabetes 2006; 55: 971–7.
61 Wallenius V, Wallenius K, Ahrén B, Rudling M, Carlsten H, Dickson SL, *et al*. Interleukin-6-deficient mice develop mature-onset obesity. Nat Med 2002; 8: 75–9.
62 Ye J, Keller JN. Regulation of energy metabolism by inflammation: a feedback response in obesity and calorie restriction. Aging (Albany NY) 2010; 2: 361–8.
63 Kopp E, Ghosh S. Inhibition of NF-kappa B by sodium salicylate and aspirin. Science 1994; 265: 956–9.
64 Pierce JW, Read MA, Ding H, Luscinskas FW, Collins T. Salicylates inhibit I kappa B-alpha phosphorylation, endothelial-leukocyte adhesion molecule expression, and neutrophil transmigration. J Immunol 1996; 156: 3961–9.
65 Shoelson SE, Lee J, Goldfine AB. Inflammation and insulin resistance. J Clin Invest 2006; 116: 1793–801.
66 Williamson RT. On the treatment of glycosuria and diabetes mellitus with sodium salicylate. Br Med J 1901; 1: 760–2.
67 Yin MJ, Yamamoto Y, Gaynor RB. The anti-inflammatory agents aspirin and salicylate inhibit the activity of I(kappa)B kinase-beta. Nature 1998; 396: 77–80.
68 Gao Z, Zuberi A, Quon MJ, Dong Z, Ye J. Aspirin inhibits serine phosphorylation of insulin receptor substrate 1 in tumor necrosis factor-treated cells through targeting multiple serine kinases. J Biol Chem 2003; 278: 24944–50.
69 Dichtl W, Dulak J, Frick M, Alber HF, Schwarzacher SP, Ares MP, *et al*. HMG-CoA reductase inhibitors regulate inflammatory transcription factors in human endothelial and vascular smooth muscle cells. Arterioscler Thromb Vasc Biol 2003; 23: 58–63.
70 Chan DC, Watts GF, Barrett PH, Beilin LJ, Mori TA. Effect of atorvastatin and fish oil on plasma high-sensitivity C-reactive protein concentrations in individuals with visceral obesity. Clin Chem 2002; 48: 877–83.
71 Preiss D, Seshasai SR, Welsh P, Murphy SA, Ho JE, Waters DD, *et al*. Risk of incident diabetes with intensive-dose compared with moderate-dose statin therapy. JAMA 2011; 305: 2556–64.
72 Burén J, Liu HX, Jensen J, Eriksson JW. Dexamethasone impairs insulin signalling and glucose transport by depletion of insulin receptor substrate-1, phosphatidylinositol 3-kinase and protein kinase B in primary cultured rat adipocytes. Eur J Endocrinol 2002; 146: 419–29.
73 Perry CG, Spiers A, Cleland SJ, Lowe GD, Petrie JR, Connell JM. Glucocorticoids and insulin sensitivity: dissociation of insulin's metabolic and vascular actions. J Clin Endocrinol Metab 2003; 88: 6008–14.
74 Böni-Schnetzler M, Thorne J, Parnaud G, Marselli L, Ehses JA, Kerr-Conte J, *et al*. Increased interleukin (IL)-1beta messenger ribonucleic acid expression in beta-cells of individuals with type 2 diabetes and regulation of IL-1beta in human islets by glucose and autostimulation. J Clin Endocrinol Metab 2008; 93: 4065–74.
75 Dinarello CA. Biologic basis for interleukin-1 in disease. Blood 1996; 87: 2095–147.
76 Maedler K, Sergeev P, Ris F, Oberholzer J, Joller-Jemelka HI, Spinas GA, *et al*. Glucose-induced beta cell production of IL-1beta contributes to glucotoxicity in human pancreatic islets. J Clin Invest 2002; 110: 851–60.
77 Ventre J, Doebber T, Wu M, MacNaul K, Stevens K, Pasparakis M,, *et al*. Targeted disruption of the tumor necrosis factor-alpha gene: metabolic consequences in obese and nonobese mice. Diabetes 1997; 46: 1526–31.
78 Schreyer SA, Chua Jr SC, LeBoeuf RC. Obesity and diabetes in TNF-alpha receptor-deficient mice. J Clin Invest 1998; 102: 402–11.
79 Dominguez H, Storgaard H, Rask-Madsen C, Steffen Hermann T, Ihlemann N, Baunbjerg Nielsen D, *et al*. Metabolic and vascular effects of tumor necrosis factor-alpha blockade with etanercept in obese patients with type 2 diabetes. J Vasc Res 2005; 42: 517–25.
80 Lo J, Bernstein LE, Canavan B, Torriani M, Jackson MB, Ahima RS, *et al*. Effects of TNF-alpha neutralization on adipocytokines and skeletal muscle adiposity in the metabolic syndrome. Am J Physiol Endocrinol Metab 2007; 293: E102–9.
81 Ofei F, Hurel S, Newkirk J, Sopwith M, Taylor R. Effects of an engineered human anti-TNF-alpha antibody (CDP571) on insulin sensitivity and glycemic control in patients with NIDDM. Diabetes 1996; 45: 881–5.
82 Paquot N, Castillo MJ, Lefèbvre PJ, Scheen AJ. No increased insulin sensitivity after a single intravenous administration of a recombinant human tumor necrosis factor receptor: Fc fusion protein in obese insulin-resistant patients. J Clin Endocrinol Metab 2000; 85: 1316–9.
83 Rosenvinge A, Krogh-Madsen R, Baslund B, Pedersen BK. Insulin resistance in patients with rheumatoid arthritis: effect of anti-TNFalpha therapy. Scand J Rheumatol 2007; 36: 91–6.
84 Matthews VB, Allen TL, Risis S, Chan MH, Henstridge DC, Watson N, *et al*. Interleukin-6-deficient mice develop hepatic inflammation and systemic insulin resistance. Diabetologia 2010; 53: 2431–41.

85 Franckhauser S, Elias I, Rotter Sopasakis V, Ferré T, Nagaev I, Andersson CX, *et al*. Overexpression of Il6 leads to hyperinsulinaemia, liver inflammation and reduced body weight in mice. Diabetologia 2008; 51: 1306–16.
86 Sadagurski M, Norquay L, Farhang J, D'Aquino K, Copps K, White MF. Human IL6 enhances leptin action in mice. Diabetologia 2010; 53: 525–35.
87 Hong EG, Ko HJ, Cho YR, Kim HJ, Ma Z, Yu TY, *et al*. Interleukin-10 prevents diet-induced insulin resistance by attenuating macrophage and cytokine response in skeletal muscle. Diabetes 2009; 58: 2525–35.
88 Fujisaka S, Usui I, Bukhari A, Ikutani M, Oya T, Kanatani Y, *et al*. Regulatory mechanisms for adipose tissue M1 and M2 macrophages in diet-induced obese mice. Diabetes 2009; 58: 2574–82.
89 Kowalski GM, Nicholls HT, Risis S, Watson NK, Kanellakis P, Bruce CR, *et al*. Deficiency of haematopoietic-cell-derived IL-10 does not exacerbate high-fat-diet-induced inflammation or insulin resistance in mice. Diabetologia 2011; 54: 888–99.
90 den Boer MA, Voshol PJ, Schröder-van der Elst JP, Korsheninnikova E, Ouwens DM, Kuipers F, *et al*. Endogenous interleukin-10 protects against hepatic steatosis but does not improve insulin sensitivity during high-fat feeding in mice. Endocrinology 2006; 147: 4553–8.
91 Kohl A, Gögebakan O, Möhlig M, Osterhoff M, Isken F, Pfeiffer AF, *et al*. Increased interleukin-10 but unchanged insulin sensitivity after 4 weeks of (1,3)(1,6)-beta-glycan consumption in overweight humans. Nutr Res 2009; 29: 248–54.
92 Tontonoz P, Spiegelman BM. Fat and beyond: the diverse biology of PPARgamma. Annu Rev Biochem 2008; 77: 289–312.
93 Ferrara A, Lewis JD, Quesenberry CP Jr, Peng T, Strom BL, Van Den Eeden SK, *et al*. Cohort study of pioglitazone and cancer incidence in patients with diabetes. Diabetes Care 2011; 34: 923–9.
94 Huang EY, Zhang J, Miska EA, Guenther MG, Kouzarides T, Lazar MA. Nuclear receptor corepressors partner with class II histone deacetylases in a Sin3-independent repression pathway. Genes Dev 2000; 14: 45–54.
95 Blander G, Guarente L. The Sir2 family of protein deacetylases. Annu Rev Biochem 2004; 73: 417–35.
96 Gilbert RE, Huang Q, Thai K, Advani SL, Lee K, Yuen DA, *et al*. Histone deacetylase inhibition attenuates diabetes-associated kidney growth: potential role for epigenetic modification of the epidermal growth factor receptor. Kidney Int 2011; 79: 1312–21.
97 Christensen DP, Dahllöf M, Lundh M, Rasmussen DN, Nielsen MD, Billestrup N, *et al*. Histone deacetylase (HDAC) inhibition as a novel treatment for diabetes mellitus. Mol Med 2011; 17: 378–390.
98 Gao Z, Yin J, Zhang J, Ward RE, Martin RJ, Lefevre M, *et al*. Butyrate improves insulin sensitivity and increases energy expenditure in mice. Diabetes 2009; 58: 1509–17.
99 Fajas L, Egler V, Reiter R, Hansen J, Kristiansen K, Debril MB, *et al*. The retinoblastoma-histone deacetylase 3 complex inhibits PPARgamma and adipocyte differentiation. Dev Cell 2002; 3: 903–10.
100 Guan HP, Ishizuka T, Chui PC, Lehrke M, Lazar MA. Corepressors selectively control the transcriptional activity of PPARgamma in adipocytes. Genes Dev 2005; 19: 453–61.
101 Miard S, Fajas L. Atypical transcriptional regulators and cofactors of PPARgamma. Int J Obes (Lond) 2005; 29: S10–2.
102 Zhang J, Henagan TM, Gao Z, Ye J. Inhibition of glyceroneogenesis by histone deacetylase 3 contributes to lipodystrophy in mice with adipose tissue inflammation. Endocrinology 2011; 152: 1829–38.
103 Rahman I. Oxidative stress, transcription factors and chromatin remodelling in lung inflammation. Biochem Pharmacol 2002; 64: 935–42.
104 Adcock IM, Ito K, Barnes PJ. Histone deacetylation: an important mechanism in inflammatory lung diseases. COPD 2005; 2: 445–55.
105 Blanchard F, Chipoy C. Histone deacetylase inhibitors: new drugs for the treatment of inflammatory diseases? Drug Discov Today 2005; 10: 197–204.
106 Dinarello CA. Inhibitors of histone deacetylases as anti-inflammatory drugs. Ernst Schering Res Found Workshop 2006; 56: 45–60.
107 Zhang L, Fang H, Xu W. Strategies in developing promising histone deacetylase inhibitors. Med Res Rev 2010; 30: 585–602.
108 Shakespear MR, Halili MA, Irvine KM, Fairlie DP, Sweet MJ. Histone deacetylases as regulators of inflammation and immunity. Trends Immunol 2011; 32: 335–43.
109 McGee SL, Hargreaves M. Histone modifications and exercise adaptations. J Appl Physiol 2011; 110: 258–63.

Acta Pharmacologica Sinica (2012) 33: 189–193
 1671-4083/12 $32.00
www.nature.com/aps

Review

Childhood obesity: a life-long health risk

Matthias BARTON*

Molecular Internal Medicine, University of Zürich, LTK Y44 G22, Winterthurerstrasse 190, 8057 Zürich, Switzerland

Childhood obesity has become major health concern for physicians, parents, and health agencies around the world. Childhood obesity is associated with an increased risk for other diseases not only during youth but also later in life, including diabetes, arterial hypertension, coronary artery disease, and fatty liver disease. Importantly, obesity accelerates atherosclerosis progression already in children and young adults. With regard to pathophysiological changes in the vasculature, the striking similarities between physiological changes related to aging and obesity-related abnormalities are compatible with the concept that obesity causes "premature" vascular aging. This article reviews factors underlying the accelerated vascular disease development due to obesity. It also highlights the importance of recognizing childhood obesity as a disease condition and its permissive role in aggravating the development of other diseases. The importance of childhood obesity for disease susceptibility later in life, and the need for prevention and treatment are also discussed.

Keywords: atherosclerosis; non-alcoholic steatohepatitis; diabetes; insulin resistance; stroke; myocardial infarction; physical exercise; cardiovascular risk; hypertension; vascular programming

Acta Pharmacologica Sinica (2012) 33: 189–193; doi: 10.1038/aps.2011.204

Childhood obesity: a health problem gone global

Childhood obesity has been of medical interest for more than 150 years[1, 2]. Until the middle of the 20th century the prevalence of obesity in the general population of the United States was relatively moderate[3]. However, in the last two decades the prevalence has risen to epidemic proportions[4–6]. In fact, 34.4 percent of the population of the United States are now considered overweight (and not obese) and 33.9 percent are considered to be obese[7], affecting more than 200 million people. Similarly, the number of children diagnosed with obesity and/or obesity-related diabetes has been continuously increasing over the past 20 years in countries around the world[8–10]. In 2010 in the United States, 17 percent of children and adolescents were obese – including those with severe obesity[11], with the prevalence of obesity having tripled since 1980[3]. Particularly worrisome is the 10.4% prevalence of obesity among the 2 to 5 year olds in the US[12], with other parts of the world catching up[13, 14]. The World Health Organization (WHO) defines obesity (in adults: BMI >30 kg/m^2) as a disease for which excessive calorie intake, in conjunction with lack of physical exercise, have been identified as major predisposing and aggravating factors[15, 16]. Obesity also serves as soil for the development of other diseases[15], particularly insulin resistance (pre-diabetes), type 2 diabetes mellitus, arterial hypertension, dyslipidemia/hypertriglyceridemia, and fatty liver disease/non-alcoholic steatohepatitis (NASH)[15, 17, 18]. At the same time, obesity also worsens these conditions once they have developed [15]. In addition, mutations in certain genes such as the leptin receptor are associated with early-onset childhood obesity and excessive body mass indices[19–21]. High birth weights or diabetes of the mother (pregnancy-associated diabetes) have been proposed as potential factors affecting postnatal health, and lack of breastfeeding has been suggested to contribute to a higher risk for obesity during adolescence[22]. A number of other factors have been associated with a higher risk to develop obesity, which include the disease susceptibility of certain ethnic groups, poverty and/or low socioeconomic status, which are often associated with a low health concerns/self-concern[3, 7]. By contrast, some Asian countries such as Japan which have a very low overall prevalence of obesity[23]. This may be in part due to composition of Asian diets, while excess access to inexpensive, high calorie food has been identified as a major factor contributing to the rising number of obese children in countries such as the USA and in European countries[24]. Not surprisingly, childhood obesity has also been steadily growing in China where over the past decades people have in part adopted Western dietary patterns[24]. Increased health risk is not limited to obesity, but already apparent with overweight. Indeed, long-term studies following the health of overweight children for more than 40 years found significantly increased risks for a number of diseases [25] (Figure 1).

* To whom correspondence should be addressed.
E-mail barton@access.uzh.ch
Received 2011-12-02 Accepted 2011-12-26

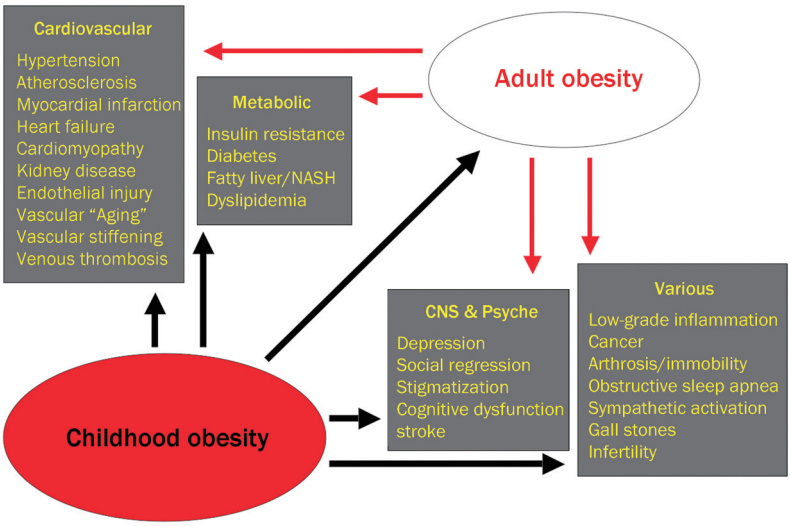

Figure 1. Aggravating effect of childhood obesity on the life-time risk for other disease conditions, including a greater risk for adult obesity, which itself continues to worsen disease development.

Atherosclerosis begins in childhood

Obese children are at a higher risk for accelerated development of vascular disease[26], which is aggravated by the worsening of risk factors secondary to obesity. Atherosclerosis, a systemic chronic inflammatory disease of the large arteries, is the main cause of cardiovascular and cerebrovascular events[27]. The disease accounts for the majority of deaths due to myocardial infarction and stroke in Western as well as in Eastern and developing countries[27]. First vascular abnormalities, inflammatory changes and plaque development can be observed in children already in the first year of life[28]; consistent with these observations, the disease process begins in utero, during which the precursor of the atherosclerotic plaque — the "fatty streak" — is already present[29, 30]. The development of fatty streaks, which represent inflammatory accumulations of macrophages in the subintimal space — is aggravated by maternal hypercholesterolemia and thus sets the basis for vascular disease later in life[30]. The cause of cardiovascular and cerebrovascular events most often is due to rupture of "soft" atherosclerotic plaques filled with a lipid core underlying a thinned fibrous cap[27], pathological findings some of which are already present in young adults[26, 31]. Plaque development is accelerated in the presence of risk factors such as arterial hypertension, dyslipidemia, diabetes, male sex, and obesity, which are equally important for children and adults[26, 31]. Interestingly, girls and young women appear to be largely protected from the aggravating effect of obesity on plaque progression[26]. Among all cardiovascular risk factors, obesity is of particular importance since it aggravates several other risk factors such as arterial hypertension, insulin resistance/diabetes, or dyslipidemia.

Childhood obesity causes changes consistent with "Premature" vascular aging

Inflammation also plays a role for insulin resistance and metabolic changes associated with obesity[32] and abnormal inflammatory activation has been reported to occur in obese children[33]. In both children and adults, obesity causes generalized injury to the vasculature. This process also involves inflammatory activation, both locally in the vascular wall[32] as well as in adipose tissue[34]. Inflammation also underlies insulin resistance (pre-diabetes) and type 2 diabetes[34], conditions originally believed to be restricted to elderly individuals, but now increasingly found in obese juveniles[35, 36]. Similarly, an important aspect of obesity-associated vascular injury obtained from preclinical and clinical studies, is that many of the vascular changes found in obesity are highly similar to those seen with aging[37], which not only represents a physiological process but in itself represents a strong and independent risk factor for future cardiovascular events[37]. As with aging[37], experimental or human obesity shows an attenuation of endothelium-dependent vasodilation[38, 39], a decrease in NO bioactivity[38, 39] in conjunction with NO synthase uncoupling[37], an increase in prostanoid-mediated endothelium-dependent contractions[40–42], telomere shortening[43–46], increased vascular stiffness[47], and increased arterial intima-media thickness[26, 48]. Obesity also increases tissue levels of endothelin-1[38, 49, 50], a strong vasoconstrictor peptide and atherogenic growth factor and proinflammatory stimulus[51]. Picard and Guarente recently reported interactions between life-span regulating genes and adipose tissue functions[52]. Thus, obesity can be considered a process which is compatible with accelerated aging which may — at least in part — explain the accelerated atherosclerosis development in children and young adults with obesity[26].

Potential role for post-natal dietary vascular programming

A few years ago results from two clinical studies were reported that childhood obesity is associated with a several fold increased risk for cardiovascular events in adult life, even if body weight had meanwhile normalized[9, 53, 54]. These very intriguing observations, which are in part supported by an earlier study[55], not only emphasize the importance of childhood obesity prevention but also suggest that still unknown mechanisms exist that must be set-off by the "childhood obesity

environment" and, once activated, remain irreversibly active until later in life irrespective of changes in body weight. Thus, possible local "post-natal dietary programming" mechanisms may contribute to the underlying disease-promoting process in the arterial wall. Alternatively, acceletated progression of atherosclerosis in youth due to obesity may simply lead to established, irreversible atherosclerotic lesions that no longer can be affected by weight normalization. Indeed, advanced coronary artery disease present in their late teenage years and death from myocardial infarction has been described in young men exposed to extremely high stress conditions[56, 57].

Continued need for disease prevention

Aside from highly complex disease processes, simple factors such as overnutrition and lack of knowledge about obesity prevention, respectively, are likely to be at least equally important. This can be exemplified by a case report from Germany where parents fed their infant almost exclusively with sugared water[58]. This infant developed severe obesity and at 2 years of age, was diagnosed with early cerebrovascular disease[58] similar to increased vascular stiffening found in obese juveniles[59], conditions normally found only at much later stages in life. Not surprisingly, reducing body weight in obese juveniles is associated with markedly improved cognitive function[60], and recent data suggest that even cerebral and cerebellar development is negatively affected by childhood obesity[61]. Thus, awareness and education of parents[12], educators, and pediatric medical staff should remain one of the key goals in order to achieve prevention of childhood obesity which, subsequently, should also result in a reduction of diseases associated with it. One of the questions is how we can monitor vascular health. The function of the vasculature, particularly endothelium-dependent vasomotion, reflects quite well the overall health status of the arterial system[62]. Human obesity, characterized by accumulation of ectopic (particularly visceral) fat[63], is associated with abnormal endothelium-dependent vasomotion and enhanced contractility to endothelin-1[64, 65]. Accordingly, a reduction in energy intake[66] or reduction in body weight[67] improves vascular function in obese patients. In human resistance arteries obesity is associated with vascular hypertrophy as indicated by an increased media-to-lumen ratio[68], and a recent important study demonstrated that functional vascular abnormalities observed in obese individuals can be largely normalized by lowering body weight by reducing intra-abdominal fat mass in adults[67]. Thus, any reduction of obesity — in children as well as adults — is likely to translate into improved overall health and survival[4, 15, 69]. Indeed, preserved endothelium-dependent vasoreactivity is associated with greater survival in patients with cardiovascular disease[62]. Possibly, reducing subcutaneous fat may also have some beneficial effect on the pro-inflammatory risk profile[70, 71].

Physical activity as therapeutic

The question remains of how to achieve a sustained reduction of childhood obesity, both at the individual level as well as for overall prevalence[72]. One of the central components of obesity prevention and therapy or – if absent a promotor of obesity — is physical exercise[4, 73–75]. Physical inactivity is a key cause contributing to and worsening childhood obesity[76], and has now even become a concern in developing countries[77]. Exercise not only has a number of beneficial effects on several risk factors associated with obesity (reduction of sympathetic activation and blood pressure, improved lipid profile, improved insulin sensitivity[4, 73–75]), but also improves consumption of excess energy stores of fat and thus helps to reduce adipose tissue mass[78]. There is recent evidence that regular exercise may even infer with cellular processes associated with vascular aging[79]. A most recent study indicates that vascular elasticity as a function of age is also increased in obese children compared with their lean counterparts[80], indicative of accelerated vascular growth and maturation and thus compatible with early aging. It is important, both for therapy and prevention of childhood obesity, that sufficient and regular exercise becomes and remains a part of children's everyday life in conjunction with normal calorie intake. It has been recently shown that weight loss in children reduces inflammatory activation[81], one of the key factors for vascular disease progression[82]. Caloric restriction prolongs life in a number of species, including rodents and primates[83, 84]. It can only be speculated that in humans "global caloric restriction" in those countries with excess access to food would have similar effects on life expectancy and overall well-being[5]. Indeed some countries have taken political measures such as issuing special taxes on fat as the dietary componant with highest energy value[85, 86]. The prevention of childhood obesity is a chance that must be taken early in life by parents, health professionals, educators, and politicians[69]. Fortunately, health agencies have already begun to implement this need into their information policies provided to parents[12] with whom children spend the most time. If we succeed with this task of promoting, achieving, and maintaining health among children — including a regular "regimen" of physical exercise[16, 87, 88] —, this will ultimately reduce the number of tomorrow's patients and enable healthy aging at a low cardiovascular risk[89].

Acknowledgements

The project was supported by the Swiss National Science Foundation (Projects Nr 108 258 and Nr 122 504).

References

1 Don WG. Remarkable case of obesity in a hindoo boy aged twelve years. Lancet 1859; 73: 363.
2 Ellis RW, Tallermann KM. Obesity in childhood: A study of fifty cases. Lancet 1934; ii: 615–20.
3 http://www.cdc.gov/obesity/data/trends.html (accessed Dec 1, 2011).
4 Barton M, Furrer J. Cardiovascular consequences of the obesity pandemic: need for action. Expert Opin Investig Drugs 2003; 12: 1757–9.
5 Olshansky SJ, Passaro DJ, Hershow RC, Layden J, Carnes BA, Brody J, *et al*. A potential decline in life expectancy in the United States in the 21st century. N Engl J Med 2005; 352: 1138–45.

6 Stewart ST, Cutler DM, Rosen AB. Forecasting the effects of obesity and smoking on U.S. life expectancy. N Engl J Med 2009; 361: 2252–60.
7 http://www.cdc.gov/obesity/data/index.html (accessed Dec 1, 2011).
8 Yanovski JA. Pediatric obesity. Rev Endocr Metab Disord 2001; 2: 371–83.
9 Ludwig DS. Childhood obesity — the shape of things to come. N Engl J Med 2007; 357: 2325–7.
10 Wright C. A US epidemic: childhood obesity. J Physician Assist Educ 2011; 21: 39–41.
11 Skelton JA, Cook SR, Auinger P, Klein JD, Barlow SE. Prevalence and trends of severe obesity among US children and adolescents. Acad Pediatr 2009; 9: 322–9.
12 http://www.cdc.gov/healthyweight/children/index.html (accessed December 1, 2011).
13 Lobstein T, Baur L, Uauy R. Obesity in children and young people: a crisis in public health. Obes Rev 2004; 5: 4–104.
14 Lobstein T. The prevention of obesity in children. Pediatr Endocrinol Rev 2004; 1: 471–5.
15 Daniels SR, Pratt CA, Hayman LL. Reduction of risk for cardiovascular disease in children and adolescents. Circulation 2011; 124: 1673–86.
16 Nadeau KJ, Maahs DM, Daniels SR, Eckel RH. Childhood obesity and cardiovascular disease: links and prevention strategies. Nat Rev Cardiol 2011; 8: 513–25.
17 Schattenberg JM, Schuppan D. Nonalcoholic steatohepatitis: the therapeutic challenge of a global epidemic. Curr Opin Lipidol 2010; 22: 479–88.
18 Ahmed MH, Abu EO, Byrne CD. Non-alcoholic fatty liver disease (NAFLD): new challenge for general practitioners and important burden for health authorities? Prim Care Diabetes 2010; 4: 129–37.
19 O'Rahilly S. Human obesity and insulin resistance: Lessons from human genetics. Clin Biochem 2011; 44: 451.
20 O'Rahilly S. Human genetics illuminates the paths to metabolic disease. Nature 2009; 462: 307–14.
21 O'Rahilly S, Farooqi IS. Human obesity as a heritable disorder of the central control of energy balance. Int J Obes (Lond) 2008; 32: S55–61.
22 Gillman MW, Rifas-Shiman SL, Camargo CA Jr, Berkey CS, Frazier AL, Rockett HR, *et al*. Risk of overweight among adolescents who were breast fed as infants. JAMA 2001; 285: 2461–7.
23 Fujita T. The metabolic syndrome in Japan. Nat Clin Pract Cardiovasc Med 2008; 5: S15–8.
24 McLellan F. Obesity rising to alarming levels around the world. Lancet 2002; 359: 1412.
25 Mossberg HO. 40-Year follow-up of overweight children. Lancet 1989; 334: 491–3.
26 McGill HC Jr, McMahan CA, Herderick EE, Zieske AW, Malcom GT, Tracy RE, *et al*. Obesity accelerates the progression of coronary atherosclerosis in young men. Circulation 2002; 105: 2712–8.
27 Libby P. Atherosclerosis: the new view. Sci Am 2002; 286: 46–55.
28 Zinserling WD. Untersuchungen über Atherosklerose. 1. Über die Aortaverfettungen bei Kindern. Virchows Arch f Path Anat 1925; 255: 677–705.
29 Napoli C, D'Armiento FP, Mancini FP, Postiglione A, Witztum JL, Palumbo G, *et al*. Fatty streak formation occurs in human fetal aortas and is greatly enhanced by maternal hypercholesterolemia. Intimal accumulation of low density lipoprotein and its oxidation precede monocyte recruitment into early atherosclerotic lesions. J Clin Invest 1997; 100: 2680–90.
30 Napoli C, Glass CK, Witztum JL, Deutsch R, D'Armiento FP, Palinski W. Influence of maternal hypercholesterolaemia during pregnancy on progression of early atherosclerotic lesions in childhood: Fate of Early Lesions in Children (FELIC) study. Lancet 1999; 354: 1234–41.
31 McGill HC Jr, McMahan CA, Zieske AW, Sloop GD, Walcott JV, Troxclair DA, *et al*. Associations of coronary heart disease risk factors with the intermediate lesion of atherosclerosis in youth. The Pathobiological Determinants of Atherosclerosis in Youth (PDAY) Research Group. Arterioscler Thromb Vasc Biol 2000; 20: 1998–2004.
32 Greenstein AS, Khavandi K, Withers SB, Sonoyama K, Clancy O, Jeziorska M, *et al*. Local inflammation and hypoxia abolish the protective anticontractile properties of perivascular fat in obese patients. Circulation 2009; 119: 1661–70.
33 Kapiotis S, Holzer G, Schaller G, Haumer M, Widhalm H, Weghuber D, *et al*. A proinflammatory state is detectable in obese children and is accompanied by functional and morphological vascular changes. Arterioscler Thromb Vasc Biol 2006; 26: 2541–6.
34 Xu H, Barnes GT, Yang Q, Tan G, Yang D, Chou CJ, *et al*. Chronic inflammation in fat plays a crucial role in the development of obesity-related insulin resistance. J Clin Invest 2003; 112: 1821–30.
35 Sinha R, Fisch G, Teague B, Tamborlane WV, Banyas B, Allen K, *et al*. Prevalence of impaired glucose tolerance among children and adolescents with marked obesity. N Engl J Med 2002; 346: 802–10.
36 Rocchini AP. Childhood obesity and a diabetes epidemic. N Engl J Med 2002; 346: 854–5.
37 Barton M. Obesity and aging: determinants of endothelial cell dysfunction and atherosclerosis. Pflugers Arch 2010; 460: 825–37.
38 Damjanovic M, Barton M. Fat intake and cardiovascular response. Curr Hypertens Rep 2008; 10: 25–31.
39 Naderali EK, Brown MJ, Pickavance LC, Wilding JP, Doyle PJ, Williams G. Dietary obesity in the rat induces endothelial dysfunction without causing insulin resistance: a possible role for triacylglycerols. Clin Sci (Lond) 2001; 101: 499–506.
40 Traupe T, Lang M, Goettsch W, Munter K, Morawietz H, Vetter W, *et al*. Obesity increases prostanoid-mediated vasoconstriction and vascular thromboxane receptor gene expression. J Hypertens 2002; 20: 2239–45.
41 Traupe T, D'Uscio L, Muenter K, Morawietz H, Vetter W, Barton M. Effects of obesity on endothelium-dependent reactivity during acute nitric oxide synthase inhibition: modulatory role of endothelin. Clin Sci (Lond) 2002; 103: 13S–5S.
42 Bhattacharya I, Damjanovic M, Gut A, Hager S, Perez-Dominguez A, Minotti R, *et al*. Childhood obesity induced by a high-fat diet causes premature vascular aging involving endothelium-dependent mechanisms. Hypertension 2008; 52: e89.
43 Buxton JL, Walters RG, Visvikis-Siest S, Meyre D, Froguel P, Blakemore AI. Childhood obesity is associated with shorter leukocyte telomere length. J Clin Endocrinol Metab 2011; 96: 1500–5.
44 Niemann B, Chen Y, Teschner M, Li L, Silber RE, Rohrbach S. Obesity induces signs of premature cardiac aging in younger patients: the role of mitochondria. J Am Coll Cardiol 2011; 57: 577–85.
45 Lee M, Martin H, Firpo MA, Demerath EW. Inverse association between adiposity and telomere length: The Fels Longitudinal Study. Am J Hum Biol 2011; 23: 100–6.
46 Diaz VA, Mainous AG, Player MS, Everett CJ. Telomere length and adiposity in a racially diverse sample. Int J Obes (Lond) 2010; 34: 261–5.
47 Tounian P, Aggoun Y, Dubern B, Varille V, Guy-Grand B, Sidi D, *et al*. Presence of increased stiffness of the common carotid artery and endothelial dysfunction in severely obese children: a prospective study. Lancet 2001; 358: 1400–4.
48 Woo KS, Chook P, Yu CW, Sung RY, Qiao M, Leung SS, *et al*. Overweight in children is associated with arterial endothelial dysfunction and intima-media thickening. Int J Obes Relat Metab Disord

2004; 28: 852–7.
49 Barton M, Carmona R, Morawietz H, d'Uscio LV, Goettsch W, Hillen H, *et al*. Obesity is associated with tissue-specific activation of renal angiotensin-converting enzyme *in vivo*: evidence for a regulatory role of endothelin. Hypertension 2000; 35: 329–36.
50 Barton M, Carmona R, Ortmann J, Krieger JE, Traupe T. Obesity-associated activation of angiotensin and endothelin in the cardiovascular system. Int J Biochem Cell Biol 2003; 35: 826–37.
51 Barton M, Yanagisawa M. Endothelin: 20 years from discovery to therapy. Can J Physiol Pharmacol 2008; 86: 485–98.
52 Picard F, Guarente L. Molecular links between aging and adipose tissue. Int J Obes Relat Metab Disord 2005; 29: S36–9.
53 Bibbins-Domingo K, Coxson P, Pletcher MJ, Lightwood J, Goldman L. Adolescent overweight and future adult coronary heart disease. N Engl J Med 2007; 357: 2371–9.
54 Baker JL, Olsen LW, Sorensen TI. Childhood body-mass index and the risk of coronary heart disease in adulthood. N Engl J Med 2007; 357: 2329–37.
55 Gunnell DJ, Frankel SJ, Nanchahal K, Peters TJ, Davey Smith G. Childhood obesity and adult cardiovascular mortality: a 57-y follow-up study based on the Boyd Orr cohort. Am J Clin Nutr 1998; 67: 1111–8.
56 Enos WF, Beyer JC, Holmes R. Pathogenesis of the coronary disease in the American soldiers killed in Korea. JAMA 1955; 158: 912–5.
57 McNamara J, Molot M, Stremple J, Cutting R. Coronary artery disease in combat casualities in Vietnam. JAMA 1971; 216: 1185–7.
58 Weghuber D, Zaknun D, Nasel C, Willforth-Ehringer A, Muller T, Boriss-Riedl M, *et al*. Early cerebrovascular disease in a 2-year-old with extreme obesity and complete metabolic syndrome due to feeding of excessively high amounts of energy. Eur J Pediatr 2007; 166: 37–41.
59 Gungor N, Thompson T, Sutton-Tyrrell K, Janosky J, Arslanian S. Early signs of cardiovascular disease in youth with obesity and type 2 diabetes. Diabetes Care 2005; 28: 1219–21.
60 Barton SB, Walker LL, Lambert G, Gately PJ, Hill AJ. Cognitive change in obese adolescents losing weight. Obes Res 2004; 12: 313–9.
61 Miller JL, Couch J, Schwenk K, Long M, Towler S, Theriaque DW, *et al*. Early childhood obesity is associated with compromised cerebellar development. Dev Neuropsychol 2009; 34: 272–83.
62 Herrmann J, Lerman A. The endothelium — the cardiovascular health barometer. Herz 2008; 33: 343–53.
63 Britton KA, Fox CS. Ectopic fat depots and cardiovascular disease. Circulation 2011; 124: e837–41.
64 Cardillo C, Campia U, Iantorno M, Panza JA. Enhanced vascular activity of endogenous endothelin-1 in obese hypertensive patients. Hypertension 2004; 43: 36–40.
65 Georgescu A, Popov D, Constantin A, Nemecz M, Alexandru N, Cochior D, *et al*. Dysfunction of human subcutaneous fat arterioles in obesity alone or obesity associated with type 2 diabetes. Clin Sci (Lond) 2011; 120: 463–72.
66 Dessi-Fulgheri P, Sarzani R, Serenelli M, Tamburrini P, Spagnolo D, Giantomassi L, *et al*. Low calorie diet enhances renal, hemodynamic, and humoral effects of exogenous atrial natriuretic peptide in obese hypertensives. Hypertension 1999; 33: 658–62.
67 De Ciuceis C, Porteri E, Rizzoni D, Corbellini C, La Boria E, Boari GE, *et al*. Effects of weight loss on structural and functional alterations of subcutaneous small arteries in obese patients. Hypertension 2011; 58: 29–36.
68 Rizzoni D, De Ciuceis C, Porteri E, Semeraro F, Rosei EA. Structural alterations in small resistance arteries in obesity. Basic Clin Pharmacol Toxicol 2012; 110: 56–62.
69 Poirier P, Giles TD, Bray GA, Hong Y, Stern JS, Pi-Sunyer FX, *et al*. Obesity and cardiovascular disease: pathophysiology, evaluation, and effect of weight loss: an update of the 1997 American Heart Association Scientific Statement on Obesity and Heart Disease from the Obesity Committee of the Council on Nutrition, Physical Activity, and Metabolism. Circulation 2006; 113: 898–918.
70 Hamdy O, Porramatikul S, Al-Ozairi E. Metabolic obesity: the paradox between visceral and subcutaneous fat. Curr Diabetes Rev 2006; 2: 367–73.
71 Marfella R, Grella R, Rizzo MR, Barbieri M, Ferraraccio F, Cacciapuoti F, *et al*. Role of subcutaneous abdominal fat on cardiac function and proinflammatory cytokines in premenopausal obese women. Ann Plast Surg 2009; 63: 490–5.
72 Wieting JM. Cause and effect in childhood obesity: solutions for a national epidemic. J Am Osteopath Assoc 2008; 108: 545–52.
73 Scheen AJ. Current management strategies for coexisting diabetes mellitus and obesity. Drugs 2003; 63: 1165–84.
74 Carroll JF, Kyser CK. Exercise training in obesity lowers blood pressure independent of weight change. Med Sci Sports Exerc 2002; 34: 596–601.
75 Kiess W, Reich A, Muller G, Galler A, Kapellen T, Raile K, *et al*. Obesity in childhood and adolescence: clinical diagnosis and management. J Pediatr Endocrinol Metab 2001; 14: 1431–40.
76 Lazarou C, Soteriades ES. Children's physical activity, TV watching and obesity in Cyprus: the CYKIDS study. Eur J Public Health 2010; 20: 70–7.
77 Onywera VO. Childhood obesity and physical inactivity threat in Africa: strategies for a healthy future. Glob Health Promot 2011; 17: 45–6.
78 Sothern MS. Obesity prevention in children: physical activity and nutrition. Nutrition 2004; 20: 704–8.
79 Werner C, Furster T, Widmann T, Poss J, Roggia C, Hanhoun M, *et al*. Physical exercise prevents cellular senescence in circulating leukocytes and in the vessel wall. Circulation 2009; 120: 2438–47.
80 Tryggestad JB, Thompson DM, Copeland KC, Short KR. Obese children have higher arterial elasticity without a difference in endothelial function: the role of body composition. Obesity (Silver Spring) 2012; 20: 165–71.
81 Van Hoorenbeeck K, Franckx H, Debode P, Aerts P, Wouters K, Ramet J, *et al*. Weight loss and sleep-disordered breathing in childhood obesity: effects on inflammation and uric acid. Obesity (Silver Spring) 2012; 20: 172–7.
82 Barton M, Minotti R, Haas E. Inflammation and atherosclerosis. Circ Res 2007; 101: 750–1.
83 Goto S, Takahashi R, Araki S, Nakamoto H. Dietary restriction initiated in late adulthood can reverse age-related alterations of protein and protein metabolism. Ann N Y Acad Sci 2002; 959: 50–6.
84 Colman RJ, Anderson RM, Johnson SC, Kastman EK, Kosmatka KJ, Beasley TM, *et al*. Caloric restriction delays disease onset and mortality in rhesus monkeys. Science 2009; 325: 201–4.
85 Wilkins R. Danes impose 25% tax increases on ice cream, chocolate, and sweets to curb disease. BMJ 2010; 341: c3592.
86 Alemanno A, Carreno I. Fat taxes in the EU between fiscal austerity and the fight against obesity. Eur J Risk Regul 2011; 4: 571–6.
87 Daniels SR, Pratt CA, Hayman LL. Recent advances in preventive cardiology and lifestyle medicine. Reduction of risk for cardiovascular disease in children and adolescents. Circulation 2011; 124: 1673–86.
88 Gutin B. Diet vs exercise for the prevention of pediatric obesity: the role of exercise. Int J Obes (Lond) 2011; 35: 29–32.
89 Barton M. Aging and biomedicine 2005: where should we go from here? Cardiovasc Res 2005; 66: 187–9.

Acta Pharmacologica Sinica (2012) 33: 194–200
 1671-4083/12 $32.00
www.nature.com/aps

Original Article

Effects of liraglutide and sibutramine on food intake, palatability, body weight and glucose tolerance in the gubra DIO-rats

Gitte HANSEN*, Jacob JELSING, Niels VRANG

Gubra aps, Agern Allé 1, DK-2970 Hørsholm, Denmark

Aim: To validate the gubra DIO-rats as a useful animal model of human obesity.
Methods: The gubra diet-induced obesity (DIO) rat model was based on male Sprague-Dawley rats with *ad libitum* access to regular chow and a palatable diet rich in fat and sugar. To evaluate the versatility of the gubra DIO-rats as a valid model of human obesity syndrome, the efficacy of 2 weight loss compounds liraglutide and sibutramine with different mechanisms of action were examined in 7-month-old gubra DIO-rats. Liraglutide (200 μg/kg, sc) was administered bi-daily, and sibutramine (5 mg/kg, *po*) was administered once daily for 23 d.
Results: Both the compounds effectively reduced the food intake, body weight and total fat mass as measured by nuclear magnetic resonance. Whereas the 5-HT reuptake inhibitor/5-HT receptor agonist sibutramine reduced the intake of both chow and the gubra-diet, the GLP-1 analogue liraglutide predominantly reduced the intake of the highly palatable diet, indicating a shift in food preference. Sibutramine lowered the insulin sensitivity index, primarily via reductions in glucose-stimulated insulin secretion.
Conclusion: This animal model responds well to 2 weight loss compounds with different mechanisms of action. Moreover, the gubra DIO-rat can be particularly useful for the testing of compounds with potential effects on diet preference.

Keywords: obesity; diet-induced obese rats; food preference; glucose tolerance; glucagon-like peptide-1 (GLP-1); 5-hydroxytryptamine (5-HT); sibutramine; liraglutide

Acta Pharmacologica Sinica (2012) 33: 194–200; doi: 10.1038/aps.2011.168

Introduction

Obesity has become one of the leading causes of death in the industrialized world and has become an increasing health concern for children[1, 2]. Currently, the only efficacious and lasting treatments for weight loss are surgical interventions, and there is an enormous unmet medical need for novel anti-obesity drugs. Hence, the availability of animal models that predictably reflect human obesity syndrome is important. Although the genetic models of obesity (*eg*, the *ob/ob* and *db/db* mice, Zucker *fa/fa* rats, Agouti mice, and MC4 knockout mice) have contributed significantly to our understanding of the molecular physiology of food intake and energy homeostasis[3, 4], the fact that human obesity is a complex interplay between environment (food, exercise) and genetics (multiple genes)[5, 6] requires animal models that reflect this complexity.

One such polygenic model is the diet-induced obese (DIO) and diet-resistant (DR) outbred rat models[7–10]. In the Levin DIO-rats, phenotypic differences in body weight gain, adiposity, and insulin sensitivity are only expressed between the outbred substrains when they are placed on diets of moderate fat, sucrose, and caloric content[11]. A major difference, however, between this experimental design and obesity in humans is that a large aspect of human susceptibility to obesity may not depend on the ability to resist weight gain when force-fed a high-fat diet. Rather, it may hinge on individual differences in the propensity to choose high-fat foods[12–14].

The gubra DIO-rat model is based on male Sprague-Dawley (SPD) rats fed a highly palatable fat- and sugar-rich diet (HPFS diet) composed of equal amounts of the chocolate spread Nutella, peanut butter and powdered chow. The rats also have access to standard pelleted chow, and hence the model allows for assessment of diet preference. Compared to other cafeteria diets, the gubra diet is easy to dispense and measure, and does not change from day-to-day[15]. The diet promotes voluntary hyperphagia that results in rapid weight gain and increases fat pad mass.

* To whom correspondence should be addressed.
E-mail gh@gubra.dk
Received 2011-09-05 Accepted 2011-11-12

To validate the gubra DIO-rat as a useful animal model of human obesity, we examined the body weight changes as well as the ingestive responses and feeding behaviors of the well-known anti-obesity agent sibutramine and the once-daily human glucagon-like peptide-1 (GLP-1) analog liraglutide for 23 d in this animal model. Sibutramine is a sympathomimetic medication that was available for long-term treatment, and the most recent drug to be withdrawn from the market due to a side effect of increased risk of cardiovascular events. Liraglutide is a long-acting GLP-1 analog available for the treatment of type 2 diabetes that has also shown clinically relevant weight loss following treatment in both diabetic[16] and non-diabetic obese patients[17].

Materials and methods

Compounds

Sibutramine (molecular weight=334.40 g/mol) was obtained from AH Diagnostics (Aarhus, Denmark). Liraglutide (molecular weight=3751.20 g/mol) was obtained from Novo Nordisk, Maaloev, Denmark.

Animals

Twenty male Sprague-Dawley rats were purchased from Taconic (Denmark). All animal experiments were conducted in accordance with internationally accepted principles for the care and use of laboratory animals, and were approved by the Danish Committee for animal research (license 2008/561-1565). The animals were housed in a standard 12-h light/dark cycle (lights on, 6:00 AM; lights off, 6:00 PM) at a room temperature of 20–22 °C and relative humidity of 50%–60%. All animals had free access to water.

Upon arrival at six weeks of age, the rats were offered a two-choice diet consisting of a standard rodent chow (Altromin #1324, Brogaarden, Denmark) and the gubra diet, a high palatable high-fat high-sugar diet made up of a paste (1:1:1) of chocolate spread (Nutella, Ferrero, Italy), peanut butter (Skippy, Unilever, USA) and powdered regular rodent chow (Altromin #1324, Brogaarden, Denmark). The rats were housed two per cage for 26 weeks (until stratification d -7). From d -7 to d 23, rats were housed one per cage. The rats had *ad libitum* access to chow, the gubra diet and water unless otherwise stated.

Drug treatment

On d -7, the rats were stratified into the following three groups based on body weight (n=6; two outliers were discarded): Vehicle (0.5% hydroxypropyl methylcellulose, Sigma, St Louis, MI); sibutramine (5 mg/kg, *po*); or liraglutide (200 μg/kg, sc). All compounds were freshly prepared and administered for 23 d via oral gavage/subcutaneous injections. Vehicle and sibutramine were administered orally once daily 2 h into the light phase, whereas liraglutide was administered subcutaneously bi-daily, two and 10 h into the light phase, respectively. The first dose was given on d 0. The liraglutide dosing was gradually increased over the first four days from 50 to 200 μg/kg. Body weight and food intake were measured daily and bi-weekly, respectively, from days 0 to 23.

Non-invasive whole body composition

Whole body composition was analyzed weekly by non-invasive EchoMRI-900 (EchoMRI, USA). The scanner (QMR systems) measured whole body fat and lean tissue mass. During the scanning procedure, the rat was placed in a restrainer for approximately one minute.

Oral glucose tolerance test (OGTT)

An OGTT was performed on d 21. Animals were mildly fasted, with access to only 50% of their daily energy requirements in the 16 h preceding the test. The amount of food administered on the day prior to the OGTT was calculated for each individual animal as the mean of the two preceding measurements of food intake. Compounds were administered 45 min prior to administration of the oral glucose load. The OGTT was carried out at 8:00 AM. Blood samples for blood glucose and plasma insulin analyses were collected from the sublingual capillaries (capillaries perforated using 23-gauge needle) at t=-60, 0, 15, 30, 60, 120, and 240 min prior to and after the oral glucose load of 2 g/kg body weight glucose (glucose: 500 mg/L, Frescenius Kabi, Sweden). The baseline blood sample (-60) was additionally analyzed for total plasma triglycerides, total cholesterol and free fatty acids (NEFA-C). Glucose and insulin area under the curve (AUC) calculations were determined as total AUC based on data from the -60 to 240 min measurements. The insulin sensitivity index (ISI) was estimated according to Matsuda and DeFronzo[18] using the following equation: $10.000/\sqrt{[(FBG*FPI)*(AUC\text{-}G*AUC\text{-}I)]}$, where FBG and FPI are fasting glucose and insulin, respectively, and AUC is the area under the curve for glucose and insulin measurements. Following the OGTT, the animals had unrestricted access to food. Two days after the OGTT, the animals were euthanized by CO_2 anesthesia. Trunk blood was collected and body white adipose tissue compartments were removed and weighed. Fat deposit weight analyses included mesenterial, retroperitoneal (right), epididymal (left) and subcutaneous inguinal (left) fat.

Blood chemistry analyses

Whole blood glucose

Blood was collected in 10-μL heparinized glass capillary tubes and immediately suspended in buffer [(0.5 mL of glucose/lactate system solution (EKF-diagnostics, Germany)], and then analysed for glucose using a BIOSEN c-Line glucose meter (EKF-diagnostics, Germany).

Insulin

A total of 100 μL of blood was collected in heparinized tubes. Plasma was separated and insulin was measured in duplicate for each data point using an ultrasensitive ELISA (Mercodia AB, Sweden).

Plasma FFA (NEFA-C)

A total of 200 μL of blood was collected in EDTA tubes con-

taining 1% NaF and the plasma was separated. The FFA content was measured using the autoanalyzer Cobas C-111 with a commercial kit (Abbott, USA).

Cholesterol and triglycerides

A total of 200 μL of blood was collected in heparinized tubes and the plasma was separated. Total triglycerides and cholesterol were measured using the autoanalyzer Cobas C-111 with a commercial kit (Roche Diagnostics, Germany).

Statistical evaluation

All data were imported into Excel 5.0 spreadsheets and subsequently subjected to relevant statistical analyses using GraphPad Prism 5.0 software. The results are presented as the mean±SEM unless otherwise stated. Statistical evaluation of the data was carried out using a one-way or a repeated measure two-way analysis of variance (ANOVA) with appropriate *post-hoc* analysis between control and treatment groups in cases where statistical significance was established ($P<0.05$; Bonferroni).

Results

Body weight analysis

Both sibutramine and liraglutide significantly reduced body weight and relative body weight changes (Figures 1A–1B). Whereas sibutramine induced weight loss stabilized after approximately two weeks of treatment (leading to a 12% drop in body weight), the liraglutide-treated rats continued to display weight loss, reaching a 15% body weight loss on the final day of the experiment (Figure 1).

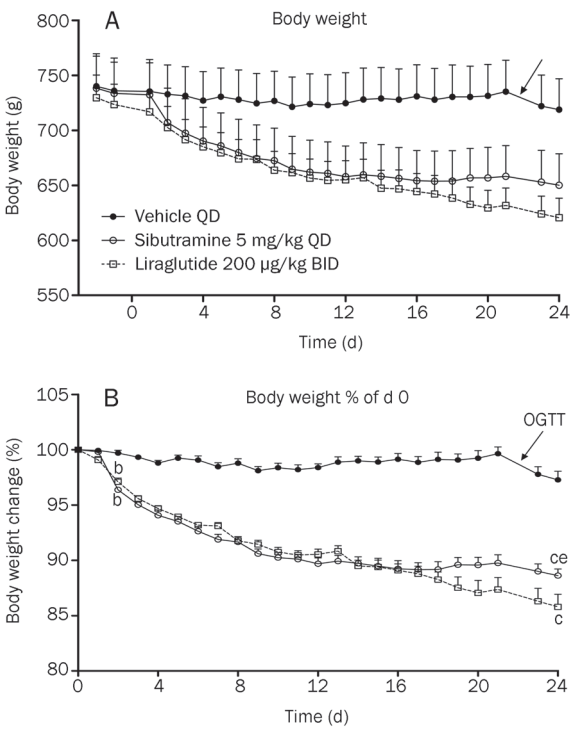

Figure 1. (A) body weight (g) and (B) body weight change (%) of gubra DIO rats treated with vehicle, sibutramine or liraglutide following a 23-d drug administration period. $^{b}P<0.05$, $^{c}P<0.01$ *vs* vehicle group. $^{e}P<0.05$ *vs* liraglutide. Data are means±SEM. $n=6$.

Food and water intake analyses

Both treatment regimens resulted in an acute drop in the intake of the gubra diet (Figures 2A–2F). Sibutramine also reduced the intake of the chow diet (Figures 2B, 2D). Liraglutide-treated rats, however, increased their intake of chow, indicating a shift in food preference from the very palatable gubra diet to chow (Figures 2B, 2D). Both treatment regimens showed unaffected water intake throughout the study period, with volumes similar to vehicle-treated rats at approximately 20–25 mL/day (data not shown).

Glucose tolerance

An OGTT was performed on day 21 (Figure 3). In the glucose tolerance test, data from an age-matched group of chow-fed SPD rats were included for comparison (Figures 3A, 3B). Although the gubra-DIO-rats do not display overt hyperglycemia during the glucose tolerance test, glucose levels in these animals were elevated compared to those in the age-matched chow-fed rats (Figures 3A, 3B). Whereas liraglutide reduced the area under the glucose curve (AUC glucose) significantly compared to vehicle, no difference in AUC was observed in sibutramine-treated rats (Figure 3B). Sibutramine, however, seemed to inhibit insulin secretion, resulting in a reduced AUC insulin (Figure 3D). Although not significant, both liraglutide- and sibutramine-treated rats tended to have lower insulin levels at the baseline (semi-fasted state) sample obtained at the -60 min time point in the OGTT (Figure 3C). As a measure of whole body insulin sensitivity, the insulin sensitivity index was calculated according to Matsuda and DeFronzo[18]. Insulin sensitivity was significantly higher in the sibutramine-treated rats compared to the vehicle-treated rats, whereas no effect on insulin sensitivity was observed following liraglutide treatment (Figure 3E). Triglyceride levels tended to be lower in both liraglutide- and sibutramine-treated rats, but not to a statistically significant extent. Likewise, no significant effects on cholesterol or free fatty acids were observed following sibutramine or liraglutide treatment, although the former tended to increase cholesterol levels compared to vehicle treatment (Table 1).

Body fat mass

Weekly measurements of whole body composition demon-

Table 1. Plasma lipids (triglyceride, cholesterol, and free fatty acids) measured in the semi-fasted state 60 min prior to glucose load on the day of the experimental OGTT following 21-d drug administration. Data are means±SEM. $n=6$. $^{b}P<0.05$ *vs* Liraglutide.

	Vehicle	Sibutramine	Liraglutide
Triglyceride (mmol/L)	1.186±0.16	1.002±0.14	0.778±0.12
Cholesterol (mmol/L)	2.916±0.15	3.350±0.14^{b}	2.756±0.11
FFA (μmol/L)	277.60±37.27	327.17±25.46	278.52±16.44

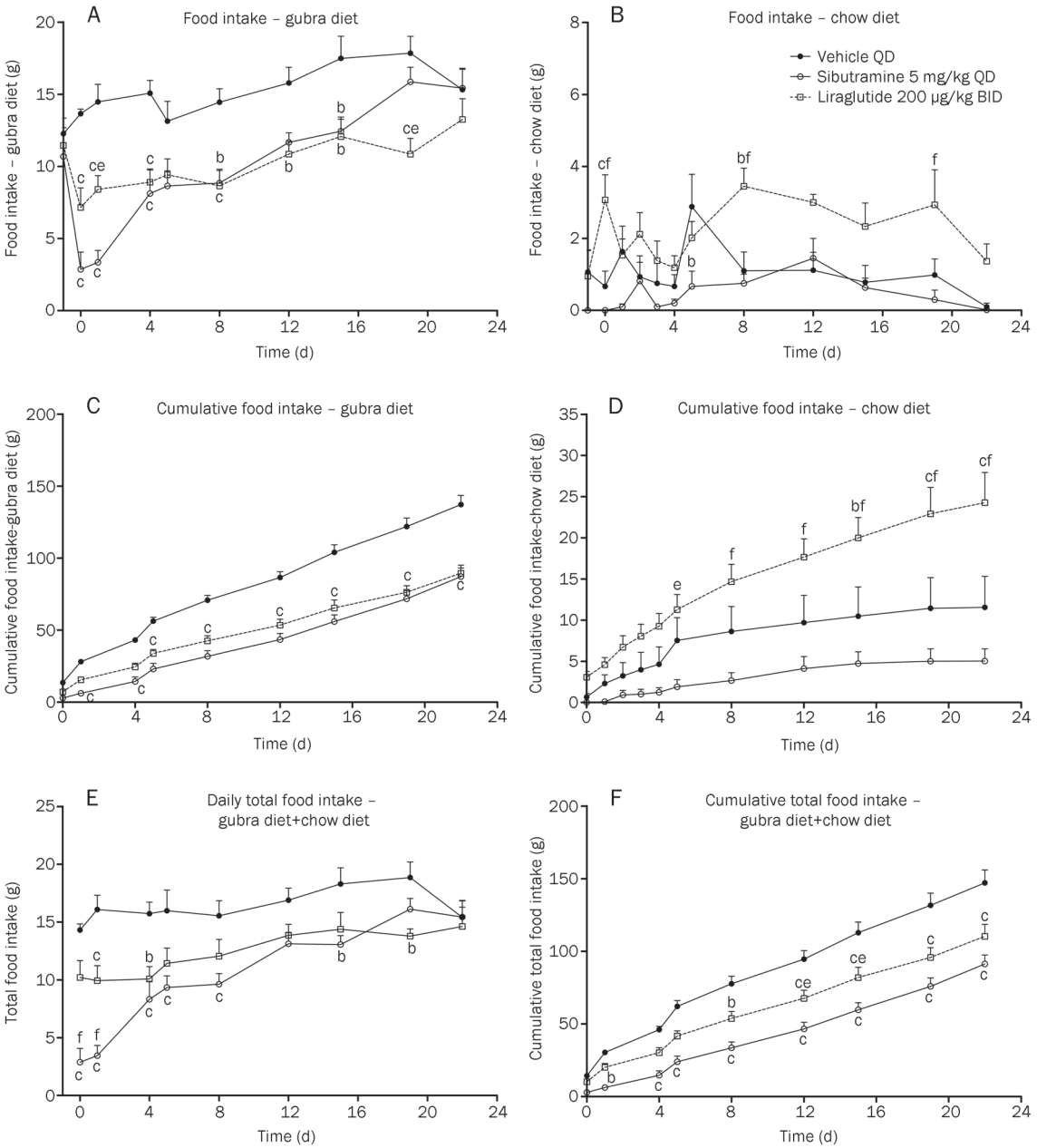

Figure 2. (A, B) daily, (C, D) cumulative intake and (E, F) total daily/cumulative intake of HPFS gubra diet and regular rodent chow (g), respectively, following a 23-d drug administration period. $^{b}P<0.05$, $^{c}P<0.01$ *vs* vehicle group. $^{e}P<0.05$, $^{f}P<0.01$ *vs* sibutramine. Data are means±SEM. $n=6$.

strated a significant reduction in total fat mass in both treatment groups (Figure 4A). No significant changes were seen in lean mass (Figure 4A). The slight initial drop in lean body mass was most likely due to the effects of the compounds on total body water. Both compounds reduced the size of all fat deposits (Figure 4B), with the most marked changes seen in the retroperitoneal and mesenterial fat pads.

Discussion

In this study, we present a detailed description of the weight gain curve, food intake and body fat composition of the gubra DIO-rat. The gubra DIO-rat has a normal Sprague-Dawley background, but displays overt obesity when fed a highly palatable fat- and sugar-rich diet for more than 14 weeks. The gubra-DIO-rats did not develop frank diabetes, but displayed elevated OGTT glucose levels compared to the age-matched chow-fed rats. We demonstrated that two different weight loss compounds, sibutramine and liraglutide, led to a 12%–15% body weight loss in this animal model, and perhaps more interestingly, that liraglutide treatment led to a shift in diet preferences with an increased craving for chow.

Dietary-induced obese animal models have played a key role in the screening of novel compounds for effects on food intake and/or body weight for many years. Thus, the first

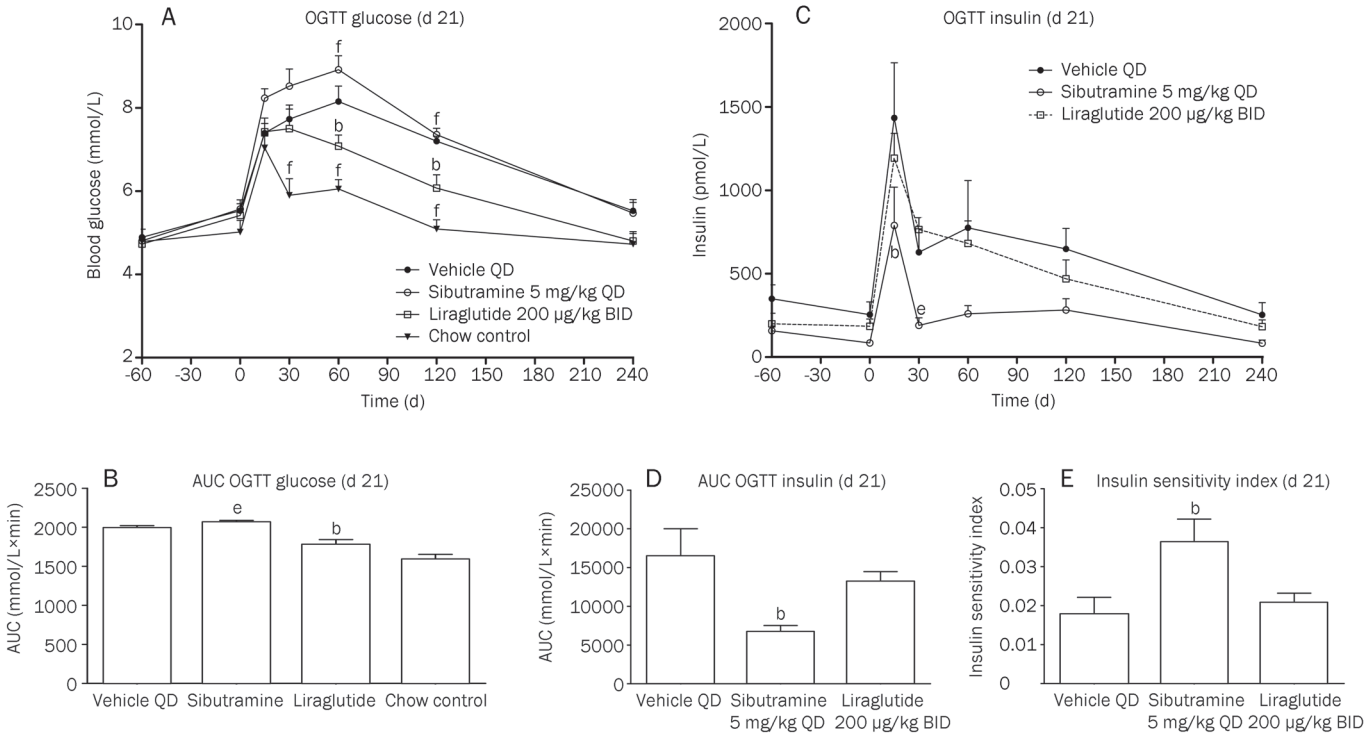

Figure 3. (A, B) blood glucose and (C, D) plasma insulin responses to an OGTT following 21-day drug administration. Rats were semi-fasted 16 h before the OGTT. Compounds were administered 45 min prior to the per oral glucose load (2 g/kg). (E) Insulin sensitivity index (CISI) calculated according to formula of Matsuda and DeFronzo, 1999. $^{b}P<0.05$ *vs* vehicle group. $^{e}P<0.05$ *vs* liraglutide. Data are means±SEM. $n=6$.

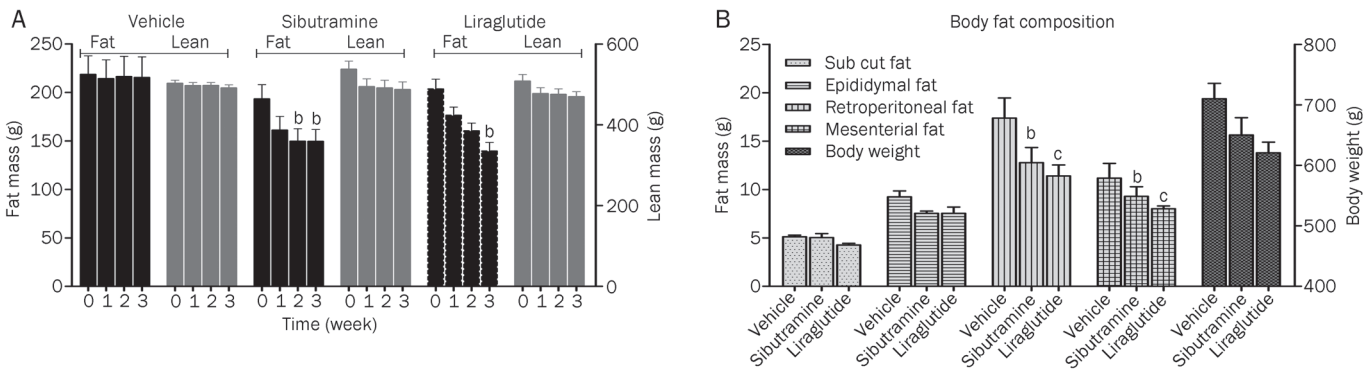

Figure 4. (A) Weekly whole body composition measuring total fat/lean body mass (g) by non-invasive EchoMRI-900 and (B) terminal fat depot analysis (g) of subcutaneous inguinal (right), epididymal (right), retroperitoneal (left), and mesenterial fat mass. $^{b}P<0.05$, $^{c}P<0.01$ *vs* vehicle group. Data are means±SEM. $n=6$.

use of a high-fat diet to induce obesity in rats was by Masek and Fabry in 1959[19]. Since then, numerous DIO models have been published using the general approach whereby diets composed of alternating components of fat and carbohydrates are administered to normal, lean rats or mice over long periods[8, 10, 20]. The so-called cafeteria diets, where animals have a choice of various palatable foods such as chocolate, peanuts etc, encourages overeating and hence provides highly relevant models for examining human diets in rodents[15, 21–23]. Although some diet-dependent differences in the phenotypes of obese animals have been reported[24], the metabolic profiles of rodents that are provided long-term access to high fat diets are reasonably uniform despite methodological variations among laboratories. In general, the currently available DIO rodent models are all based on the feeding of mice or rats diets that are high in energy, mostly from fat (*eg*, the Levin DIO, the C57BL/6J DIO) or sugar[7, 25, 26]. Once obesity has been induced, the animals exhibit stabilized body weights, marked visceral adiposity (30%–35% fat), high plasma levels of leptin, moderate insulin resistance (rather than overt diabetes) and

mild lipid abnormalities. Furthermore, the dietary-induced obesity in animals is polygenic in nature, ie, the susceptibility for weight gain is due to many different genes. In these respects, the animals display similar symptoms to those observed in common human obesity, and the factors contributing to the initiation and maintenance of obesity are similar between animals and man.

The pharmacological approaches for reducing body weight include the development of compounds which reduce food intake or absorption of fat from the gastrointestinal tract, increase energy utilization or act by a combination of these mechanisms. Modest weight loss as low as 5% of initial body weight can lead to favorable improvements in blood pressure, lipid profile, insulin sensitivity and glucose tolerance[27–29]. Thus, an anti-obesity drug[23, 30] that delivers an approximate 10% weight loss in animals with dietary-induced obesity would appear to be a sensible positive control in DIO studies.

In the current study, we aimed to validate the gubra DIO-rat as a useful animal model of human obesity. Six-week-old Sprague-Dawley rats were offered a two-choice diet consisting of standard rodent chow diet or the gubra diet, a highly palatable high-fat, high-sugar diet. After a six-month feeding period, body weight changes, ingestive responses and feeding behaviors were examined following daily administration of sibutramine and liraglutide for 23 d. Compared to the vehicle control, chronic administration of either sibutramine or liraglutide to high-fat/sugar-fed DIO-rats caused significant reductions in body weight gain, which is in agreement with previously reported data using other rodent DIO models[14, 15, 31–34]. The body weight loss observed in both groups was mainly caused by decreasing levels of total fat mass as revealed by the weekly measurements of whole body composition.

As expected, liraglutide as well as sibutramine administration was associated with a significant acute reduction in total caloric intake. Interestingly, however, liraglutide shifted the choice of food, with a significant decrease in the palatable gubra diet consumption accompanied by a relative increase in chow consumption. This shift in food preference by liraglutide is in agreement with previously published data of candy-fed obese Sprague-Dawley rats[15]. The exact mechanism for this effect of pharmacological treatment with a GLP-1 analogue is currently not known. However, it is known that not all drugs that reduce the motivation to eat do so through actions on satiety; therefore, other CNS systems associated with the pleasure or rewarding aspects of food intake, such as the opioid or dopaminergic systems, must also be considered[35]. Interestingly, altered preference for food has also been reported from patients who undergo gastric bypass surgery and exhibit altered attitudes towards and preferences for healthier food[36]. Given that gastric bypass surgery has been shown to enhance meal-induced GLP-1 secretion[37], it is tempting to speculate that the shift in food preference is related to the GLP-1 system.

Besides their weight reducing effects, and in agreement with previously published data, liraglutide was able to improve glucose tolerance[14], and sibutramine improved the insulin sensitivity index (ISI)[10]. The latter was primarily obtained via reductions in glucose-stimulated insulin secretion. The fact that the gubra DIO model rats never developed frank diabetes, which occurs in many other DIO models, is most likely attributable to our feeding regimen where the rats do not eat the high-fat diet only, but can choose freely between chow and the palatable chocolate diet.

Conclusion

Taken together, the gubra DIO model rat, which is fed a two-choice diet composed of highly palatable fat- and sugar-rich food and regular chow, seems to be a valuable polygenetic DIO model for screening compounds primarily affecting food intake and body weight. This model is therefore preferable to other DIO models where animals are force-fed high fat diets without choice, which is very unlike the human situation.

Author contribution

Niels VRANG, Gitte HANSEN, and Jacob JELSING designed research; Natascha LELLING and Gitte HANSEN performed research; Gitte HANSEN analyzed data; Niels VRANG, Gitte HANSEN, and Jacob JELSING wrote the paper.

References

1 Procter KL. The aetiology of childhood obesity: a review. Nutr Res Rev 2007; 20: 29–45.
2 Wang Y. Cross-national comparison of childhood obesity: the epidemic and the relationship between obesity and socioeconomic status. Int J Epidemiol 2001; 30: 1129–36.
3 Carroll L, Voisey J, van Daal A. Mouse models of obesity. Clin Dermatol 2004; 22: 345–9.
4 Kennedy AJ, Ellacott KL, King VL, Hasty AH. Mouse models of the metabolic syndrome. Dis Model Mech 2010; 3: 156–66.
5 Farooqi IS. Genetic, molecular and physiological insights into human obesity. Eur J Clin Invest. 2011; 41: 451–5.
6 Travers and McCarthy 2011
7 Levin BE, Dunn-Meynell AA, Balkan B, Keesey RE. Selective breeding for diet-induced obesity and resistance in Sprague-Dawley rats. Am J Physiol 1997; 273: R725–730.
8 Levin BE, Keesey RE. Defense of differing body weight set points in diet-induced obese and resistant rats. Am J Physiol 1998; 274: R412–419.
9 Archer ZA, Rayner DV, Rozman J, Klingenspor M, Mercer JG. Normal distribution of body weight gain in male Sprague-Dawley rats fed a high-energy diet. Obes Res 2003; 11: 1376–83.
10 Madsen AN, Hansen G, Paulsen SJ, Lykkegaard K, Tang-Christensen M, Hansen HS, *et al*. Long-term characterization of the diet-induced obese and diet-resistant rat model: a polygenetic rat model mimicking the human obesity syndrome. J Endocrinol 2010; 206: 287–96.
11 Levin BE, Triscari J, Hogan S, Sullivan AC. Resistance to diet-induced obesity: food intake, pancreatic sympathetic tone, and insulin. Am J Physiol 1987; 252: R471–8.
12 Smith BK, Kelly LA, Pina R, York DA, Bray GA. Preferential fat intake increases adiposity but not body weight in Sprague-Dawley rats. Appetite 1998; 31: 127–39.
13 Smith BK, Andrews PK, West DB. Macronutrient diet selection in thirteen mouse strains. Am J Physiol Regul Integr Comp Physiol 2000; 278: R797–805.
14 Raun K, von Voss P, Knudsen LB. Liraglutide, a once-daily human

glucagon-like peptide-1 analog, minimizes food intake in severely obese minipigs. Obesity (Silver Spring) 2007; 15: 1710–6.
15 Raun K, von Voss P, Gotfredsen CF, Golozoubova V, Rolin B, Knudsen LB. Liraglutide, a long-acting glucagon-like peptide-1 analog, reduces body weight and food intake in obese candy-fed rats, whereas a dipeptidyl peptidase-IV inhibitor, vildagliptin, does not. Diabetes 2007; 56: 8–15.
16 Buse JB, Rosenstock J, Sesti G, Schmidt WE, Montanya E, Brett JH, *et al*. Liraglutide once a day versus exenatide twice a day for type 2 diabetes: a 26-week randomised, parallel-group, multinational, open-label trial (LEAD-6). Lancet 2009; 374: 39–47.
17 Astrup A, Rossner S, Van Gaal L, Rissanen A, Niskanen L, Al Hakim M, *et al*. Effects of liraglutide in the treatment of obesity: a randomised, double-blind, placebo-controlled study. Lancet 2009; 374: 1606–16.
18 Matsuda M, DeFronzo RA. Insulin sensitivity indices obtained from oral glucose tolerance testing: comparison with the euglycemic insulin clamp. Diabetes Care 1999; 22: 1462–70.
19 Masek J, Fabry P. High-fat diet and the development of obesity in albino rats. Experientia 1959; 15: 444–5.
20 Mercer JG, Archer ZA. Diet-induced obesity in the Sprague-Dawley rat: dietary manipulations and their effect on hypothalamic neuropeptide energy balance systems. Biochem Soc Trans 2005; 33: 1068–72.
21 Sampey BP, Vanhoose AM, Winfield HM, Freemerman AJ, Muehlbauer MJ, Fueger PT, *et al*. Cafeteria diet is a robust model of human metabolic syndrome with liver and adipose inflammation: comparison to high-fat diet. Obesity (Silver Spring) 2011; 19: 1109–17.
22 Naderali EK, Williams G. Effects of short-term feeding of a highly palatable diet on vascular reactivity in rats. Eur J Clin Invest 2001; 31: 1024–8.
23 Fisas A, Codony X, Romero G, Dordal A, Giraldo J, Merce R, *et al*. Chronic 5-HT6 receptor modulation by E-6837 induces hypophagia and sustained weight loss in diet-induced obese rats. Br J Pharmacol 2006; 148: 973–83.
24 Buettner R, Parhofer KG, Woenckhaus M, Wrede CE, Kunz-Schughart LA, Schölmerich J, *et al*. Defining high-fat-diet rat models: metabolic and molecular effects of different fat types. J Mol Endocrinol 2006; 36: 485–501.
25 Collins S, Martin TL, Surwit RS, Robidoux J. Genetic vulnerability to diet-induced obesity in the C57BL/6J mouse: physiological and molecular characteristics. Physiol Behav 2004; 81: 243–8.
26 Vrang N, Madsen AN, Tang-Christensen M, Hansen G, Larsen PJ. PYY(3-36) reduces food intake and body weight and improves insulin sensitivity in rodent models of diet-induced obesity. Am J Physiol Regul Integr Comp Physiol 2006; 291: R367–75.
27 Blackburn G. Effect of degree of weight loss on health benefits. Obes Res 1995; 3: 211s–216s.
28 Follick MJ, Abrams DB, Smith TW, Henderson LO, Herbert PN. Contrasting short- and long-term effects of weight loss on lipoprotein levels. Arch Intern Med 1984; 144: 1571–4.
29 Yanovski SZ, Bain RP, Williamson DF. Report of a National Institutes of Health-Centers for Disease Control and Prevention workshop on the feasibility of conducting a randomized clinical trial to estimate the long-term health effects of intentional weight loss in obese persons. Am J Clin Nutr 1999; 69: 366–72.
30 Bray GA. Drug treatment of obesity. Rev Endocr Metab Disord 2001; 2: 403–18.
31 Boozer CN, Leibel RL, Love RJ, Cha MC, Aronne LJ. Synergy of sibutramine and low-dose leptin in treatment of diet-induced obesity in rats. Metabolism 2001; 50: 889–93.
32 Bush EN, Shapiro R, Brune ME, Knourek-Segel VE, Droz BA, Fev T, Lin E, Jacobsen PB. Chronic treatment with either dexfenfluramine or sibutramine in diet-switched diet-induced obese mice. Endocrine. 2006; 29: 375–81.
33 Mashiko S, Ishihara A, Iwaasa H, Moriya R, Kitazawa H, Mitobe Y, *et al*. Effects of a novel Y5 antagonist in obese mice: combination with food restriction or sibutramine. Obesity 2008; 16: 1510–5.
34 Larsen PJ, Fledelius C, Knudsen LB, Tang-Christensen M. Systemic administration of the long-acting GLP-1 derivative NN2211 induces lasting and reversible weight loss in both normal and obese rats. Diabetes 2001; 50: 2530–9.
35 Halford JC. Lorcaserin — not a new weapon in the battle with appetite. Nat Rev Endocrinol 2010; 6: 663–4.
36 Olbers T, Bjorkman S, Lindroos A, Maleckas A, Lonn L, Sjostrom L, *et al*. Body composition, dietary intake, and energy expenditure after laparoscopic Roux-en-Y gastric bypass and laparoscopic vertical banded gastroplasty: a randomized clinical trial. Ann Surg 2006; 244: 715–22.
37 Rodieux F, Giusti V, D'Alessio DA, Suter M, Tappy L. Effects of gastric bypass and gastric banding on glucose kinetics and gut hormone release. Obesity (Silver Spring) 2008; 16: 298–305.

Acta Pharmacologica Sinica (2012) 33: 201–207
 1671-4083/12 $32.00
www.nature.com/aps

Original Article

Association of *ALOX15* gene polymorphisms with obesity-related phenotypes in Chinese nuclear families with male offspring

Yao-hua KE#, Wen-jin XIAO#, Jin-wei HE, Hao ZHANG, Jin-bo YU, Wei-wei HU, Jie-mei GU, Gao GAO, Hua YUE, Chun WANG, Yun-qiu HU, Miao LI, Yu-juan LIU, Wen-zhen FU, Zhen-lin ZHANG*

Metabolic Bone Disease and Genetics Research Unit, Department of Osteoporosis and Bone Diseases, the Shanghai Sixth People's Hospital, Shanghai Jiaotong University, Shanghai 200233, China

Aim: Genetic variation in ALOX12, which encoded human 12-lipoxygenase, was found to be associated with fat mass in young Chinese men. The objective of this study was to investigate the relationship between single nucleotide polymorphisms (SNPs) and haplotypes in the ALOX15 gene and obesity-related phenotypes in Chinese nuclear families with male offspring.
Methods: We recruited 1,296 subjects from 427 nuclear families with male offspring and genotyped five SNPs (rs9894225, rs748694, rs2619112, rs2619118, and rs916055) in the ALOX15 gene locus. The total fat mass (TFM), trunk fat mass (tFM), leg fat mass (LFM) and arm fat mass (AFM) were measured using dual-energy X-ray absorptiometry (DXA). The percentage of fat mass (PFM) was the ratio of TFM and body weight. The association between SNPs and haplotypes of ALOX15 and obesity-related phenotypic variation was measured using quantitative transmission disequilibrium test (QTDT).
Results: Using QTDT to measure family-based genetic association, we found that rs916055 had a statistically significant association with PFM (P=0.038), whereas rs916055 had a marginal but statistically insignificant association with tFM (P=0.093). The multiple-parameter 1000 permutations test agreed with the family-based association results: both showed that rs916055 had a statistically significant association with PFM (P=0.033).
Conclusion: rs916055 in ALOX15 gene was significantly associated with the percentage of fat mass in Chinese nuclear families with male offspring in the family-based association study using QTDT approach.

Keywords: obesity; fat mass; *ALOX15*; lipoxygenase; single nucleotide polymorphism; obesity-related phenotypes; family-based association study; quantitative transmission disequilibrium test

Acta Pharmacologica Sinica (2012) 33: 201–207; doi: 10.1038/aps.2011.167

Introduction

There has been an alarming increase in the number of patients with metabolic syndrome, a disorder with a constellation of conditions that includes glucose intolerance, obesity, dyslipidemia and hypertension. Obesity is the central and causal component of this syndrome[1], but the underlying mechanisms have not been fully elucidated. It is now widely accepted that the activation of inflammatory and oxidative stress is one of the common causes of obesity and largely contributes to the related pathological outcomes[2–4]. Several factors are responsible for inflammation in obesity, such as elevated nuclear-factor kappaB (NF-κB) activity, the presence of free fatty acids, and increased levels of adipokines including tumor necrosis factor-alpha (TNFα), interleukins (ILs), resistin and leptin[2, 5, 6]. Oxidative stress activates kinases such as c-Jun N-terminal kinase (JNK) and mitogen-activated protein kinase (MAPK) and inhibits NF-κB kinase (IKK). These kinases may directly interfere insulin signaling or indirectly enhance inflammatory processes via common biochemical pathways (*ie*, NF-κB)[7–9]. Exploring the interface between inflammation and oxidative stress at a molecular and genetic level will enhance our understanding of obesity and the complications associated with it.

The lipoxygenase pathway, which generates proinflammatory metabolites from arachidonic acid, has recently attracted a great deal of attention for its potential role in obesity and atherosclerosis disease. Expression of 12/15-lipoxygenase is elevated in adipocytes isolated from insulin resistant obese

# The two authors contributed equally to this work.
* To whom correspondence should be addressed.
E-mail ZZL2002@medmail.com.cn
Received 2011-09-14 Accepted 2011-11-11

Zucker rats relative to lean rats[10]. A diet high in fat induced macrophage infiltration into the adipose tissue of wild-type but not 12/15-lipoxygenase gene knock-out mice[11]. The addition of the 12/15-lipoxygenase metabolic products, 12(*S*)-HETE and 15(*S*)-HETE, directly to 3T3-LI adipose cells significantly upregulated the expression of key proinflammatory genes (*TNF-a, IL-6,* and *IL-12*) and downregulatesd an important anti-inflammatory gene (*adiponectin*)[12]. These findings support the hypothesis that 12/15-lipoxygenase is important for obesity. The human 12/15 lipoxygenase is encoded by arachidonate lipoxygenase 12/15 (*ALOX12/15*), both of which are located on chromosome 17p13, a region that is linked to obesity-related traits in several independent studies[13]. More recently, we have shown that genetic variation in *ALOX12* is associated with total fat mass (TFM) in young Chinese men[14]. An analysis of tar *ALOX12* cDNA showed that *ALOX12* raised 12-HETE and 15-HETE levels but had a greater effect on 12-HETE[15]. This finding suggests that two *ALOX* genes may, at least to some extent, be similar in function. Furthermore, UV-irradiation suppressed *ALOX12* expression, whereas it up-regulated *ALOX15* expression. Treatment with *ALOX15* metabolites significantly suppressed insulin-like growth factor II induced-*ALOX12* expression in human keratinocyte cells[16]. Together, these findings have raised our interest in assessing whether the *ALOX15* pathway is involved in the etiology of obesity. In the present study, we performed family-based association studies of *ALOX15* using the quantitative transmission disequilibrium test (QTDT) to determine whether SNPs in *ALOX15* are associated with obesity-related phenotypic variation in a sample of Chinese nuclear families used in a previous study.

Materials and methods

Subjects

We recruited 1296 individuals from 427 nuclear families whose offspring were sons from 2004 to 2007. The average family size was 3.03. Four hundred two families had one child, and 25 families had two children. Each study subject completed a questionnaire concerning his or her age, sex, medical history, family history, marital status, physical activity, alcohol use, dietary habits and smoking history. All of the male offspring were healthy. Exclusion criteria were the same as previously reported[14, 17] .

All the study subjects belonged to the Chinese Han ethnic group and were residents of Shanghai which is located approximately halfway along the coast of China. The study was approved by the Ethics Committee of the Sixth People's Hospital affiliated with Shanghai Jiao Tong University. All of the subjects involved in the study signed informed consent documents before entering the project.

Body composition measurements

A total-body dual-energy X-ray absorptiometry (DXA) scan was performed using pan-beam technology (GE-LUNAR Prodigy, USA; enhanced whole-body detector, software version 5.71). A standard soft-tissue examination to analyze body composition consisted of TFM measurements, regional measurements of trunk fat mass (tFM) and arm (AFM) and leg fat mass (LFM) measurement. Height was measured using a stadiometer. Arm and leg fat mass together constitute extremity fat mass. Trunk fat mass (tFM) is an indicator of the tendency of adipose to accumulate in the central trunk region. The tFM has been found to correlate well with abdominal fat. All male progeny were measured for body composition, as described above. The machine was calibrated daily, and the coefficient of variability (*CV*) values of the DXA measurements (which were obtained from fifteen individuals repeatedly measured three times) were calculated to be 3.72% for AFM, 3.28% for LFM, 2.52% for tFM and 1.69% for TFM. The long-term reproducibility of our DXA data during the trial, based on repeated weekly phantom measurements using standardized equipment, was 0.45%. The body mass index (BMI) was defined as weight/height^2 (units of kilogram/meter^2). The percentage of fat mass (PFM) is the TFM divided by body weight.

Genotyping

SNPs were selected using the following criteria: (1) validation status (validated experimentally in human populations). (2) degree of heterozygosity (*ie*, minor allele frequency (MAF)>0.1) and (3) reported to the dbSNP (SNP database) by multiple sources. A total of five SNPs within *ALOX15* were selected: rs9894225, rs748694, rs2619112, rs2619118, and rs916055. Three of the five SNPs (rs2619112, rs2619118, and rs916055) are tagging SNPs (tagSNPs). They were selected from HapMap (hapmap.org). The algorithm removes SNPs with pairwise linkage disequilibrium (LD) values that exceed a certain threshold (r^2=0.8). The other two SNPs (rs9894225 and rs748694) were located in the *ALOX15* promoter region, which is known to contain multiple regulatory elements[18, 19]. Study subjects were genotyped for all five SNPs. The TaqMan allelic discrimination assay (Applied Biosystems, Foster City, CA, USA) was used for genotyping, while primer and probe sequences were optimized with the SNP assay-by-design service from Applied Biosystems. Amplification reactions were performed on the Mx3000P Real-Time PCR System (Stratagene, Santa Clara, CA). The probe for one allele in the two-allele PCR system was labeled with 6-carboxyfluorescein (FAM) dye and the other probe was labeled with hexachlorofluorescein phosphoramidite (HEX) dye. Twenty nanograms of genomic DNA was amplified in 96-well plates in the presence of the 1×TaqMan probe and primer mix and the 1×TaqMan Universal PCR Master Mix (Applied Biosystems). The PCR program consisted of an initial cycle at 95 °C for 10 min, followed by 40 cycles at 95 °C for 15 s and 60 °C for 1 min.

Linkage disequilibrium (LD) and haplotype analyses

Haplotypes were constructed from the population genotype data using the algorithm constructed by Stephens *et al* (2001) and the PHASE program (version 2.0.2)[20]. The significance threshold for linkage disequilibrium (LD) between the gene markers was based on the haplotypes and allele frequencies determined by the Haploview (version 3.2)[21]. We examined

the LD coefficients, D′ and r^2 , between all pairs of biallelic loci. The frequencies of genotypes and haplotypes were calculated with genotypic data from the unrelated parents of nuclear families.

Statistical analyses

Allele frequencies were estimated by gene counting. The Hardy-Weinberg equilibrium was measured by a χ^2 goodness-of-fit test. The orthogonal model in the QTDT program was used to test for population stratification, linkage, and family-based association between SNPs and haplotypes and obesity-related phenotypes. (The QTDT software package is available online at http://www.sph.umich.edu/csg/abecasis/QTDT/index.html.) This method of statistical analysis, as defined by the QTDT software, extends the trio-based transmission disequilibrium test (TDT) to quantitative trait data and uses genotypic data from available siblings and parents. Because all of the children in the nuclear families were sons and the effects of the parent's phenotypes were excluded in the QTDT analyses, sex was not used as a covariate to adjust for the sons' phenotypic variations. However, raw obesity phenotypic measurements, such as BMI, TFM, tFM, AFM, LFM, and percentage of fat mass (PFM), which are covariates, were adjusted by age. Because false-positive results can confound conclusions, the reliability of our results was assessed by performing a permutation procedure (1000 simulations) to generate empirical *P* values[22, 23]. The statistical power was estimated with Piface (version 1.65) (http://www.math.uiowa.edu/~rlenth/Power/) taking into account the sample size, minor allele frequency of every genotype and variation in obesity phenotypes. The distribution of the obesity-related phenotypic data was calculated by performing the Shapiro-Wilk test. A *P*-value of less than 0.05 was considered significant for all the analyses.

Results

Characteristics of the study subjects

The DNA of 15 individuals could not be subjected to genotypic analysis due to the poor quality of DNA obtained after amplification. Twelve sons were removed from the study when initial analysis showed that they deviated from Mendelian inheritance. This left a total of 1215 individuals from 400 nuclear families in the study. The basic characteristics of the study subjects are shown in Table 1. Because the effects of the parents' phenotypes were excluded from the statistical analysis (QTDT), we only made use of the body composition measurements of the sons.

Table 1. Basic characteristics of the subjects (Mean±SD).

Variation	Father (*n*=400)	Mother (*n*=400)	Son (*n*=415)
Age (years)	61.10±7.07	58.39±6.37	30.14±6.09
Height (m)	1.68±6.04	1.56±5.45	1.73±5.91
Weight (kg)	69.63±9.48	58.28±8.22	70.55±10.57
BMI (kg/m^2)	24.76±3.10	24.01±3.12	23.55±3.24
Arms fat mass (kg)	–	–	1.27±0.73
Legs fat mass (kg)	–	–	4.66±1.87
Trunk fat mass (kg)	–	–	9.38±4.37
Total fat mass (kg)	–	–	15.89±6.86
Percentage of fat mass	–	–	0.22±0.07

SNP genotyping and linkage disequilibrium

Five SNPs in *ALOX15* were examined initially; however, rs9894225 was excluded from further analysis when only one SNP (GG) was found after genotypic analysis, despite the use of multiple strategies to identify additional SNPs. The remaining four SNPs were in Hardy-Weinberg equilibrium (Table 2).

To gain further insight into the pattern of LD between alleles at polymorphic loci, pairwise disequilibrium measures (D′) were calculated. As shown in Figure 1, three SNPs (rs2619112, rs2619118, and rs916055) constituted one block. The SNP rs748694 was an "orphan", independent of the block. LD was observed for each SNP, with D′ values ranging from 0.69 to 0.72. Using the likelihood method implemented by PHASE, we inferred that 8 different haplotypes were presented in our population, using a likelihood method based on a PHASE. The most common haplotype (TGT) had a frequency of 42.4% (haplotype1), and four common haplotypes (TGT, CAC, TGC, and TAC) accounted for 86.6% of the haplotypes identified within our sample population of total unrelated parents (Table 3).

Association between SNPs and haplotypes and obesity-related phenotypes

All 400 families were included in the following analyses because the effects of the parents' phenotypes were excluded

Table 2. Information of the analyzed *ALOX15* SNPs in this study.

SNP	Physical position	Location and function	Allele change	Amino acid change	HWE	MAF in dbSNP	MAF in this study
rs9894225	4149933	Promoter	A>G	NA	0.22	0.26	1.00
rs748694	4496938	Promoter	A>G	NA	0.83	0.47	0.32
rs2619112	4482134	Intron 12	A>G	NA	0.90	0.49	0.40
rs2619118	4487026	Intron	C>T	NA	0.55	0.48	0.49
rs916055	4481583	3′-UTR	C>T	NA	0.32	0.42	0.39

NA=not applicable; MAF: minor allele frequency; HWE: Hardy-Weinberg equilibrium.

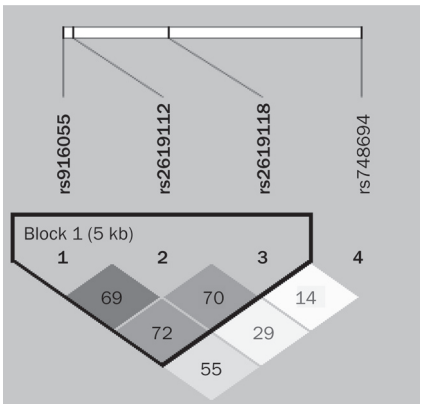

Figure 1. LD patterns for the ALOX15 gene. The increasing degree of darkness of the cells from white to black represents the increasing strength of LD. There is a strong LD (0.6<D′<0.8) across rs2619112, rs2619118, and rs916055. Rs748694 is not included for LD analysis.

Table 3. Frequency of *ALOX15* haplotypes for all available SNPs.

Index	rs916055	rs2619112	rs2619118	Frequency
1	T	G	T	0.424
2	C	A	C	0.266
3	T	G	C	0.103
4	T	A	C	0.073
5	C	G	C	0.067
6	C	A	T	0.055
7	T	A	T	0.007
8	C	G	T	0.006

Table 4. *P* values of tests for population stratification, total association, and within-family association using QTDT.

	rs748694	rs2619112	rs2619118	rs916055
Tests of population stratification				
BMI	0.894	0.355	0.919	0.755
Arm fat mass	0.222	0.329	0.814	0.687
Leg fat mass	0.099	0.364	0.576	0.441
Trunk fat mass	0.478	0.256	0.653	0.491
Total fat mass	0.142	0.132	0.680	0.312
Percentage of fat mass	0.108	0.220	0.294	0.361
Tests of total association				
BMI	0.934	0.575	0.845	0.589
Arm fat mass	0.740	0.564	0.354	0.372
Leg fat mass	0.862	0.543	0.569	0.198
Trunk fat mass	0.585	0.776	0.478	0.437
Total fat mass	0.928	0.558	0.402	0.173
Percentage of fat mass	0.775	0.844	0.075	**0.042**
Tests of within-family association				
BMI	0.939	0.588	0.850	0.992
Arm fat mass	0.541	0.767	0.589	0.360
Leg fat mass	0.202	0.822	0.954	0.146
Trunk fat mass	0.587	0.662	0.732	0.511
Total fat mass	0.275	0.499	0.723	0.093
Percentage of fat mass	0.186	0.309	0.520	**0.038**
P 1000 permutation of within-family association				
BMI	0.938	0.612	0.850	0.985
Arm fat mass	0.580	0.775	0.634	0.331
Leg fat mass	0.180	0.817	0.942	0.170
Trunk fat mass	0.834	0.223	0.297	0.135
Total fat mass	0.388	0.617	0.797	0.170
Percentage of fat mass	0.194	0.353	0.540	**0.033**

All body compositon values are adjusted for age. Bold indicates significant *P* values ($P<0.05$).

from the QTDT test. The results of the QTDT are summarized in Table 4. The analysis showed that there were 258, 278, 302, and 284 informative families at SNPs rs748694, rs2619112, rs2619118, and rs916055, respectively. We did not find significant population stratification in our samples. For the total and the family-based association analyses performed on the 400 nuclear families, we found that only rs916055 was significantly associated with PFM ($P=0.042$, and $P=0.038$, respectively), rs916055 had a marginal but insignificant association with tFM ($P=0.093$) in the family-based association results. No other SNP showed significant evidence of association (in either family-based association or the total family association) with any body composition parameters. Results of the multiple-parameter test involving 1000 permutations, greed with family-based association results. In this case, rs916055 also had a significant association with PFM ($P=0.033$).

Figure 1 is a graphical representation of pairwise LD as measured by D′. The results showed a region of substantial LD between rs2619112, rs2619118, and rs916055. Four common haplotypes accounted for 86.6% of the haplotypes in the sample population of unrelated parents (Table 3). The haplotype analysis is an important source of information that complements the LD analysis of SNPs and was generated using genotypic data from the three SNPs. We also investigated the association between obesity phenotypes and the four common haplotypes identified here. The TDT analysis showed that there were 288, 245, 105, and 84 informative families at haplotypes TGT, CAC, TGC and TAC, respectively. Significant population stratification was found for haplotype TGC with regard to the PFM ($P=0.027$). For total family association analysis, we detected a significant association between the most common haplotype (TGT) and PFM ($P=0.032$). However, we failed to find significant evidence of any link between a haplotype and obesity-related phenotypes by family-based association or the 1000 permutations test ($P>0.05$) (data not shown).

Discussion

It has become evident that the activation of inflammation and oxidative stress is involved in the development of obesity and its complications[2, 5–7]. The chronic inflammation caused by the recruitment of macrophages and the secretion of chemok-

Table 5. *P* values of association of haplotypes of *ALOX15* with obesity related phenotypes using QTDT.

	TGT	CAC	TGC	TAC
Tests of population stratification				
BMI	0.942	0.278	0.910	0.824
Arm fat mass	0.711	0.590	0.393	0.534
Leg fat mass	0.986	0.394	0.076	0.964
Trunk fat mass	0.546	0.510	0.218	0.450
Total fat mass	0.556	0.348	0.077	0.481
Percentage of fat mass	0.871	0.364	**0.027**	0.754
Tests of total association				
BMI	0.766	0.773	0.884	0.858
Arm fat mass	0.160	0.387	0.410	0.737
Leg fat mass	0.259	0.494	0.978	0.468
Trunk fat mass	0.378	0.591	0.892	0.959
Total fat mass	0.179	0.502	0.964	0.706
Percentage of fat mass	**0.032**	0.812	0.656	0.671
Tests of within-family association				
BMI	0.834	0.433	0.869	0.902
Arm fat mass	0.209	0.802	0.896	0.797
Leg fat mass	0.415	0.931	0.174	0.672
Trunk fat mass	0.291	0.955	0.301	0.587
Total fat mass	0.171	0.878	0.169	0.772
Percentage of fat mass	0.157	0.430	0.163	0.971
P 1000 permutation of within-family association				
BMI	0.843	0.447	0.871	0.912
Arm fat mass	0.225	0.814	0.888	0.768
Leg fat mass	0.428	0.935	0.199	0.624
Trunk fat mass	0.269	0.911	0.267	0.536
Total fat mass	0.282	0.923	0.261	0.776
Percentage of fat mass	0.180	0.459	0.147	0.961

All body compositon values are adjusted for age. Bold indicates significant *P* values ($P<0.05$).

ines and adipocytokines, affects adipose function[5, 6]. The products of lipoxygenases raise the expression of MCP-1, IL-6, TNF, and adhesion molecules in macrophages and vascular cells[24, 25]. Moreover, 12/15-lipoxygenases exacerbate oxidative stress by attacking mitochondria, leading to the production of reactive oxygen species (ROS)[26]. Recently, Almeida *et al*[27] demonstrated that the lipoxygenase-oxidized polyunsaturated fatty acids (PUFA) activates the ROS/FoxO/PPARγ catenin cascade, which results in elevated oxidative stress and PPARγ expression and reduced canonical Wnt signaling (the latter is the pathway linked to adipose inflammation). Therefore, lipoxygenase pathways may play an important role in the development of obesity. Indeed, previous studies have identified *ALOX5*[28, 29] and *ALOX12*[14] as susceptibility genes for obesity. *ALOX15*, another member of the lipoxygenases family, has been linked to obesity risk in several studies[13]. In the present study, we investigated the relationship between *ALOX15* gene polymorphisms and obesity-related phenotypes in a large group of Chinese nuclear families. Significant association was found between SNP rs916055 and PFM through QTDT analysis. The 1000 permutation test confirmed the results of the family-based association study.

The SNP rs916055 is located in the 3′-UTR of *ALOX15*. This region is important for the translational regulation of gene expression, particularly during embryonic development and differentiation[30]. Studies shown that the presence of an alternative differentiation control element (DICE) in the 3′-UTR of the *ALOX15* gene alters *ALOX15* mRNA and protein expression[24, 31]. Another SNP (rs11568131) within the *ALOX15* locus was shown to be significantly associated with the expression of key proinflammatory genes, such as those coding for IL-6, TNF, and IL-1, all of which influence obesity[32]. According to Hapmap, rs11568131 is in high LD with rs916055 (D′=1) (HapMap Data Phase III/Rel#2, Feb09, on NCBIB36 assembly, dbSNP b126), although rs11568131 displays a modest heterozygosity (MAF=0.155). Furthermore, one SNP (rs916055) has been shown to have significant association with bone mineral density (BMD) within the lumbar portion of the spine in postmenopausal women[33]. Because the genomic organization of mammalian ALOX is highly conserved[34], we speculated that SNP rs916055, which is located within the 3′-UTR of ALOX15 may affect the binding of the transcriptional machinery, which might, in turn, generate potentially functional RNA variants. However, no other SNPs or haplotypes were found to have a significant association with any obesity-related phenotype. All of the SNPs in this study had high heterozygosity (MAF>0.2), which increased our power to detect associations. This does not exclude the existence of common variants with low penetrance or rare variants with high penetrance, which make a contribution to the susceptibility to complex diseases[35, 36]. For example, a rare nonsynonymous SNP in *ALOX15*, rs34210653, was recently found to be associated with a higher risk of coronary heart disease[37]. To our knowledge, this is the first study to investigate the possible influence of *ALOX15* genetic variation on obesity in humans. Further studies should be conducted with a larger sample population and high density SNP genotyping among different ethnic groups to confirm our results.

This study has several strengths. First, more obesity-related phenotypes were examined in this study than are normally employed in such studies. The phenotypes, include TFM, tFM, LFM, and AFM, but not BMI. BMI has been widely used as a surrogate phenotype; however, it alone may not be sufficiently accurate to be used to indicate the proportion of fat in the body or the relative contributions of body muscle and fat[38]. DXA is a reliable and convenient method of assessing obesity and is considered the golden standard for anthropometric measures[39]. Although CT and MRI scans can also provide these measurements, those methods are limited by costs, radiation exposure and other factors[40]. DXA analyses can yield information on the fat composition of body segments, such as the hip, trunk and limbs. It is well known that abdominal or visceral fat is strongly associated with metabolic disturbances and cardiovascular disease[41–43]. Studies indicate

that DXA-based measurements of the fat mass in the trunk region strongly correlate with CT and MRI scans of abdominal fat[44–46]. In the present study, we measured the total, central (trunk) and peripheral (leg and arm) fat mass in young men aged 20–40 years. Another strength of this study is the use of QTDT analysis. Family-based associations are unaffected by population stratification. Thus, QTDT avoids the false-positive and false-negative results that occur more than with other association analyses[47]. With 400 nuclear families in our sample, the test has a power of >80% to identify a candidate gene as a quantitative trait locus (QTL), which can explain ~10% of the variation in the obesity phenotypes. We also performed permutations (1000 simulations) to generate empirical *P*-values[15, 16], which helps to eliminate false-positive results generated by multiple QTDT tests.

Our study is limited by several factors. First, we selected only five SNPs of *ALOX15* for the study. Second, the aim of this study was to explore the impact of *ALOX15* gene on obesity-related phenotypes; however, only 9% of the sons were obese (a BMI of 30 or higher is considered obese). A larger obese population should be recruited for the next study.

In conclusion, we found that the SNP rs916055 had a significant family-based association with PFM in nuclear families with young males using the QTDT approach to demonstrate linkage. Further studies to validate our results should be conducted with larger samples, a great proportion of obese individuals and rare SNPs from different ethnic groups.

Acknowledgements

This study was supported by the National Natural Science Foundation of China (Grant Nos 81170803, 30570819, 30800387, 81070692, and 81000360), the Program of Shanghai Subject Chief Scientist (No 08XD1403000) and STCSM (Nos 10D21950100 and 08411963100).

Author contribution

Zhen-lin ZHANG designed the research; Yao-hua KE, Wen-jin XIAO, Jin-wei HE, Jin-bo YU, Gao GAO, Hua YUE, Chun WANG, and Wen-zhen FU performed the research; Hao ZHANG, Jin-bo YU, Wei-wei HU, Jie-mei GU, and Yu-juan LIU recruited research subjects; Yun-qiu HU and Miao LI took fat mass and lean mass measurements. Zhen-lin ZHANG contributed new analytical tools; Wen-jin XIAO and Zhen-lin ZHANG analyzed the data; Wen-jin XIAO wrote the paper.

References

1 Monteiro R, Azevedo I. Chronic inflammation in obesity and the metabolic syndrome. Mediators Inflamm 2010. doi: 10.1155/2010/289645.
2 Shah A, Mehta N, Reilly MP. Adipose inflammation, insulin resistance, and cardiovascular disease. J Parenter Enteral Nutr 2008; 32: 638–44.
3 Ketonen J, Pilvi T, Mervaala E. Caloric restriction reverses high-fat diet-induced endothelial dysfunction and vascular superoxide production in C57B1/6 mice. Heart Vessels 2010; 25: 254–62.
4 Kobayasi R, Akamine EH, Davel AP, Rodrigues MA, Carvalho CR, Rossoni LV. Oxidative stress and inflammatory mediators contribute to endothelial dysfunction in high-fat diet-induced obesity inmice. J Hypertens 2010; 28: 2111–9.
5 Barry S, Camillo R. Anti-inflammatory nutrition as a pharmacological approach to treat obesity. J Obes 2011; doi:10.1155/2011/431985.
6 Bastard JP, Maachi M, Lagathu C, Kim MJ, Caron M, Vidal H, *et al*. Recent advances in the relationship between obesity, inflammation, and insulin resistance. Eur Cytokine Netw 2006; 171: 4–12.
7 Qatanani M, Lazar MA. Mechanisms of obesity-associated insulin resistance: many choices on the menu. Genes Dev 2007; 211: 1443–55.
8 Yuan M, Konstantopoulos N, Lee J. Reversal of obesity and diet-induced insulin resistance with salicylates or targeted disruption of IKKB. Science 2001; 293: 1673–7.
9 Skalen K, Gustafsson M, Rydberg EK, Hultén LM, Wiklund O, Innerarity TL, *et al*. Subendothelial retention of atherogenic lipoproteins in early atherosclerosis. Nature 2002; 417: 750–4.
10 Nadler JL, Pei H, Bevard M, Bruce A. Reduced macrophage infiltration in visceral adipose tissue of 12-lipoxygenase knockout mice. Arterioscler Thromb Vasc Biol 2007; 27: E48.
11 Chakrabarti SK, Cole BK, Wen Y, Keller SR, Nadler JL. 12/15-lipoxygenase products induce inflammation and impair insulin signaling in 3T3-L1 adipocytes. Obesity 2009; 17: 1657–63.
12 Sears DD, Miles PD, Chapman J, Ofrecio JM, Almazan F, Thapar D, *et al*. 12/15-lipoxygenase is required for the early onset of high fat diet-induced adipose tissue inflammation and insulin resistance in mice. PLoS One 2009; 4: e7250.
13 Rankinen T, Zuberi A, Chagnon YC, Weisnagel SJ, Argyropoulos G, Walts B. The human obesity gene map: the 2005 update. Obesity 2006; 14: 529–644.
14 Xiao WJ, He JW, Zhang H, Hu WW, Gu JM, Yue H, *et al*. ALOX12 polymorphisms are associated with fat mass but not peak bone mineral density in Chinese nuclear families. Int J Obes 2011; 35: 378–86.
15 Chen XS, Kurre U, Jenkins NA, Copeland NG, Funk CD. cDNA cloning, expression, mutagenesis of C-terminal isoleucine, genomic structure, and chromosomal localizations of murine 12-lipoxygenases. J Biol Chem 1994; 269: 13979–87.
16 Yoo H, Jeon B, Jeon MS, Lee H, Kim TY. Reciprocal regulation of 12- and 15-lipoxygenases by UV-irradiation in human keratinocytes. FEBS Lett 2008; 582: 3249–53.
17 Gao G, Zhang ZL, He JW, Zhang H, Yue H, Hu WW, *et al*. No association of the polymorphisms of the frizzled-related protein gene with peak bone mineral density in Chinese nuclear families. BMC Med Genet 2010; 11: 1.
18 Kelavkar U, Wang S, Montero A, Murtagh J, Shah K, Badr K. Human 15-lipoxygenase gene promoter: analysis and identification of DNA binding sites for IL-13-induced regulatory factors in monocytes. Mol Biol Rep 1998; 25: 173–82.
19 Urano T, Shiraki M, Fujita M, Hosoi T, Orimo H, Ouchi Y, *et al*. Association of a single nucleotide polymorphism in the lipoxygenase ALOX15 5′-flanking region (-5229G/A) with bone mineral density. J Bone Miner Metab 2005; 23: 226–30.
20 Stephens M, Smith NJ, Donnelly P. A new statistical method for haplotype reconstruction from population data. Am J Human Genet 2001; 68: 978–89.
21 Barrett JC, Fry B, Maller J, Daly MJ. Haploview: analysis and visualization of LD and haplotype maps. Bioinformatics 2005; 21: 263–5.
22 Zhang ZL, He JW, Qin YJ, Hu YQ, Li M, Zhang H, *et al*. Association between myostatin gene polymorphisms and peak BMD variation in Chinese nuclear families. Osteoporos Int 2008; 19: 39–47.
23 Zhang ZL, He JW, Qin YJ, Hu YQ, Li M, Liu YJ, *et al*. Association between SNP and haplotypes in PPARGC1 and adiponectin genes and

bone mineral density in Chinese nuclear families. Acta Pharmacol Sin 2008; 28: 287–95.
24 Kritzik MR, Ziober AF, Dicharry S, Conrad DJ, Sigal E. Characterization and sequence of an additional 15-lipoxygenase transcript and of the human gene. Biochim Biophys Acta 1997; 1352: 267–81.
25 Saltiel AR, Kahn CR. Insulin signalling and the regulation of glucose and lipid metabolism. Nature 2001; 414: 799–806.
26 Pallast S, Arai K, Wang X, Lo EH, van Leyen K. 12/15-Lipoxygenase targets neuronal mitochondria under oxidative stress. J Neurochem 2009; 111: 882–9.
27 Almeida M, Ambrogini E, Han L, Manolagas SC, Jilka RL. Increased lipid oxidation causes oxidative stress, increased peroxisome proliferator-activated receptor-gamma expression, and diminished pro-osteogenic Wnt signaling in the skeleton. J Biol Chem 2009; 284: 27438–48.
28 Mehrabian M, Schulthess FT, Nebohacova M, Castellani LW, Zhou Z, Hartiala J, *et al*. Identification of *ALOX5* as a gene regulating adiposity and pancreatic function. Diabetologia 2008: 51: 978–88.
29 Mehrabian M, Allayee H, Stockton J, Lum PY, Drake TA, Castellani LW, *et al*. Integrating genotypic and expression data in a segregating mouse population to identify 5-lipoxygenase as a susceptibility gene for obesity and bone traits. Nat Genet 2005; 37: 1224–33.
30 Wickens M, Anderson P, Jackson RJ. Life and death in the cytoplasm: messages from the 3′ end. Curr Opin Genet Dev 1997; 7: 220–32.
31 Thiele BJ, Berger M, Huth A, Reimann I, Schwarz K, Thiele H. Tissue-specific translational regulation of alternative rabbit 15-lipoxygenase mRNAs differing in their 3′-untranslated regions. Nucleic Acids Res 1999; 27: 1828–36.
32 Fairfax BP, Vannberg FO, Radhakrishnan J, Hakonarson H, Keating BJ, Hill AV, *et al*. An integrated expression phenotype mapping approach defines common variants in LEP, ALOX15, and CAPNS1 associated with induction of IL-6. Hum Mol Genet 2010; 19: 720–30.
33 Cheung CL, Chan V, Kung AW. A differential association of ALOX15 polymorphisms with bone mineral density in pre- and post-menopausal women. Hum Hered 2008; 65: 1–8.
34 Fuck CD. Molecular biology in the eicosanoid field. Prog Nucleic Acid Res Mol Biol 1993; 45: 67–98.
35 Schork NJ, Murray SS, Frazer KA, Topol EJ. Common *vs* rare allele hypotheses for complex diseases. Curr Opin Genet Dev 2009; 19: 212–9.
36 Schork NJ, Wessel J, Malo N. DNA sequence-based phenotypic association analysis. Adv Genet 2008; 60: 195–217.
37 Assimes TL, Knowles JW, Priest JR, Basu A, Borchert A, Volcik KA, *et al*. A near null variant of 12/15-LOX encoded by a novel SNP in *ALOX15* and the risk of coronary artery disease. Atherosclerosis 2008; 198: 136–44.
38 Ode JJ, Pivarnik JM, Reeves MJ, Knous JL. Body mass index as a predictor of percent fat in college athletes and nonathletes. Med Sci Sports Exerc 2007; 39: 403–9.
39 Glickman SG, Marn CS, Supiano MA, Dengel DR. Validity and reliability of dual energy X-ray absorptiometry for the assessment of abdominal adiposity. J Appl Physiol 2004; 97: 509–14.
40 Goodpaster BH. Measuring body fat distribution and content in humans. Curr Opin Clin Nutr Metab Care 2002; 5: 481–7.
42 Pi-Sunyer FX. The epidemiology of central fat distribution in relation to disease. Nutr Rev 2004; 62: S120–6.
42 Bray GA, Jablonski KA, Fujimoto WY, Barrett-Connor E, Haffner S, Hanson RL, *et al*. Relation of central adiposity and body mass index to the development of diabetes in the Diabetes Prevention Program. Am J Clin Nutr 2008; 87: 1212–8.
43 Fox CS, Massaro JM, Hoffmann U, Pou KM, Maurovich-Horvat P, Liu CY, *et al*. Abdominal visceral and subcutaneous adipose tissue compartments: association with metabolic risk factors in the Framingham Heart Study. Circulation 2007; 116: 39–48.
44 Snijder MB, Visser M, Dekker JM, Seidell JC, Fuerst T, Tylavsky F, *et al*. The prediction of visceral fat by dual-energy X-ray absorptiometry in the elderly: a comparison with computed tomography and anthropometry. Int J Obes Relat Metab Disord 2002; 26: 984–93.
45 Kamel EG, McNeill G, Han TS, Smith FW, Avenell A, Davidson L, *et al*. Measurement of abdominal fat by magnetic resonance imaging, dual-energy X-ray absorptiometry and anthropometry in non-obese men and women. Int J Obes Relat Metab Disord 1999; 23: 686–92.
46 Lee K, Lee S, Kim YJ, Kim YJ. Waist circumference, dual-energy X-ray absortiometrically measured abdominal adiposity, and computed tomographically derived intra-abdominal fat area on detecting metabolic risk factors in obese women. Nutrition 2008; 24: 625–31.
47 Liu C, Xu D, Sjoberg J, Forsell P, Björkholm M, Claesson HE. Transcriptional regulation of 15-lipoxygenase expression by promoter methylation. Exp Cell Res 2004; 297: 61–7.

Acta Pharmacologica Sinica (2012) 33: 208–209
 1671-4083/12 $32.00
www.nature.com/aps

Research Highlight

Hormone level and dopamine tells the value of food

Zuo-ren WANG*

Acta Pharmacologica Sinica (2012) 33: 208–209; doi: 10.1038/aps.2011.211; published online 16 Jan 2012

Ideal food should be delicious and nutritious. But sometimes, the food you eat is delicious but not nutritious, or nutritious but not delicious. To let animals know which to be delicious or nutritious is an important or valuable question. In a recent article published in *Nature Neuroscience*[1], Friedman JM *et al* addressed this question and showed that the level of hormone leptin and dopamine system co-regulated the reward value of food in mice.

Leptin, a 16 kDa protein encoded by the Ob (Obese) gene, is a hormone that has a central role in regulation of fat metabolism, appetite and the balance between energy intake and consumption[2]. Leptin was identified and its role in fat metabolism was firstly revealed by Friedman JM *et al* in 1994. In mouse genetic screen study, they found that mutation in the genes encoding either leptin itself or leptin's receptor caused massively obese in mice, and this could be rescued by injections of leptin. These findings in mice coincided with the observations that humans carrying homozygous mutations in leptin gene suffered severe obesity. These results indicated that leptin signals are important in regulating fat metabolism. Later studies revealed that instead of a signal to consume the surfeit of fat, leptin is a signal informing the brain of enough nutrients in the body. Thus, when an animal is full up, its leptin level goes high that in turn sends a satiety signal to the brain and stop the animal from eating more. On the contrary, when an animal is in hunger, its leptin level drops, thus sends less satiety signal to the brain; and this drive the animal to looking for nutritious food.

Dopamine is a neurotransmitter involved in modulating many important brain functions. Dopamine is released by the dopaminegic neurons in hypothalamus, substantia nigra and especially ventral tegmental area (VTA) — a brain region tightly linked with rewarding process. Many studies showed that rewarding process is highly related to the activation of the dopaminegic neurons in the VTA of the middle brain[3]. A trick that the authors used in their research is to mimic the rewarding process by specifically activating of the dopaminegic neurons in VTA.

The technique that Friedman JM *et al* used in this article is optogentectics, a recently developed tool, in which light-activatable cation channel (*eg*, Channelrhodopsin II, ChR2) or light-activatable chloride pump (*eg*, Halorhodopsin from Natromonas, NPHR) are used to activate or silent the function of the interested neurons[4]. They generated a kind of genetically engineered mice, in which ChR2 protein was specifically expressed in the dopaminegic neuron in VTA. An optic fiber was then introduced to the VTA of the mice. When laser pulses were delivered to VTA through the optic fiber, the dopaminegic neurons were activated, mimicking a rewarding process. Next, they measured the preference index of the mice to two kinds of "sugar", sucrose and sucralose. Sucrose is a kind of natural sugar with nutrient, which sucralose is a synthetic sweetener with very low calories. They found that the mice naturally prefer the nutritious sucrose to the low-calorie sucralose, suggesting that nutrient of sucrose confer it a higher rewarding value, and sucralose has a lower rewarding value. Interestingly, this could be reversed when sucralose was paired with activation of the dopaminegic neurons. When the sucralose solution was applied to the mice, laser pulses were simultaneously delivered to activate the dopaminegic neurons in VTA. In this scenario, the mice switched to prefer sucralose. These results suggest that preference to a food not only depends on the sensation on the tongue, but also the brain judgment of its reward value of the food. Furthermore, the authors investigated whether the leptin level affects the judgment of food reward value. When the mice were deprived for food for 24 h, the dropping of leptin level coincided with that the value of sucrose increased. Upregulation of leptin by injection can reverse this effect. These results indicated that leptin could regulate the reward value of nutrient.

The findings made by the authors are not only important to our fundamental understanding of the regulatory mecha-

Institute of Neuroscience, State Key Laboratory of Neuroscience, Shanghai Institutes for Biological Sciences, Chinese Academy of Sciences, Shanghai 200031, China
Correspondence: Prof Zuo-ren WANG (zuorenwang@ion.ac.cn)

nisms of appetite and fat metabolism, but also provide important clues for weight control and therapeutics for metabolism-related disorders, such as obesity and nervosa. If the leptin level in people with obesity or nervosa can be modulated, their appetite or desire for food, and their body weight can be controlled.

1 Domingos AI, Vaynshteyn J, Voss HU, Ren X, Gradinaru V, Zang F, *et al*. Leptin regulates the reward value of nutrient. Nat Neurosci 2011; 14: 1562–8.
2 Friedman JM. Leptin at 14 y of age: an ongoing story. Am J Clin Nutr 2009; 89: 973S–979S.
3 Schultz W. Getting formal with dopamine and reward. Neuron 2002; 36: 241–63.
4 Fenno L, Yizhar O, Deisseroth K. The development and application of optogenetics. Annu Rev Neurosci 2011; 34: 389–412.

Acta Pharmacologica Sinica 2012: 210–211
 1671-4083/12 $32.00
www.nature.com/aps

Research Highlight

Novel agents inhibit human leukemic cells

Wei-ping YU[1, *], Juan LI[2]

Acta Pharmacologica Sinica (2012) 33: 210–211; doi: 10.1038/aps.2011.207; published online 9 Jan 2012

Ouabain (OUA) and pyrithione zinc (PZ) have been proved as the potential drugs for treating acute myeloid leukemia (AML). Selected from a screening among 1040 Food and Drug Administration-approved pharmacological agents, both drugs show ability to induce apoptosis of the culturing AML cells, exhibiting the poisoning effect on the cells. Studies also reveal the efficiency of the drugs in inhibiting the growth of human AML cells injected into the mice lacking of immunity and killing primary AML cells from the peripheral blood of AML patients[1].

AML is a quickly progressive malignant disease characterized by too many immature blood-forming cells in the bone marrow and blood which interfere with the production of normal blood cells. In normal process of the formation and development of blood cells, a normal cell is gradually matured from immature blood-forming cells without uncontrolled growth. However, a single malignant AML cell accumulates genetic and/or epigenetic changes which "freeze" the cell in its immature state and prevent differentiation in AML[2]. When this is combined with other abnomal changes which disrupt genes controlling proliferation, the result is uncontrolled proliferation and/or abnormal survival of an immature clone of cells, leading to the clinical entity of AML[3]. The malignant cell often possesses surface marker CD34, a marker of primitive blood cells[4]. Therefore, to eliminate the malignant cells, a successful drug treatment of AML has to inhibit cell proliferation and/or induce cell death including apoptosis and necrosis. Since gene regulatory networks that govern these malignant cells are very complicated, the discovery of drugs that have different targets on AML cells is an attractive but difficult endeavor[5].

The conventional drugs for AML treatment such as cytarabine, idarubicin or daunorubicin target the cell cycle or nuclear DNA. They are not effective against the $CD34^+$ malignant cells which are usually the quiescent cells. In addition, it is found that the nuclear factor-κB (NF-κB) transcription factor is aberrantly activated in $CD34^+$ malignant AML cells to support abnormal proliferation and resistance to apoptosis triggered by therapeutic agents, suggesting that NF-κB inhibition may be an important therapeutic target[6]. In other tumors, loss of NF-κB is associated with increased apoptosis and sensitivity to chemotherapy. However, the commonly used AML chemotherapeutics (*eg*, cytarabine and anthracyclines) actually activate, rather than inhibit, NF-κB, providing a survival advantage to the malignant cells[7]. Overall, it is urgent to ask for novel drug options targeting AML cells independent of cell cycle or nuclear DNA, relating to NF-κB activity and the $CD34^+$ malignant cells. Recently, Tailler *et al*[1] report that they have created a system, suitable to screen more than 1000 compounds in one single experiment, and successfully identified two potential drugs inducing AML cell death by this way.

OUA, a specific ligand of Na^+/K^+ ATPase, has been used for more than 200 years for the treatment of cardiac insufficiency by inhibiting Na^+/K^+ ATPase activity. In addition to this effect, recent studies have indicated that OUA is also able to induce apoptosis and inhibit cell proliferation in solid tumors, the mechanisms involved include its binding to the Na^+/K^+ ATPase resulting in intracellular Na^+ and Ca^{2+} levels increment and a variety of mechanisms mostly to be irrelevant for AML cells[8]. PZ is an antifungal and antibacterial agent for external use in clinic. Tailler *et al*[1] find that both OUA and PZ can trigger AML cell death by inhibiting NF-κB dependent survival signaling and hence stimulating mitochondrial pathway of apoptosis. Moreover, both OUA and PZ can inhibit the tumor formation of human AML cells injected into the mice lacking of immunity and induce the death of $CD34^+$ malignant cells from AML patients. Therefore, they conclude that, unlike the conventional drugs, both OUA and PZ exert significant anticancer effects on human AML cells by the mechanisms that are not involved with DNA damage, cell cycle arrest or differentiation, reactive oxygen species (ROS)

[1]*Department of Pathophysiology, Medical School of Southeast University, Nanjing 210009, China;*
[2]*Department of Hematology, the Affiliated Drum Tower Hospital of Nanjing University Medical School, Najing 210008, China*
Correspondence: Prof Wei-ping YU
(wpylg@hotmail.com)

increment and protein structural change. They also demonstrate that both OUA and PZ had no significant toxicity on the mice at doses which bring about high antileukemic efficiency and no synergistic effect with the conventional drugs.

The findings by Tailler *et al*[1] in the experimental and preclinical AML treatments with OUA and PZ serve to highlight two promising antileukemic agents whose activity should be evaluated in prospective clinical studies. However, it is necessary to clarify some related preliminary questions. First, it is not enough to conclude that OUA and PZ induce apoptosis through a mechanism independently of ROS in AML cells, only by the result that inhibiting the nitric oxide synthesis failed to suppress OUA- or PZ-induced apoptosis. It needs further confirmation that no other kinds of ROS such as hydroxyl radical and superoxide anion radical involved, by FACS analysis of generation of ROS in AML cells treated with OUA or PZ. Second, the doses of the drugs used in AML patients for effectively killing the malignant cells with no toxicity should be determined, which may quite different from that used in mice. Third, the precise antileukemic mode of action of PZ should be elucidated, and pharmacokinetics experiments of PZ should be done when it is for internal use. In addition to testing the new therapeutics, researchers should be able to explain, if it is not by chance or not due to their structure, the pharmacological reason that these two drugs with different medical usage have the same cell death-inducing effects on AML cells with similar underline mechanisms.

1 Tailler M, Senovilla L, Lainey E, The'pot S, Me' tivier D, Se'bert M, *et al*. Antineoplastic activity of ouabain and pyrithione zinc in acute myeloid leukemia. Oncogene 2011. doi: 10.1038/onc.2011.521.
2 Fialkow PJ. Clonal origin of human tumors. Biochim Biophys Acta.1976; 458: 283–321.
3 Fialkow PJ, Janssen JW, Bartram CR. Clonal remissions in acute nonlymphocytic leukemia: evidence for a multistep pathogenesis of the malignancy. Blood 1991; 77: 1415–7.
4 Bonnet D, Dick JE. Human acute myeloid leukemia is organized as a hierarchy that originates from a primitive hematopoietic cell. Nat Med 1997; 3: 730–7.
5 McDermott SP, Eppert K, Notta F, Isaac M, Datti A, Al-Awar R, *et al*. A small molecule screening strategy with validation on human leukemia stem cells uncovers the therapeutic efficacy of kinetin riboside. Blood 2011. doi: 10.1182/blood-2011-01-330019.
6 Griessinger E, Frelin C, Cuburu N, Imbert V, Dageville C, Hummelsberger M, *et al*. Preclinical targeting of NF-kappaB and FLT3 pathways in AML cells. Leukemia 2008; 22: 1466–9.
7 Jordan CT, Guzman ML. Mechanisms controlling pathogenesis and survival of leukemic stem cells. Oncogene 2004; 23: 7178–87.
8 Chen JQ , Contreras RG, Wang R, Fernandez SV, Shoshani L, Russo IH, *et al*. Sodium/potasium ATPase (Na^+, K^+-ATPase) and ouabain/related cardiac glycosides: a new paradigm for development of anti-breast cancer drugs? Breast Cancer Res Treat 2006; 96: 1–15.

Acta Pharmacologica Sinica 2012: 212–213
 1671-4083/12 $32.00
www.nature.com/aps

Research Highlight

Novel targeted therapy for acute myeloid leukemia with a dual FLT3 and JAK2 inhibitor

Yin-jun LOU*

Acta Pharmacologica Sinica (2012) 33: 212–213; doi: 10.1038/aps.2011.206; published online 9 Jan 2012

Acute myeloid leukemia (AML) is a highly malignant hematopoietic tumor. The use of all-*trans* retinoic acid (ATRA) and arsenic trioxide, which began from China, has resulted in revolution of the acute promyelocytic leukemia (APL) that appears curable in more than 70% of patients[1]. However, the treatment regimen for non-APL AML particularly in older patients has progressed little in the past two decades. Intensive efforts have been made toward the development of novel target agents, which are based on new-found pathophysiological events crucial for cancers. FMS-related tyrosine kinase 3 (FLT3), which is mutated in about 30% patients of AML, is the most ideal target for molecular therapy. Over the past decade, a number of FLT3 inhibitors have been studied in clinical trials. However, the results were often transient because of secondary resistance developed[2]. In addition, genetic lesions and aberrations involving Janus-associated kinase 2 (JAK2) have been found to be associated with a wide spectrum of hematological malignancies[3]. Recently, S Hart *et al* reported that pacritinib (SB1518), a dual JAK2/FLT3 inhibitor, emerged as an ideal new therapeutic agent for acute myelogenous leukemia in a preclinical study[4].

Pacritinib is a potent and selective inhibitor of FLT3 and JAK2 with IC_{50} of 23 and 22 nmol/L, respectively[5]. In the study, the authors demonstrated pacritinib led to a dose-dependent decrease of FLT3 auto-phosphorylation and downstream effectors of STAT5, ERK1/2, AKT phosphorylation in FLT3-internal-tandem duplication (ITD) cell lines (MV4-11, MOLM-13) and in FLT3-wt-bearing cell line (RS4;11). The agent inhibited the proliferation of MV4-11, MOLM-13 and RS4; 11 cells with IC_{50} of 47, 67, and 930 nmol/L, respectively. Furthermore, the JAK2V617F-harboring cell line, SET-2, was also very sensitive to pacritinib (IC_{50}=220 nmol/L). Flow cytometry analysis showed that the agent could induce G_1 arrest and caspase-dependent apoptotsis. Pacritinib inhibited the proliferation of 14 primary AML samples with the IC_{50} ranging from 190 nmol/L to 1300 nmol/L, with concomitant inhibition of phosphorylation of FLT3, STAT3, and STAT5. The two samples harboring the FLT3-ITD mutation were among the most sensitive. Moreover, pacritinib was also highly active in *in vivo* models of FLT3-ITD driving cell lines. In MV4-11 tumor-bearing mice, pacritinib (once daily for 21 consecutive days) induced dose-dependent inhibition of tumor growth. Complete regression was observed in 3/10 and 8/8 mice in the groups receiving 50 and 100 $mg \cdot kg^{-1} \cdot day^{-1}$, respectively. In the MOLM-13 model, pacritinib treatment (150 mg/kg bid for 7 consecutive days) resulted in tumor growth inhibition of 83%. Finally, higher activity of JAK/STAT signaling was confirmed in FLT3-linifanib/ABT-869 resistant cells (MV4-11-R). Pacritinib was highly effective in the resistant cell lines. A combination of FLT3 inhibitor linifanib with JAK family inhibitor ruxolitinib showed the synergistic effect on MV4-11 cells.

Interestingly, pacritinib entered the clinic in 2008 has completed Phase 2 trials for myelofibrosis. It has shown promising clinical activity and a favorable safety profile. The agent has received orphan drug designation from the US and the EU regulatory authorities. In summary, the preliminary results of the dual inhibitor of FLT3 and JAK2 were promising. Hope remains that pacritinib will be become an effective therapeutic adjunct to our current treatment approach to AML. Results from near future clinical trials will answer the question whether the dual inhibitor of FLT3 and JAK2 will be a real successful targeted agent.

As the next generation sequence technology advanced, more genetic and molecular changes in cancers including AML were discovered[6]. Multiple different genetic changes may cooperate in cancers. New mutations in signaling pathway or alternate pathway will emerge when treated by only one specific target agent[7]. Thus, from a clini-

Department of Hematology, Institute of Hematology, the First Affiliated Hospital of Zhejiang University, School of Medicine, Hangzhou 310003, China
Correspondence: Dr Yin-jun LOU
(louyinjun@yahoo.com.cn)

cal point of view there are at least two important aspects in this study. First, the resistant of target therapy could be possible reversed by simultaneously blocking two or more signaling pathways. It indicates a new strategy to screen for agents for an effective targeted cancer therapy. Second, since there are a handful of FLT3, JAK2 inhibitors or other kinase inhibitors have already been discovered and are currently being developed for clinical trials. It is rationale to designing trials in a more effective manner by combining one targeted drugs along with other agents that target alternate mechanisms of disease pathogenesis.

1 Wang ZY, Chen Z. Acute promyelocytic leukemia: from highly fatal to highly curable. Blood 2008; 111: 2505–15.
2 Fathi A, Levis M. FLT3 inhibitors: a story of the old and the new. Curr Opin Hematol 2011; 18: 71–6.
3 Stein BL, Crispino JD, Moliterno AR. Janus kinase inhibitors: an update on the progress and promise of targeted therapy in the myeloproliferative neoplasms. Curr Opin Oncol 2011; 23: 609–16.
4 Hart S, Goh KC, Novotny-Diermayr V, Hu CY, Hentze H, Tan YC, *et al*. Pacritinib (SB1518), a JAK2/FLT3 inhibitor for the treatment of acute myeloid leukemia. Blood Cancer J 2011; 1: e44.
5 Hart S, Goh KC, Novotny-Diermayr V, Tan YC, Madan B, Amalini C, *et al*. SB1518, a novel macrocyclic pyrimidine-based JAK2 inhibitor for the treatment of myeloid and lymphoid malignancies. Leukemia 2011; 25: 1751–9.
6 Mardis ER, Ding L, Dooling DJ, Larson DE, McLellan MD, Chen K, *et al*. Recurring mutations found by sequencing an acute myeloid leukemia genome. N Engl J Med 2009; 361: 1058–66.
7 Wagle N, Emery C, Berger MF, Davis MJ, Sawyer A, Pochanard P, *et al*. Dissecting therapeutic resistance to RAF inhibition in melanoma by tumor genomic profiling. J Clin Oncol 2011; 29: 3085–96.

Acta Pharmacologica Sinica (2012) 33: 214–220
 1671-4083/12 $32.00
www.nature.com/aps

Original Article

Temperature- and concentration-dependence of kainate-induced γ oscillation in rat hippocampal slices under submerged condition

Cheng-biao LU[1, *], Zhi-hua WANG[1], Yan-hong ZHOU[2], Martin VREUGDENHIL[3]

[1]Department of Automation, Institute of Electrical Engineering, Yanshan University, Qinhuangdao 066004, China; [2]Department of Computer, Institute of Mathematics and Information Technology, Hebei Normal University of Science and Technology, Qinhuangdao 066004, China; [3]Department of Neurophysiology, University of Birmingham, Birmingham, West Midlands, United Kingdom

Aim: Fast neuronal network oscillation at the γ frequency band (γ oscillation: 30–80 Hz) has been studied extensively in hippocampal slices under interface recording condition. The aim of this study is to establish a method for recording γ oscillation in submerged hippocampal slices that allows simultaneously monitoring γ oscillation and the oscillation-related intracellular events, such as intracellular Ca^{2+} concentration or mitochondrial membrane potentials.
Methods: Horizontal hippocampal slices (thickness: 300 μm) of adult rats were prepared and placed in a submerged or an interface chamber. Extracellular field recordings were made in the CA3c pyramidal layer of the slices. Kainate, an AMPA/kainate receptor agonist, was applied via perfusion. Data analysis was performed off-line.
Results: Addition of kainate (25–1000 nmol/L) induced γ oscillation in both the submerged and interface slices. Kainate increased the γ power in a concentration-dependent manner, but the duration of steady state oscillation was reduced at higher concentrations of kainate. Long-lasting γ oscillation was maintained at the concentrations of 100–300 nmol/L. Under submerged condition, γ oscillation was temperature-dependent, with the maximum power achieved at 29 ℃. The induction of γ oscillation under submerged condition also required a fast rate of perfusion (5–7 mL/min) and showed a fast dynamic during development and after the washout.
Conclusion: The kainite-induced γ oscillation recorded in submerged rat hippocampal slices is useful for studying the intracellular events related to neuronal network activities and may represent a model to reveal the mechanisms underlying the normal neuronal synchronizations and diseased conditions.

Keywords: γ oscillation; neuronal network; hippocampus; kainite; submerged slice

Acta Pharmacologica Sinica (2012) 33: 214–220; doi: 10.1038/aps.2011.159; published online 23 Jan 2012

Introduction

Neuronal network oscillations at the gamma frequency band (γ oscillations, 30–80 Hz) generated in the cortex play an important role in learning and memory[1, 2]. These oscillations provide a timing mechanism for controlling information processing[1, 3]. Impairments of γ oscillations have been associated with Alzheimer's disease[4] and normal aging. Both *in vivo*[5] and *in vitro*[6, 7] studies have suggested that intrahippocampally generated γ activity emerges from the rhythmic activity of interneurons that receive converging inputs from pyramidal neurons and control their firing through divergent outputs. The similarity in the timing of the unit discharges to the field potentials observed both *in vivo* and *in vitro* have validated the *in vitro* γ models.

In vitro models of hippocampal γ oscillations rely on a depolarizing drive provided by specific agonists for the metabotropic glutamate, muscarinic acetylcholine or kainate receptors. Most *in vitro* oscillations have been shown to be accurate experimental models for the study of *in vivo* γ oscillations[5, 8, 9]. Although *in vitro* γ oscillations are primarily studied under interface conditions and have provided valuable information for an understanding of the mechanisms of oscillatory activities, the limitation of this model is its inability to detect intracellular events, such as intracellular calcium concentrations or mitochondrial functions in individual neurons, which are critical for neuronal network oscillations[10]. To study intracellular events related to γ oscillations, an *in vitro* γ recording under submerged conditions is essential. Previous studies reported the difficulty of inducing and maintaining γ oscillations under submerged conditions[7, 11, 12]. Here, we aim to develop

* To whom correspondence should be addressed.
E-mail cblu@ysu.edu.cn
Received 2011-06-29 Accepted 2011-10-26

a method for recording persistent γ oscillations under submerged conditions that is capable of simultaneously monitoring γ oscillations and oscillation-related intracellular events.

By optimizing the experimental conditions, we established a method in which persistent γ oscillations can be reliably induced in the hippocampal CA3 area and that provides a superior model for the study of cellular mechanisms underlying γ oscillations.

Materials and methods

Animal model

All procedures were carried out under UK home office license and in accordance with the regulation of the UK Animals Act, 1998 and associated guidance. All efforts were made to minimize animal suffering, reduce the number of animals used, and utilize alternatives to *in vivo* techniques, if available.

Young adult rats (3–4 months) were anesthetized by intraperitoneal injection of a ketamine (76 mg/kg)/medetomidine (1 mg/kg) mixture and then sacrificed by cervical dislocation. The brain was quickly removed and immersed in an ice-cold sucrose-ACSF solution saturated with 95% O_2/5% CO_2 and contained the following (in mmol/L): 189 sucrose, 2.5 KCl, 0.5 $CaCl_2$, 10 $MgCl_2$, 26 $NaHCO_3$, 1.25 NaH_2PO_4, and 10 glucose. Horizontal hippocampal slices were cut into 300-μm sections using an Integraslice (Campden Instruments, UK). The slices were then stored in an interface chamber at room temperature (22–23 °C) bubbled with a mixture of 95% O_2/5% CO_2.

Test procedure

A slice was placed in an interface or submerged chamber and allowed to equilibrate for an hour in artificial ACSF before recording. The bath temperature was measured using a digital temperature meter (Hanna Instruments, Ann Arbor, Michigan, USA). Temperature alterations in the recording chambers were achieved by either increasing or decreasing the water temperature in the water bath. For interface slices, the temperature and perfusion rate were maintained at 31–32 °C and 2–3 mL/min, respectively. The optimal conditions for γ activity in the submerged slices were 28–29 °C and 5–7 mL/min for temperature and perfusion rate, respectively. The composition of ACSF was (in mmol/L) 125 NaCl, 26 $NaHCO_3$, 3 KCl, 2 $CaCl_2$, 1.25 NaH_2PO_4, 1 $MgCl_2$, and 10 D-glucose, and its pH was equilibrated with a mixture of 95% O_2/5% CO_2 at pH 7.4. The slices were visualized with a stereo microscope (Leica MZ8, Micro Instruments, Oxford, UK). Electrodes (2 to 4 MΩ) were pulled from borosilicate glass capillaries of 1.2 mm OD×0.69 mm ID (Harvard Apparatus, Edenbridge, Kent, UK) using a P-97 horizontal micropipette puller (Sutter Instrument Company, Novato, CA, USA) and filled with ACSF.

The electrodes were placed in the stratum radiatum (SR) of area CA3 in the hippocampus for the interface chamber, as the SR appears to be most reliable location to induce γ oscillation. For the same reason, the stratum pyramidale (SP) of the CA3 is used for the submerged recording of KA-induced γ oscillation. The coherence of the γ oscillations was studied by placing one electrode in CA3c and moving a second electrode in ~200-μm steps along the cell layer of the Ammon horn. After recording a baseline for approximately 5–10 min, γ oscillations were induced by adding various concentrations of KA.

The extracellular microelectrodes were connected to an AC-DC amplifier (Neurolog System, Digitimer, Welwyngarden City, UK). The signals were sampled at 5 kHz using a CED 1401 interface and low-pass filtered at 2.5 kHz using a Neurolog NL-125 filter unit (Digitimer). For the continuous recording in submerged slices, signals were sampled at 1 kHz and filtered at 0.5 kHz. A Humbug noise-eliminator (Digitimer) was used to remove line noise. Signal 2 and Spike 2 were used for data acquisition. Data analysis was performed off-line using Spike 2 and Signal 2 (Cambridge electronic design [CED], Cambridge, UK), SigmaStat (SPSS Inc, USA) and Microsoft Excel software.

The power of network oscillations was measured using fast Fourier transformation (FFT) over 20–100 s of data, which quantifies the proportional power of each wavelength within the data section. The summated power value of the γ oscillation is a summation of powers ranging between 20–60 Hz *in vitro*, first adopted by Fisahn *et al*[6].

Statistical analysis

The data are expressed as the mean and standard error of the mean, with *n* indicating the number of slices.

Results

KA-induced γ oscillations

Extracellular field recordings were made in the hippocampal CA3c pyramidal layer in both submerged and interface slices. KA-induced γ oscillations developed in a time-dependent manner. At 100 nmol/L, KA-induced oscillations required 2–10 min to reach the peak (n=8) for submerged slices and 30–70 min (n=7) for interface recordings. The oscillations lasted longer than 30 min and for a few hours for the submerged and interface slice recordings, respectively. After washout of KA, the oscillations generally required 20–30 min to recover in submerged recordings but could take hours to recover in the interface recordings.

Power spectra analysis indicated that the dominant oscillation frequency in the submerged and interface recordings were approximately 25 and 40 Hz, respectively (Figure 1). A frequency of 25 Hz was at the lower range of γ oscillations (20–59 Hz). This frequency was associated with the lower temperature in the recording chamber in the submerged slices (29 °C).

Temperature dependence

The optimum temperature for KA-induced γ oscillations under submerged conditions was determined, and the temperature affected γ oscillations in the submerged slices. Increasing the temperature from 23–36 °C altered the frequency and power of the oscillation. Representative traces of oscillatory activity at 25 and 29 °C are shown in Figure 2A. The frequency of oscillations increased from 18 to 25 Hz as the temperature increased from 25 to 29 °C (Figure 2B). The temperature-dependence

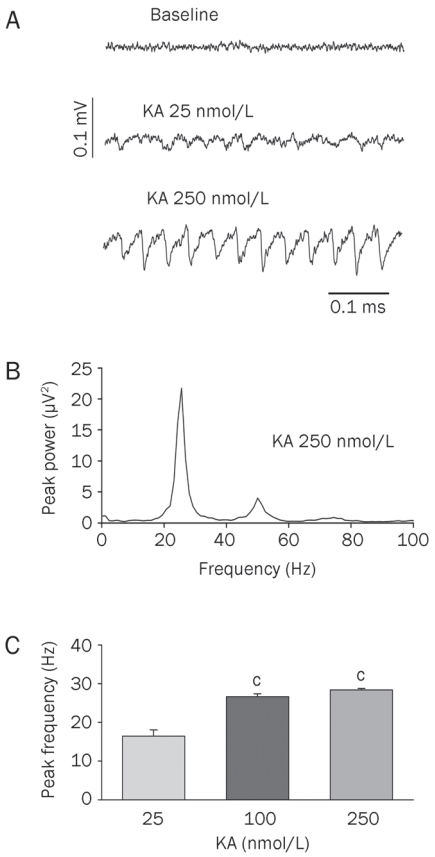

Figure 1. Kainate-induced γ oscillations. A) Example traces of oscillatory activities induced by various concentrations of KA in submerged slices. B) Power spectra from oscillations induced by KA (250 nmol/L) show that the peak frequency for submerged slice is 25 Hz. C) Bar graphs show the average peak frequency of oscillatory activity induced by various concentration of KA in submerged slices. $^{c}P<0.01$, compared with 25 nmol/L KA group, ANOVA.

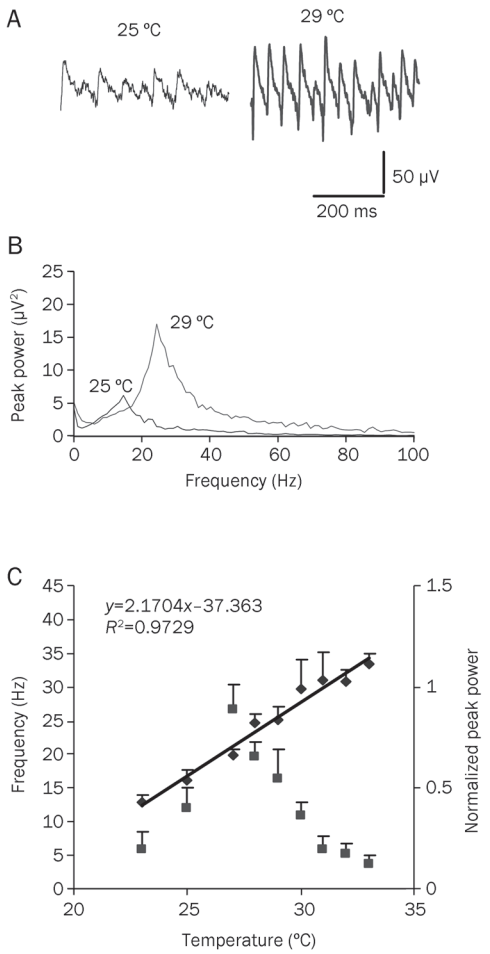

Figure 2. Oscillatory activity is temperature-dependent. A) Examples of KA-induced field potentials in a submerged slice at 25 °C and 29 °C. Recordings were made in SP of CA3. B) Power spectra at different temperatures, corresponding to the field potentials in A. C) Plots of oscillation frequency (diamond) and the peak power of oscillations (square) as a function of temperature for the submerged slices.

of oscillation frequency over a range of temperatures from 23–33 °C is depicted in Figure 2C. Based on the linear fit, the calculated change in response to a 1 °C increase in temperature corresponds to a 2.3±0.4 Hz increase in the oscillation frequency (n=7). Although the oscillation frequency was positively correlated with temperature over a range of 23–33 °C, γ power was only correlated with temperature within a limited temperature range. Increasing the temperature increased the γ power (Figure 2C). The highest γ power was achieved at 27–29 °C. As the temperature was further increased, the γ power was reduced (Figure 2C).

Concentration dependence

KA increased the γ power (Figure 3) in both interface and submerged slices in a concentration-dependent manner. At 25 nmol/L KA, the average γ power was 303±154 μV^2 (n=7) and 26±13 μV^2 (n=8) for the interface and submerged slices, respectively. At 100 nmol/L KA, the γ power increased to 2308±691 μV^2 (n=7) and 195±91 μV^2 (n=8) for the interface and submerged slices, respectively. At 250 nmol/L KA, the γ power further increased for both interface and submerged conditions (Figure 3C, 3D). Increasing the KA concentration also accelerated the development of γ oscillations, as represented by a reduction in the time to reach peak power. For the interface slices, the time to peak γ power was 110±16.4 min, 103±4.6 min, and 27±4.9 min for 25 nmol/L, 100 nmol/L, and 250 nmol/L KA, respectively. For the submerged slices, the time to peak γ power was 68±7.9 min, 12.2±2.2 min, and 4.7±1.97 min for 25 nmol/L, 100 nmol/L, and 250 nmol/L KA, respectively.

Although the maximum γ powers under both conditions increased by KA in a concentration-dependent manner, γ maintenance appeared to be reduced at higher KA concentrations. At 25 nmol/L KA, the steady state of γ oscillations lasted for a few hours in the interface slices (n=7) and longer than 50 min in the submerged slices (n=8), but at 250 nmol/L, the steady state of γ oscillations was maintained for less than an hour for the interface slices ($P<0.01$, compared with that of

the 25 nmol/L KA interface slice group) and less than 30 min for submerged slices (P<0.01, compared with that of the 25 nmol/L KA submerged slice group). In 5 submerged slices tested, high concentrations of KA (1.5 μmol/L) induced rapidly developing (2–3 min), strong γ oscillations, which lasted for only a couple of minutes (Figure 3F).

Area and layer specificity

In interface chamber recordings, the strongest γ oscillations were usually recorded in the CA3c area (closest to the hilus), followed by CA3b and CA3a[13]. Representative results of γ oscillations recorded from these three areas (CA3a, CA3b, and CA3c) from an interface slice are shown in Figure 4A–4D. These recordings were repeated in the submerged slices, and similar results were obtained (data not shown). Therefore, γ oscillations were routinely recorded in the submerged slices in the CA3c area. Oscillatory activity can be recorded in the somatic (stratum pyramidale, SP) and apical dendritic layer (stratum radiatum, SR), with positive population synaptic potentials in the somatic region (SP) and negative potentials in the SR (Figure 4E). In the interface slices, the strongest γ oscillations were recorded in the SR, followed by the SP and stratum oriens (SO). In the submerged slices, the γ power was highest in the SP, followed by the SR and SO (Figure 4F).

Oscillations are mediated by both excitatory and inhibitory synapses

KA-induced γ oscillations require KA receptor activation as well as excitatory glutamatergic and inhibitory GABAergic neurotransmission. The effects of the AMPA/KA receptor blocker, NBQX, and the $GABA_A$ receptor blocker, GABAzine, were tested on KA-induced (100 nmol/L) γ oscillations. On average, the γ power was reduced to 0.9%±0.3% that of the control (100%) by NBQX (n=4, P<0.01) and to 3.1%±2.1% of the control by GABAzine (n=4, P<0.05). After 20 min washout of GABAzine, the γ oscillations partially recovered (47%±20% of control, n=4), but no significant recovery was observed after NBQX washout (1.2%±0.2% of control). TTX (1 μmol/L) reduced the γ powers to 24.2%±3.8% (P<0.05, n=4) that of the control at 20 min of application, which did not recover at washout (0.54%±0.26% of the control, data not shown).

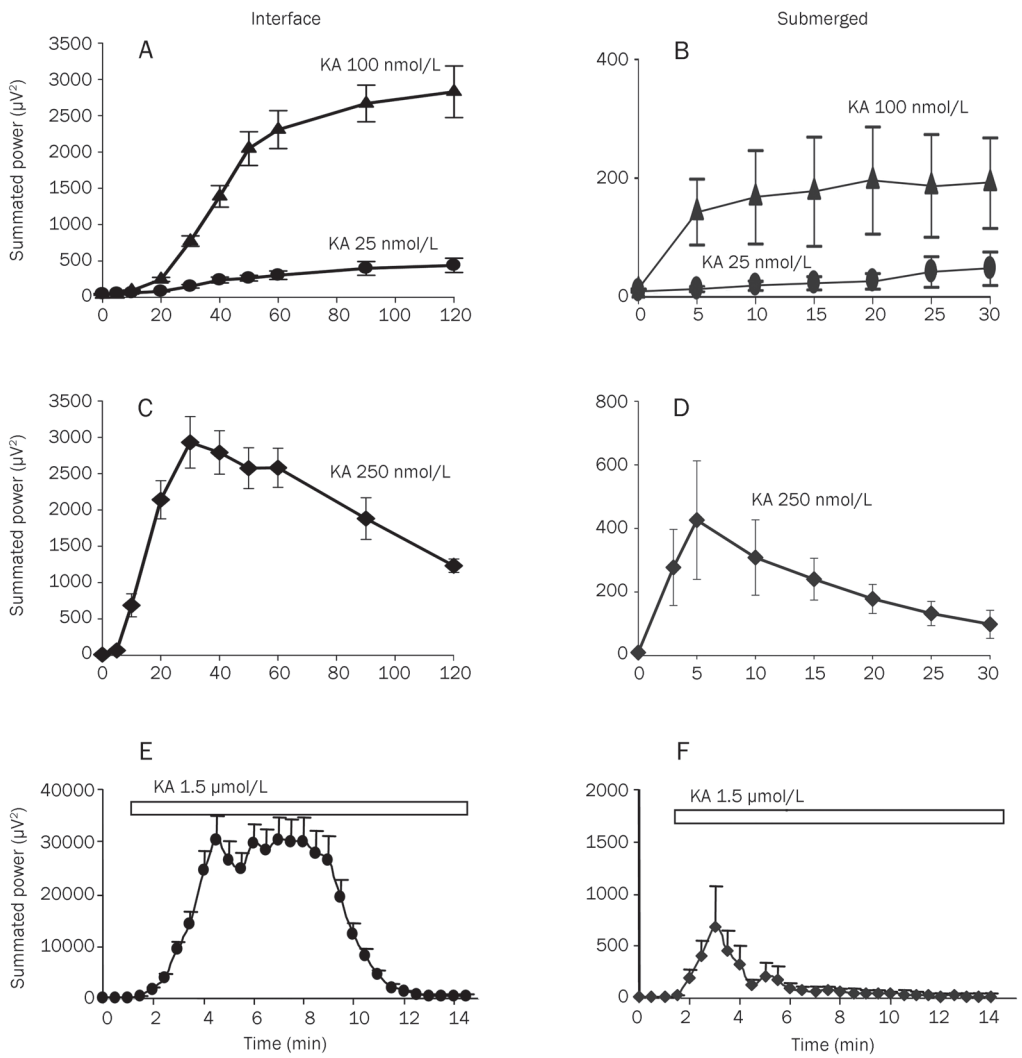

Figure 3. Time-effect curves of summated power at various KA concentrations. Left panel (A, C, E) and right panel (B, D, F) show the summated powers of γ oscillations recorded under interface and submerged conditions, respectively. Larger concentrations of KA (250 nmol/L and 1.5 μmol/L) induced larger amplitude of γ oscillations but reduced temporal stability in both interface (C, E) and submerged slices (D, F). Each data point represents the mean±SEM.

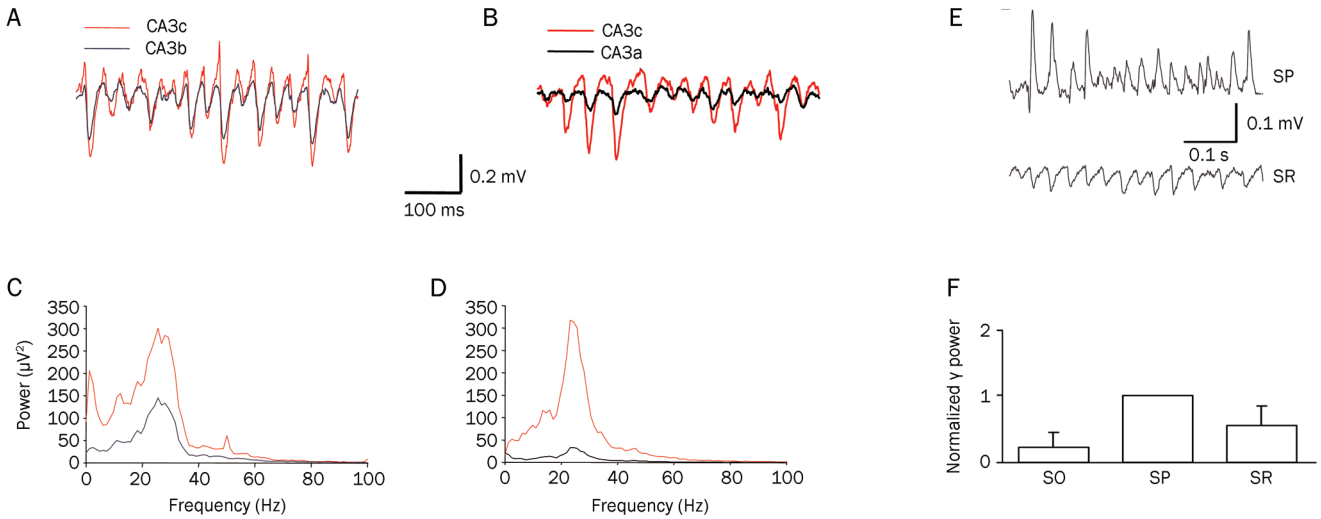

Figure 4. Area and layer specificity of γ oscillations. A) Representative recordings of γ oscillations from CA3c (red) and CA3b (blue). B) Representative recordings of γ oscillations from CA3c (red) and CA3a (black). C) Power spectra from the recordings of γ oscillations shown in panel A. D) Power spectra from the recordings of γ oscillations shown in panel B. E) γ oscillations show positivity recorded in SP and negativity recorded in SR. The recording electrode was moved from SO to SP and then to SR and recordings were made at each position. F) Normalized γ powers at different layers of hippocampus in CA3c area. For the comparison, summated γ power from each location was normalised to the power in SP. Data are given as mean±SEM. For interface slices, *n*=17 for the recordings from all the three layers; for submerged slices, *n*=13 for the recordings at SP and SR and *n*=5 for the recordings at SO.

Effect of perfusion rate on γ oscillations

The effect of perfusion rate on γ oscillations over the range of 1.35–10.5 mL/min in both interface and submerged recordings is shown in Figure 5. In the interface recordings, there was no obvious change in the power of γ oscillations with increased perfusion rate (line with open circles). In the submerged recordings, increasing the perfusion rate from 1.35–7 mL/min increased the power of the γ oscillations, whereas the higher perfusion rates (10.5 mL/min) reduced the power (line with filled diamonds). The optimal perfusion rate was determined to be 7 mL/min.

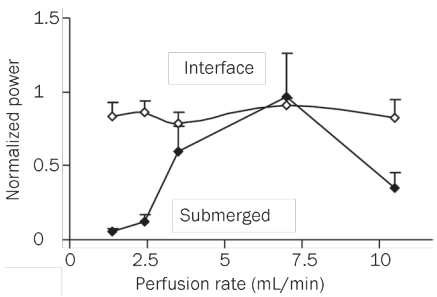

Figure 5. Effect of perfusion rate on γ oscillations in interface and submerged slices. Varying the perfusion rate did not alter γ oscillation strength in interface slices at 1.35–10.5 mL/min, but affect γ oscillation in submerged slices. The optimum perfusion rate for the submerged slices is 5–7 mL/min. Data are presented as mean±SEM. *n*=5 slices

Discussion

We determined the optimal conditions for the induction of persistent γ oscillations in submerged slices. Previous *in vitro* studies showed that γ frequency network oscillations lasting for tens of minutes could be routinely induced in hippocampal slices using an interface-type recording chamber[6, 14–16]. In contrast, oscillations induced using submerged-type slice chambers, designed for visually guided patch-clamp recordings using infrared DIC optics, lasted only a few seconds and were qualitatively different from those recorded under interface conditions[11, 13].

The optimal temperature for γ oscillations recorded under submerged conditions is 28–29 °C, a few degrees less than that under the interface conditions (32–33 °C). The reason that a relatively low temperature is required for γ oscillations under submerged conditions remains to be determined, but the possibilities include the following situations: 1) because tissues consume less oxygen at lower temperatures, the relatively low temperature may help maintain the γ oscillations and 2) the relatively low temperature may help maintain the mitochondrial membrane potential ($\Delta\Psi_m$)[17], which is critical for the maintenance of the proton gradient necessary for ATP synthesis in mitochondria. Warming the chamber from 22 to 32 °C was reported to depolarize the mitochondrial membrane potential and reduce ATP synthesis in cells of the carotid body[17].

The oscillation frequency induced by KA in the submerged slices was at the lower range of the γ band. Previous studies have shown that γ oscillations typically have a peak frequency of ~35 Hz[6] under interface conditions. The difference in the peak frequency in this study and those of previous reports may be explained by the temperature at which the experiments were conducted. Our recordings indicate that a 1 °C

change in temperature correlates with an alteration of oscillation frequency of 2.3 Hz (a 9.2% change per degree). Our results are in line with a previous report in interface slices[18], which showed an 8.3% reduction in frequency per degree of change in CCh-induced oscillations, and another report in hippocampal slices[19], which showed an 8.8% reduction per degree in tetanically evoked γ oscillations. Temperature-related changes in the oscillation frequency are likely associated with changes in inhibitory postsynaptic potential (IPSP) duration. GABAergic IPSP duration is also known to be a key determinant of oscillation frequency[20], and GABAergic IPSPs are prolonged at lower temperatures[18, 21]. Temperature may also affect excitatory synaptic transmission[22] and contribute to the temperature dependence of oscillation frequency; indeed, gamma oscillation is dependent on both excitatory and inhibitory neurotransmissions.

The oscillation polarity is positive in the SP, where the neuronal somata are located, but negative in the apical dendrites in both interface and submerged slices. The polarity at the soma is positive because GABA, released from presynaptic interneurons, activates GABAA receptors at the postsynaptic membrane of the principle cell, causing Cl^- influx and thereby leaving a positive charge outside the soma. The positive potential in the extracellular recordings is caused by a positive charge flowing out of the cell, a process called the "source" in current source density analysis[23, 24]. Whether the source is an active or passive process depends on the intracellular recording of the soma; if this recording shows a hyperpolarized current (IPSC) coinciding with the source, then the source is likely to be active[25] because hyperpolarization is caused by Cl^- influx. In contrast, the negative field potential in the stratum radium (neuronal dendrite location) is due to the positive charge flowing into the dendrite. This process is called a "sink" in current source density analysis. A passive sink is caused by an active source of GABA in the soma, whereas an active sink is caused by the release of glutamate from recurrently excited synapses activating synaptic receptors and causing a positive charge (Na^+) influx. The positive polarity of the KA-induced γ oscillations recorded in the SP in the slices in this study is likely due to active sources[25].

KA-induced γ oscillations in the submerged slices in the hippocampal CA3 can be blocked by either NBQX or GABAzine, suggesting that both pyramidal neurons (excitatory) and interneurons (inhibitory) are involved in γ oscillations. These oscillations are similar to those recorded *in vitro* in the entorhinal cortex caused by kainate receptor activation[26], *in vitro* in the hippocampus caused by cholinergic activation[6, 16, 27] and *in vivo* in the hippocampus[5] but are different from the γ oscillations recorded in the CA1[14, 15, 28, 29], which showed that both chemically and electrically interconnected interneuronal networks were involved without any contribution from pyramidal cells. The sodium channel blocker, TTX, also largely reduced γ oscillations, suggesting that neuronal action potentials (spikes) contribute to the network oscillations[30].

The recovery after a 20-min drug washout showed different dynamics for different blockers: partial recovery for GABAzine, limited recovery for NBQX and no recovery for TTX. The difference in washout dynamics may be related to the chemical and physical properties of the different drugs. For example, the antagonist NBQX typically cannot be washed out easily due to its lipophilic nature[31]. The limited washout time (20 min) in this study may have contributed to the limited recovery of these drugs. Under prolonged washout times (up to 1 h), there was a dramatic recovery of the γ oscillation for the NBQX and TTX treatment groups in some cases.

The development dynamics of KA-induced γ oscillation are largely dependent on the concentration of KA. High concentrations of KA (1–2 μmol/L) induced a rapid collapse in γ oscillations, suggesting that strong membrane depolarization blocks neurotransmission[32]. The micromolar KA-induced rapid collapse of γ oscillations may be related to the high demand for ATP in fast network oscillations, causing the neurons to rapidly run out of energy. Therefore, a concentration of KA in the nanomolar range is suitable for the induction of persistent γ oscillations.

Under submerged conditions, γ oscillation requires a fast perfusion rate (5–7 mL/min), indicating the nature of high oxygen demand for fast network oscillations. A high perfusion rate, although providing a rapid exchange of fresh solution, may cause mechanical damage to the brain slice, which likely explains the reduced power of the γ oscillations under a high perfusion rate of 10.5 mL/min in this study.

In summary, the KA-induced submerged oscillatory activity in the γ frequency band in this study is similar to that recorded in the interface recordings with respect to the neurotransmitters and synapses involved but with faster dynamics during development and after the washout. Under submerged conditions, γ oscillations can be induced by KA at nanomolar concentrations and at a relatively low temperature. This model will provide neuroscientists, pharmacologists and clinical researchers with a useful tool to study the network mechanisms underlying normal neuronal synchronization and neuronal disorders, such as Alzheimer's disease and schizophrenia, which are known to involve cognitive dysfunction and the impairment of oscillatory activity.

Acknowledgements

This work was supported by MRC (Medical Research Council) and National Natural Science Foundation of China (Grant No 31070938).

Author contribution

Lu CB: designed, performed experiments and wrote paper; Wang ZH: performed experiments; Zhou YH: analyzed data; Vreugdenhil M: designed research and wrote paper.

References

1 Lisman JE, Idiart M. Storage of 7+/-2 short-term memories in oscillatory subcycles. Science 1995; 267: 1512–5.
2 Jensen O, Lisman JE. Novel lists of 7+/-2 known items can be reliably stored in an oscillatory short-term memory network: interaction with long-term memory. Learn Mem 1996; 3: 257–63.

3 Herrmann CS, Munk MHJ, Engel AK. Cognitive functions of gamma-band activity: memory match and utilization. Trends Cogn Sci 2004; 8: 347–55.
4 Driver JA, Logroscino G, Buring JE, Gaziano JM, Kurth T. A prospective cohort study of cancer incidence following the diagnosis of Parkinson's disease. Cancer Epidemiol Biomarkers Prev 2007; 16: 1260–5.
5 Csicsvari J, Jamieson B, Wise KD, Buzsáki G. Mechanisms of gamma oscillations in the hippocampus of the behaving rat. Neuron 2003; 37: 311–22.
6 Fisahn A, Pike FG, Buhl EH, Paulsen O. Cholinergic induction of network oscillations at 40 Hz in the hippocampus *in vitro*. Nature 1998; 394: 186–9.
7 Gloveli T, Dugladze T, Saha S, Monyer H, Heinemann U, Traub RD, *et al*. Differential involvement of oriens/pyramidale interneurones in hippocampal network oscillations *in vitro*. J Physiol 2005; 562: 131–47.
8 Steriade M, Amzica F, Contreras D. Synchronization of fast (30–40 Hz) spontaneous cortical rhythms during brain activation. J Neurosci 1996; 16: 392–417.
9 Penttonen M, Kamondi A, Acsady L, Buzsaki G. Gamma frequency oscillation in the hippocampus of the rat: intracellular analysis *in vivo*. Eur J Neurosci 1998; 10: 718–28.
10 Kann O, Huchzermeyer C, Kovacs R, Wirtz S, Schuelke M. Gamma oscillations in the hippocampus require high complex I gene expression and strong functional performance of mitochondria. Brain 2011; 134: 345-58.
11 McMahon LL, Williams JH, Kauer JA. Functionally distinct groups of interneurons identified during rhythmic carbachol oscillations in hippocampus *in vitro*. J Neurosci 1998; 18: 5640–51.
12 Kawaguchi Y. Distinct firing patterns of neuronal subtypes in cortical synchronized activities. J Neurosci 2001; 21: 7261–72.
13 Vreugdenhil M, Toescu EC. Age-dependent reduction of gamma oscillations in the mouse hippocampus *in vitro*. Neuroscience 2005; 132:1151-7.
14 Whittington MA, Traub RD, Jefferys JG. Synchronized oscillations in interneuron networks driven by metabotropic glutamate receptor activation. Nature 1995; 373: 612–5.
15 Boddeke H, Best R, Boeijinga P. Synchronous 20 Hz rhytmic activity in hippocampal networks induced by activation of metabotropic glutamate receptors *in vitro*. Neuroscience 1997; 76: 653–8.
16 Palhalmi J, Paulsen O, Freund T, Hajos N. Distinct properties of carbachol-and DHPG-induced network oscillations in hippocampal slices. Neuropharmacology 2004; 47: 381–9.
17 Duchen MR, Biscoe T. Relative mitochondrial membrane potential and $[Ca^{2+}]_i$ in type I cells isolated from the rabbit carotid body. J Physiol 1992; 450: 33–61.
18 Dickinson R, Awaiz S, Whittington M, Lieb W, Franks N. The effects of general anaesthetics on carbachol-evoked gamma oscillations in the rat hippocampus *in vitro*. Neuropharmacology 2003; 44: 864–72.
19 Javedan SP, Fisher RS, Eder HG, Smith K, Wu J. Cooling abolishes neuronal network synchronization in rat hippocampal slices. Epilepsia 2002; 43: 574–80.
20 Traub RD, Whittington MA, Buhl EH, Jefferys JG, Faulkner HJ. On the mechanism of the gamma → beta frequency shift in neuronal oscillations induced in rat hippocampal slices by tetanic stimulation. J Neurosci 1999; 19: 1088–105.
21 Banks MI, Li TB, Pearce RA. The synaptic basis of GABAA, slow. J Neurosci 1998; 18: 1305–17.
22 Adelson J, Bhardwaj H, Kannan P. Changes in synaptic delay and EPSP amplitude induced by TEA with 3,4-DAP, temperature and post-tetanic potentiation. Pioneering Neurosci 2004; 5: 53–60.
23 Tenke CE, Schroeder CE, Arezzo JC, Vaughan HG. Interpretation of high-resolution current source density profiles: a simulation of sublaminar contributions to the visual evoked potential. Exp Brain Res 1993; 94: 183–92.
24 Martinez DP, Freeman WJ. Periglomerular cell action on mitral cells in olfactory bulb shown by current source density analysis. Brain Res 1984; 308: 223–33.
25 Mann EO, Suckling JM, Hajos N, Greenfield SA, Paulsen O. Perisomatic feedback inhibition underlies cholinergically induced fast network oscillations in the rat hippocampus *in vitro*. Neuron 2005; 45: 105–17.
26 Cunningham MO, Davies CH, Buhl EH, Kopell N, Whittington MA. Gamma oscillations induced by kainate receptor activation in the entorhinal cortex *in vitro*. J Neurosci 2003; 23: 9761–9.
27 Hájos N, Pálhalmi J, Mann EO, Németh B, Paulsen O, Freund TF. Spike timing of distinct types of GABAergic interneuron during hippocampal gamma oscillations *in vitro*. J Neurosci 2004; 24: 9127–37.
28 Hormuzdi SG, Pais I, LeBeau FE, Towers SK, Rozov A, Buhl EH, *et al*. Impaired electrical signaling disrupts gamma frequency oscillations in connexin 36-deficient mice. Neuron 2001; 31: 487–95.
29 Traub RD, Whittington MA, Buhl EH, LeBeau FE, Bibbig A, Boyd S, *et al*. A possible role for gap junctions in generation of very fast EEG oscillations preceding the onset of, and perhaps initiating, seizures. Epilepsia 2001; 42: 153–70.
30 Cunningham MO, Whittington MA, Bibbig A, Roopun A, LeBeau FE, Vogt A, *et al*. A role for fast rhythmic bursting neurons in cortical gamma oscillations *in vitro*. Proc Natl Acad Sci U S A 2004; 101: 7152–7.
31 Smeraski CA, Dunwiddie TV, Diao L, Finger TE. NMDA and non-NMDA receptors mediate responses in the primary gustatory nucleus in goldfish. Chem Senses 1999; 24: 37–46.
32 Fisahn A. Kainate receptors and rhythmic activity in neuronal networks: hippocampal gamma oscillations as a tool. J Physiol 2005; 562: 65–72.

Acta Pharmacologica Sinica (2012) 33: 221–229
 1671-4083/12 $32.00
www.nature.com/aps

Original Article

Exhaustive swimming differentially inhibits $P2X_1$ receptor- and α_1-adrenoceptor-mediated vasoconstriction in isolated rat arteries

Lu LI[2], Tao WU[3], Cong WEI[1], Jian-ke HAN[1], Zhen-hua JIA[1], Yi-ling WU[1, *], Lei-ming REN[2, *]

[1]Integration of Traditional and Western Medical Research Academy of Hebei Province, Shijiazhuang 050035, China; [2]Department of Pharmacology, Institute of Chinese Integrative Medicine, Hebei Medical University, Shijiazhuang 050017, China; [3]Department of Hand Surgery, The Third Affiliated Hospital of Hebei Medical University, Shijiazhuang 050051, China

Aim: To investigate the effects of exhaustive swimming exercise on P2X1 receptor- and α1-adrenoceptor-mediated vasoconstriction of different types of arteries in rats.
Methods: Male Wistar rats were divided into 2 groups: the sedentary control group (SCG) and the exhaustive swimming exercise group (ESEG). The rats in the ESEG were subjected to a swim to exhaustion once a day for 2 weeks. Internal carotid, caudal, pulmonary, mesenteric arteries and aorta were dissected out. Isometric vasoconstrictive responses of the arteries to α,β-methylene ATP (α,β-MeATP) or noradrenaline (NA) were recorded using a polygraph.
Results: The exhaustive swimming exercise did not produce significant change in the EC_{50} values of α,β-MeATP or NA in vasoconstrictive response of most of the arteries studied. The exhaustive swimming exercise inhibited the vasoconstrictive responses to P2X1 receptor activation in the internal carotid artery, whereas it reduced the maximal vasoconstrictive responses to α1-adrenoceptor stimulation in the caudal, pulmonary, mesenteric arteries and aorta. The rank order of the reduction of the maximal vasoconstriction was as follows: mesenteric, pulmonary, caudal, aorta.
Conclusion: Exhaustive swimming exercise differentially affects the P2X1 receptor- and α1-adrenoceptor-regulated vasoconstriction in internal carotid artery and peripheral arteries. The ability to preserve purinergic vasoconstriction in the peripheral arteries would be useful to help in maintenance of the basal vascular tone during exhaustive swimming exercise.

Keywords: exhaustive exercise; swimming; α_1-adrenoceptor; $P2X_1$ receptor; vasoconstriction; artery

Acta Pharmacologica Sinica (2012) 33: 221–229; doi: 10.1038/aps.2011.148

Introduction

Regularly engaging in moderate exercise provides many well-established health benefits, including the prevention of, or a reduction in, the deleterious effects of pathological conditions such as hypertension, coronary artery disease, atherosclerosis, diabetes mellitus, and osteoporosis[1–3]. However, the beneficial effects of exercise are lost with overexertion, which causes the production of free radicals[4] and subsequent damage to lipids, proteins, and DNA. Exhaustive exercise has been shown to lead to tissue damage in animals[5, 6]. It has also been reported that exhaustive exercise resulted in significant impairment of regional left ventricular systolic and diastolic function in rats[7]. In the right ventricle of the human heart, tissue Doppler measurements of systolic and early diastolic function have been found to decrease significantly after prolonged strenuous exercise compared to pre-training values[8].

Functional changes in the vasculature of animals subjected to physical exercise have attracted considerable attention for many years. Acute exercise significantly attenuates α-adrenoceptor-mediated vasoconstriction of the thoracic aorta isolated from rabbits[9], and chronic exercise also decreases adrenergic agonist-induced vasoconstriction in the isolated thoracic aorta and carotid artery of spontaneously hypertensive rats[10]. It has also been reported that sedentary (control) and exercise-trained rats show no difference in the maximum levels of vasoconstriction induced by noradrenaline (NA) or phenylephrine in the isolated thoracic aorta[11]. Moderate levels of exercise did not alter either the myogenic regulation of the arterial diameter stimulated by increased transmural pressure or the smooth muscle responses to a thromboxane agonist in control and *db/db* mice[12]. Chronic treadmill running sig-

* To whom correspondence should be addressed.
E-mail ren-leiming@263.net(Lei-ming REN);
yilingwu5109@163.com(Yi-ling WU).
Received 2011-01-22 Accepted 2011-10-10

nificantly enhanced myogenic vasoconstriction in the coronary resistance arteries isolated from female pigs[13]. Potential reasons for this discrepancy might be differences among arteries studied, the laboratory animals used and the exercise modes employed.

It is well known that the sympathetic and purinergic cotransmission involving NA and adenosine 5′-triphosphate (ATP) exists in a variety of blood vessels. The neurogenic vasoconstriction induced by electrical field stimulation consists of a purinergic (prazosin-resistant) component and an adrenergic (prazosin-sensitive) component in different blood vessels. P2X and P2Y receptors are widely distributed throughout the cardiovascular system and are important in the regulation of vascular tone[14]. The $P2X_1$ purinoceptor is the primary P2X subtype expressed on most vascular smooth muscle cells[15], and is responsible for purinergic arterial contraction[16, 17]. α,β-Methylene ATP (α,β-MeATP) is considered to be a useful reagent to investigate $P2X_1$ receptor-mediated vasoconstriction[18]. It has been reported that rats with diet-induced obesity have enhanced sympathetic nerve-mediated vasoconstriction via upregulation of purinergic and adrenergic neurotransmission[19]. Vidal *et al*[20], however, have indicated that α,β-MeATP significantly inhibits vasoconstrictive responses to electrical field stimulation in the tail arteries of spontaneously hypertensive rats, but does not inhibit these responses in the tail arteries of normal rats. Therefore, the purpose of this study was to examine whether there is similar or differential inhibition of α_1-adrenoceptor- and $P2X_1$ purinoceptor-mediated vasoconstriction in the aorta and the internal carotid, caudal, pulmonary and mesenteric arteries in healthy rats after exhaustive swimming exercise.

Materials and methods

Animals

Male Wistar rats weighing 300–350 g (aged 12–13 weeks) were housed one per cage in a temperature-controlled room (24±1 °C) with a 12 h light/dark cycle and received approximately 50% of their daily food intake[6] and tap water *ad libitum*. The commercial standard chow was purchased from Hebei Medical University. Rats were randomly divided into two groups: a sedentary control group (SCG) and an exhaustive swimming exercise group (ESEG). All animals used in this study received humane care in compliance with institutional animal care guidelines. All procedures performed were approved by the Local Institutional Committee.

Chemicals

[–]-Noradrenaline bitartrate (NA), α,β-methylene adenosine 5′-triphosphate lithium salt (α,β-MeATP), desmethylimipramine hydrochloride, deoxycorticosterone acetate, yohimbine hydrochloride, propranolol hydrochloride and acetylcholine hydrochloride were obtained from the Sigma Chemical Company, USA. The above reagents were dissolved in distilled water except for deoxycorticosterone acetate which was dissolved in 1,2-propanediol. The final concentration of 1,2-propanediol in the tissue bath did not affect the vascular responses to NA.

Training protocols

To familiarize the rats with water immersion and reduce water-induced stress, the rats of the ESEG were made to swim in an apparatus holding no less than a water depth of 60 cm for 15 min daily at 8:30 am for 6 days/week during the first week. After the rats had adapted to the swimming exercise, the animals were subjected to a swim to exhaustion with a weight equivalent to 3% of their body weight tied to their tails[21] for two weeks. The training, began from 8:30 am to 11:30 am[22], was conducted daily for 6 days/week by the same person. Exhaustion was defined by two criteria: the rats remained below the water surface for 10 s, and the rats showed a lack of a "righting reflex" when they were placed on a flat surface[21]. Simultaneously, the rats of the SCG were kept in a small chamber holding a water depth of 10 cm. The water temperature was maintained at 34–36 °C[23].

Arterial preparations

Rats of the ESEG and SCG were anesthetized by subcutaneous injection of urethane (1.5 g/kg) 24 h after the last exhaustive swimming session then sacrificed by cutting the femoral artery, resulting in exsanguination. After the chest and abdomen were opened by a midline incision, the thoracic aorta, right pulmonary artery and superior mesenteric artery were carefully removed. An anterior midline incision was made on the neck to expose the carotid artery. The left and right internal carotid arteries were identified from their origin at the common carotid artery bifurcation to their entry points into the skull and were isolated. The caudal artery was surgically exposed from the ventral side then dissected from surrounding tissues and removed. These isolated arteries were maintained in ice-cold oxygenated Krebs-Henseleit (K-H) solution (133 mmol/L NaCl, 4.7 mmol/L KCl, 1.35 mmol/L NaH_2PO_4, 16.3 mmol/L $NaHCO_3$, 0.61 mmol/L $MgSO_4$, 7.8 mmol/L glucose and 2.52 mmol/L $CaCl_2$). The vascular endothelium of each artery was removed by gently rubbing the lumen with a scored polythene cannula, the external diameter of which was slightly smaller than the internal diameter of the blood vessel. A ring segment (4 mm long) without endothelium was mounted horizontally in a 10-mL organ bath, and the isometric tension was recorded by a polygraph (ERT-884, Youlin Electron Co, Kaifeng, China). Preloads were applied to the preparations of internal carotid artery (1.0 g), caudal artery (0.75 g), pulmonary artery (1.0 g), mesenteric artery (1.0 g), and aorta (2.0 g)[24]. The preparations were allowed to equilibrate for 1 h in K-H solution. The solution was maintained at 37 °C and aerated with 95% O_2 and 5% CO_2 (pH 7.4). Successful removal of the arterial endothelium was confirmed by the loss of the relaxation response to acetylcholine (ACh, 1 μmol/L) in precontracted arterial rings treated with NA.

Experimental protocols

Before performing the following procedures, a cumulative dose-response curve for NA (0.0001–100 μmol/L) was con-

structed for each of the arterial preparations to observe the vasoconstrictive responsiveness, followed by further equilibration for 1 h. After the isolated arterial experiments were performed, a dose-response curve for KCl (10–120 mmol/L) was constructed in the arterial preparations, and the wet weight of each preparation was recorded.

Vasoconstrictive responses to NA in the aorta and the internal carotid, caudal, pulmonary, and mesenteric arteries

In the arterial preparations used to construct a second cumulative dose-response curve for NA, desmethylimipramine (0.1 μmol/L), deoxycorticosterone (5 μmol/L), yohimbine (0.3 μmol/L) and propranolol (1 μmol/L) were added to the organ bath for 30 min to block neuronal or extra-neuronal uptake of NA and to block α_2- and β-adrenoceptors, respectively. The second cumulative dose-response curve for NA (0.0001–100 μmol/L) was constructed for each arterial preparation of the aorta and the internal carotid, caudal, pulmonary, and mesenteric arteries to observe α_1-adrenoceptor-regulated vasoconstriction.

Vasoconstrictive responses to α,β-MeATP in the aorta and the internal carotid, caudal, pulmonary, and mesenteric arteries

Because α,β-MeATP rapidly desensitizes its own receptors, a single concentration of α,β-MeATP at 0.1, 1.0, 10, or 100 μmol/L was added to the organ bath (each arterial preparation was exposed to α,β-MeATP only once) for each arterial preparation, and the resultant responses of several preparations exposed to different concentrations were grouped together to form a dose-response curve[25].

Statistical analysis

Vasoconstrictive responses to NA and α,β-MeATP were expressed as the maximal changes in tension (g) and were further normalized to wet tissue weight (g/mg tissue). Values presented here are the mean±SEM. Two-way ANOVA was used to evaluate any differences between the two sets of dose-response curves. If the *F* statistic was significant, it was compared to the individual datum with its respective control value by Bonferroni's test. We compared the EC_{50} values of the agonists, the maximal vasoconstriction to KCl and the wet tissue weight of arterial preparations between the two groups using an unpaired *t*-test. *P* values less than 0.05 were considered to be statistically significant. The data were analyzed using GraphPad Prism version 5.00 (San Diego, California, USA).

Results

Effect of exhaustive swimming exercise on wet tissue weight and the vasoconstrictive response to KCl

The wet weight of the mesenteric arterial ring segments in the SCG was 0.73±0.02 mg, which was significantly lower than that in the ESEG (0.85±0.02 mg) ($P<0.01$, Figure 1A). The values of the wet weights of the internal carotid, caudal, pulmonary, and aortic arterial ring segments in the SCG were not significantly different from those in the ESEG ($P>0.05$, Figure 1A). The maximal vasoconstrictive responses to KCl in the mesenteric and caudal arteries in the SCG were 1.72±0.05 g/mg tissue and 3.27±0.10 g/mg tissue, respectively. These responses were much greater than those of the ESEG; the vasoconstrictive responses in the mesenteric and caudal arteries were 1.46±0.06 g/mg tissue and 2.85±0.10 g/mg tissue, respectively ($P<0.01$, Figure 1B). There were no significant differences in the maximal vasoconstrictive responses to KCl of the internal carotid artery, pulmonary artery and the aorta between the SCG and the ESEG rats ($P>0.05$, Figure 1B). However, the range of EC_{50} values for KCl in the 5 types of arteries subsequently exposed to the second administration of NA ranged from 17.23 to 31.74 mmol/L, and the EC_{50} values of KCl in the SCG were not significantly different from those in the ESEG (Table 1).

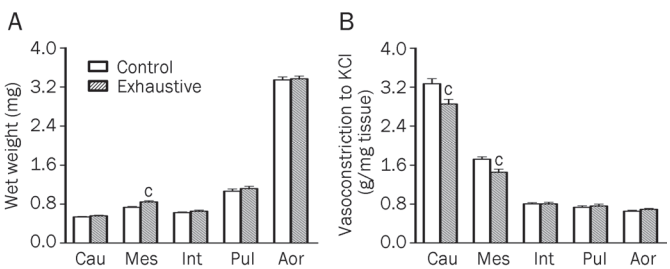

Figure 1. Tissue wet weight (A) and vasoconstriction to 120 mmol/L KCl (B) in the rat mesenteric (Mes), caudal (Cau), pulmonary (Pul), internal carotid (Int) arteries and aorta (Aor) from the sedentary control group (SCG, *n*=29−34) and the exhaustive swimming exercise group (ESEG, *n*=28−35). Data were expressed as mean±SEM. $^cP<0.01$ *vs* SCG.

Table 1. The -log EC_{50} (mol/L) for NA and α,β-MeATP as well as EC_{50} (mmol/L) for KCl in various isolated arterial preparations. NA group, *n*=8−15; α,β-MeATP group, *n*=20−24; KCl group, *n*=8−15. $^cP<0.01$ *vs* SCG.

Artery	SCG			ESEG		
	NA	α,β-MeATP	KCl	NA	α,β-MeATP	KCl
Internal carotid	7.15±0.07	5.36±0.22	20.20±1.17	7.36±0.18	4.71±0.22	21.38±0.64
Caudal	6.70±0.05	6.19±0.18	29.25±1.45	6.78±0.06	6.09±0.15	31.74±1.45
Mesenteric	6.98±0.08	5.70±0.18	23.25±0.64	7.00±0.11	5.51±0.23	21.36±1.86
Aorta	7.43±0.04	4.97±0.14	20.71±1.39	7.11±0.10^c	4.90±0.22	21.10±1.58
Pulmonary	7.58±0.07	5.40±0.34	17.23±1.46	7.54±0.07	5.62±0.21	20.22±0.85

The vasoconstrictive responsiveness of the aorta and the internal carotid, caudal, pulmonary, and mesenteric arteries to NA

Before analyzing the difference in the vasoconstrictive responses to either α_1-adrenoceptor stimulation or $P2X_1$ purinoceptor stimulation between the two rat groups, we examined the vasoconstrictive responsiveness of the selected arteries individually. In the rats of the SCG, there were no significant differences in the vasoconstrictive responses to the first exposure to NA in the internal carotid, caudal, pulmonary, mesenteric artery or aorta between the preparations subsequently exposed to the second administration of NA and those subsequently exposed to α,β-MeATP (P>0.05, Figure 2A–6A). The same results were observed in the rats from the ESEG (P>0.05, Figure 2B–6B).

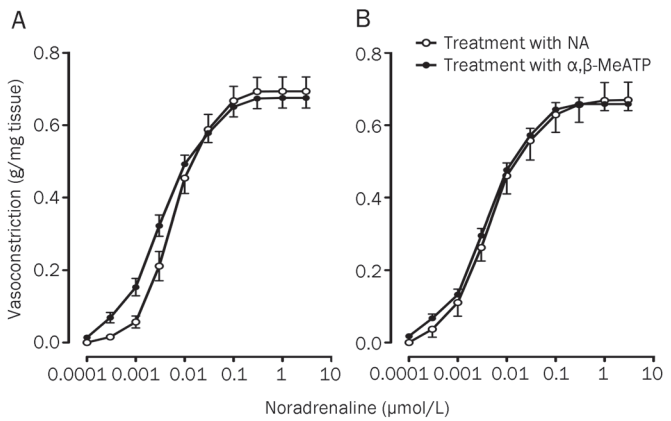

Figure 2. A comparison of the vasoconstrictive responses to noradrenaline between the preparations exposing to the second administration of noradrenaline (treatment with NA; n=10, left; n=9, right) and those exposing to α,β-methylene ATP (treatment with α,β-MeATP; n=24, left; n=24, right) in the rat pulmonary arteries from the sedentary control group (A) and the exhaustive swimming exercise group (B). Data were expressed as mean±SEM.

Effect of exhaustive swimming exercise on the vasoconstrictive responses to NA in the aorta and the internal carotid, caudal, pulmonary, and mesenteric arteries

A second exposure of the 5 selected arteries to NA (0.0001–100 μmol/L) produced vasoconstrictive responses in a dose-dependent manner in the rats of the SCG and the ESEG. The exhaustive swimming exercise significantly decreased the vasoconstrictive response to NA in the pulmonary and caudal arterial preparations (P<0.01, Figure 7A and 8A), reaching a maximal inhibition of 13.68% in the pulmonary artery and 9.48% in the caudal artery. In the mesenteric arterial preparation, the inhibition of vasoconstrictive response to NA by exhaustive swimming exercise was more potent, reaching a maximal inhibition of 21.02% (P<0.01, Figure 9A). Exhaustive swimming exercise significantly inhibited the vasoconstrictive responses to NA in the aorta, but the maximal response was not affected (Figure 10A). The vasoconstrictive response

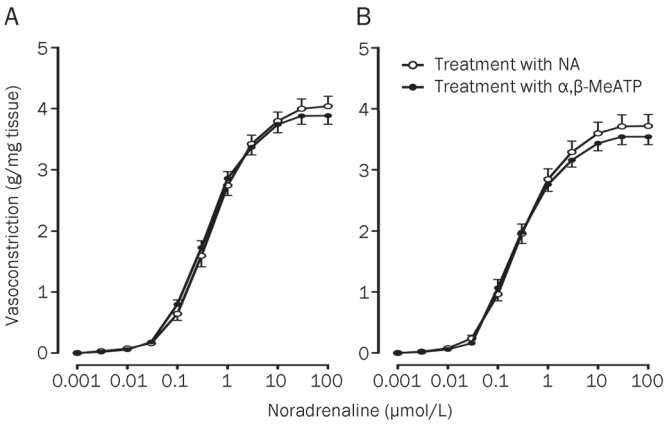

Figure 3. A comparison of the vasoconstrictive responses to noradrenaline between the preparations exposing to the second administration of noradrenaline (treatment with NA; n=11, left; n=15, right) and those exposing to α,β-methylene ATP (treatment with α,β-MeATP; n=20, left; n=20, right) in the rat caudal arteries from the sedentary control group (A) and the exhaustive swimming exercise group (B). Mean±SEM.

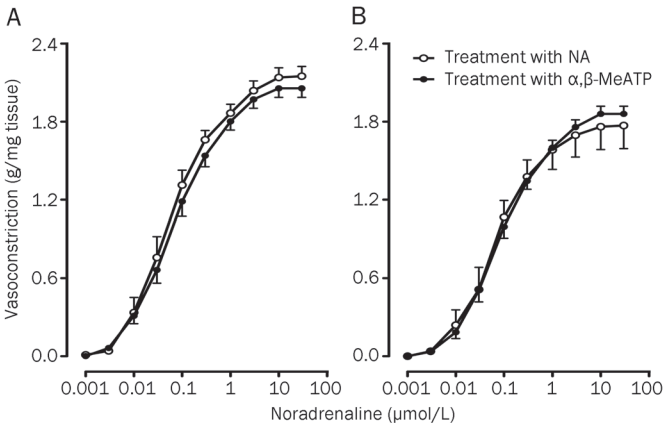

Figure 4. A comparison of the vasoconstrictive responses to noradrenaline between the preparations exposing to the second administration of noradrenaline (treatment with NA; n=11, left; n=9, right) and those exposing to α,β-methylene ATP (treatment with α,β-MeATP; n=22, left; n=22, right) in the rat mesenteric arteries from the sedentary control group (A) and the exhaustive swimming exercise group (B). Data were expressed as mean±SEM.

to NA in the internal carotid arterial preparation was not significantly affected by exhaustive swimming exercise (P>0.05, Figure 11A). The range of the negative log(EC_{50}) values (where the EC_{50} values are expressed as mol/L) for the 5 types of arteries given a second treatment with NA was 6.70–7.58. In the thoracic aorta, the negative log(EC_{50}) value of NA in the SCG (7.43±0.04) was slightly larger than that in the ESEG (7.11±0.10) (P<0.01); however, the EC_{50} values of NA in the SCG were not significantly different from those in the ESEG in the other 4 types of arteries (Table 1).

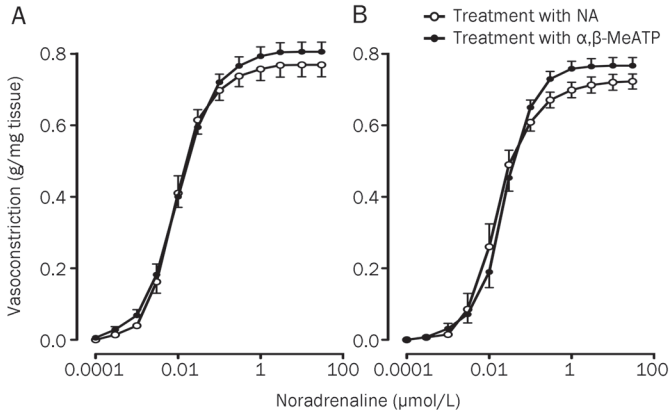

Figure 5. A comparison of the vasoconstrictive responses to noradrenaline between the preparations exposing to the second administration of noradrenaline (treatment with NA; *n*=11, left; *n*=8, right) and those exposing to α,β-methylene ATP (treatment with α,β-MeATP; *n*=23, left; *n*=22, right) in the rat thoracic aorta from the sedentary control group (A) and the exhaustive swimming exercise group (B). Data were expressed as mean±SEM.

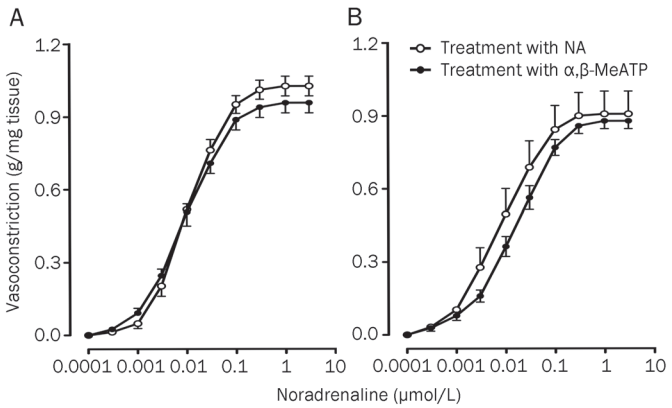

Figure 6. A comparison of the vasoconstrictive responses to noradrenaline between the preparations exposing to the second administration of noradrenaline (treatment with NA; *n*=9, left; *n*=8, right) and those exposing to α,β-methylene ATP (treatment with α,β-MeATP; *n*=20, left; *n*=20 right) in the rat internal carotid arteries from the sedentary control group (A) and the exhaustive swimming exercise group (B). Data were expressed as mean±SEM.

Effect of exhaustive swimming exercise on vasoconstrictive responses to α,β-MeATP in the aorta and the internal carotid, caudal, pulmonary, and mesenteric arteries

α,β-MeATP (0.1–100 μmol/L) produced vasoconstriction in the internal carotid, caudal, pulmonary, and mesenteric arteries, as well as the aorta, in a dose-dependent manner in the rats of the SCG and the ESEG. The vasoconstrictive responses to α,β-MeATP in the caudal artery, pulmonary artery, mesenteric artery and the aorta were not significantly affected by exhaustive swimming exercise (P>0.05, Figure 7B–10B). However, exhaustive swimming exercise significantly decreased

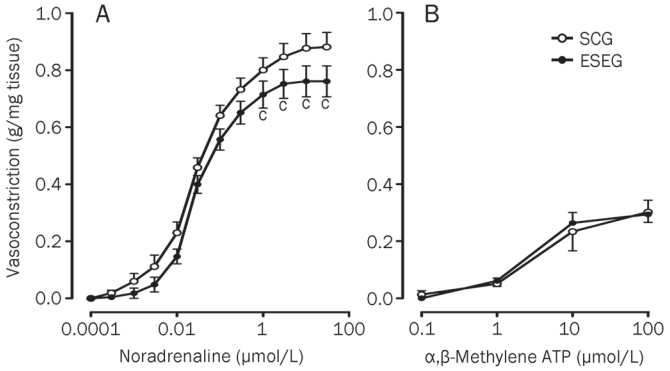

Figure 7. A comparison of the vasoconstrictive responses to the second administration of noradrenaline (A) or to α,β-methylene ATP (B) in the rat pulmonary arteries between the sedentary control group (SCG; *n*=10, A; *n*=5–7, B) and the exhaustive swimming exercise group (ESEG; *n*=9, A; *n*=5–7, B). Mean±SEM. Statistical significance was analyzed by two-way ANOVA in A: ^cP<0.01 *vs* SCG.

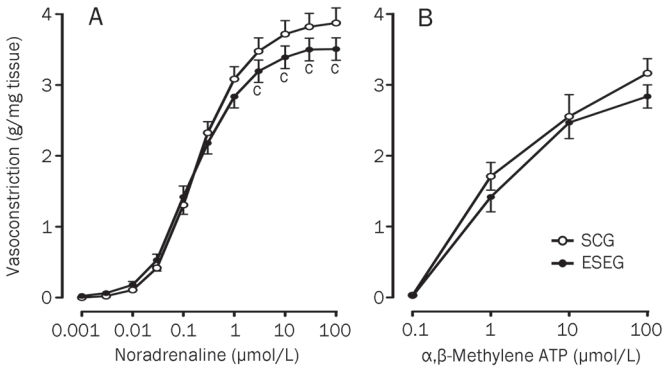

Figure 8. A comparison of the vasoconstrictive responses to the second administration of noradrenaline (A) or to α,β-methylene ATP (B) in the rat caudal arteries between the sedentary control group (SCG; *n*=11, A; *n*=5, B) and the exhaustive swimming exercise group (ESEG; *n*=15, A; *n*=5, B). Data were expressed as mean±SEM. Statistical significance was analyzed by two-way ANOVA in A: ^cP<0.01 *vs* SCG.

the vasoconstrictive response to α,β-MeATP in the internal carotid arterial preparations, reaching a maximum inhibition of 50.38% (P<0.01, Figure 11B). The range of the negative log(EC_{50}) values for α,β-MeATP in the 5 types of arteries was 4.71–6.19, and the EC_{50} values of α,β-MeATP in the SCG were not significantly different from those in the ESEG (Table 1).

Discussion

The co-transmission of NA and ATP is well established in the sympathetic innervation of a variety of blood vessels in animals. However, in this study, we discovered that exhaustive swimming exercise did not affect the EC_{50} values of NA or α,β-MeATP, but this type of exercise significantly decreased the $P2X_1$ receptor-mediated vasoconstriction in the rat internal carotid artery. Conversely, the vasoconstrictive response to

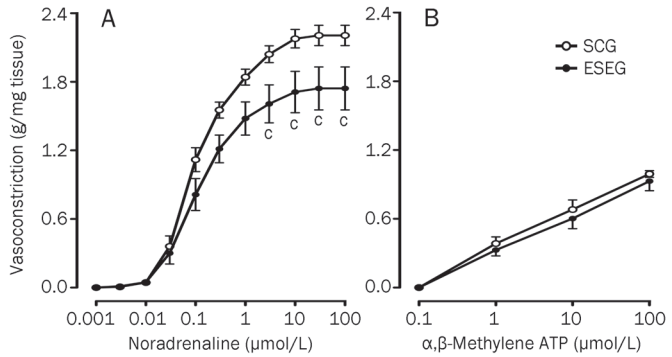

Figure 9. A comparison of the vasoconstrictive responses to the second administration of noradrenaline (A) or to α,β-methylene ATP (B) in the rat mesenteric arteries between the sedentary control group (SCG; *n*=11, A; *n*=5−6, B) and the exhaustive swimming exercise group (ESEG; *n*=9, A; *n*=5−6, B). Data were expressed as mean±SEM. $^{c}P<0.01$ *vs* SCG.

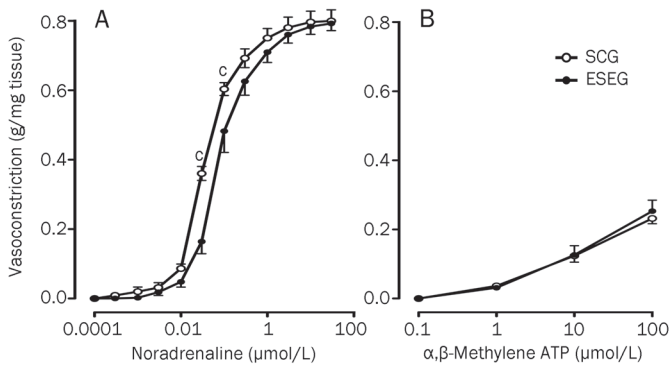

Figure 10. A comparison of the vasoconstrictive responses to the second administration of noradrenaline (A) or to α,β-methylene ATP (B) in the rat thoracic aorta between the sedentary control group (SCG; *n*=11, A; *n*=5−6, B) and the exhaustive swimming exercise group (ESEG; *n*=8, A; *n*=5−6, B). Data were expressed as mean±SEM. $^{c}P<0.01$ *vs* SCG.

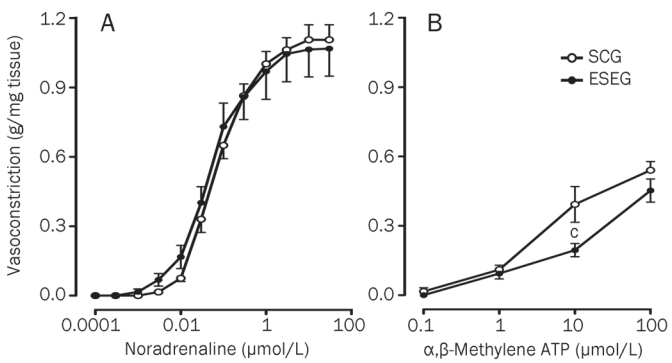

Figure 11. A comparison of the vasoconstrictive responses to the second administration of noradrenaline (A) or to α,β-methylene ATP (B) in the rat internal carotid arteries between the sedentary control group (SCG; *n*=9, A; *n*=5, B) and the exhaustive swimming exercise group (ESEG; *n*=8, A; *n*=5, B). Data were expressed as mean±SEM. $^{c}P<0.01$ *vs* SCG.

α_1-adrenoceptor, but not $P2X_1$ receptor, activation was inhibited in the caudal artery, pulmonary artery, mesenteric artery and the aorta obtained from rats subjected to the exhaustive swimming exercise.

Before observing the vasoconstrictive responses to α_1-adrenoceptor or $P2X_1$ receptor stimulation, we examined the vasoconstrictive responsiveness of each artery. In the rats of the SCG and the ESEG, there were no significant differences in the vasoconstrictive responses to the first exposure to NA (Figure 2–6) in the internal carotid, caudal, pulmonary, and mesenteric artery along with the aorta. No significant differences in vasoconstrictive responsiveness between the preparations that were either exposed to a second administration of NA or to α,β-MeATP were observed, suggesting that the 5 types of arteries obtained from the SCG rats and the ESEG rats were comparable in the present study. Because the EC_{50} values of KCl treatment were significantly greater in different types of arteries treated with α,β-MeATP than NA[24], and the maximum vasoconstrictive response to KCl in the rat mesenteric and caudal arteries in the SCG were greater than the response in the ESEG, we expressed the vasoconstrictive responses to NA and α,β-MeATP as g/mg tissue. Concomitantly, we found the exhaustive swimming exercise did not alter the EC_{50} values of KCl.

It has been reported that long-term swimming exercise significantly reduces the vasoconstrictive response to phenylephrine in the rat mesenteric artery and thoracic aorta when the endothelium is intact, but not in the endothelium-denuded arteries[26, 27]. Chronic exercise also enhances endothelium-mediated vasodilatation in the endothelium-intact aorta and mesenteric artery, but this exercise does not affect NA-induced vasoconstriction in the endothelium-denuded arteries isolated from spontaneously hypertensive rats[28]. Moreover, exercise training increases acetylcholine-induced relaxation and eNOS protein levels in the porcine pulmonary artery[29, 30], but not in the pulmonary artery from hypertensive rats[31]. Therefore, we removed the vascular endothelium of the isolated mesenteric, pulmonary, caudal and internal carotid arteries from the rat to directly observe the changes in α_1-adrenoceptor- and $P2X_1$ receptor-mediated vascular smooth muscle contractions because several studies suggest that exercise affects not only the vasoconstriction of vascular smooth muscles[32, 33], but also the function of the vascular endothelium[26, 27].

NA induces vasoconstriction and vasodilatation via α-adrenoceptors and β-adrenoceptors. Furthermore, Carter *et al*[34] reported that though α_2-adrenoceptors do not play a large role in NA-mediated vasoconstriction of the thoracic aorta in normotensive rats, there is an increased role of these receptors in hypertensive rats. Prior to measuring vasoconstrictive responsiveness after a second treatment with NA in this study, we added several reagents (propranolol, yohimbine, desmethylimipramine and deoxycorticosterone) to the organ bath to block β-adrenoceptors and α_2-adrenoceptors, as well as neuronal and extra-neuronal uptake of NA. This allows for the measurement of vasoconstriction after a second exposure of each arterial preparation to NA to be attributed to

α_1-adrenoceptors alone.

Though it is widely accepted that the $P2X_1$ receptor seems to be the most important P2X subtype in the vascular smooth muscle, this concept is not observed in functional studies. Nori *et al*[35] observed the coexpression of three P2X receptor mRNAs ($P2X_1$, $P2X_2$, and $P2X_4$) in the rat vascular smooth muscle. However, it was reported that the $P2X_4$ receptor did not couple to a vasomotor response[36], and the $P2X_2$ receptor was mainly expressed in nerves and arterial endothelial cells and only found at low levels in smooth muscle cells[37]. Recently, Wallace *et al*[38] investigated the expression of P2X receptors in the tail and mesenteric arteries of rats aged 4, 6, and 12 weeks by using immunohistochemistry. $P2X_1$ receptor-specific immunoreactivity was associated with the smooth muscle layer of both arteries from all rats of all three ages, and the $P2X_4$ receptor was weakly expressed in the smooth muscle layer of the tail artery in 4- and 6-week-old rats along with the mesenteric artery of 4- and 12-week-old rats. Immunoreactivity of the other subtypes of the P2X receptor family was not detected in the smooth muscle layer of arteries in 6- and 12-week-old rats[38]. In our study, we used 12–13-week-old rats (300–350 g), and the vascular endothelium of the regional arteries was removed. This age of rats combined with the use of α,β-MeATP (which is inactive as an agonist at the recombinant $P2X_2$ purinoceptor[39]) allows us to assume that the $P2X_1$ purinoceptors are primarily involved in the vasoconstrictive response to α,β-MeATP.

This study was the first investigation of measuring the changes in the $P2X_1$ receptor-regulated vasoconstriction of regional arteries from rats subjected to the exhaustive swimming exercise. We also compared the effects of exhaustive swimming exercise on both α_1-adrenoceptor- and $P2X_1$ receptor-mediated vasoconstriction in the isolated internal carotid, caudal, pulmonary and mesenteric arteries along with the aorta. Our study clearly showed that the vasoconstrictive responses to α_1-adrenoceptor stimulation in the aorta and the caudal, pulmonary and mesenteric arteries from the exhaustively exercised rats were significantly smaller than those from the normal rats, and a rank order of the decrease in the maximal vasoconstriction was determined as follows: mesenteric artery, pulmonary artery, caudal artery, aorta. Similar results were reported in the endothelium-denuded aorta[32] and mesenteric artery[33] from normal rats subjected to physical exercise. Moreover, we found that the $P2X_1$ receptor-mediated vasoconstriction in all 5 arterial subtypes was not affected by exhaustive exercise. Using an isolated perfused splenic artery, Yang *et al*[40] observed two peaks of vasoconstriction in response to periarterial nerve stimulation: an initial transient constriction induced by the purinergic ligand ATP and a second peak response consisting primarily of an adrenergic component. Our recent study demonstrated that the maximal vasoconstriction mediated by $P2X_1$ receptors reached at least 40% of those mediated by α_1-adrenoceptors in the rat internal carotid, mesenteric and pulmonary arteries. $P2X_1$ receptor-mediated vasoconstriction even reached 80% in the caudal artery[24], which suggested that purinergic transmission can be useful to maintain the basal vascular tone and could be important to the hemodynamic control in rats subjected to exhaustive swimming exercise. Sugawara *et al*[41] also suggested that a reduction in α-adrenoceptor-mediated vascular tone contributes to improved arterial compliance in healthy adults who engage in endurance exercise.

In contrast to the rat caudal artery, pulmonary artery, mesenteric artery and the aorta, the vasoconstrictive response to α_1-adrenoceptor stimulation in the rat internal carotid artery was not significantly affected by exhaustive swimming exercise. However, the vasoconstrictive response to $P2X_1$ receptor stimulation in the internal carotid artery from the exhaustively exercised rats was significantly reduced. The reason for this difference is still unclear based on the data from the present study. Normally, the brain is entirely dependent upon glucose as an energy substrate as implied by cerebral metabolic ratio, which is close to 6.0[42]. After exhaustive exercise, the cerebral metabolic ratio drops to 1.7, suggesting a link between brain metabolism and central fatigue[43].

It was reported recently that the ratio of ischemic-to-nonischemic blood flow decreases from 6 to 24 months of age, and the capillary density of nonischemic and ischemic muscle also decreases in an age-dependent manner in wild-type mice[44]. Swimming training was shown to reduce the formation of abnormal vessels and promoted collateral artery formation in the ischemic limbs of aged wild-type mice[44]. We plan to observe and clarify the effect of exhaustive swimming on vasoconstriction mediated by purinoceptors or adrenoceptors in aged rats in the near future. Maiorana *et al*[45] reported that chronic heart failure patients engaging in aerobic exercise had no changes in the wall thickness and the wall-to-lumen ratio of the brachial artery, while patients engaging in resistance exercise had a significantly reduced brachial artery wall thickness and wall-to-lumen ratio. The method of exhaustive swimming used in our study does not fall within the categories of either aerobic exercise or resistance exercise. It is unclear whether aerobic exercise affects the vasoconstriction mediated by purinoceptors and adrenoceptors in the same manner as resistance exercise does in normal or heart failure model animals.

Overall, the results of the present study showing the different effects of exhaustive swimming exercise on the vasoconstriction mediated by α_1-adrenoceptors and $P2X_1$ receptors between rat internal carotid artery and the peripheral arteries could help to explain that stress or injury can mediate different vascular responses in animals and humans and could be associated with tissue or organ functions. In conclusion, the exhaustive swimming exercise differentially affects the vasoconstriction regulated by $P2X_1$ receptors and α_1-adrenoceptors in the rat internal carotid artery and the peripheral arteries, and the ability to preserve purinergic vasoconstriction of the peripheral arteries is useful in maintaining the basal vascular tone during exhaustive swimming exercise.

Acknowledgements

This work was supported by a grant from the National Program on Key Basic Research Project of China (973 Program)

(No 2005CB523301).

Author contribution

Lei-ming REN and Yi-ling WU designed the research. Lu LI, Tao WU, Cong WEI, and Jian-ke HAN performed the research. Zhen-hua JIA analyzed the data.

References

1 Kingwell BA. Nitric oxide-mediated metabolic regulation during exercise: effects of training in health and cardiovascular disease. FASEB J 2000; 14: 1685–96.
2 Sutoo D, Akiyama K. Regulation of brain function by exercise. Neurobiol Dis 2003; 13: 1–14.
3 Larson EB, Wang L. Exercise, aging, and Alzheimer disease. Alzheimer Dis Assoc Disord 2004; 18: 54–6.
4 Sastre J, Asensi M, Gasco E, Pallardo FV, Ferrero JA, Furukawa T, *et al*. Exhaustive physical exercise causes oxidation of glutathione status in blood: prevention by antioxidant administration. Am J Physiol 1992; 263: R992–5.
5 Banerjee AK, Mandal A, Chanda D, Chakraborti S. Oxidant, antioxidant and physical exercise. Mol Cell Biochem 2003; 253: 307–12.
6 Fehrenbach E, Northoff H. Free radicals, exercise, apoptosis, and heat shock proteins. Exerc Immunol Rev 2001; 7: 66–89.
7 Huang CC, Lin TJ, Chen CC, Lin WT. Endurance training accelerates exhaustive exercise-induced mitochondrial DNA deletion and apoptosis of left ventricle myocardium in rats. Eur J Appl Physiol 2009; 107: 697–706.
8 Aslani A, Babaee Bigi MA, Moaref AR, Aslani A. Effect of extreme exercise on myocardial function as assessed by tissue Doppler imaging. Echocardiography 2009; 26: 1036–40.
9 Howard MG, DiCarlo SE, Stallone JN. Acute exercise attenuates phenylephrine-induced contraction of rabbit isolated aortic rings. Med Sci Sports Exerc 1992; 24: 1102–7.
10 Chen Hi H, Chiang IP, Jen CJ. Exercise training increases acetylcholine-stimulated endothelium-derived nitric oxide release in spontaneously hypertensive rats. J Biomed Sci 1996; 3: 454–60.
11 Graham DA, Rush JW. Exercise training improves aortic endothelium-dependent vasorelaxation and determinants of nitric oxide bioavailability in spontaneously hypertensive rats. J Appl Physiol 2004; 96: 2088–96.
12 Moien-Afshari F, Ghosh S, Elmi S, Khazaei M, Rahman MM, Sallam N, *et al*. Exercise restores coronary vascular function independent of myogenic tone or hyperglycemic status in *db/db* mice. Am J Physiol Heart Circ Physiol 2008; 295: H1470–80.
13 Korzick DH, Laughlin MH, Bowles DK. Alterations in PKC signaling underlie enhanced myogenic tone in exercise-trained porcine coronary resistance arteries. J Appl Physiol 2004; 96: 1425–32.
14 Boarder MR, Hourani SM. The regulation of vascular function by P2 receptors: multiple sites and multiple receptors. Trends Pharmacol Sci 1998; 19: 99–107.
15 Collo G, North RA, Kawashima E, Merlo-Pich E, Neidhart S, Surprenant A, *et al*. Cloning of $P2X_5$ and $P2X_6$ receptors and the distribution and properties of an extended family of ATP-gated ion channels. J Neurosci 1996; 16: 2495–507.
16 Galligan JJ, Hess MC, Miller SB, Fink GD. Differential localization of P2 receptor subtypes in mesenteric arteries and veins of normotensive and hypertensive rats. J Pharmacol Exp Ther 2001; 296: 478–85.
17 Vial C, Evans RJ. P2X(1) receptor-deficient mice establish the native P2X receptor and a $P2Y_6$-like receptor in arteries. Mol Pharmacol 2002; 62: 1438–45.
18 Erlinge D, Burnstock G. P2 receptors in cardiovascular regulation and disease. Purinergic Signal 2008; 4: 1–20.
19 Haddock RE, Hill CE. Sympathetic overdrive in obesity involves purinergic hyperactivity in the resistance vasculature. J Physiol 2011; 589: 3289–307.
20 Vidal M, Hicks PE, Langer SZ. Differential effects of alpha-beta-methylene ATP on responses to nerve stimulation in SHR and WKY tail arteries. Naunyn Schmiedebergs Arch Pharmacol 1986; 332: 384–90.
21 Thomas DP, Marshall KI. Effects of repeated exhaustive exercise on myocardial subcellular membrane structures. Int J Sports Med 1988; 9: 257–60.
22 Peijie C, Hongwu L, Fengpeng X, Jie R, Jie Z. Heavy load exercise induced dysfunction of immunity and neuroendocrine responses in rats. Life Sci 2003; 72: 2255–62.
23 Sun B, Wang JH, Lv YY, Zhu SS, Yang J, Ma JZ. Proteomic adaptation to chronic high intensity swimming training in the rat heart. Comp Biochem Physiol Part D Genomics Proteomics 2008; 3: 108–17.
24 Li L, Jia ZH, Chen C, Wei C, Han JK, Wu YL, *et al*. Physiological significance of P2X receptor-mediated vasoconstriction in five different types of arteries in rats. Purinergic Signal 2011; 7: 221–9.
25 Wihlborg AK, Slätt J, Sun X, Zhao XH, Malmsjö M, Bergman J, *et al*. 2,2′-Nitrophenylisatogen potentiates P2X1 receptor mediated vascular contraction and blood pressure elevation. Drug Dev Res 2003; 59: 82–7.
26 Jansakul C, Hirunpan P. Effects of exercise training on responsiveness of the mesenteric arterial bed to phenylephrine and KCl in male rats. Br J Pharmacol 1999; 127: 1559–66.
27 Jansakul C. Effect of swimming on vascular reactivity to phenylephrine and KCl in male rats. Br J Pharmacol 1995; 115: 587–94.
28 Yen MH, Yang JH, Sheu JR, Lee YM, Ding YA. Chronic exercise enhances endothelium-mediated dilation in spontaneously hypertensive rats. Life Sci 1995; 57: 2205–13.
29 Johnson LR, Parker JL, Laughlin MH. Chronic exercise training improves ACh-induced vasorelaxation in pulmonary arteries of pigs. J Appl Physiol 2000; 88: 443–51.
30 Johnson LR, Rush JW, Turk JR, Price EM, Laughlin MH. Short-term exercise training increases ACh-induced relaxation and eNOS protein in porcine pulmonary arteries. J Appl Physiol 2001; 90: 1102–10.
31 Goret L, Reboul C, Tanguy S, Dauzat M, Obert P. Training does not affect the alteration in pulmonary artery vasoreactivity in pulmonary hypertensive rats vasoreactivity in pulmonary hypertensive rats. Eur J Pharmacol 2005; 527: 121–8.
32 Izawa T, Morikawa M, Mizuta T, Nagasawa J, Kizaki T, Oh-ishi S, *et al*. Decreased vascular sensitivity after acute exercise and chronic exercise training in rat thoracic aorta. Res Commun Mol Pathol Pharmacol 1996; 93: 331–42.
33 Chies AB, de Oliveira AM, Pereira FC, de Andrade CR, Correa FM. Phenylephrine-induced vasoconstriction of the rat superior mesenteric artery is decreased after repeated swimming. J Smooth Muscle Res 2004; 40: 249–58.
34 Carter RW, Begaye M, Kanagy NL. Acute and chronic NOS inhibition enhances alpha(2)- adrenoreceptor-stimulated RhoA and Rho kinase in rat aorta. Am J Physiol Heart Circ Physiol 2002; 283: H1361–9.
35 Nori S, Fumagalli L, Bo X, Bogdanov Y, Burnstock G. Coexpression of mRNAs for $P2X_1$, $P2X_2$, and $P2X_4$ receptors in rat vascular smooth muscle: an *in situ* hybridization and RT-PCR study. J Vasc Res 1998; 35: 179–85.
36 Ralevic V, Burnstock G. Receptors for purines and pyrimidines. Pharmacol Rev 1998; 50: 413–92.
37 Hansen MA, Dutton JL, Balcar VJ, Barden JA, Bennett MR. P2X

(purinergic) receptor distributions in rat blood vessels. J Auton Nerv Syst 1999; 75: 147–55.

38 Wallace A, Knight GE, Cowen T, Burnstock G. Changes in purinergic signalling in developing and ageing rat tail artery: importance for temperature control. Neuropharmacology 2006; 50: 191–208.

39 Brake AJ, Wagenbach MJ, Julius D. New structural motif for ligand-gated ion channels defined by an ionotropic ATP receptor. Nature 1994; 371: 519–23.

40 Yang XP, Chiba S. Effects of a selective neuropeptide Y Y(1) receptor antagonist BIBP 3226 on double peaked vasoconstrictor responses to periarterial nerve stimulation in canine splenic arteries. Br J Pharmacol 2000; 130: 1699–705.

41 Sugawara J, Komine H, Hayashi K, Yoshizawa M, Otsuki T, Shimojo N, *et al*. Reduction in alpha-adrenergic receptor-mediated vascular tone contributes to improved arterial compliance with endurance training. Int J Cardiol 2009; 135: 346–52.

42 Dalsgaard MK, Quistorff B, Danielsen ER, Selmer C, Vogelsang T, Secher NH. A reduced cerebral metabolic ratio in exercise reflects metabolism and not accumulation of lactate within the human brain. J Physiol 2004; 554: 571–8.

43 Volianitis S, Fabricius-Bjerre A, Overgaard A, Stromstad M, Bjarrum M, Carlson C, *et al*. The cerebral metabolic ratio is not affected by oxygen availability during maximal exercise in humans. J Physiol 2008; 586: 107–12.

44 Cheng XW, Kuzuya M, Kim W, Song HZ, Hu L, Inoue A, *et al*. Exercise training stimulates ischemia-induced neovascularization via phosphatidylinositol 3-kinase/Akt-dependent hypoxia-induced factor-1 alpha reactivation in mice of advanced age. Circulation 2010; 122: 707–16.

45 Maiorana AJ, Naylor LH, Exterkate A, Swart A, Thijssen DH, Lam K, *et al*. The impact of exercise training on conduit artery wall thickness and remodeling in chronic heart failure patients. Hypertension 2011; 57: 56–62.

Acta Pharmacologica Sinica (2012) 33: 230–236
 1671-4083/12 $32.00
www.nature.com/aps

Original Article

PKCα regulates vasopressin-induced aquaporin-2 trafficking in mouse kidney collecting duct cells *in vitro* via altering microtubule assembly

Hong ZHAO[1, #], Xi YAO[2, #], Tao-xia WANG[2], Wen-min JIN[1], Qian-qian JI[1], Xiao YANG[1], Qiu-hong DUAN[3], Li-jun YAO[2, *]

[1]Department of Trauma Surgery, Tongji Hospital, Huazhong University of Science & Technology, Wuhan 430030, China; [2]Departments of Nephrology, Union Hospital, Huazhong University of Science & Technology, Wuhan 430030, China; [3]Department of Biochemistry and Molecular Biology, Tongji Medical College, Huazhong University of Science & Technology, Wuhan 430022, China

Aim: Aquaporin-2 (AQP2) is a vasopressin-regulated water channel located in the collecting tubule and collecting duct cells of mammalian kidney. The aim of this study is to investigate whether PKCα plays a role in vasopressin-induced AQP2 trafficking in mouse inner medullary collecting duct 3 (mIMCD3) cells.

Methods: AQP2-mIMCD3 stable cell line was constructed by transfection of mouse inner medullary collecting duct 3 (mIMCD3) cells with AQP2-GFP construct. Then the cells were transfected with PKCα shRNA, PKCα A/25E, or PKCα scrambled shRNA. The expression levels of PKCα, AQP2, and phospho-S256-AQP2 were analyzed using Western blot. The interaction between AQP2 and PKCα was examined using immunoprecipitation. The distribution of AQP2 and microtubules was studied using immunocytochemistry. The AQP2 trafficking was examined using the biotinylation of surface membranes.

Results: Treatment of AQP2-mIMCD3 cells with 100 μmol/L of 1-desamino-8-*D*-arginine vasopressin (DdAVP) for 30 min stimulated the translocation of AQP2 from the cytoplasm to plasma membrane through influencing the microtubule assembly. Upregulation of active PKCα by transfection with PKCα A/25E plasmids resulted in de-polymerization of α-tubulin and redistributed AQP2 in the cytoplasm. Down-regulation of PKCα by PKCα shRNA partially inhibited DdAVP-stimulated AQP2 trafficking without altering α-tubulin distribution. Although 100 μmol/L of DdAVP increased AQP2 phosphorylation at serine 256, down-regulation of PKCα by PKCα shRNA did not influence DdAVP-induced AQP2 phosphorylation, suggesting that AQP2 phosphorylation at serine 256 was independent of PKCα. Moreover, PKCα did not physically interact with AQP2 in the presence or absence of DdAVP.

Conclusion: Our results suggested that PKCα regulates AQP2 trafficking induced by DdAVP via microtubule assembly.

Keywords: PKCα; 1-desamino-8-*D*-arginine vasopressin (DdAVP); aquaporin-2; microtubule; kidney; medullary collecting duct

Acta Pharmacologica Sinica (2012) 33: 230–236; doi: 10.1038/aps.2011.160; published online 2 Jan 2012

Introduction

Protein kinase C alpha (PKCα) is a member of the classic PKC family[1], which is widely expressed in the mammalian kidney[2–4] and contributes to various kidney functions, including substrate absorption and urine concentration[5, 6]. PKCα-mediated cytoskeleton remodeling results in endocytosis in epithelial cells, which increases the uptake of various substrates, such as NHE3 and albumin[7–9]. PKCα is localized in glomeruli, the intercalated cells of the cortical collecting duct, and the medullary-collecting duct in the mouse kidney[4]. Genetic knockout mice that lack PKCα exhibit decreased glomerular filtration rate, increased urinary output and lower urinary osmolarity, accompanied by normal water intake and normal levels of the plasma antidiuretic hormone arginine vasopressin (AVP)[5]. These results strongly suggest that PKCα-mediated urine concentration primarily occurs within the medullary collecting duct.

Aquaporin-2 (AQP2) is a vasopressin-regulated water channel in the principal cells of the connecting tubule and the collecting duct in the kidney[10, 11]. AQP2 is stored in an intracellular compartment and plays an important role in the regulation of urine concentration[12–15]. AVP stimulates AQP2 translocation to the plasma membrane for the re-absorption of water. AQP2 is removed from the plasma membrane and returned to the intracellular compartment when the stimulation in terminated[16–18]. In addition, AVP also regulates AQP2 mRNA and protein levels, which mediates long-term regula-

# These two authors contributed equally to this paper.
* To whom correspondence should be addressed.
E-mail drylj@hotmail.com
Received 2011-06-28 Accepted 2011-10-28

tion[19, 20]. Both short- and long-term regulation mechanisms are involved in the pathophysiology of AQP2-mediated urine concentration[21]. Although PKC is involved in angiotensin II-mediated AQP2 expression and trafficking[22], our previous study demonstrated that AQP2 expression is only slightly different between PKCα knockout mice and wild-type mice[5], which strongly suggests that the long-term AQP2 regulation mechanism does not contribute to PKCα-mediated urine concentration. AQP2 transportation is partially regulated by the cytoskeleton[23–25], and PKCα-mediated remodeling of the actin cytoskeleton is involved in constitutive albumin uptake in the renal proximal tubule[9]. However, the contribution of PKCα to AQP2 trafficking, the role of the cytoskeleton in PKCα-mediated AQP2 transportation and the mechanism of PKCα regulation of AQP2 translocation are less well understood.

We hypothesized that PKCα mediates AQP2 trafficking via cytoskeleton distribution because of the important role of PKCα in urine concentration and cytoskeleton remodeling. Therefore, this study revealed the crosstalk among PKCα, AVP and AQP2 in trafficking and cytoskeletal remodeling in mIMCD3 cell.

Materials and methods

Constructs, antibodies, and reagents

The pEF-nero-PKCα A/25E vector was a gift from Dr Gottfried BAIER (Institute for Medical Biology and Human Genetics, University of Innsbruck, Innsbruck, Austria). The AQP2-GFP-pCMV6 construct was purchased from Origene (Rockville, MD, USA). Lipofectamine plus and geneticin (G418) were purchased from Invitrogen (Shanghai, China). Protein A/G-agarose beads and primary antibodies against phosphor-S256-AQP2, AQP2, PKCα, and GAPDH were purchased from Santa Cruz (Heidelberg, Germany). The primary antibody against α-tubulin was purchased from Calbiochem (Darmstadt, Germany). The secondary goat anti-rabbit IgG conjugated with Cy3 antibody and the analogue 1-desamino-8-*D*-arginine vasopressin (DdAVP) were purchased from Sigma (Shanghai, China). DAPI was purchased from Vector Burlingame (San Diego, CA, USA). Sulfo-Link NHS-LC-biotin and streptavidin-agarose beads were purchased from Pierce (Beijing, China). Major apparatuses included a Mini-PROTEAN II Electrophoresis Cell (Bio-Rad, Shanghai, China) and a confocal laser-scanning microscope (Olympus FV500, Japan).

Cells and cell culture

Immortalized mouse inner medullary collecting duct 3 (mIMCD3) cells were kindly provided by Dr John M LUK (Department of Urology, University of Hong Kong, Hong Kong, China). mIMCD3 cells were maintained in Dulbecco's modified Eagle's medium/Ham's F12 (1:1) (GIBCO, Invitrogen, Shanghai, China) supplemented with 10% fetal bovine serum (GIBCO, Invitrogen, Shanghai, China) and 2% penicillin-streptomycin (Amresco, Shanghai, China) in a humidified atmosphere with 5% CO_2 at 37 °C.

Generation of pGCsi-U6/Neo PKCα shRNA plasmid

Three siRNAs were designed and synthesized by Invitrogen (Shanghai, China) according to the cDNA sequence of PKCα (NM_011101): #1, GTCCTTCACGTTCAAATTA; #2, GTGCAGTATGAAACTCAAA; and #3, CCATCCAACAACCTGGACA. The siRNAs were cloned into the eukaryotic expression plasmid pGCsi-U6/Neo (Genechem, Shanghai, China). The constructed pGCsi-U6/Neo-PKCα-siRNA vector was transfected into mIMCD3 cells. Western blotting was used to evaluate the suppression of PKCα expression in different cell groups.

Transfection

Transfection of mIMCD3 cells with the AQP2-GFP construct was performed using Lipofectamine 2000 (Shanghai, China) according to the manufacturer's instructions. The cells were maintained in medium containing 400 μg/mL geneticin for 24 h after transfection. Individual neomycin-resistant colonies were selected and expanded for 14 d after transfection.

AQP2-GFP was stably expressed in mIMCD3 cells (AQP2-mIMCD3 cells) that were transiently transfected with a eukaryotic expression vector encoding the constitutively activated form of PKCα A/25E (pEF-nero-PKCα A/25E)[26] using Lipofectamine 2000 according to the manufacturer's instructions. AQP2-mIMCD3 cells were transfected with three pGCsi-U6/Neo-PKCα shRNAs and scrambled shRNA using Lipofectamine 2000 according to the manufacturer's instructions to evaluate the inhibition efficiency of the siRNAs. The cells were harvested 48 h after transfection, and Western blot and immunofluorescence were used to evaluate the transfection efficiency.

Immunocytochemical staining

AQP2-mIMCD3 cells were divided into 3 groups: (1) Scrambled shRNA transfected; (2) PKCα A/25E vector transfected; and (3) PKCα shRNA transfected. The cells in each group were treated with 100 μmol/L DdAVP for 30 min. DdAVP was removed, and the cells were incubated with culture medium for 2 h (washout). The cells were then fixed in 4% paraformaldehyde for 10 min, rinsed twice in PBS, and blocked for 15 min in a blocking/permeabilization solution (PBS containing 0.1% BSA and 0.3% Triton X-100). The cells were washed with PBS and pre-incubated in PBS containing 1% BSA for 20 min. The cells were incubated with an α-tubulin antibody (at a final concentration of 2 μg/mL) at 4 °C overnight. The cells were washed with PBS and incubated in the secondary goat anti-rabbit IgG conjugated with Cy3 antibody (at a final concentration of 2 μg/mL) for 1.5 h at RT. Finally, the cells were washed twice with PBS and mounted with DAPI for confocal laser-scanning microscopy equipped with a CoolSNAP HQ camera.

Biotinylation of surface membrane proteins

Identifiably transfected AQP2-mIMCD3 cells were cultured on polylysine-coated 60-mm dishes for 48 h and treated with

DdAVP for 0 min, 30 min, or 30 min followed by a 2-h washout. The cells were washed three times with PBS/glycine (137 mmol/L NaCl, 2.7 mmol/L KCl, 10 mmol/L Na_2HPO_4, 1.8 mmol/L KH_2PO_4, pH 8.0, and 5 mmol/L glycine) and twice with PBS[27]. An ice-cold biotinylation reagent (0.5 mg/mL in PBS) was immediately added to cells. The biotinylation reagent was removed after a 10-min incubation on ice, and the cells were washed three times with PBS/glycine.

Immunoblotting and immunoprecipitation

Transfected and DdAVP-treated cells were lysed in RIPA buffer (10 mmol/L Tris-HCl, 0.15 mol/L NaCl, 1% NP-40, 1% Na-deoxycholate, 0.5% SDS, 0.02% sodium azide, and 1 mmol/L EDTA, pH 7.4). The cell lysates were clarified by centrifugation at 1000×*g* for 10 min at 4 °C. Protein concentrations were measured using the bicinchoninic acid protein assay reagent kit (Pierce, Thermo Fisher Scientific, Beijing, China) and adjusted to the same concentration using lysine buffer. A 0.5-mL aliquot of the cell lysates was incubated with 50 μL of streptavidin-agarose beads at 4 °C overnight to capture biotinylated proteins, 50 μL of protein A/G-agarose beads plus the AQP2 antibody to capture total AQP2, or 50 μL of protein A/G-agarose beads plus the PKCα antibody to capture total PKCα. The beads were pelleted, washed, and boiled for 5 min in 50 μL of cracking buffer (50 mmol/L Tris-HCl [pH 7.0], 10% glycerol, 2% SDS, and 2% β-mercaptoethanol). The eluted immunoprecipitates were separated on 10% polyacrylamide gels and transferred electrophoretically to PVDF membrane. The membranes were blocked for 90 min with blocking buffer during gentle shaking and incubated overnight with antibodies against AQP2 (0.5 μg/mL), phospho-S256-AQP2 (0.5 μg/mL), PKCα (0.5 μg/mL) or GAPDH (0.5 μg/mL). The membranes were incubated with an HRP-conjugated IgG (0.1 μg/mL) for 2 h at room temperature. Finally, the immunoreactive signals were visualized using an ECL reagent (Beyotime, Shanghai, China) and quantified using the Image J program (NIH, Bethesda, MD, USA).

Statistical analyses

The values are presented as the means±SEM. The data were analyzed using SPSS software. Statistical significance of differences was assessed using unpaired *t*-tests or two-way ANOVAs. A value of $P<0.05$ was viewed as statistically significant.

Results

Inhibition of PKCα and the overexpression of AQP2 in mIMCD3 cells

All three PKCα shRNA plasmids (#1, #2, and #3) and PKCα scrambled shRNA plasmids were transfected into mIMCD3 cells to select the shRNAs with the highest inhibition efficiency to PKCα. Crude proteins were extracted from the harvested cells 48 h after transfection and subjected to Western blotting using the PKCα antibody. PKCα shRNA #1 plasmids exhibited the greatest inhibitory effect on PKCα, but all three PKCα shRNAs demonstrated visible inhibition ($P<0.01$) (Figure 1A).

The transfection of mIMCD3 with the AQP2-GFP-pCMV6 plasmid produced 12 geneticin-resistant clones, 10 of which were subjected to Western blot analysis (data not shown). The clone that amply expressed AQP2 was selected and named WT-7. A strong signal at 30 kDa in the selected AQP2-mIMCD3 stable cell line (WT-7) was observed, but no signal was detected in nontransfected mIMCD3 cells (Figure 1B).

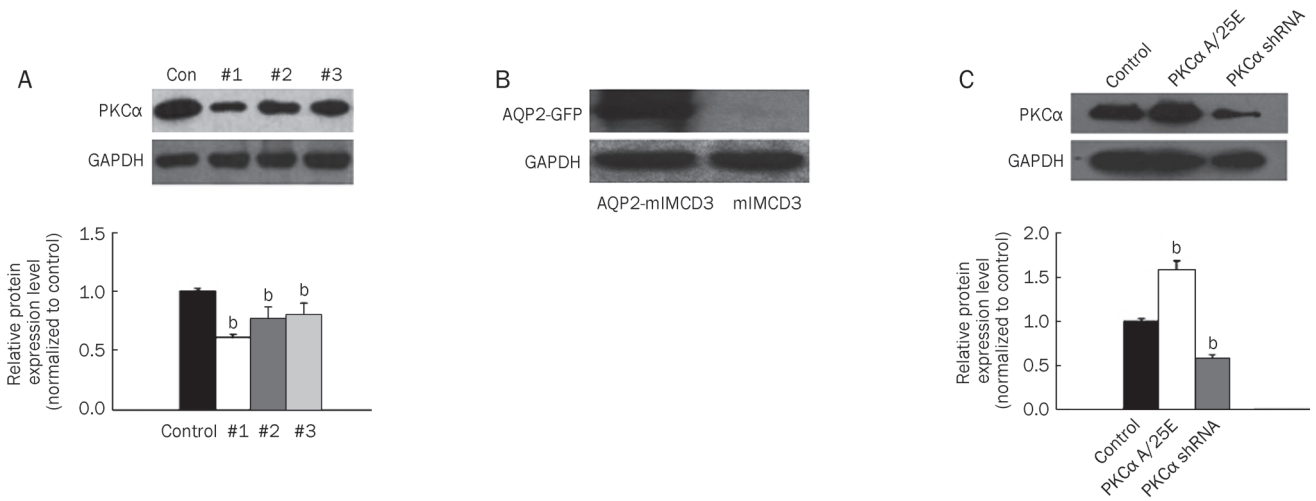

Figure 1. Inhibition of PKCα and the overexpression of AQP2 in mIMCD3 cells. (A) PKCα shRNA plasmid #1, #2, #3, and PKCα scramble shRNA plasmid (control) were transfected into mIMCD3 cells respectively. Forty-eight hours after transfection, crude proteins extracted from harvested cells were subjected to Western blot using antibodies against PKCα. Representative blot was shown (left) and quantitative analysis of PKCα protein levels were normalized to control group (n=3 each group) (right). $^bP<0.05$ *vs* control group. (B) AQP2-mIMCD3 stable cell line was generated by transfecting to express AQP2-GFP (See Materials and methods). The expression of AQP2-GFP was detected in selected WT7 stable cell lines. (C) AQP2-GFP stably expressed WT7 cells were transfected with scramble shRNA (Con), PKCα A/25E constructs or PKCα shRNA, respectively. Forty-eight hours after transfection, crude proteins extracted from harvested cells were subjected to Western blot using antibodies against PKCα (left). Quantitative analysis of PKCα protein levels were normalized to control group (n=3 each group) (right). $^bP<0.05$ *vs* control group.

These results suggest the successful preparation of AQP2-mIMCD3 stable cell lines.

The WT-7 stable cell line was used to investigate PKCα expression following different transfections of PKCα scrambled shRNA, PKCα A/25E, and PKCα shRNA (#1) using Western blot. The transfection of PKCα A/25E significantly enhanced PKCα expression, but PKCα shRNA (#1) dramatically suppressed PKCα expression ($P<0.05$) (Figure 1C). The WT-7 cell line and PKCα A/25E and PKCα shRNA (#1) plasmids were utilized in subsequent experiments.

DdAVP enhanced the phosphorylation of AQP2 and PKCα *in vitro*

The physical association of AQP2 with endogenous PKCα was examined *in vitro* in WT7 cell lines to reveal the direct role of PKCα on AQP2. Cells with or without DdAVP treatment for 30 min were lysed, and PKCα was immunoprecipitated using anti-PKCα antibodies. The immunoprecipitates were analyzed using Western blot and AQP2 antibodies. Strong signals for AQP2 and PKCα were detected in whole cell lysates and immunoprecipitates, but no AQP2 signal was detected in PKCα immunoprecipitates (Figure 2). These results suggest that PKCα did not interact with AQP2 *in vitro*. However, DdAVP treatment enhanced AQP2 phosphorylation at serine 256. Down-regulation of PKCα by shRNA did not alter DdAVP-mediated AQP2 phosphorylation at serine 256. These data indicated that PKCα did not influence DdAVP-induced AQP2 phosphorylation at serine 256 (Figure 2).

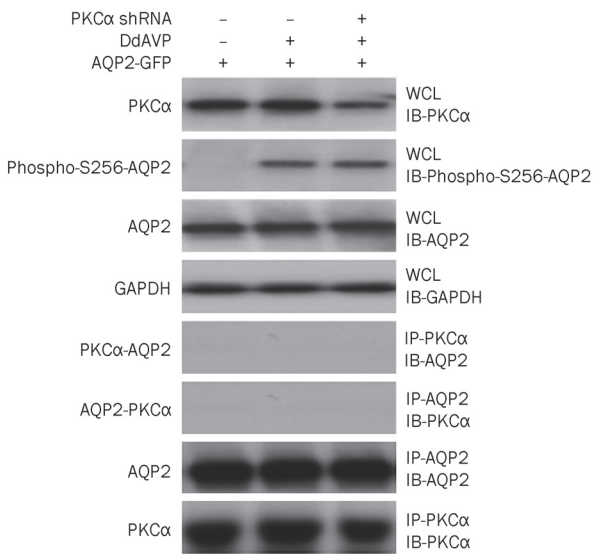

Figure 2. DdAVP enhanced the phosphorylation of AQP2 and AQP2 did not physically interact with PKCα *in vitro*. AQP2-GFP stably expressed WT7 cells were transfected with indicated constructs. Forty-eight hours after transfection, cells were treated with or without DdAVP for 30 min. Cells were then lysed and immunoprecipitation was performed with anti-PKCα and anti-AQP2 antibodies. Crude proteins from whole cell lysates and the immunoprecipitates were subjected to Western blot with indicated antibodies.

PKCα expression influenced the distribution of α-tubulin and DdAVP-mediated AQP2 trafficking in mIMCD cells

An increase in PKCα activity induces the re-organization of microtubules in proximal tubular cells[9]. Therefore, PKCα-induced alterations in microtubule architecture were investigated. Most cells that were transfected with scrambled shRNA plasmid or PKCα shRNA plasmids exhibited a prominent dense network of microtubules around the nucleus with a considerably lower microtubule content in the cell periphery under basal conditions. The constitutive activation of PKCα increased microtubule formation in the cell periphery (Figure 3, upper panel and middle panel). AQP2-mIMCD3 cells (WT7 cells) were incubated with DdAVP for 30 min followed by a 2-h washout to evaluate the involvement of PKCα in AVP-induced microtubule formation in the cell periphery. Cells that were transfected with the control and PKCα A/25E plasmids displayed increased microtubule formation in the cell periphery following DdAVP stimulation. In contrast, the down-regulation of PKCα expression using shRNA inhibited DdAVP-induced microtubule depolymerization (Figure 3, lower panel). Taken together, these data strongly indicated that the expression of PKCα regulated microtubule distribution in mIMCD cells.

The role of PKCα in DdAVP-induced AQP2 trafficking was investigated because PKCα influences microtubule reorganization, and the DdAVP-induced depolymerization of microtubules affects the redistribution of AQP2 to the plasma membrane[25, 28, 29]. Immunofluorescence analyses indicated that AQP2 was primarily localized around the nucleus under basal condition. Treatment with DdAVP for 30 min produced a pronounced increase in AQP2 localization in the plasma membrane. DdAVP washout restored the perinuclear localization of AQP2. The expression of constitutively activated PKCα produced a wide distribution of AQP2 throughout the cytoplasm in contrast to AQP2 localization around the nucleus under basal conditions. DdAVP also induced the translocation of AQP2 to the plasma membrane in the PKCα A/25E transfected group. The down-regulation of PKCα expression by shRNA interference inhibited DdAVP-induced AQP2 translocation to the plasma membrane (Figure 3).

Regulation of PKCα expression influenced DdAVP-stimulated plasma location of AQP2

mIMCD-3 surface membrane proteins were biotinylated following DdAVP treatment for 0 min, 30 min, and 30 min followed by a 2-h washout to confirm the immunofluorescence results. Biotinylated proteins were captured from whole-cell lysates using streptavidin beads, separated by SDS-PAGE and probed using an AQP2 antibody. Immunoprecipitation was performed in whole cell lysates in parallel using AQP2-specific antibodies. The DdAVP-induced increase in biotin-AQP2 was partially inhibited by PKCα down-regulation with shRNA transfection, but biotin-AQP2 was enhanced by the overexpression of PKCα A/25E (Figure 4). Moreover, different treatments only marginally affected the total amount of

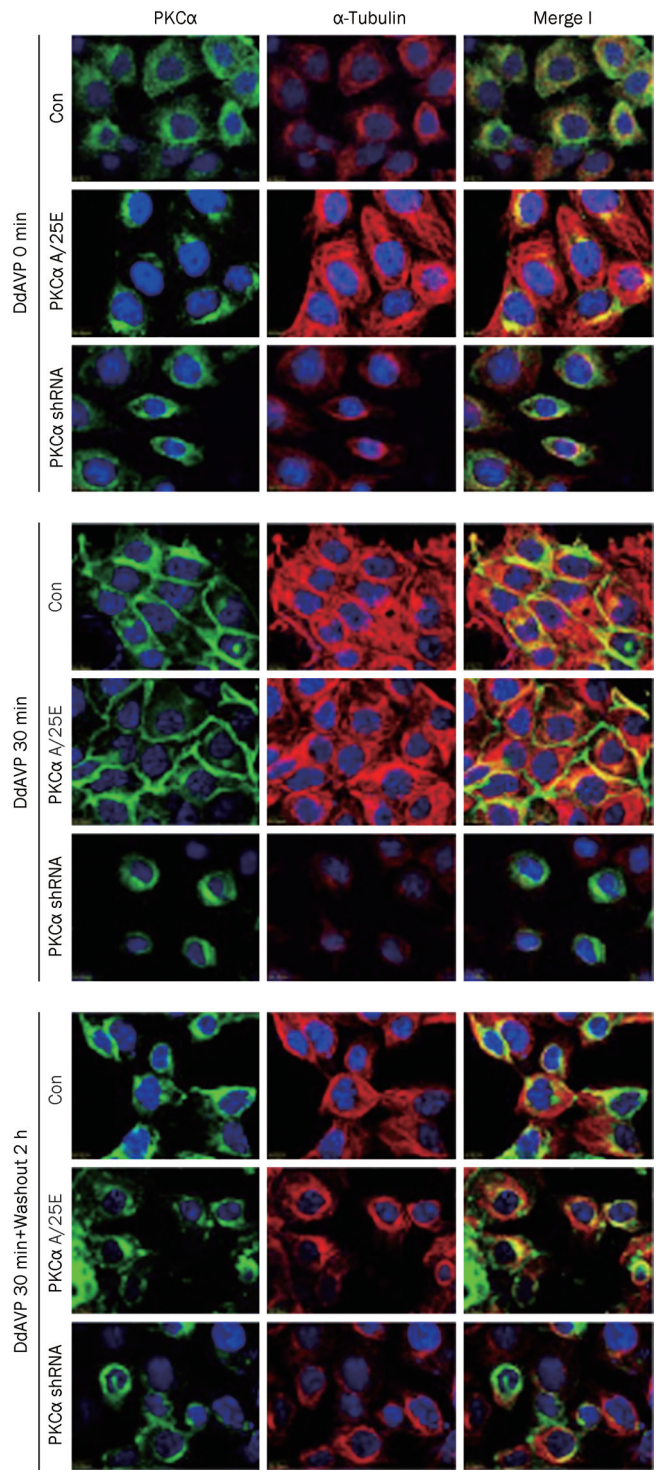

Figure 3. PKCα expression influenced the distribution of α-tubulin and DdAVP-mediated AQP2 trafficking in mIMCD3 cells. AQP2-GFP stably expressed WT7 cells were transfected with PKCα cramble shRNA (Con), PKCα A/25E constructs or PKCα shRNA constructs. Forty-eight hours after transfection, cells were treated with or without DdAVP for 0 min, 30 min or 30 min followed by 2 h washout. Cells were then fixed, permeablized and stained with antibodies aganist PKCα (green) and α-tubulin (red) for immunofluorescence. Nuclear was stained by DAPI (blue).

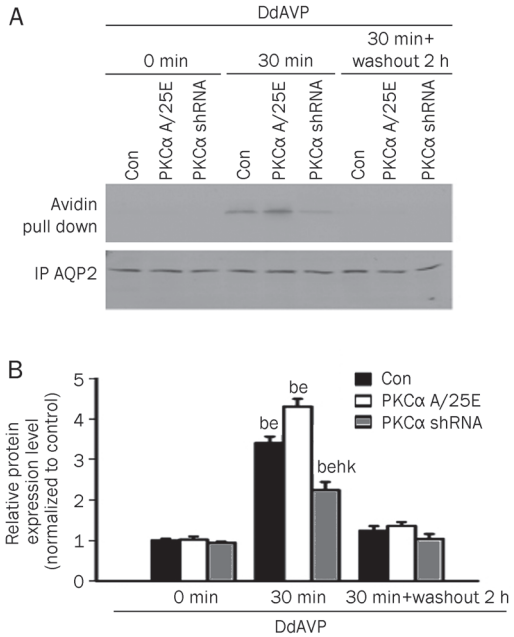

Figure 4. Regulation of PKCα expression influenced DdAVP stimulated plasma location of AQP2. (A) AQP2-GFP stably expressed WT7 cells were transfected with indicated constructs. Forty-eight hours after transfection, surface membrane proteins were biotinylated at 0 min, DdAVP treated 30 min, and DdAVP treated 30 min followed by 2 h washout. Whole cell lysates were subjected to avidin pulldown assay using streptavidin-agarose beads or immunoprecipitation (IP) using anti-AQP2 antibodies. The recovered proteins were separated by SDS-PAGE and analyzed by Western blot for AQP2 as described in Materials and Methods. For each condition, the detected signals from avidin-pulldown assay and AQP2 immunoprecipitation were from same SDS-PAGE gel. (B) Signals from 3 independent experiments were quantified by densitometry. The intensity of the AQP2 signals from the avidin pulldowns were normalized to the corresponding AQP2 IP signals under each condition. Data were represented as mean±SEM. $^{b}P<0.05$ *vs* DdAVP 0 min group. $^{e}P<0.05$ vs DdAVP 30 min+2 h washout group. $^{h}P<0.05$ *vs* DdAVP 30 min con group. $^{k}P<0.05$ *vs* DdAVP 30 min PKCα A/25E group.

AQP2 as determined by AQP2 immunoprecipitation (Figure 4). These results were consistent with the AQP2 translocation observed by immunofluorescence detection and demonstrated that PKCα participated in DdAVP-mediated AQP2 translocation in mIMCD cells.

Discussion

PKCα exhibits different expression patterns in mouse and rat kidneys. For example, PKCα localizes in the proximal tubule of mice but not rats[3, 4]. Our previous study demonstrated that PKCα contributes to urine concentration in the mouse kidney[5]. The use of cell lines that originate from mouse IMCD cells is reasonable because AQP2 is primarily expressed in collecting duct principal cells, and the effect of PKCα on urine concentrating occurs in the inner medulla. In the present study, AQP2 trafficking was examined in an mIMCD3 cell line that was derived from mouse IMCD and exhibited the properties of IMCD cells. However, immortalized mIMCD3 cells

lack AQP2 expression[30], and AQP2 is only briefly expressed in primary cultured IMCD cells[31]. Therefore, we generated AQP2-mIMCD3 stable cell lines for the following experiments. Our results demonstrated that AQP2 was located in intracellular vesicles in non-stimulated mIMCD3 cells. DdAVP treatment induced the translocation of AQP2 from the cytoplasm to the plasma membrane, and DdAVP washout reversed AQP2 localization from the plasma membrane to the cytoplasm (Figure 4). Therefore, AQP2-mIMCD3 cells provide an optimal cell model to investigate AQP2 trafficking.

AQP2 phosphorylation at serine 256 by PKA plays an important role in AQP2 trafficking[32, 33]. However, the phosphorylation of AQP2 at serine 256 is not sufficient to maintain the presence of the water channel at the plasma membrane[34], and the PKC-induced internalization of AQP2 in collecting duct cells does not depend on the phosphorylation state of AQP2[35, 36]. Our study demonstrated that DdAVP increased AQP2 phosphorylation, and the inhibition of PKCα expression did not influence DdAVP-mediated AQP2 phosphorylation at serine 256, which is consistent with previous reports. These results strongly suggest that AQP2 phosphorylation at serine 256 is PKCα independent. However, the ability of PKCα to phosphorylate AQP2 at other phosphorylation sites, such as serine 231, remains unclear. Our results indicated that PKCα did not interact with AQP2 *in vitro*. Therefore, the ability of PKCα to mediate the trafficking of phosphorylated AQP2 requires further investigation.

The disruption of microtubules induces AQP2 translocation to the plasma membrane[13, 23, 29], and PKCα is involved in cytoskeletal remodeling during cell motility, phagocytosis, neurite outgrowth and the regulation of cytoskeleton-associated proteins[37–40]. Therefore, the impact of PKCα on the cytoskeleton in AQP2-mIMCD3 cells was investigated. Microtubules are part of the cytoskeleton and consist of α, β, and γ tubulins[41]. α-Tubulin is the major cytoskeletal protein related to cell trafficking. The role of PKCα in the assembly of α-tubulin was determined. PKCα overexpression or inhibition produced a constitutively active form of PKCα or down-regulated expression of PKCα, respectively, which resulted in the de- and re-polymerization of α-tubulin, respectively. Moreover, PKCα down-regulation prevented DdAVP-mediated α-tubulin depolymerization. These data indicated that PKCα is involved in the assembly of α-tubulin in AQP2-mIMCD3 cells, which is consistent with previous reports[9].

The microtubule-dependent transport of AQP2 is predominantly responsible for AQP2 trafficking and localization inside of the cell after its internalization, but it is not responsible for the exocytic transport of the water channel[25]. In the present study, the overexpression of constitutively active PKCα produced a wide distribution of AQP2 throughout the cytoplasm, which is in contrast to its translocation to the plasma membrane. This result indicates that other factors/proteins rather than α-tubulin are required for AQP2 translocation to the plasma membrane[40]. Furthermore, the consistent inhibition of α-tubulin depolymerization by the down-regulation of PKCα expression produced a loss in DdAVP-mediated AQP2 translocation. This result confirms that α-tubulin is a key element for the proper localization of AQP2 in the cytoplasmic compartment.

In summary, the use of stably expressing AQP2-mIMCD3 cells demonstrated that PKCα did not functionally associate with AQP2. The down-regulation of PKCα expression altered the distribution of α-tubulin and inhibited DdAVP-mediated AQP2 trafficking. However, constitutively activated PKCα rescued or aggravated these changes. These data directly demonstrated that PKCα mediates AQP2 trafficking by influencing the assembly of α-tubulin and underscore the complexity of the molecular events of PKCα-mediated urine concentration.

Acknowledgements

This work was supported by the National Natural Science Foundation of China (No 30871173).

Author contribution

Dr Li-jun YAO designed the research and wrote the paper; Dr Hong ZHAO performed biotinlyation of cell surface protein experiment; Xi YAO performed Western blot and immunocytochemistry experiment; Tao-xia WANG prepared plasmids and analysed data; Wen-min JIN performed cell culture experiment; Qian-qian JI contributed reagents preparation; Dr Xiao YANG wrote the paper; Dr Qiu-hong DUAN performed the research.

References

1 Mellor H, Parker PJ. The extended protein kinase C superfamily. Biochem J 1998; 332: 281–92.
2 Ostlund E, Mendez CF, Jacobsson G, Fryckstedt J, Meister B, Aperia A. Expression of protein kinase C isoforms in renal tissue. Kidney Int 1995; 47: 766–73.
3 Pfaff IL, Wagner HJ, Vallon V. Immunolocalization of protein kinase C isoenzymes alpha, beta1 and betaII in rat kidney. J Am Soc Nephrol 1999; 10: 1861–73.
4 Redling S, Pfaff IL, Leitges M, Vallon V. Immunolocalization of protein kinase C isoenzymes alpha, beta I, beta II, delta, and epsilon in mouse kidney. Am J Physiol Renal Physiol 2004; 287: F289–F298.
5 Yao L, Huang DY, Pfaff IL, Nie X, Leitges M, Vallon V. Evidence for a role of protein kinase C-alpha in urine concentration. Am J Physiol Renal Physiol 2004; 287: F299–304.
6 Yao LJ, Leitges M, Vallon V. Mice lacking protein kinase C beta present modest increases in systolic blood pressure and NH_4Cl-induced metabolic acidosis. Kidney Blood Press Res 2006; 29: 36–42.
7 Kim JH, Lee-Kwon W, Park JB, Ryu SH, Yun CH, Donowitz M. Ca^{2+}-dependent inhibition of Na^+/H^+ exchanger 3 (NHE3) requires an NHE3-E3KARP-alpha-actinin-4 complex for oligomerization and endocytosis. J Biol Chem 2002; 277: 23714–24.
8 Qualmann B, Kessels MM, Kelly RB. Molecular links between endocytosis and the actin cytoskeleton. J Cell Biol 2000; 150: F111–F116.
9 Hryciw DH, Pollock CA, Poronnik P. PKC-alpha-mediated remodeling of the actin cytoskeleton is involved in constitutive albumin uptake by proximal tubule cells. Am J Physiol Renal Physiol 2005; 288: F1227–F1235.
10 Fushimi K, Uchida S, Hara Y, Hirata Y, Marumo F, Sasaki S. Cloning

and expression of apical membrane water channel of rat kidney collecting tubule. Nature 1993; 361: 549–52.
11 Nielsen S, DiGiovanni SR, Christensen EI, Knepper MA, Harris HW. Cellular and subcellular immunolocalization of vasopressin-regulated water channel in rat kidney. Proc Natl Acad Sci U S A 1993; 90: 11663–7.
12 Takata K, Matsuzaki T, Tajika Y. Aquaporins: water channel proteins of the cell membrane. Prog Histochem Cytochem 2004; 39: 1–83.
13 Tajika Y, Matsuzaki T, Suzuki T, Ablimit A, Aoki T, Hagiwara H, *et al*. Differential regulation of AQP2 trafficking in endosomes by microtubules and actin filaments. Histochem Cell Biol 2005; 124: 1.
14 Rojek A, Fuchtbauer EM, Kwon TH, Frokiaer J, Nielsen S. Severe urinary concentrating defect in renal collecting duct-selective AQP2 conditional-knockout mice. Proc Natl Acad Sci U S A 2006; 103: 6037–42.
15 Takata K, Matsuzaki T, Tajika Y, Ablimit A, Hasegawa T. Localization and trafficking of aquaporin 2 in the kidney. Histochem Cell Biol 2008; 130: 197–209.
16 Nielsen S, Chou CL, Marples D, Christensen EI, Kishore BK, Knepper MA. Vasopressin increases water permeability of kidney collecting duct by inducing translocation of aquaporin-CD water channels to plasma membrane. Proc Natl Acad Sci U S A 1995; 92: 1013–7.
17 Yamamoto T, Sasaki S, Fushimi K, Ishibashi K, Yaoita E, Kawasaki K, *et al*. Vasopressin increases AQP-CD water channel in apical membrane of collecting duct cells in Brattleboro rats. Am J Physiol 1995; 268: C1546–C1551.
18 Boone M, Deen PM. Physiology and pathophysiology of the vasopressin-regulated renal water reabsorption. Pflugers Arch 2008; 456: 1005–24.
19 Hozawa S, Holtzman EJ, Ausiello DA. cAMP motifs regulating transcription in the aquaporin 2 gene. Am J Physiol 1996; 270: C1695–C1702.
20 Matsumura Y, Uchida S, Rai T, Sasaki S, Marumo F. Transcriptional regulation of aquaporin-2 water channel gene by cAMP. J Am Soc Nephrol 1997; 8: 861–7.
21 Hasler U, Leroy V, Martin PY, Feraille E. Aquaporin-2 abundance in the renal collecting duct: new insights from cultured cell models. Am J Physiol Renal Physiol 2009; 297: F10–F18.
22 Li C, Wang W, Rivard CJ, Lanaspa MA, Summer S, Schrier RW. Molecular mechanisms of angiotensin II stimulation on aquaporin-2 expression and trafficking. Am J Physiol Renal Physiol 2011; 300: F1255–F1261.
23 Noda Y, Horikawa S, Kanda E, Yamashita M, Meng H, Eto K, *et al*. Reciprocal interaction with G-actin and tropomyosin is essential for aquaporin-2 trafficking. J Cell Biol 2008; 182: 587–601.
24 Takata K. Aquaporin-2 (AQP2): its intracellular compartment and trafficking. Cell Mol Biol 2006; 52: 34–9.
25 Vossenkamper A, Nedvetsky PI, Wiesner B, Furkert J, Rosenthal W, Klussmann E. Microtubules are needed for the perinuclear positioning of aquaporin-2 after its endocytic retrieval in renal principal cells. Am J Physiol Cell Physiol 2007; 293: C1129–C1138.
26 Baier-Bitterlich G, Uberall F, Bauer B, Fresser F, Wachter H, Grunicke H, *et al*. Protein kinase C-theta isoenzyme selective stimulation of the transcription factor complex AP-1 in T lymphocytes. Mol Cell Biol 1996; 16: 1842–50.
27 Goel M, Zuo CD, Schilling WP. Role of cAMP/PKA signaling cascade in vasopressin-induced trafficking of TRPC3 channels in principal cells of the collecting duct. Am J Physiol Renal Physiol 2010; 298: F988–F996.
28 Hays RM, Condeelis J, Gao Y, Simon H, Ding G, Franki N. The effect of vasopressin on the cytoskeleton of the epithelial cell. Pediatr Nephrol 1993; 7: 672–9.
29 Nedvetsky PI, Tamma G, Beulshausen S, Valenti G, Rosenthal W, Klussmann E. Regulation of aquaporin-2 trafficking. Handb Exp Pharmacol 2009, 190: 133–57.
30 Umenishi F, Narikiyo T, Schrier RW. Effect on stability, degradation, expression, and targeting of aquaporin-2 water channel by hyperosmolality in renal epithelial cells. Biochem Biophys Res Commun 2005; 338: 1593–9.
31 Maric K, Oksche A, Rosenthal W. Aquaporin-2 expression in primary cultured rat inner medullary collecting duct cells. Am J Physiol 1998; 275: F796–801.
32 Katsura T, Gustafson CE, Ausiello DA, Brown D. Protein kinase A phosphorylation is involved in regulated exocytosis of aquaporin-2 in transfected LLC-PK1 cells. Am J Physiol 1997; 272: F817–F822.
33 Christensen BM, Zelenina M, Aperia A, Nielsen S. Localization and regulation of PKA-phosphorylated AQP2 in response to V(2)-receptor agonist/antagonist treatment. Am J Physiol Renal Physiol 2000; 278: F29–F42.
34 Nejsum LN, Zelenina M, Aperia A, Frokiaer J, Nielsen S. Bidirectional regulation of AQP2 trafficking and recycling: involvement of AQP2-S256 phosphorylation. Am J Physiol Renal Physiol 2005; 288: F930–F938
35 Van Balkom BW, Savelkoul PJ, Markovich D, Hofman E, Nielsen S, van der Sluijs P, *et al*. The role of putative phosphorylation sites in the targeting and shuttling of the aquaporin-2 water channel. J Biol Chem 2002; 277: 41473–9.
36 Kamsteeg EJ, Hendriks G, Boone M, Konings IB, Oorschot V, van der Sluijs P, *et al*. Short-chain ubiquitination mediates the regulated endocytosis of the aquaporin-2 water channel. Proc Natl Acad Sci U S A 2006; 103: 18344–9.
37 Holm A, Tejle K, Gunnarsson T, Magnusson KE, Descoteaux A, Rasmusson B. Role of protein kinase C alpha for uptake of unopsonized prey and phagosomal maturation in macrophages. Biochem Biophys Res Commun 2003; 302: 653–8.
38 Beaudry H, Gendron L, Guimond MO, Payet MD, Gallo-Payet N. Involvement of protein kinase C alpha (PKC alpha) in the early action of angiotensin II type 2 (AT2) effects on neurite outgrowth in NG108-15 cells: AT2-receptor inhibits PKC alpha and p21ras activity. Endocrinology 2006; 147: 4263–72.
39 Belin RJ, Sumandea MP, Allen EJ, Schoenfelt K, Wang H, Solaro RJ, *et al*. Augmented protein kinase C-alpha-induced myofilament protein phosphorylation contributes to myofilament dysfunction in experimental congestive heart failure. Circ Res 2007; 101: 195–204.
40 Abeyweera TP, Chen X, Rotenberg SA. Phosphorylation of alpha6-tubulin by protein kinase Calpha activates motility of human breast cells. J Biol Chem 2009; 284: 17648–56.
41 Nogales E, Wolf SG, Downing KH. Structure of the alpha beta tubulin dimer by electron crystallography. Nature 1998; 391: 199–203.

Acta Pharmacologica Sinica (2012) 33: 237–241
 1671-4083/12 $32.00
www.nature.com/aps

Original Article

Glucagon-like peptide 1 receptor plays a critical role in geniposide-regulated insulin secretion in INS-1 cells

Li-xia GUO[1, 2], Zhi-ning XIA[1, *], Xue GAO[2], Fei YIN[2], Jian-hui LIU[2, *]

[1]College of Bioengineering, Chongqing University, Chongqing 400030, China; [2]Research Centre of Medicinal Chemistry and Chemical Biology, Chongqing Technology and Business University, Chongqing 400067, China

Aim: To explore the role of the glucagon-like peptide 1 receptor (GLP-1R) in geniposide regulated insulin secretion in rat INS-1 insulinoma cells.
Methods: Rat INS-1 insulinoma cells were cultured. The content of insulin in the culture medium was measured with ELISA assay. GLP-1R gene in INS-1 cells was knocked down with shRNA interference. The level of GLP-1R protein in INS-1 cells was measured with Western blotting.
Results: Geniposide (0.01–100 μmol/L) increased insulin secretion from INS-1 cells in a concentration-dependent manner. Geniposide (10 μmol/L) enhanced acute insulin secretion in response to both the low (5.5 mmol/L) and moderately high levels (11 mmol/L) of glucose. Blockade of GLP-1R with the GLP-1R antagonist exendin (9–39) (200 nmol/L) or knock-down of GLP-1R with shRNA interference in INS-1 cells decreased the effect of geniposide (10 μmol/L) on insulin secretion stimulated by glucose (5.5 mmol/L).
Conclusion: Geniposide increases insulin secretion through glucagon-like peptide 1 receptors in rat INS-1 insulinoma cells.

Keywords: geniposide; glucagon-like peptide 1 receptor; insulin secretion; type 2 diabetes mellitus; RNA interference

Acta Pharmacologica Sinica (2012) 33: 237–241; doi: 10.1038/aps.2011.146; published online 21 Nov 2011

Introduction

Type 2 diabetes mellitus involves defects in both insulin secretion and insulin sensitivity. Multiple insulin secretion defects could occur, including the absence of pulsatility[1], loss of the early phase of insulin secretion after glucose stimulation[2], decreased basal and stimulated concentrations of insulin in the plasma[3], excess secretion of pro-hormone, and progressive decreases in insulin secretory capacity[4]. Thus, the regulation of insulin secretion in pancreatic β cells has long been considered important for the prevention and treatment of type 2 diabetes mellitus[4].

Emerging data have shown that GLP-1 functions through its receptor to regulate insulin secretion and glucose metabolism and is, therefore, a potentially important target in the treatment of type 2 diabetes. GLP-1 is able to improve insulin secretion in subjects with impaired glucose tolerance and type 2 diabetes[5]. Studies have demonstrated that increased expression or activity of GLP-1R is beneficial to β cell functions, including insulin synthesis/secretion[6], proliferation[7], neogenesis[7], and anti-apoptosis[8]. Unfortunately, GLP-1 has a half-life of less than 2 minutes in the circulatory system owing to rapid degradation by dipeptidyl peptidase-4 (DPP IV)[9].

Utilizing a high-throughput screening assay, we previously identified geniposide as a potent agonist of GLP-1R and possessed neurotrophic and neuroprotective properties[10–12]. However, it is unknown whether geniposide is able to improve insulin secretion in pancreatic β cells. In the present study we examined the effect of geniposide on insulin secretion in INS-1 cells. The results demonstrate that geniposide increased insulin secretion in a dose-dependent manner and enhanced glucose-stimulated insulin secretion in INS-1 cells. We have further observed that exendin (9–39), an antagonist of GLP-1R, and GLP-1R siRNA decreased the effect of geniposide on glucose-stimulated insulin secretion in INS-1 cells.

Materials and methods

Cell culture

An INS-1 rat insulinoma cell line was purchased from the CCTCC (China Center for Type Culture Collection). The cells

* To whom correspondence should be addressed.
E-mail znxia@cqu.edu.cn (Zhi-ning XIA);
jhliu@ctbu.edu.cn (Jian-hui LIU)
Received 2011-05-25 Accepted 2011-09-30

were grown in a humidified atmosphere with 5% CO_2 at 37 °C. The culture medium was RPMI-1640 containing 11 mmol/L glucose, which was supplemented with 10% FBS, 10 mmol/L HEPES, 100 U/mL penicillin, 100 μg/mL streptomycin, 2 mmol/L *L*-glutamine, 1 mmol/L sodium pyruvate, and 50 μmol/L mercaptoethanol. Cells were passaged every week following trypsinization.

Geniposide induces insulin secretion in a concentration-dependent manner

To investigate the effect of geniposide on insulin secretion, INS-1 cells were seeded onto 12-well plates and cultured for 24 h. The cells were washed twice with Krebs-Ringer bicarbonate buffer (KRBH; 129 mmol/L NaCl, 4.8 mmol/L KCl, 1.2 mmol/L $MgSO_4$, 1.2 mmol/L KH_2PO_4, 2.5 mmol/L $CaCl_2$, 5 mmol/L $NaHCO_3$, 0.1% BSA, 10 mmol/L HEPES; pH 7.4) and starved for 2 h in KRBH buffer. Then, the cells were incubated with fresh KRBH containing different concentrations of geniposide (0, 0.01, 0.1, 1.0, 10, or 100 μmol/L) for 1 h. The supernatants were collected to determine the insulin content using commercial kit (Linco Research, Inc, Missouri, USA) according to the kit' instructions.

Effect of geniposide on insulin secretion stimulated by glucose

To explore the influence of geniposide on glucose-stimulated insulin secretion, INS-1 cells were seeded onto 12-well plates and cultured for 24 h. After the cells were washed two times with fresh KRBH and starved for 2 h in fresh KRBH, the cells were incubated with 10 μmol/L geniposide in the absence or presence of indicated concentrations of glucose for 1 h. The supernatants were collected and analyzed for insulin concentration using commercial kit (Linco Research, Inc, Missouri, USA) according to the kit' instructions.

The role of GLP-1R in geniposide-inducing insulin secretion

To probe the role of GLP-1R, we investigated the effect of an antagonist for GLP-1R on insulin secretion in the presence of a low concentration of glucose. INS-1 cells were starved for 2 h in fresh KRBH, placed for 1 h in fresh KRBH containing 200 nmol/L exendin (9–39), and then treated for 1 h with 5.5 mmol/L glucose in the presence or absence of 10 μmol/L geniposide. The supernatants were collected to probe the insulin concentration using commercial kits.

To further explore the role of GLP-1R in the regulatory effects of geniposide on insulin secretion, we constructed a stable INS-1 cell line with the GLP-1R silenced by a shGLP-1R plasmid, which was optimized in our previous work[11]. The level of GLP-1R expression was analyzed with Western blot and real-time PCR. The primers were 5′-TATTGGCTCATCATACGCTTG-3′ (GLP-1R sense), 5′-GTCTGCATTTGATGTCGGTCT-3′ (GLP-1R antisense), 5′-AAGTTCAACGGCACAGTCAAG-3′ (GAPDH sense) and 5′-CCAGTAGACTCCACGACATACTCA-3′ (GAPDH antisense). The mRNA and protein levels of GLP-1R are about 35.4% and 21% those of the control, respectively. Using the same protocol as introduced in Materials and Methods, we determined the insulin secretion induced by geniposide in INS-1 cells in which GLP-1R had been knocked down.

Statistical analysis

Data are expressed as the means±SD from at least three independent experiments. When significance was detected, the differences between the treatments were analyzed using a one-way ANOVA with the Origin 8.0 Pair-Sample *t*-Test. The significance level was set at $P<0.05$.

Results

Geniposide regulates insulin secretion in INS-1 cells

As shown in Figure 1, geniposide elicited concentration-dependent increases in insulin secretion in β cells. Similar to GLP-1, geniposide also increased acute insulin secretion in response to both low and moderately high glucose levels (Figure 2).

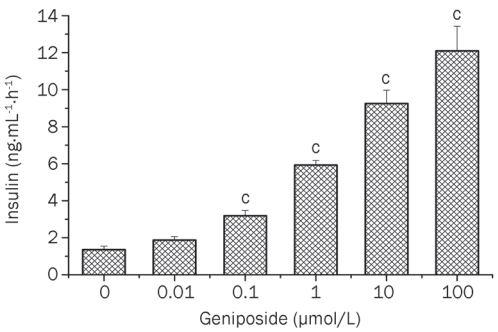

Figure 1. Geniposide induces insulin secretion in a concentration-dependent manner in INS-1 cells. The INS-1 cells at passages of 68–73 were seeded at 5×10^5 cells/well in 12-well-plates. The next day, the cells were washed twice with KRBH buffer and starved in KRBH buffer for 2 h. The media was changed with fresh KRBH containing different concentrations of geniposide (0, 0.01, 0.1, 1.0, 10, or 100 μmol/L). Following 1-h incubation, the medium was collected and analyzed for insulin concentration. Data are expressed as means±SD from 4 independent experiments. $^cP<0.01$ *vs* control by one-way ANOVA followed by the Pair-Sample *t*-Test using Origin 8.0 software.

In normoglycemic subjects, glucose-stimulated insulin secretion is characterized by a biphasic pattern, with the peak of the first phase rising abruptly 3–5 min after glucose stimulation and lasting for about 10 min[4]. To determine whether geniposide induces changes in both phases of insulin secretion, we tested the influence of geniposide on biphasic insulin secretion in INS-1 cells in the absence or presence of low glucose levels. It was observed that geniposide enhanced insulin secretion in both phases when glucose was present (Figure 3).

GLP-1R plays an important role in geniposide-induced insulin secretion in INS-1 cells.

Our previous work showed that geniposide was an agonist of GLP-1R[10–12]. To investigate the role of GLP-1R in glucose-stimulated insulin secretion, we determined the effect of

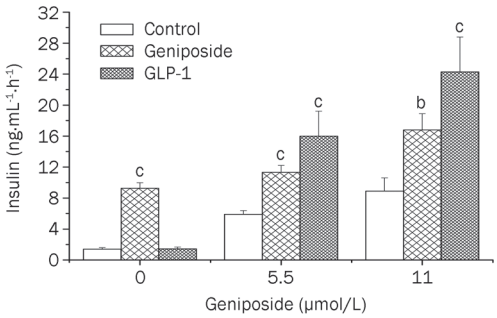

Figure 2. Geniposide potentiates glucose-stimulated insulin secretion in INS-1 cells. INS-1 cells were seeded in 12-well-plates and continued to incubate for 24 h; the cells were washed twice with fresh KRBH and starved in KRBH buffer for 2 h. The media was changed with fresh KRBH containing different concentrations of glucose (0, 5.5, or 11 mmol/L) with or without 10 μmol/L geniposide or GLP-1 (330 nmol/L). Following 1-h incubation, the medium was collected and analyzed for insulin concentration. Data are expressed as means±SD from 6 independent experiments. $^{b}P<0.05$, $^{c}P<0.01$ *vs* control at the same glucose concentration by one-way ANOVA followed by the Pair-Sample *t*-Test using Origin 8.0 software.

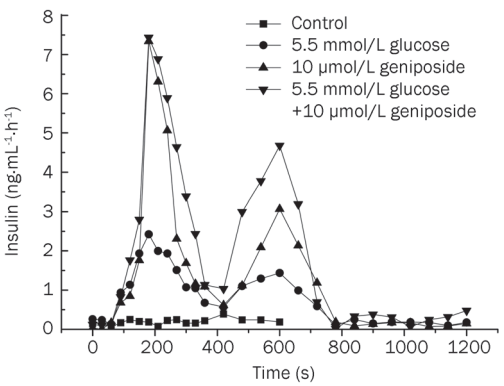

Figure 3. Effects of geniposide on the biphasic glucose-stimulated insulin secretion in INS-1 cells. INS-1 cells were treated with 10 μmol/L geniposide in the presence or absence of 5.5 mmol/L glucose (G5.5) for 20 min. The media were collected in a 30-s intermediate to determine the insulin secretion with ELISA. Data are expressed as mean of two independent experiments.

geniposide on insulin secretion in the presence or absence of a GLP-1R antagonist, exendin (9–39) amide. The data demonstrate that pretreatment with 200 nmol/L exendin (9–39) for 1 h prevented the geniposide-induced increase in insulin secretion in INS-1 cells (Figure 4A).

We also checked the effect of GLP-1R interference on geniposide-induced insulin secretion in INS-1 cells. The results showed that, in INS-1 cells in which GLP-1R had been knocked down, the level of insulin secretion induced by 5.5 mmol/L glucose did not differ from that of the control cells. These results suggest that glucose-stimulated insulin secretion is not dependent upon GLP-1R. However, in contrast to normal cultured INS-1 cells, geniposide failed to enhance glucose

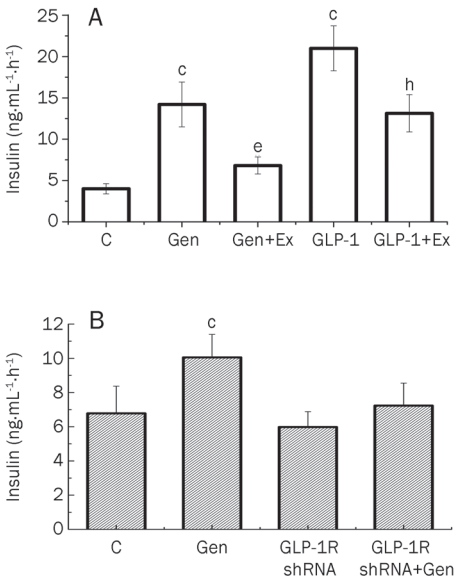

Figure 4. GLP-1R plays a critical role in geniposide-induced insulin secretion in INS-1 cells. (A) After the attached INS-1 cells were washed twice and starved for 2 h, the media was changed with KRBH buffer containing 5.5 mmol/L glucose, and INS-1 cells were treated with geniposide (10 μmol/L) or GLP-1 (330 nmol/L) in the presence or absence of GLP-1 receptor antagonist, exendin (9–39) (Ex, 200 nmol/L) for 1 h. (B) GLP-1R-interferred INS-1 cells and control cells were treated with 5.5 mmol/L glucose for 1 h in the presence or absence of 10 μmol/L geniposide, respectively. The media were collected to determine the level of insulin secretion. Data are expressed as means±SD from 6 independent experiments. $^{c}P<0.01$ *vs* control. $^{e}P<0.05$ *vs* geniposide group; $^{h}P<0.05$ *vs* GLP-1 group by one-way ANOVA followed by the Pair-Sample *t*-Test using Origin 8.0 software.

stimulated insulin secretion in GLP-1R- knockdown INS-1 cells (Figure 4B). Taken together with the effect of exendin (9–39) on geniposide regulation of glucose-stimulated insulin secretion, these results indicate that GLP-1R plays an important role in geniposide regulation of insulin secretion in INS-1 cells.

Discussion

Type 2 diabetes mellitus is a metabolic disorder that manifests mainly as abnormalities in pancreatic insulin secretion and the peripheral actions of insulin. During the progression of diabetes, the mass of β cells is reduced, with a concomitant decrease in the amount of insulin secreted. An effective therapeutic option is to use drugs to boost the production and release of insulin by pancreatic islets. For example, sulfonylurea-based drugs that act on the β-cell secretory apparatus augment the release of insulin, overcoming peripheral insulin resistance and restoring normoglycemia in type 2 diabetic patients. Nonetheless, treatment with sulfonylureas is associated with side-effects, such as non-optimal normoglycemic control, which triggers protracted hypoglycemic episodes, worsens myocardial function, and potentially causes weight gain[13, 14].

Alternatively, natural hypoglycemic compounds may offer

advantages over the drugs currently used for diabetes. For example, plant-derived iridoids, of which many are dietary constituents, may serve as promising candidates for the development of therapeutics to prevent or treat diabetes. Jin *et al* reported that aucubin lowers blood glucose and protects the pancreas from oxidative stress in streptozotocin-induced diabetes. Thus, aucubin might have potential as a safe preventive agent against diabetes[15]. In the present study, we examined the effect of geniposide, one of the main iridoid glucoside of *Gardenia fruit*, on insulin secretion and GLP-1R. We found, for the first time, that geniposide induces insulin secretion in β-cells in a dose-dependent manner and that geniposide has a synergistic effect on insulin secretion in INS-1 cells in the presence of low and moderately high doses of glucose. We also observed that geniposide directly induced insulin secretion in INS-1 cells in the absence of glucose. These results may be a consequence of the activation of GLP-1R by geniposide, which regulates the concentration of Ca^{2+} through a signal pathway, or changes in the energy balance of INS-1 cells, which alters the ATP ratio and further regulates the activity of ATP-sensitive K^+ channels.

GLP-1 is an incretin, which is released in response to carbohydrate and fat intake and enhances glucose-stimulated insulin secretion[16]. An increasing number of studies have demonstrated the benefits of GLP-1 for increasing pancreatic β cell mass and function. Because GLP-1 exerts its beneficial effects through binding and activating its receptor, GLP-1R is a valuable target for the treatment of diabetes[17]. However, GLP-1 has an extremely short half-life owing to rapid degradation by DPP IV, which limits the therapeutic value of exogenous GLP-1[9]. Therefore, it is important to develop small molecules that are able to activate GLP-1R. The ability of geniposide to activate GLP-1R has previously been demonstrated in neurons[10, 12]. However, the effects of this compound on the regulation of insulin secretion and GLP-1R are poorly understood. It is conceivable that GLP-1R agonists can play a role as anti-diabetic agents and as tools for researching islet metabolism. Nevertheless, our findings about the action of geniposide on β-cell insulin secretion warrant investigation into the molecular mechanisms involved. Moreover, we also observed that both exendin (9–39) and GLP-1R siRNA off-set the effect of geniposide on insulin secretion, suggesting that GLP-1R plays a critical role in the geniposide-induced increase in insulin secretion by INS-1 cells.

Additionally, the observed increase in glucose-stimulated insulin secretion in INS-1 cells following incubation with geniposide was especially evident during the first-phase of insulin secretion. In type 2 diabetes mellitus, the first-phase of insulin secretion is abolished and late phase secretion is reduced and delayed[18]. The early phase of insulin secretion is pivotal in the transition from the fasting state to the fed state with a different function[19]. A reduction in the first-phase of insulin secretion has been found both in patients with overt type 2 diabetes mellitus and at the early stage of disease development, which involves impaired glucose tolerance and a slightly elevated fasting glucose[20]. The effect of geniposide on insulin secretion through activation of GLP-1R suggests that geniposide may be a potential therapeutic agent for the prevention or treatment of type 2 diabetes.

Acknowledgements

This work was supported by grants from the National Natural Science Foundation of China (30973576), the Key Project of the Chinese Ministry of Education (209098), the Chongqing Science & Technology committee (CSTC, 2009BA5069, 2009BB5373, 2011jjA1396), the Chongqing Municipal Education Committee (KJ090710; KJ090733) and the Innovative Research Team Development Program at the University of Chongqing (No KJTD201020). The authors are grateful to Prof Yan-wen WANG from the Institute for Nutrisciences and Health, and the National Research Council of Canada for providing suggestions and corrections during the preparation of this manuscript.

Author contribution

Jian-hui LIU and Zhi-ning XIA designed the research; Li-xia GUO, Zhi-ning XIA, Xue GAO, Fei YIN, and Jian-hui LIU performed the research; and Jian-hui LIU and Li-xia GUO analyzed the data and wrote the paper.

References

1 Bergsten P. Pathophysiology of impaired pulsatile insulin release. Diabetes Metab Res Rev 2000; 16: 179–91.
2 Kano Y, Kanatsuna T, Nakamura N, Kitagawa Y, Mori H, Kajiyama S, *et al*. Defect of the first-phase insulin secretion to glucose stimulation in the perfused pancreas of the nonobese diabetic (NOD) mouse. Diabetes 1986; 35: 486–90.
3 Hartter E, Svoboda T, Ludvik B, Schuller M, Lell B, Kuenburg E, *et al*. Basal and stimulated plasma levels of pancreatic amylin indicate its co-secretion with insulin in humans. Diabetologia 1991; 34: 52–4.
4 Guillausseau PJ, Meas T, Virally M, Laloi-Michelin M, Medeau V, Kevorkian JP. Abnormalities in insulin secretion in type 2 diabetes mellitus. Diabetes Metab 2008; 34 Suppl 2: S43–8.
5 Arulmozhi DK, Portha B. GLP-1 based therapy for type 2 diabetes. Eur J Pharm Sci 2006; 28: 96–108.
6 Kielgast U, Holst J, Madsbad S. Treatment of type 1 diabetic patients with glucagon-like peptide-1 (GLP-1) and GLP-1R agonists. Curr Diabetes Rev 2009; 5: 266–75.
7 Egan JM, Bulotta A, Hui H, Perfetti R. GLP-1 receptor agonists are growth and differentiation factors for pancreatic islet beta cells. Diabetes Metab Res Rev 2003; 19: 115–23.
8 Cornu M, Thorens B. GLP-1 protects beta-cells against apoptosis by enhancing the activity of an IGF-2/IGF1-receptor autocrine loop. Islets 2009; 1: 280–2.
9 Ahren B, Winzell MS, Wierup N, Sundler F, Burkey B, Hughes TE. DPP-4 inhibition improves glucose tolerance and increases insulin and GLP-1 responses to gastric glucose in association with normalized islet topography in mice with beta-cell-specific overexpression of human islet amyloid polypeptide. Regul Pept 2007; 143: 97–103.
10 Liu JH, Zheng XX, Yin F, Hu YH, Guo LX, Deng X, *et al*. Neurotrophic property of geniposide for inducing the neuronal differentiation of PC12 cells. Int J Dev Neurosci 2006; 24: 419–24.
11 Yin F, Liu JH, Zheng XX, Guo LX. GLP-1 receptor plays a critical role in geniposide-induced expression of heme oxygenase-1 in PC12 cells. Acta Pharmacol Sin 2010; 31: 540–5.

12 Liu JH, Yin F, Zheng XX, Jing JJ, Hu YH. Geniposide, a novel agonist for GLP-1 receptor, prevents PC12 cells from oxidative damage via MAP kinase pathway. Neurochem Int 2007; 51: 361–9.
13 Martin S, Kolb H, Beuth J, van Leendert R, Schneider B, Scherbaum WA. Change in patients' body weight after 12 months of treatment with glimepiride or glibenclamide in type 2 diabetes: a multicentre retrospective cohort study. Diabetologia 2003; 46: 1611–7.
14 Jennings AM, Wilson RM, Ward JD. Symptomatic hypoglycemia in NIDDM patients treated with oral hypoglycemic agents. Diabetes Care 1989; 12: 203–8.
15 Jin L, Xue HY, Jin LJ, Li SY, Xu YP. Antioxidant and pancreas-protective effect of aucubin on rats with streptozotocin-induced diabetes. Eur J Pharmacol 2008; 582: 162–7.
16 Marguet D, Baggio L, Kobayashi T, Bernard AM, Pierres M, Nielsen PF, *et al*. Enhanced insulin secretion and improved glucose tolerance in mice lacking CD26. Proc Natl Acad Sci U S A 2000; 97: 6874–9.
17 Verspohl EJ. Novel therapeutics for type 2 diabetes: incretin hormone mimetics (glucagon-like peptide-1 receptor agonists) and dipeptidyl peptidase-4 inhibitors. Pharmacol Ther 2009; 124: 113–38.
18 Davies MJ, Rayman G, Grenfell A, Gray IP, Day JL, Hales CN. Loss of the first phase insulin response to intravenous glucose in subjects with persistent impaired glucose tolerance. Diabet Med 1994; 11: 432–6.
19 Del Prato S, Marchetti P, Bonadonna RC. Phasic insulin release and metabolic regulation in type 2 diabetes. Diabetes 2002; 51: S109–16.
20 Widen EI, Eriksson JG, Ekstrand AV, Groop LC. The relationship between first-phase insulin secretion and glucose metabolism. Acta Endocrinol (Copenh) 1992; 127: 289–93.

Acta Pharmacologica Sinica (2012) 33: 242–249
 1671-4083/12 $32.00
www.nature.com/aps

Original Article

Plumbagin inhibits cell growth and potentiates apoptosis in human gastric cancer cells *in vitro* through the NF-κB signaling pathway

Jing LI[1], Lin SHEN[1, *], Fu-rong LU[1, *], You QIN[2], Rui CHEN[1], Jia LI[3], Yan LI[1], Han-zi ZHAN[5], Yuan-qiao HE[4]

[1]Department of Traditional Chinese Medicine, Union Hospital, Tongji Medical College, Huazhong University of Science and Technology, Wuhan 430022, China; [2]Cancer Center, Union Hospital, Tongji Medical College, Huazhong University of Science and Technology, Wuhan 430022, China; [3]Department of Acupuncture & Moxibustion, Hubei University of Chinese Medicine, Wuhan 430065, China; [4]Department of Laboratory Animal Science, Nanchang University, Nanchang 330031, China; [5]University of Pittsburgh School of Medicine, Pittsburgh, Pennsylvania, USA

Aim: To investigate the effects and underlying mechanisms of plumbagin, a naphthoquinone derived from medicinal plant Plumbago zeylanica, on human gastric cancer (GC) cells.
Methods: Human gastric cancer cell lines SGC-7901, MKN-28, and AGS were used. The cell viability was examined using CCK-8 viability assay. Cell proliferation rate was determined using both clonogenic assay and EdU incorporation assay. Apoptosis was detected via Annexin V/propidium iodide double-labeled flow cytometry. Western blotting was used to assess the expression of both NF-κB-regulated gene products and TNF-α-induced activation of p65, IκBα, and IKK. The intracellular location of NF-κB p65 was detected using confocal microscopy.
Results: Plumbagin (2.5–40 μmol/L) concentration-dependently reduced the viability of the GC cells. The IC_{50} value of plumbagin in SGC-7901, MKN-28, and AGS cells was 19.12, 13.64, and 10.12 μmol/L, respectively. The compound (5–20 μmol/L) concentration-dependently induced apoptosis of SGC-7901 cells, and potentiated the sensitivity of SGC-7901 cells to chemotherapeutic agents TNF-αand cisplatin. The compound (10 μmol/L) downregulated the expression of NF-κB-regulated gene products, including IAP1, XIAP, Bcl-2, Bcl-xL, tumor factor (TF), and VEGF. In addition to inhibition of NF-κB p65 nuclear translocation, the compound also suppressed TNF-α-induced phosphorylation of p65 and IKK, and the degradation of IκBα.
Conclusion: Plumbagin inhibits cell growth and potentiates apoptosis in human GC cells through the NF-κB pathway.

Keywords: plumbagin; anticancer drug; TNF-α; cisplatin; gastric carcinoma; apoptosis; NF-κB

Acta Pharmacologica Sinica (2012) 33: 242–249; doi: 10.1038/aps.2011.152; published online 9 Jan 2012

Introduction

Gastrointestinal cancers comprise a large percentage of malignancies and cancer-related deaths, among which gastric and colorectal cancers are most common[1]. Approximately 700 000 annual deaths make gastric cancer (GC) the second leading cause of mortality in the world[2]. Nearly two-thirds of gastric cancer mortality occurs in developing countries. In China, the death rate is 42%[2]. Despite the rapid progress in surgical techniques and chemotherapies, prognosis for patients with GC is usually poor. Therefore, it is urgent to find an effective therapy against this malignant disease.

Recently, dietary components and phytochemicals were shown to be effective in treating various human diseases[3, 4]. Plumbagin (5-hydroxy-2-methyl-1,4-naphthoquinone) is a quinonoid constituent derived from the roots of the medicinal plant *Plumbago zeylanica*. This plant has been safely used for centuries in traditional ayurvedic and Chinese medicine[5]. Plumbagin has been reported to exhibit anti-microbial properties[6], anti-atherosclerotic effects[7], and anticancer activities both *in vitro* and *in vivo*[5]. Previous findings suggest that plumbagin can inhibit cell proliferation and induce apoptosis in breast carcinomas[8], suppress promotion and metastasis in prostate cancer[5], and induce cell cycle arrest and apoptosis in melanoma cells[9]. The results of these studies have shown that plumbagin has enormous potential as an anticarcinogenic agent. However, the effectiveness of plumbagin in the treatment of GC, as well as its mechanism of action, has not been

* To whom correspondence should be addressed.
E-mail shenlinhb@yahoo.com.cn (Lin SHEN);
furonglulove@163.com (Fu-rong LU)
Received 2011-08-07 Accepted 2011-10-09

investigated.

Although it is clear from previous studies that plumbagin acts as an anticancer agent by inducing apoptosis and halting cell proliferation, how plumbagin mediates these effects is not fully understood. Evidence in the current literature suggests that plumbagin can suppress the activation of nuclear factor-κB (NF-κB) in A549 human lung cancer cells[10]. Plumbagin can also modulate the activation of p65 and IκBα kinase, leading to the activation of apoptosis in several cancer cell lines[11]. Plumbagin may also inhibit the expression of NF-κB-regulated gene products, such as B-cell lymphoma-2 (Bcl-2)[12], Bcl-xL[12], and vascular endothelial growth factor (VEGF)[11]. Therefore, it is possible that plumbagin exerts its anticarcinogenic action by regulating the NF-κB pathway.

NF-κB is a ubiquitous and evolutionarily conserved transcription factor that is activated in a wide variety of tumors[13] and plays a pivotal role in tumorigenesis[13, 14]. The NF-κB proteins, and other proteins associated with the NF-κB pathway, have been linked to cellular transformation, proliferation, apoptosis suppression, and angiogenesis[14]. In GC cells, NF-κB was shown to be constitutively activated[15], and the activation of NF-κB has been touted as a prognostic parameter in gastric carcinoma[16]. Thus, agents that suppress NF-κB activation have great potential to be effective in the prevention and treatment of GC. Two NF-κB-suppressing compounds include paeoniflorin[17] and wogonin[18], which were shown to cause GC cell apoptosis by regulating the activation of NF-κB.

Because plumbagin has been reported to inhibit the activation of NF-κB, and NF-κB plays a pivotal role in gastric carcinoma, we hypothesized that plumbagin may exert its anticarcinogenic effects in human GC cells by blocking the NF-κB pathway.

Materials and methods

Materials

Plumbagin, dimethyl sulfoxide (DMSO), and propidium iodide (PI) were purchased from Sigma-Aldrich (St Louis, MO, USA). Plumbagin was dissolved in DMSO to a concentration of 200 mmol/L and stored in a dark-colored bottle at -20 °C. This stock solution was further diluted in cell culture medium immediately before use. Tumor necrosis factor-α (TNF-α) was purchased from Pepro Tech Inc (Rocky Hill, NJ, USA). The antibodies against Bcl-2, VEGF, tumor factor (TF), β-actin, and Cy3-labeled goat anti-rabbit IgG were obtained from Santa Cruz Biotechnology (Santa Cruz, CA, USA). The IAP1 antibody was provided by Epitomic, Inc (Burlingame, CA, USA). The Anti-Bcl-xL, anti-XIAP, and anti-histone H2B antibodies were purchased from Bioworld Technology (Minneapolis, MN, USA). The antibodies against IκB kinase α (IKKα), NF-κB p65, phospho-p65 (Ser 536), IκBα, phospho-IκBα (Ser 32), goat anti-mouse-HRP conjugate, and goat anti-rabbit-HRP conjugate were purchased from Cell Signaling Technology (Beverly, MA, USA). The penicillin, streptomycin, RPMI-1640 medium, and fetal bovine serum (FBS) were obtained from GIBCO BRL Life Technologies (Grand Island, NY, USA).

Cell culture

Human gastric cancer cell lines, SGC-7901, MKN-28, and AGS, were cultured in RPMI-1640 medium supplemented with 10% FBS, 100 U/mL penicillin, and 100 μg/mL streptomycin. Cells were incubated in a humidified atmosphere of 5% CO_2 at 37 °C.

Cell viability and proliferation assay

Cell viability was assessed using the Cell Counting Kit-8 assay (CCK-8, Dojindo Laboratories, Kumamoto, Japan)[19]. Briefly, GC cells were grown in 96-well plates (10 000 cells/well) overnight without treatment. The cells were then incubated with varying concentrations of plumbagin and collected at several different time points. At the time of collection, 10 μL of kit reagent, WST-8 [2-(2-methoxy-4-nitrophenyl)-3-(4-nitrophenyl)-5-(2,4-disulfonyl)-2*H*-tetrazolium], was added to each well and incubated for 4 h at 37 °C. Thereafter, the optical density (*OD*) was measured at 450 nm using a 96-well multiscanner autoreader (Thermo Electron Corp, Waltham, MA, USA).

The effect of plumbagin on cell proliferation was determined using both a clonogenic assay and an EdU (5-ethynyl-2′-deoxyuridine) incorporation assay. Briefly, SGC-7901 cells were cultured in 30 mm dishes and treated with plumbagin at various concentrations (0, 5, 10, and 20 μmol/L) for 6 h. After treatment, the medium was removed and replaced with fresh medium. Cells were grown for 10 d at 37 °C to allow for colony formation. Subsequently, the cells were washed with phosphate-buffered saline (PBS), fixed with 4% formaldehyde for 15 min at room temperature and stained with 0.5% crystal violet. The images were collected, and the number of colonies in each well were counted.

Proliferating cells were stained with EdU using the Cell-Light EdU DNA Cell Proliferation Kit (RIBOBio Co, Guangzhou, China)[20]. The cells were seeded in 96-well culture plates and exposed to media with or without plumbagin. All cells were treated with 50 μmol/L of EdU for 4 h at 37 °C. After being fixed with 4% paraformaldehyde for 15 min, the cells were treated with 0.5% Triton X-100 for 20 min and rinsed with PBS three times. Thereafter, the cells were exposed to 100 μL of 1×Apollo® reaction cocktail for 30 min and incubated with 5 μg/mL of Hoechst 33342 to stain the cell nuclei for 30 min. Images were captured using a fluorescent microscope (Olympus, Tokyo, Japan).

Apoptotic cell detection

An Annexin-V-FITC kit (Bender Medsystems, Burlingame, CA, USA) was used according to the manufacturer's instructions. Briefly, the plumbagin-treated GC cells were resuspended in 500 μL binding buffer, followed by staining with an Annexin-V-FITC and PI solution for 30 min at room temperature in the dark. The samples were analyzed immediately using the FACSCalibur flow cytometer (Becton, Dickinson and Co, San Jose, CA, USA).

Western blot analysis

Cells seeded in 10 cm dishes were treated with 10 μmol/L or 5 μmol/L of plumbagin. Total cell extracts were prepared using M-PER mammalian protein extraction reagent and protease inhibitors (Pierce, Rorkford, IL, USA). The cytoplasmic and nuclear extracts were prepared using the Nuclear and Cytoplasmic Protein Extraction Kit (Beyotime, Jiangsu, China). Protein concentrations were determined using the BCA protein assay (Pierce, Rorkford, IL, USA). Equivalent amounts of protein (30 μg) were loaded per lane, resolved by SDS-polyacrylamide gel electrophoresis (8%–12%), and transferred to PVDF membranes. After being blocked with a 5% skim milk solution for 1 h, the membranes were incubated with their respective primary antibodies overnight at 4 °C, followed by secondary antibody incubations for 1 h at room temperature. The proteins were visualized using an enhanced chemiluminescence system (ECL, Beyotime Institute of Biotechnology, Jiangsu, China).

Immunofluorescence for NF-κB p65 localization

The effect of plumbagin on the nuclear translocation of p65 was examined by immunofluorescence[21]. Briefly, GC cells were washed in PBS and fixed with 4% paraformaldehyde for 15 min at room temperature. The fixed cells were permeabilized with 0.5% Triton-X 100 in PBS for 10 min and blocked with a 5% bovine serum albumin in PBS. The anti-NF-κB p65 antibody was diluted 1:100 and incubated overnight at 4 °C. The cells were then incubated with Cy3-labeled secondary antibodies for 1 h and mounted with Hoechst 33342 stain. Images were captured using an A1Si confocal laser-scanning microscope (Nikon, Japan).

Statistical analysis

The data are presented as the mean±SD. The Student's *t*-test was used to determine the significance between groups. *P* values of less than 0.05 were considered to be significant. All statistical analyses were performed using the SPSS (Statistical Package for the Social Sciences) 13.0 software.

Results

Plumbagin decreased viability and inhibited the proliferation of GC cells

Cell viability was assayed by treating GC cell lines, including SGC-7901, MKN-28, and AGS cells, with various concentrations of plumbagin followed by analysis using the CCK-8 viability assay. We observed that cellular viability was suppressed by plumbagin in a dose-dependent manner in all three of the GC cell lines (Figure 1A). The IC_{50} values of plumbagin in SGC-7901, MKN-28, and AGS cells were 19.12 μmol/L, 13.64 μmol/L, and 10.12 μmol/L, respectively.

The EdU incorporation assay was performed to detect whether plumbagin could affect the number of proliferating cells. We determined that the number of EdU-positive cells in the plumbagin group was reduced compared to the control group. This indicated that plumbagin inhibited the proliferation of SGC-7901 cells *in vitro* (Figures 1B and 1C).

To determine the effect of the long-term antiproliferative activity of plumbagin, we used clonogenic assays. The clonogenicity of SGC-7901 cells in the plumbagin groups was reduced in a concentration-dependent manner (Figure 1D). We observed an inhibition of more than 30% for colony formation (Figure 1E).

Plumbagin enhanced the cell apoptosis of GC cells

The amount of apoptotic cell death was quantified with Annexin V-FITC/PI double-labeled flow cytometry. The SGC-7901 cells were pretreated with varying concentrations of plumbagin. This led to an increase in the amount of apoptosis in this cell line (Figure 2A). The total apoptosis rates were 1.77%±0.31%, 8.00%±1.67%, 30.57%±1.25%, and 35.33%±1.31% at plumbagin concentrations of 0 μmol/L, 5 μmol/L, 10 μmol/L, and 20 μmol/L of plumbagin, respectively.

Plumbagin suppressed the expression of NF-κB-regulated gene products

NF-κB is known to regulate the expression of IAP1, XIAP, Bcl-2, and Bcl-xL, all of which are associated with cancer cell survival[22–24]. To investigate whether plumbagin inhibits the expression of these proteins, whole-cell protein extracts were prepared and analyzed by Western blotting with the specific antibodies. Plumbagin decreased the expression of these proteins in a time-dependent manner (Figure 3A).

We also determined the effect of plumbagin on the NF-κB-dependent gene products that are involved in angiogenesis and metastasis. We found that plumbagin downregulated the expression of both VEGF and TF (Figure 3B).

Plumbagin inhibited TNF-α-induced phosphorylation and nuclear translocation of NF-κB p65

We investigated the effect of plumbagin on p65 nuclear translocation and its phosphorylation status. In general, p65 is located in the cytoplasm in untreated cells, and TNF-α-induced p65 is detected in the nuclei. In cells pretreated with plumbagin, the TNF-α-induced nuclear translocation of p65 was almost completely suppressed (Figure 4A).

Modifications of p65, such as phosphorylation, play an important role in NF-κB transcriptional activity[25]. Therefore, we examined the effect of plumbagin on the phosphorylation and expression of p65 in both nuclear extracts (NE) and cytoplasmic extracts (CE) by Western blot. In the nuclear protein extracts from the TNF-α-treated cells, the accumulation of both total and phosphorylated p65 increased in a time-dependent manner. Concurrently, the expression of p65 in cytoplasmic extracts decreased gradually upon TNF-α stimulation. The p65 nuclear translocation and phosphorylation induced by TNF-α were markedly suppressed in the plumbagin-pretreated GC cells (Figure 4B).

Plumbagin inhibited both TNF-α-induced degradation of IκBα and the phosphorylation of IκBα and IKKα

It is well known that after the phosphorylation, ubiquitination, and proteolytic degradation of IκBα, the p50-p65 heterodimer

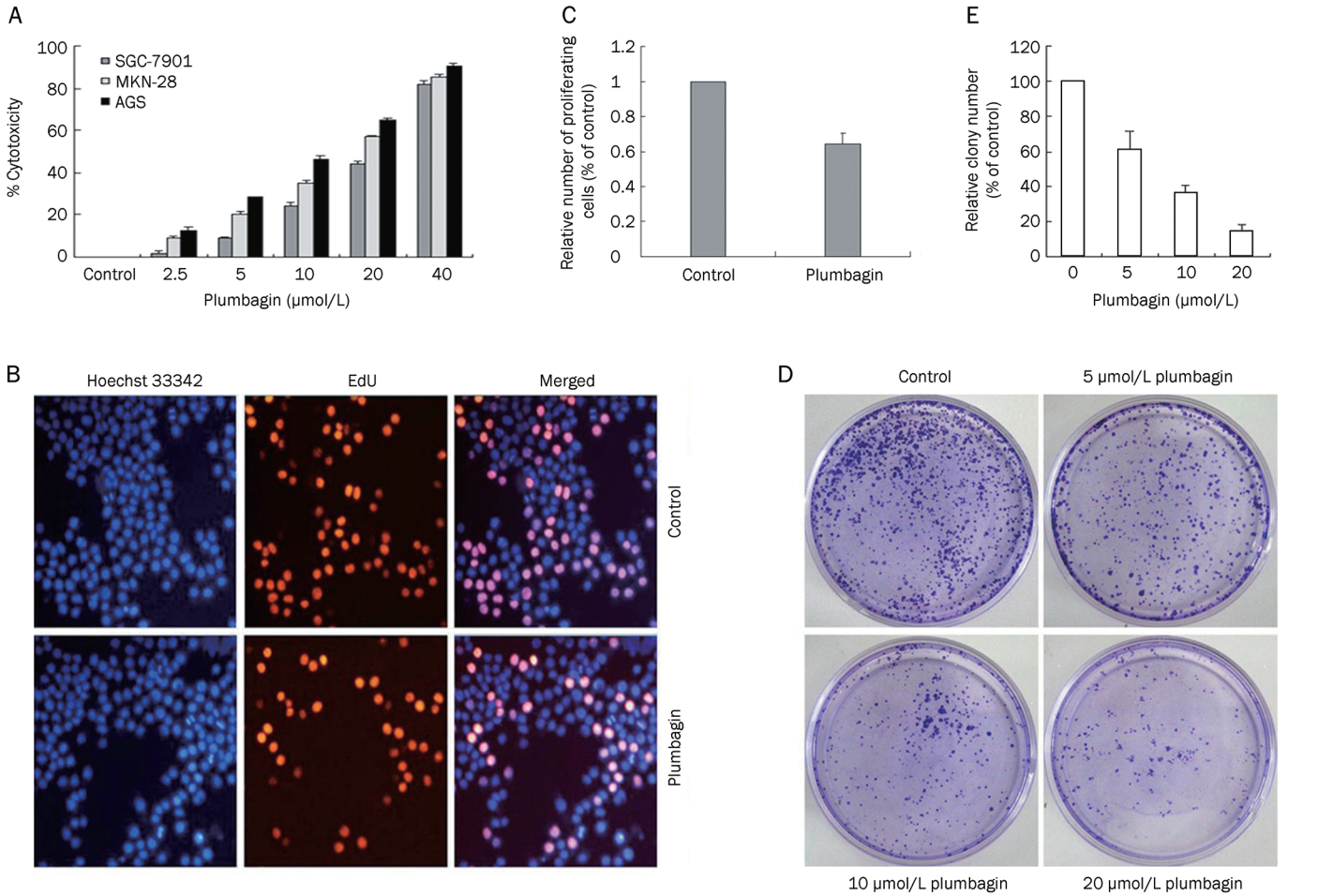

Figure 1. Plumbagin decreased viability and inhibited proliferation of GC cells. (A) Cell viability in plumbagin-treated SGC-7901, MKN-28, and AGS cells. The cells were treated with indicated concentrations (0–40 μmol/L) of plumbagin for 24 h. (B–C) Plumbagin inhibited the cellular DNA replication in SGC-7901 cells (magnification×200). Cells were incubated with 5 μmol/L plumbagin for 12 h. The EdU-labeled replicating cells were examined under a fluorescent microscope. The red and blue cells were counted in a blind manner. (D–E) Plumbagin decreased the number of colony-forming cells. Cells were treated with indicated concentrations of plumbagin (0, 5, 10, and 20 μmol/L) for 6 h, and then the medium was replaced by fresh medium. Cells were allowed to grow for 10 d. The formed cell clones were counted in a blind manner. The data shown are the mean from three independent experiments.

is released and translocates to the nucleus[13]. To determine whether plumbagin inhibited p65 nuclear translocation was due to the degradation and phosphorylation of IκBα, we exposed the cells (pretreated with or without plumbagin) to TNF-α for varying amounts of time. IκBα was degraded in the control cells; however, in the plumbagin pretreated cells, TNF-α failed to induce the degradation of IκBα. Furthermore, TNF-α increased IκBα phosphorylation in the control cells but had no effect on the plumbagin-pretreated cells (Figure 5). These results indicated that plumbagin suppressed both TNF-α-induced IκBα degradation and the activation of IκBα, which occurs prior to p65 nuclear translocation.

The phosphorylation of IκBα required activation of IKK. To examine the effect of plumbagin on IKKα activation, we investigated whether plumbagin could influence TNF-α-induced IKKα phosphorylation. Indeed, plumbagin suppressed TNF-α-dependent IKKα phosphorylation. Both the TNF-α and plumbagin treatments had a weak effect on IKKα protein expression (Figure 5).

Plumbagin potentiated apoptosis induced by TNF-α as well as cisplatin

Because TNF-α and the chemotherapeutic agent cisplatin are two anticancer agents that are commonly used in the clinic, we investigated whether plumbagin affects TNF-α- and/or cisplatin-induced apoptosis. The results displayed an increase in the cytotoxic effect induced by either TNF-α or cisplatin in the presence of plumbagin. This suggests that plumbagin potentiated the apoptotic effects of both TNF-α and cisplatin (Figure 6).

Discussion

The aim of this study was to investigate whether plumbagin has an anticancer effect on human GC cells via inhibition of

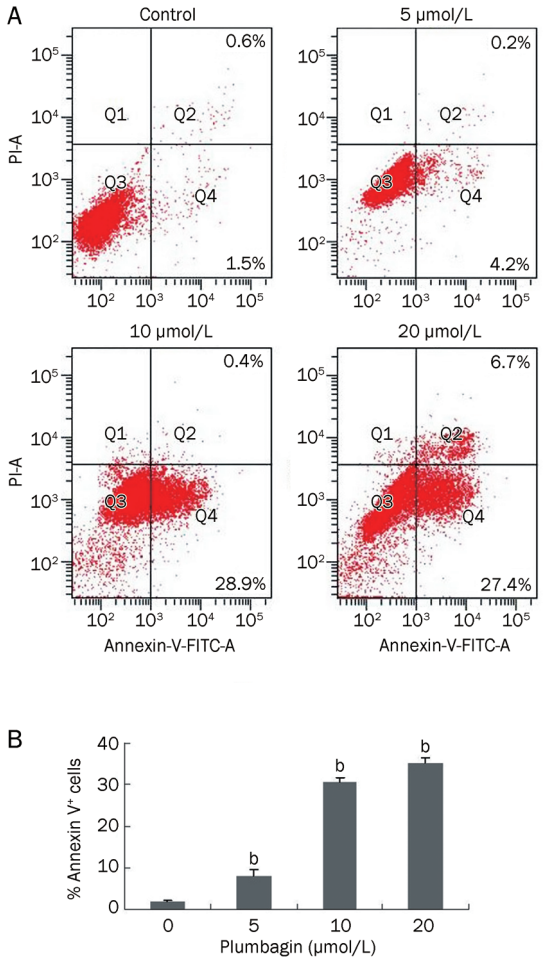

Figure 2. Plumbagin enhanced cell apoptosis of GC cells. (A) Plumbagin induced apoptosis of SGC-7901 cells. Cells were incubated with 0, 5, 10, and 20 μmol/L plumbagin for 12 h. The apoptosis was analyzed by Annexin V-FITC/PI double-staining assay. (B) The degree of apoptotic cell death was quantified. Data represented the mean±SD of three individual experiments ($^bP<0.05$).

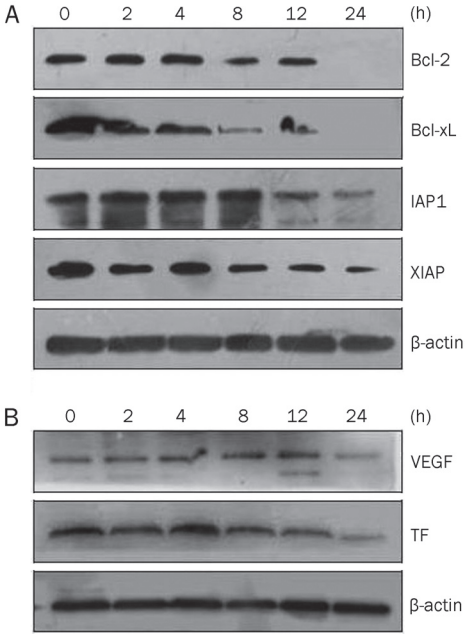

Figure 3. Plumbagin suppressed the expression of NF-κB-regulated gene products. (A) Plumbagin decreased the expression of NF-κB-regulated anti-apoptotic proteins. (B) Plumbagin suppressed the expression of VEGF and TF. SGC-7901 cells were incubated with 10 μmol/L plumbagin for different time periods (0, 2, 4, 8, 12, and 24 h). Whole-cell extracts were prepared and measured by Western blot analysis using the relevant antibodies.

the NF-κB pathway. We identified, for the first time, that GC cells treated with plumbagin underwent growth inhibition, apoptosis and increased chemosensitivity in a dose-dependent manner. We also observed that the protein expression levels of various anti-apoptotic proteins were downregulated by plumbagin in a time-dependent manner. Furthermore, we determined that plumbagin suppressed both NF-κB activation and the expression of NF-κB-regulated gene products. The effects of plumbagin on the NF-κB pathway largely explained how plumbagin increased the chemosensitivity of GC cells.

It is interesting to note that plumbagin caused apoptosis in human GC cell lines, including the well-differentiated MKN-28 cells, and the partially-differentiated SGC-7901 and AGS cell lines. The effective concentration of plumbagin necessary to induce GC cell death is comparable with several existing natural products that have been tested on human GC cells, such as wogonin and curcumin[18, 26]. The downregulated anti-apoptotic proteins that we observed upon treatment with plumbagin, including IAP1, XIAP, Bcl-2, and Bcl-xL, are the main reasons for increased apoptosis. Because Bcl-2 and Bcl-xL are key members in the mitochondrial apoptotic pathway, we conclude that mitochondria may be one of the pathways for apoptosis.

We determined that plumbagin was able to suppress the expression of proteins involved in anti-apoptosis (*ie*, IAP1, XIAP, Bcl-2, and Bcl-xL), angiogenesis (VEGF), and metastasis (TF)[27, 28], all of which are linked to, and regulated by, NF-κB. Based on our findings, we hypothesized that plumbagin may have an effect on the NF-κB pathway in GC cells. Indeed, plumbagin blocked the nuclear translocation of NF-κB p65. Plumbagin also caused the downregulation of both the expression and phosphorylation of NF-κB p65 in nucleus induced by TNF-α.

Exposing cancer cells to TNF-α initiates numerous intracellular signaling cascades, most of which activate the IKK complex, which consists of IKKα, IKKβ, and IKKγ[29]. In the current study, plumbagin inhibited TNF-α-induced phosphorylation of IKKα. IκBα is phosphorylated at serine residues 32 and 34 by IKKs, and this phosphorylation triggers the degradation of IκBα, which allows for the release and translocation of p65 into the nucleus to activate the transcription of target genes[29]. We observed that plumbagin inhibited TNF-α-induced degradation of IκBα by suppressing its phosphorylation. Similar to our data, several studies have shown that some natural constituents, such as berberine, berbamine, and curcumin,

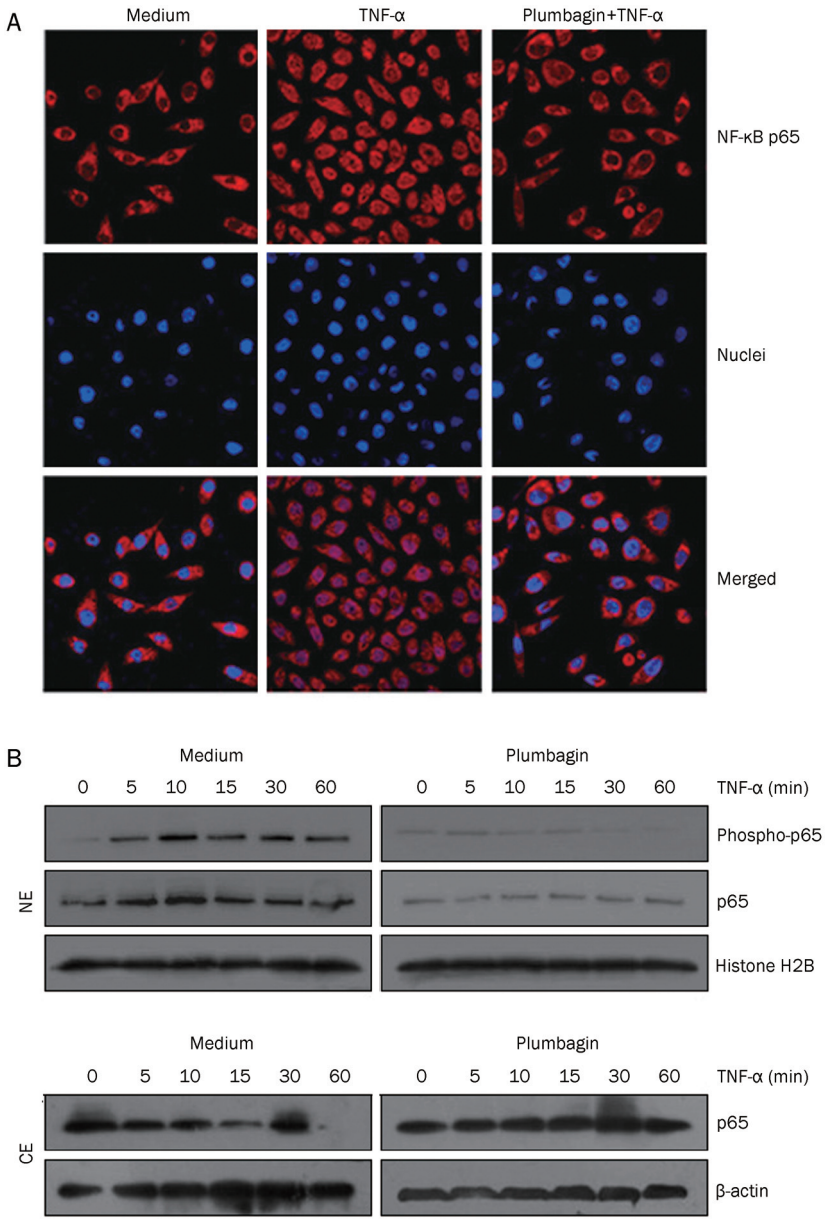

Figure 4. Plumbagin inhibited TNF-α-induced phosphorylation and nuclear translocation of NF-κB p65. (A) Plumbagin inhibited TNF-α-induced p65 localization by immunofluorescence analysis. SGC-7901 cells were either pretreated or untreated with 5 μmol/L plumbagin for 4 h and then exposed to 0.1 nmol/L TNF-α for 30 min (magnification×400). (B) Plumbagin inhibited TNF-α-induced phosphorylation and nuclear translocation of p65. SGC-7901 cells were first treated or untreated with 5 μmol/L plumbagin for 4 h and then exposed to 0.1 nmol/L TNF-α for indicated times. Nuclear extracts (NE) and cytoplasmic extracts (CE) were prepared and analyzed by Western blot with antibodies against p65 and phospho-p65. The antibodies of anti-β-actin and anti-histone H2B were used as controls.

can suppress the activation of NF-κB and its target genes and cause apoptosis in various cancer cells[30–32]. Whether plumbagin is a selective inhibitor of other transcription factors in GC cells remains to be elucidated.

Chemotherapy is widely used in the treatment of numerous malignancies and is a potent therapeutic method; however, chemoresistance remains a major obstacle in the chemotherapeutic treatment of cancer. Overexpression of transcription factors, such as NF-κB, contributes to enhanced cancer cell survival and chemoresistance[33]. Interestingly, we found that plumbagin potentiated apoptosis induced by TNF-α or cisplatin. Plumbagin, in combination with TNF-α or cisplatin, was more effective than the single agent alone. This might be explained by the fact that the apoptosis induced by TNF-α or cisplatin can be suppressed by the activation of NF-κB[34, 35], which is inhibited by plumbagin. This again suggests that plumbagin could be a useful therapeutic strategy in human GC.

Given its strong anticancer abilities, the toxicity of plumbagin has been extensively evaluated. In rodents, plumbagin had dose-related toxic side effects, including diarrhea, skin rashes, and hepatic and reproductive toxicity[11]. Plumbagin did not exhibit significant toxicity on normal tissues at a dose of 2 $mg \cdot kg^{-1} \cdot d^{-1}$ [9]. Additional preclinical and prospective randomized clinical trials are required to determine the full potential of this agent.

In summary, our findings strongly indicate that plumbagin acts as an anticancer agent by inhibiting cell proliferation, inducing apoptosis, and potentiating the chemosensitivity of GC cells. These effects are, in part, mediated by suppressing both NF-κB activation and the expression of NF-κB-regulated gene products. Based on the evidence provided

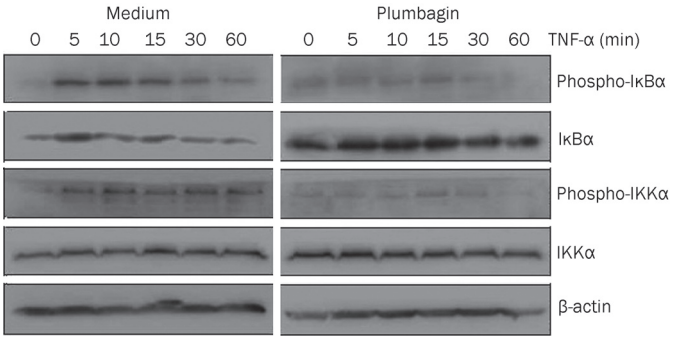

Figure 5. Plumbagin inhibited TNF-α-induced degradation of IκBα, phosphorylation of IκBα and IKKα. Plumbagin inhibited TNF-α induced IκBα degradation, phosphorylation of IκBα and IKKα. SGC-7901 cells were first exposed to 5 μmol/L plumbagin for 4 h and then treated with 0.1 nmol/L TNF-α for the indicated times and analyzed by Western blotting using various antibodies.

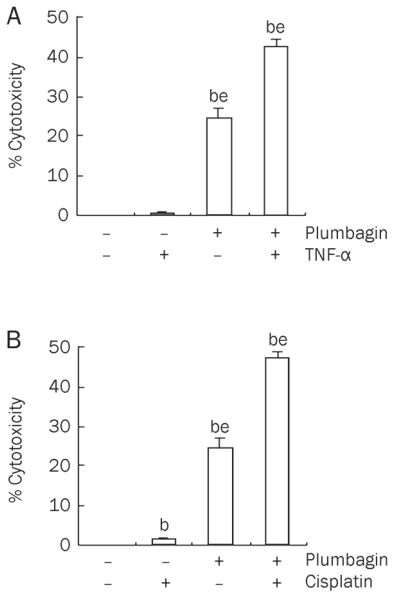

Figure 6. Plumbagin potentiated apoptotic effects of TNF-α and cisplatin. (A–B) SGC-7901 cells were pretreated with 10 μmol/L plumbagin for 2 h, and then treated with 0.1 nmol/L TNF-α and cisplatin for 24 h. Cell viability was then analyzed by the CCK-8 method. Data represented the mean±SD of three individual experiments ($^bP<0.05$ compared to control group. $^eP<0.05$ compared with TNF-α or cisplatin treatment only).

here, plumbagin should be strongly considered as a basis for the development of novel pharmaceutical agents that target human GC cells to improve the treatment of this disease.

Acknowledgements

This work was supported by grants from the National Natural Science Foundation of China (No 81072945 and No 81001670). The authors are grateful to the Department of Central Laboratory, Union Hospital, Tongji Medical College, Huazhong University of Science and Technology, Wuhan, China, for allowing us to use their experimental facilities and providing us their technical support.

Author contribution

Jing LI, You QIN, Rui CHEN, and Jia LI performed the experiments. Jing LI, Lin SHEN, and Fu-rong LU participated in the design of the study and prepared the manuscript. Yan LI, Han-zi ZHAN, and Yuan-qiao HE contributed to the analyses and interpretation of the data and performed the statistical analysis. Han-zi ZHAN revised the manuscript.

References

1 Qiao L, Wong BC. Targeting apoptosis as an approach for gastrointestinal cancer therapy. Drug Resist Update 2009; 12: 55–64.
2 Parkin DM, Bray F, Ferlay J, Pisani P. Global cancer statistics, 2002. CA Cancer J Clin 2005; 55: 74–108.
3 Surh YJ. Cancer chemoprevention with dietary phytochemicals. Nat Rev Cancer 2003; 3: 768–80.
4 Lu FR, Shen L, Qin Y, Gao L, Li H, Dai Y. Clinical observation on trigonella foenum-graecum L total saponins in combinaiton with sulphanylureas in the treatment of type 2 diabetes mellitus. Chin J Integr Med 2008; 14: 56–60.
5 Aziz MH, Dreckschmidt NE, Verma AK. Plumbagin, a medicinal plant-derived naphthoquinone, is a novel inhibitor of the growth and invasion of hormone — refractory prostate cancer. Cancer Res 2008; 68: 9024–32.
6 Mossa JS, El-Feraly FS, Muhammad I. Antimycobacterial constituents from Juniperus procera, Ferula communis and Plumbago zeylanica and their *in vitro* synergistic activity with isonicotinic acid hydrazide. Phytother Res 2004; 18: 934–37.
7 Ding YX, Chen ZJ, Liu S, Che D, Vetter M, Chang CH. Inhibition of Nox-4 activity by plumbagin, a plant-derived bioactive naphthoquinone. J Pharm Pharmacol 2005; 57: 111–6.
8 Kuo PL, Hsu YL, Cho CY. Plumbagin induces G_2-M arrest and autophagy by inhibiting the AKT/mammalian target of rapamycin pathway in breast cancer cells. Mol Cancer Ther 2006; 5: 3209–21.
9 Wang CC, Chiang YM, Sung SC, Hsu YL, Chang JK, Kuo PL. Plumbagin induces cell cycle arrest and apoptosis through reactive oxygen species/c-Jun N-terminal kinase pathways in human melanoma A375. S2 cells. Cancer Lett 2008; 259: 82–98.
10 Shieh JM, Chiang TA, Chang WT, Chao CH, Lee YC, Huang GY, *et al*. Plumbagin inhibits TPA-induced MMP-2 and u-PA expressions by reducing binding activities of NF-kappaB and AP-1 via ERK signaling pathway in A549 human lung cancer cells. Mol Cell Biochem 2010; 335: 181–93.
11 Sandur SK, Ichikawa H, Sethi G, Ahn KS, Aggarwal BB. Plumbagin (5-hydroxy-2-methyl-1,4-naphthoquinone) suppresses NF-kappaB activation and NF-kappaB-regulated gene products through modulation of p65 and IkappaBalpha kinase activation, leading to potentiation of apoptosis induced by cytokine and chemotherapeutic agents. J Biol Chem 2006; 281: 17023–33.
12 Hsu YL, Cho CY, Kuo PL, Huang YT, Lin CC. Plumbagin (5-hydroxy-2-methyl-1,4-naphthoquinone) induce apoptosis and cell cycle arrest in A549 cells through p53 accumulation via c-Jun NH_2-terminal kinase–mediated phosphorylation at serine 15 *in vitro* and *in vivo*. J Pharmacol Exp Ther 2006; 318: 484–94.
13 Aggarwal BB. Nuclear factor-kappaB: the enemy within. Cancer Cell 2004; 6: 203–8.
14 Gupta SC, Kim JH, Prasad S, Aggarwal BB. Regulation of survival, proliferation, invasion, angiogenesis, and metastasis of tumor cells

through modulation of inflammatory pathways by nutraceuticals. Cancer Metast Rev 2010; 29: 405–34.
15 Li Q, Yu YY, Zhu ZG, Ji YB, Zhang Y, Liu BY, *et al*. Effect of NF-kappaB constitutive activation on proliferation and apoptosis of gastric cancer cell lines. Eur Surg Res 2005; 37: 105–10.
16 Yamanaka N, Sasaki N, Tasaki A, Nakashima H, Kubo M, Morisaki T, *et al*. Nuclear factor-kappaB p65 is a prognostic indicator in gastric carcinoma. Anticancer Res 2004; 24: 1071–5.
17 Wu H, Li W, Wang T, Shu Y, Liu P. Paeoniflorin suppress NF-kappaB activation through modulation of I kappaB alpha and enhances 5-fluorouracil-induced apoptosis in human gastric carcinoma cells. Biomed Pharmacother 2008; 62: 659–66.
18 Zhao Q, Wang J, Zou MJ, Hu R, Zhao L, Qiang L, *et al*. Wogonin potentiates the antitumor effects of low dose 5–fluorouracil against gastric cancer through induction of apoptosis by down-regulation of NF-kappaB and regulation of its metabolism. Toxicol Lett 2010; 197: 201–10.
19 Park HH, Lee KY, Kim SH, Lee YJ, Koh SH. L-DOPA-induced neurotoxicity is reduced by the activation of the PI3K signaling pathway. Toxicology 2009; 265: 80–6.
20 Lv L, Xiao XY, Gu ZH, Zeng FQ, Huang LQ, Jiang GS. Silencing USP22 by asymmetric structure of interfering RNA inhibits proliferation and induces cell cycle arrest in bladder cancer cells. Mol Cell Biochem 2011; 346: 11–21.
21 Pandey MK, Sung B, Ahn KS, Kunnumakkara AB, Chaturvedi MM, Aggarwal BB. Gambogic acid, a novel ligand for transferrin receptor, potentiates TNF–induced apoptosis through modulation of the nuclear factor–kappaB signaling pathway. Blood 2007; 110: 3517–25.
22 Li C, Yang Z, Zhai C, Qiu W, Li D, Yi Z, *et al*. Maslinic acid potentiates the anti–tumor activity of tumor necrosis factor alpha by inhibiting NF–kappaB signaling pathway. Mol Cancer 2010; 9: 73.
23 Olsen LS, Hjarnaa PJ, Latini S, Holm PK, Larsson R, Bramm E, *et al*. Anticancer agent CHS 828 suppresses nuclear factor-kappa B activity in cancer cells through downregulation of IKK activity. Int J Cancer 2004; 111: 198–205.
24 Tamatani M, Che YH, Matsuzaki H, Ogawa S, Okado H, Miyake S, *et al*. Tumor necrosis factor induces Bcl-2 and Bcl-x expression through NFkappaB activation in primary hippocampal neurons. J Biol Chem 1999; 274: 8531–8.
25 Yang F, Tang E, Guan K, Wang CY. IKK beta plays an essential role in the phosphorylation of RelA/p65 on serine 536 induced by lipopolysaccharide. J Immunol 2003; 170: 5630–5.
26 Cai XZ, Wang J, Li XD, Wang GL, Liu FN, Cheng MS, *et al*. Curcumin suppresses proliferation and invasion in human gastric cancer cells by downregulation of PAK1 activity and cyclin D1 expression. Cancer Biol Ther 2009; 8: 1360–8.
27 Ma YY, He XJ, Wang HJ, Xia YJ, Wang SL, Ye ZY, *et al*. Interaction of coagulation factors and tumor–associated macrophages mediates migration and invasion of gastric cancer. Cancer Sci 2010; 102: 336–42.
28 Xie TX, Aldape KD, Gong W, Kanzawa T, Suki D, Kondo S, *et al*. Aberrant NF-kappaB activity is critical in focal necrosis formation of human glioblastoma by regulation of the expression of tissue factor. Int J Oncol 2008; 33: 5–15.
29 Ducut Sigala JL, Bottero V, Young DB, Shevchenko A, Mercurio F, Verma IM. Activation of transcription factor NF-kappaB requires ELKS, an IkappaB kinase regulatory subunit. Science 2004; 304: 1963–7.
30 Pandey MK, Sung B, Kunnumakkara AB, Sethi G, Chaturvedi MM, Aggarwal BB. Berberine modifies cysteine 179 of IkappaBalpha kinase, suppresses nuclear factor-kappaB-regulated antiapoptotic gene products, and potentiates apoptosis. Cancer Res 2008; 68: 5370–9.
31 Liang Y, Xu RZ, Zhang L, Zhao XY. Berbamine, a novel nuclear factor kappaB inhibitor, inhibits growth and induces apoptosis in human myeloma cells. Acta Pharmacol Sin 2009; 12: 1659–65.
32 Aggarwal S, Ichikawa H, Takada Y, Sandur SK, Shishodia S, Aggarwal BB. Curcumin (diferuloylmethane) down-regulates expression of cell proliferation and antiapoptotic and metastatic gene products through suppression of IkappaBalpha kinase and Akt activation. Mol Pharmacol 2006; 69: 195–206.
33 Dhandapani KM, Mahesh VB, Brann DW. Curcumin suppresses growth and chemoresistance of human glioblastoma cells via AP-1 and NFkappaB transcription factors. J Neurochem 2007; 102: 522–38.
34 Wang X, Chen W, Lin Y. Sensitization of TNF-induced cytotoxicity in lung cancer cells by concurrent suppression of the NF-kappaB and Akt pathways. Biochem Biophys Res Commun 2007; 355: 807–12.
25 Giri DK, Aggarwal BB. Constitutive activation of NF-kappaB causes resistance to apoptosis in human cutaneous T cell lymphoma HuT-78 cells. Autocrine role of tumor necrosis factor and reactive oxygen intermediates. J Biol Chem 1998; 273: 14008–14.

Acta Pharmacologica Sinica (2012) 33: 250–260
 1671-4083/12 $32.00
www.nature.com/aps

Original Article

Suppression of human lung cancer cell proliferation and metastasis *in vitro* by the transducer of ErbB-2.1 (TOB1)

Yang JIAO#, Ke-kang SUN#, Lin ZHAO, Jia-ying XU, Li-li Wang, Sai-jun FAN*

Key Laboratory of Radiation Biology, School of Radiation Medicine and Protection, Medical College of Soochow University, Suzhou 215123, China

Aim: To investigate the effects of the transducer of ErbB-2.1 (TOB1) on the proliferation, migration and invasion of human lung cancer cells *in vitro*.

Methods: Human lung cancer cell lines (95-D, A549, NCI-H1299, NCI-H1975, NCI-H661, NCI-H446, NCI-H1395, and Calu-3) and the normal human bronchial epithelial (HBE) cell line were tested. The expression levels of TOB1 in the cells were determined with Western blot and RT-PCR analyses. TOB1-overexpressing cell line 95-D/TOB1 was constructed using lipofectamine-induced TOB1 recombinant plasmid transfection and selective G418 cell culture. The A549 cells were transcend-transfected with TOB1-siRNA. MTT assay, flow cytometry and Western blot analysis were used to examine the effects of TOB1 on cancer cell proliferation and wound healing. Transwell invasive assay was performed to evaluate the effects of TOB1 on cancer cell migration and invasion. The activity of MMP2 and MMP9 was measured using gelatin zymography assay.

Results: The expression levels of TOB1 in the 8 human lung cancer cell lines were significantly lower than that in HBE cells. TOB1 overexpression inhibited the proliferation of 95-D cells, whereas TOB1 knockdown with TOB1-siRNA promoted the growth of A549 cells. Decreased cell migration and invasion were detected in 95-D/TOB1 cells, and the suppression of TOB1 enhanced the metastasis in A549 cells. TOB1 overexpression not only increased the expression of the phosphatase and tensin homolog (PTEN), an important tumor suppressor, but also regulated the downstream effectors in the PI3K/PTEN signaling pathway, including Akt, ERK1/2, *etc*. In contrast, decreased expression of TOB1 oppositely regulated the expression of these factors. TOB1 also regulates the gelatinase activity of MMP2 and MMP9 in lung cancer cells.

Conclusion: The results demonstrate that the PI3K/PTEN pathway, which is essential for carcinogenesis, angiogenesis, and metastasis, may be one of the possible signaling pathways for regulation of proliferation and metastasis of human lung cancer cells by TOB1 *in vitro*.

Keywords: human lung cancer cells; transducer of ErbB-2.1 (TOB1); PTEN; carcinogenesis; metastasis; RNA interference

Acta Pharmacologica Sinica (2012) 33: 250–260; doi: 10.1038/aps.2011.163; published online 12 Dec 2011

Introduction

As one of the leading causes of cancer mortality in the world and the most common occupational cancer, lung cancer is becoming the biggest challenge for basic science[1]. Despite advances in surgery, radiotherapy, and chemotherapy, the mortality rate of lung cancer has not been substantially reduced over the past decades, largely because of potential metastasis. Metastasis is one of the most lethal attributes of cancer, responsible for about 90% of human cancer deaths[2]. Lung cancer metastasis involves a complex series of steps, including cellular migration, local invasion, dissemination, and angiogenesis. The inhibition of one of these processes can substantially prevent secondary tumors from spreading in the body[3, 4].

The tumor suppressor protein, which functions in cell cycle regulation, apoptosis induction, DNA damage repair, and metastasis inhibition, is a potential therapeutic target in lung cancer[5–7]. One of the promising examples is *p53*, whose mutation has been detected in 90% of small cell lung cancers and in 50% of non–small cell lung cancer. In 2006, Cristofanilli *et al*[8] reported that adenovirus mediates p53 overexpression,

#These authors contributed equally to this work.
*To whom correspondence should be addressed.
E-mail sjfan@suda.edu.cn
Received 2011-08-18 Accepted 2011-11-03

which induces cell apoptosis in p53-null cells. These data documented a safety profile, encouraging clinical trials of adenovirus-mediated p53 in the therapy of lung cancer. However, evidence concerning other tumor suppressors thought to be responsible for lung cancer carcinogenesis, migration, and invasion still needs to be clarified.

The transducer of ErbB-2.1 (*TOB1*) gene was initially identified as a member of the anti-proliferative TOB/BTG (transducer of ErbB-2/B-cell translocation gene) protein family, which was first discovered in the 1990s[9]. In mammalian cells, this family consists of *BTG1*, *BTG2*, *BTG3*, *BTG4*, *TOB1*, and *TOB2*. All the protein products of the family members possess the potential ability to restrain cell growth[10–13]. Carcinogenesis and tumor progression in lung, liver, and lymph nodes were observed in mice lacking TOB1[14]. Furthermore, TOB1 deletion and dysfunction were also reported in human malignancies[15, 16]. These studies suggest that *TOB1* acts as a tumor suppressor gene. Accumulating studies have also found that TOB1 might inhibit cell proliferation through its intervention in oncogenic pathways, including the epidermal growth factor and the TGF-β/Smad signal pathways[17-19]. Although TOB1 expression is reduced in clinical lung cancer samples[15], the effects of *TOB1* on lung cancer proliferation and metastasis *in vitro* are poorly understood. The signaling pathways or the related mechanisms remain unclear.

In the present study, using Lipofectamine-mediated TOB1 recombinant plasmid and siRNA transfection of lung cancer cell lines, the effects of TOB1 on lung cancer proliferation, invasion, and migration are investigated *in vitro*. The possible pathways involved in its regulation of lung cancer tumorigenesis and metastasis are explored.

Materials and methods

Cell culture

The normal human bronchial epithelial (HBE) cell line and eight human lung cancer cell lines (95-D, A549, NCI-H1299, NCI-H1975, NCI-H661, NCI-H446, NCI-H1395, and Calu-3) were purchased from American Type Culture Collection (Manassas, VA, USA). Calu-3 cells were maintained in Dulbecco's modified Eagle's medium (DMEM). The other cells were seeded onto tissue culture dishes containing RPMI-1640 supplemented with 10% fetal calf serum (FCS), *L*-glutamine (5 mmol/L), non-essential amino acids (5 mmol/L), penicillin (100 U/mL), and streptomycin (100 U/mL) (Invitrogen, Carlsbad, CA, USA), at 37 °C in a humidified 5% CO_2 atmosphere.

Plasmids, siRNAs, and transfection

The full-length human TOB1 cDNA was derived using polymerase chain reaction (PCR), using specific primers designed according to the TOB1 reference sequence from GenBank (NM_005749.2), and then cloned into the eukaryotic expression vector pcDNA3.0 (Invitrogen, Carlsbad, CA, USA). Three siRNA that target TOB1 mRNA and control (scrambled-sequence) siRNA were designed and synthesized by Invitrogen. For stable transfection, the cells were transfected using Lipofectamine 2000™. After an additional 24-h incubation, 500 μg/mL G418 (Sigma-Aldrich, MO, USA) was applied. After four weeks, the cell clones that overexpressed TOB1 were identified and obtained. Treatments with siRNA were performed as previously described[20]. Subconfluent lung cancer cells were transfected with each siRNA (40 nmol/L) using Lipofectamine™ RNAiMAX reagent (Invitrogen, Carlsbad, CA, USA). Before the start of the following experiment, the cells were incubated for another 48 h. The TOB1 inhibition efficiency by siRNA was determined using Western blot analysis. siRNA #1 exhibited about 30% decreased TOB1 expression, whereas no effect on TOB1 expression was observed in the control siRNA. Therefore, siRNA #1 was selected for further studies. The sequences for TOB1-siRNA #1 is as follows (5′ to 3′): GCUGUAAGCCCUACCUUCATT
UGAAGGUAGGGCUUACAGCTT

Cell viability assay

Cell proliferation was determined using a 3-[4,5-dimethylthiazol-2-yl]-2,5-diphenyl-tetrazolium bromide (MTT) viability assay, the most commonly used assay for determining cell growth and death. The MTT survival assay has been described in detail in previous studies[21]. Exponentially growing cells were recultured (5000 cells/well) overnight in 96-well tissue culture plates. Up to 20 μL of MTT (Sigma-Aldrich, MO, USA) was directly added to the media in each well, with a final concentration of 2 mg/mL. After 4-h incubation, the medium containing MTT was discarded, and 120 μL of dimethyl sulfoxide was added for 10 min. The absorbance was measured using an enzyme-linked immunosorbent assay reader at 570 nm, with the absorbance at 630 nm as the background correction. The cell viability was expressed as the percentage of untreated controls. All experiments were performed at least three times.

Cell cycle assays

The cells were removed with trypsin and collected into centrifuge tubes together with the culture medium. All the contents were centrifuged for 5 min at 1800×*g*. The supernate was poured out, washed once with 1×phosphate-buffered saline (PBS), and centrifuged for another 5 min. The cells were finally fixed with 5 mL of pre-cooled 70% ethanol for at least 4 h. The fixed cells were centrifuged and washed with 1×PBS. After centrifugation, the cell pellets were resuspended in 500 μL of propidium iodine (10 μg/mL) containing 300 μg/mL RNase (Sigma-Aldrich, USA). The cells were then incubated on ice for 30 min, and then filtered with a 53-μm nylon mesh. The cell cycle distribution was calculated from 10 000 cells using ModFit LT software (Becton Dickinson, CA, USA) using FACS Calibur (Becton Dickinson, San Jose, CA, USA).

Transwell invasion assay

The invasion assay was carried out using Transwell (Millipore, Billerica, MA, USA), as previously described[20]. The filter surfaces (8 μm pore size) of the Transwell plates were uniformly coated with 25 mg of Matrigel overnight at 4 °C before the experiment. The lower chamber was filled with culture

medium containing 10% FCS. The subconfluent proliferating cells were carefully transferred onto the coated upper surface of the chamber. After 24-h incubation, the filter was gently removed, and the upper surface of the filter was wiped to remove all attached cells. The cells that invaded through the Matrigel and attached to the lower surface of the filter were fixed with 4% paraformaldehyde and stained with Giemsa. Three replicates were conducted for each condition, and 15 random fields in each replicate were chosen and counted using an Olympus CKX41 inverted microscope. The results are presented as the ratio of cells that invaded relative to the cells that invaded in the control conditions (cells seeded in serum-free media, and invaded towards 10% FCS in DMEM). The results were obtained from at least three independent experiments.

Wound healing assay

In vitro cell migration was assessed using the scratch wound assay. The cells were subcultured onto six-well tissue culture plates to confluent cell monolayers using culture medium containing 10% FCS. The "wounds" were carefully created manually on the monolayers using sterile pipette tips, and the cellular debris was washed off with the desired medium. Phase contrast images of certain fixed positions in the wound area were taken at 0, 24, and 48 h after scratching using Olympus CKX41 microscope with a digital camera. In the images, the edge of the initial wound area was marked with lines using Image-Pro® Plus software (Media Cybernetics, Carlsbad, CA, USA). The edge of the initial wound area was overlaid with the image taken at 24 and 48 h after scratching. The number of cells migrating into the initial wound area was counted at 24 and 48 h after scratching. The data were obtained from three independent assays.

Western blot and immunoprecipitation (IP)/immunoblot analyses

Cell lysates were prepared and Western blot analysis was performed as previously described[22]. Equal aliquots of total cell protein (50 μg per lane) were electrophoresed on sodium dodecyl sulfate (SDS)-polyacrylamide gels, transferred onto polyvinylidene fluoride (PVDF) membranes, and then blotted using the following primary antibodies (Santa Cruz Biotech, Santa Cruz, CA, USA, 1:1000 dilution): β-actin (C-4), TOB (E-1), TOB1 (H-18), cyclin B1 (D-11), cyclin D1 (A-12), cyclin E (E-4), CDK2 (M2), PTEN (N-19), EGFR (1003), ERK1/2 (T-183), p-ERK1/2 (T185+Y187+T202+Y204), Akt (11E7), p-Akt (ser473), p-IκB-α (B9), NF-κB (P65A), MMP-2 (2C1), MMP-9 (6-6B), γ-catenin (G-20), α-catenin (C-19), β-catenin (BD1080), E-cadherin (G-10); and secondary antibody horseradish peroxidase-labeled goat anti-mouse (GAM-007) and goat anti-rabbit (SC-2004) IgG. For the IP/Western blot, 1 mg lysate was immunoprecipitated with 1 μg of anti-TOB (E-1) antibody at 4 °C overnight. Protein A-Sepharose beads were added and incubated at 4 °C for 2 h, and the protein-bead complex was washed 5 times with radioimmunoprecipitation assay lysis buffer. The SDS-polyacrylamide gel electrophoresis (PAGE) was then performed to separate the immunoprecipitates. The anti-TOB1 (H-18) and anti-PTEN (N-19) antibodies were applied for immunoblot. The protein bands were visualized using an enhanced chemiluminescence system (Union Bioscience Corporation, Hangzhou, China) with prestained markers as molecular size standards. The densitometry of the protein bands was quantified with Quantity One (Bio-Rad, Hercules, CA, USA), and the values were expressed relative to β-actin (control for loading and transfer). At least three independent experiments were performed for each cell type studied.

Semiquantitative reverse transcription (RT)-PCR analysis

mRNA expression was determined using semiquantitative RT-PCR assays. The PCR reaction conditions and cycle numbers were rigorously adjusted so that each reaction occurred within the linear range of amplification. The detailed methods for RNA isolation, cDNA synthesis, and RT-PCR analyses have been previously described[23]. For specific intent genes, the PCR primers were as follows: GAPDH sense, 5′-CAACTACATGGTCTACATGTTCC-3′, anti-sense, 5′-CAACCTGGTCCTCAGTGTAG-3′; TOB1 sense, 5′-GGATCGACCCATTTGAGGTTTCT-3′, anti-sense, 5′-CTACCCAAGCCAAGCCCATACAG-3′; PTEN sense, 5′-AGACCATAACCCACCACA-3′, anti-sense, 5′-TTGACGGCT CCTCTACTG-3′. The PCR products were analyzed via electrophoresis through 1% agarose gels containing 0.1 mg/mL ethidium bromide (EB). The gels were photographed under ultraviolet light. The mRNA expression levels were quantified by densitometry of the cDNA bands using software Quantity One (Bio-Rad, Hercules, CA, USA). At least three independent experiments were performed for each cell type studied.

Gelatin zymography assay

The MMP-2 and MMP-9 activity of the supernates of lung cancer cells 95-D transfected or untransfected with TOB1 recombinant plasmid, as well as the RNAi-treated A549 cells, were identified using gelatin zymography assay as previously described[24]. At 24 h after transfection, all the cells were seeded onto 6-well plates at a final density of 3.0×10^5 cells/well. The supernatants were harvested after 24 h of additional incubation, and the conditioned media were collected by centrifugation at 13 000 r/min for 5 min to remove the debris. The concentrations of the samples were quantified using bicinchoninic acid assay (Beyotime Institute of Biotechnology, Haimen, China). Then, 20 μg of each protein sample was loaded under non-reducing conditions onto 10% SDS-polyacrylamide gel containing 500 μg/mL gelatin (Amresco, Slon, OH, USA). After electrophoresis under 165 V for 1.5 h, the gels were washed twice using washing buffer (50 mmol/L Tris-Cl pH 7.6, 10 mmol/L $CaCl_2$) with 2.5% Triton X-100 for 30 min. Then, the gels were incubated overnight in zymography developing buffer containing 50 mmol/L Tris-HCl, pH 7.5, 10 mmol/L $CaCl_2$, 150 mmol/L NaCl, and 0.02% NaN_3 at 37 °C. Then, 0.05% Coomassie Brilliant Blue R-250 was utilized for gel staining, followed by destaining with a solution containing 30% methanol and 10% acetic acid. The gelatinase activity of the matrix metalloproteinases (MMPs) was then visualized as clear bands against the blue-stained background,

and the density of the bands was analyzed using Quantity One software. At least three individual experiments were conducted with independent protein samples.

Statistical analysis

The data are presented as means and standard deviations (SD). Statistical comparisons of the experimental results between the treated group and the control group were made using two-tailed Student's *t*-test. All statistical tests were performed using SPSS version 17.0. P value ≤0.05 between groups was considered significant.

Results

TOB1 expression is decreased in eight lung cancer cell lines

TOB1 plays a role in suppressing the carcinogenesis of cancers, such as lung, thyroid, and breast cancers. However, the functional role of TOB1 in lung cancer has not yet been fully explored. To investigate the effect of TOB1 on proliferation and metastasis of lung cancer cells, the TOB1 expression levels in the eight lung cancer cell lines and in the normal bronchial epithelial cell line HBE were first analyzed using Western blot analyses and RT-PCR assays. As shown in Figure 1, the levels TOB1 protein and mRNA expression levels all decreased in the eight lung cancer cell lines, although at different levels. Compared with the immortalized normal epithelial cell line HBE, TOB1 mRNA expression decreased from 10% to 90% in almost all of the eight lung cancer cell lines (P<0.05, Figure 1A and 1C). Similar results were confirmed in TOB1 protein expression, as shown in Figure 1B and 1D, wherein the TOB1 protein levels decreased from 100% in the HBE cells to 20% to 80%. These *in vitro* data confirmed the findings of previous studies by Iwanaga *et al*[15] that reducing TOB1 expression is an important event in lung cancer.

Ectopic expression of TOB1 regulates the proliferation of human lung cancer cells through alternation of the cell cycle

According to gain-of-function and loss-of-function approaches, the lung cancer cell lines 95-D and A549 were selected as model systems because 95-D cells express almost-deleted TOB1, whereas A549 cells express moderate TOB1. Using Lipofectamine and G418-mediated plasmid stable transfection, multiple clones stably transfected with TOB1 were selected and confirmed through RT-PCR and Western blot analysis in 95-D/TOB1 (Figure 2A). To investigate whether downregulated TOB1 expression enhances the aggressiveness of lung cancer cells, three different siRNA that target TOB1 and a control siRNA with a random sequence were generated and induced into A549 cells by transcend transfection. The efficacy of the siRNA was confirmed (Figure 2B). siRNA #1 efficiently reduced TOB1 expression in both the mRNA and protein level; thus, it was selected for further studies.

MTT viability assays were conducted to elucidate the potential biological effects of TOB1 in lung cancer cells. As shown in Figure 2C, the 95-D/TOB1 transfectants displayed about 50% reduction in proliferation rate compared with the "mock"-transfected 95-D cells on d 4 and d 7. Conversely, the A549/siRNA-TOB1–transfected cells showed a pronounced increase in growth rate at d 4, and about 20% increase in proliferation on d 7. The results imply that TOB1 plays a key role in the growth control of lung cancer cells. Cell cycle analysis was

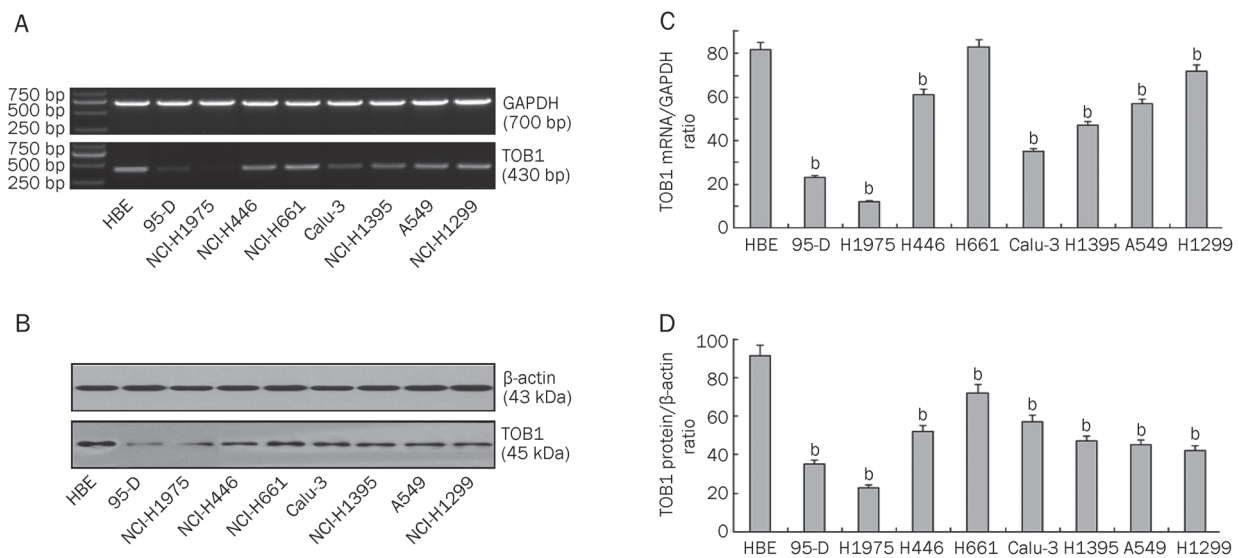

Figure 1. TOB1 expression is variably decreased in eight lung cancer cell lines. (A) Expression of TOB1 mRNA in lung cancer cell lines assayed via RT-PCR; GAPDH was used as the loading control. Total RNA was extracted from normal and lung cancer cells. The 430 bp TOB1 cDNA fragments were separated and visualized by 1% agarose gel electrophoresis and ethidium bromide staining. (B) Expression of TOB1 protein in normal epithelial cell line HBE and eight lung cancer cell lines, separately assayed via Western blot analysis with β-actin as the loading control. Whole cell lysates (50 μg) from each of the nine cell lines were separated using SDS-PAGE and transferred onto PVDF membranes. Bands were visualized using monoclonal anti-TOB1 antibodies with a chemiluminescence detection system. All experiments were performed independently at least three times. Mean±SD. ^bP<0.05 *vs* HBE cells.

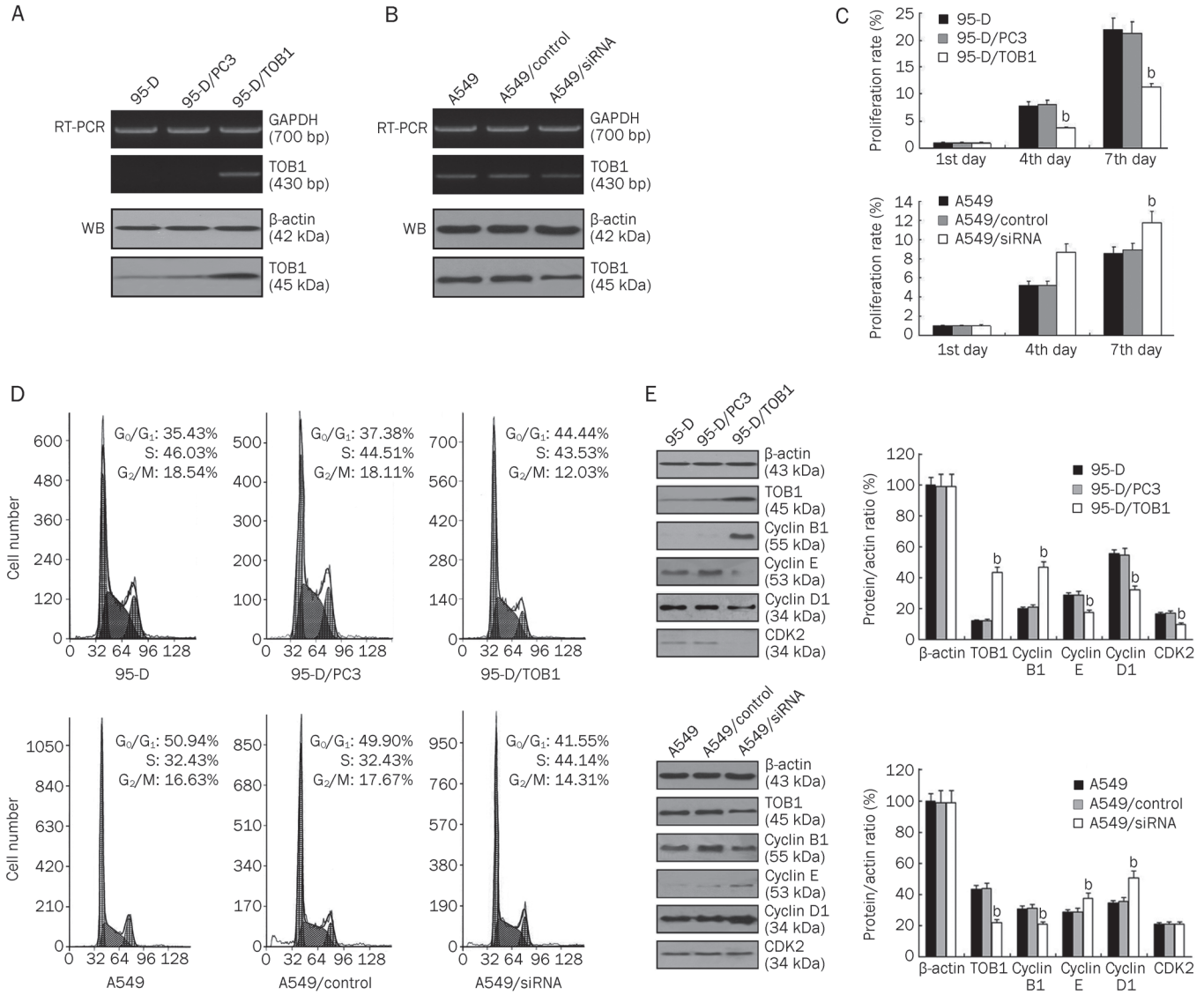

Figure 2. TOB1 regulates proliferation and modulates cell cycle progression of the non-small cell lung cancer cell lines 95-D and A549. (A) Ectopic TOB1 expression was confirmed via RT-PCR and immunoblotting in a 95-D/TOB1 transfectant and compared with vector-transfected parental cells. GAPDH and β-actin were used as the loading controls. (B) TOB1 expression was significantly reduced (at least 30%) in A549/siRNA-TOB1 cells compared with the parental and control siRNA-transfected A549 cells. TOB1 expression was subjected to RT-PCR and Western blot using specific primer and monoclonal TOB1 antibody. GAPDH gene and β-actin protein expression were utilized as the loading controls. (C) TOB1 overexpression suppresses 95-D cell proliferation in MTT viability assays. In contrast, increased cell growth was observed in the A549/siRNA-TOB1 cells. A total of 4000 cells from each cell line were seeded in a 24-well plate. Cells were counted at d 1, 4, and 7. All samples were prepared in triplicate. The proliferation rate was measured as fold changes in cell growth. (D) TOB1 overexpression induced G_1 phase and G_2/M phase arrest in the 95-D lung cancer cell line. The decreased TOB1 expression caused a decrease in the G_1 population and an increase in the S phase population of A549 cells. Sub-confluent proliferating cells were stained with propidium iodide and subjected to FACS analysis to determine the cell cycle distribution. (E) In the 95-D cells, TOB1 overexpression increased cyclin B1 expression, and negatively regulated the expression of cyclin D1, cyclin E, and CDK2. TOB1-siRNA transfection increased the expression of cyclin D1 and cyclin E, but slightly reduced cyclin B1 expression. The cells were harvested using trypsin and centrifugation. Equal aliquots of the total protein (50 μg) were analyzed by SDS-PAGE and blotted to detect cyclin B1, cyclin D1, and cyclin E protein expression. The protein expression was expressed as fold changes in band density, with β-actin as the loading control. All the experiments were performed independently at least three times. Mean±SD. $^bP<0.05$ *vs* the control group.

then performed on the TOB1 transfectants and TOB1 knock-down lung cancer cells. The results in Figure 2D suggest that relative to the parental and vector-transfected "mock" cells, exogenous TOB1 overexpression in the 95-D cells significantly induced cell accumulation in the G_1 phase (t=7.16; P<0.05) and a modest decrease in percentage from 18% to 12% in the G_2/M population (t=6.83; P<0.05). Conversely, decreased TOB1 expression caused a decrease in the G_1 population (t=4.30;

$P<0.05$) and an increase in the S phase population ($t=7.01$; $P<0.05$) compared with the parental or control siRNA-transfected A549 cells.

The functional role of TOB1 expression on cell cycle modulators was further investigated. The alterations in the different cyclins in TOB1-overexpressing or siRNA-TOB1 lung cancer cells were evaluated and compared with the parental or "mock" cells using Western blot analysis. Figure 2E shows that cyclin B1 expression increased three-fold in the 95-D/TOB1 cells, but remarkably decreased in the siRNA-TOB1 A549 cells. The expression levels of cyclin E, CDK2, and cyclin D1 were significantly suppressed in the 95-D/TOB1 cells. In contrast, cyclin E and cyclin D1 expression were both increased in the A549/siRNA-TOB1-transfected cells. These results suggest that TOB1 might partly participate in cell cycle progression regulation by adjusting cyclin expression.

Alteration of the aggressiveness of lung cancer cells by TOB1 protein

A critical event in tumor metastasis and progression is the ability of tumor cells to invade the extracellular matrix, allowing tumor cells to move beyond the restrictions of the primary tumor environment. To examine the competence of cells to invade through biological matrices *in vitro*, Transwell assay was carried out as described previously[20]. The results show that compared with the parental cells, amplified TOB1 expression vigorously inhibited the ability of the 95-D cells to invade through the filter coated with Matrigel. As shown in Figure 3A, the invasion rate of 95-D/TOB1 cells decreased by more than 80% corresponding to the parental and vector-transfected cells ($t=68.56$; $P<0.05$). In contrast, the invasion rate of A549 cells transfected with TOB1-siRNA increased by 2.5-fold ($t=5.17$; $P<0.05$) in contrast to the control cells (Figure 3B).

To determine whether the decreased invasiveness caused by TOB1 is associated with cell motility, the effect of TOB1 on cell migration capacity was analyzed using a wound healing assay[25]. The cells were scratch-wounded with sterile pipette tips and post-incubated for an additional 48 h. Figure 3C and 3D show that cell flattening and spreading along the edges of the wound were significantly more obvious in the A549/siRNA cells than in the A549 cells ($t=6.51$; $P<0.05$), and were significantly lesser in 95-D/TOB1 cells than in the parental lung cancer cells ($t=5.93$; $P<0.05$).

Taken together, these results indicate that *TOB1* gene expression significantly inhibits cell invasion and migration *in vitro*, and the knockdown of TOB1 conversely increases the ability of lung cancer cells to invade and migrate.

TOB1 mediates anti-metastasis effects through alterations of PTEN-mediated modulation of downstream signaling

RT-PCR and Western blot analysis were utilized to identify additional targets of TOB1 that might be involved in down-regulating lung cancer metastasis. PTEN, an important tumor suppressor mutated in a wide range of malignancies second only to p53, which is a central negative regulatory factor of epidermal growth factor receptor (EGFR) downstream of phosphoinositide 3 kinase (PI3K)-Akt (Akt8 virus oncogene cellular homolog) pathway. It plays a key role in cell proliferation, survival, and malignant transformation by regulating the mitogen-activated protein kinase (MAPK) and the PI3K/Akt and integrin-focal adhesion kinase (FAK) pathways. Recent studies have investigated several signaling pathways, such as MAPK and Akt, through which TOB1 conducts its tumor suppressor activity. In lung cancer, the functional pathways of TOB1 remain to be elucidated.

In the present study, RT-PCR was used to detect the effects of TOB1 on PTEN mRNA expression. TOB1 overexpression in the 95-D cells increased PTEN mRNA expression up to two-fold in the control cells, whereas PTEN mRNA was reduced in the TOB1-siRNA–transfected A549 cells (Figure 4A). Western blot analysis was then conducted to identify the effects of TOB1 on the PI3K/PTEN pathways. The results show that TOB1 overexpression slightly decreased EGFR expression, thereby significantly suppressing the expression of downstream effecters Akt and ERK1/2, but had no obvious effects on the expression of these proteins. Reduced NF-κB (p65) and increased IκB-α phosphorylation were observed in the 95-D/TOB1 cells. TOB1 overexpression amplified E-cadherin expression and slightly downregulated α-/β-/γ-catenin (Figure 4B). In addition, decreased MMP-2 and MMP-9 expression were also detected in the 95-D/TOB1 cells. In the TOB1-knockdown A549 cells, the contradictory effects on almost all these downstream factors were confirmed, as shown in Figure 4C. The variations in gene expression caused by the different TOB1 expression levels suggest that TOB1 might be a multifunctional regulator of the metastasis of lung cancer cells. The effects of TOB1 expression on the activities of MMPs were also determined with a gelatin zymography assay, as shown in Figure 4D. TOB1-overexpressing 95-D cells exhibited decreased MMP2 ($t=4.61$; $P<0.05$) and MMP9 ($t=6.19$; $P<0.05$) activity in contrast to the parental and mock-transfected cells. RNAi-induced TOB1 knockdown in the A549 cells increased MMP2 activity to some extent ($t=9.10$; $P<0.05$).

These results reveal the ability of TOB1 to regulate most of the important downstream factors of the PI3K/PTEN signal pathway; therefore, the potential interaction between PTEN and TOB1 was further examined through an IP/immunoblot assay. The results indicate that the presence of PTEN protein in the TOB1 IP of the A549 cells containing the wild-type *PTEN* gene and moderate *TOB1* gene expression, as shown in Figure 4E. In the TOB1-suppressed A549 cells, this protein–protein association was still observed, but to a lesser extent. Neither PTEN nor TOB1 was found in the normal mouse IgG IP, which was the negative control for the IP assay (data not shown). The results imply that TOB1 is actually associated with PTEN in the A549 cells.

Discussion

Recently, accumulated evidence has indicated that the *TOB1* gene is involved in the negative regulation of cell growth and functions as a tumor suppressor[26–28]. Alterations in TOB1 expression have been reported in a variety of human malig-

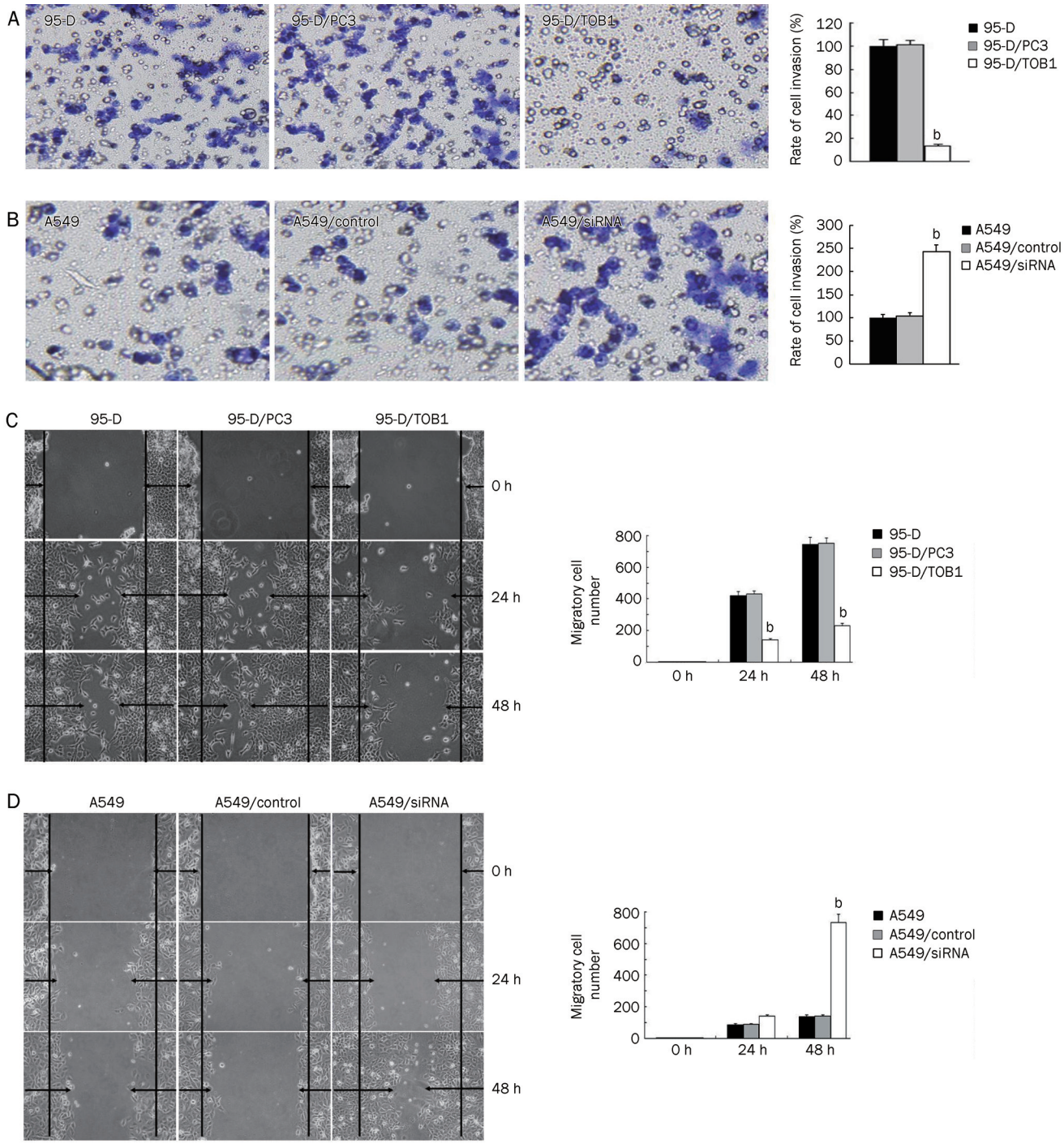

Figure 3. TOB1 expression is inversely correlated with lung cancer cell metastasis *in vitro*. (A) TOB1 overexpression prevented highly invasive 95-D cells from invading. 95-D, 95-D/PC3, and 95-D/TOB1 cells grown to subconfluence were trypsinized and transferred into the upper compartment of the modified Transwell chambers (3×10^5 cells/chamber). RPMI 1640 plus 10% FCS (500 μL/chamber) as a chemo attracter was added to the lower compartment. After 24 h incubation, the invasive cells attached to the lower surface of the Matrigel-coated filter were fixed, stained, and photographed under a phase contrast microscope and then counted in 15 randomly selected microscopic fields. $^bP<0.05$ *vs* the control group. (B) Less invasive A549 cells regained their invasiveness with the knockdown of TOB1 expression. Exponential A549, A549/control siRNA, and A549/siRNA-TOB1 cells were seeded onto the modified Transwell chambers (3×10^5 cells/chamber). After 24 h of chemoattraction with 10% FCS, the cells that invaded through the artificial basement membrane were visualized, counted, and analyzed. $^bP<0.05$ *vs* the control group. (C) Ectopic TOB1 expression decreased lung cancer cell migration ability. Confluent 95-D, 95-D/PC3, and 95-D/TOB1 cells cultured in six-well dishes were carefully wounded using sterile pipette tips. After 12 or 24 h, the cells were photographed under a phase contrast microscope. (D) Confluent A549, A549/control siRNA, and A549/siRNA-TOB1 cells were also wounded as described above. The number of cells migrating into the initial wound area was counted and expressed as mean±SD. $^bP<0.05$ *vs* the control group. All experiments were performed at least three times independently.

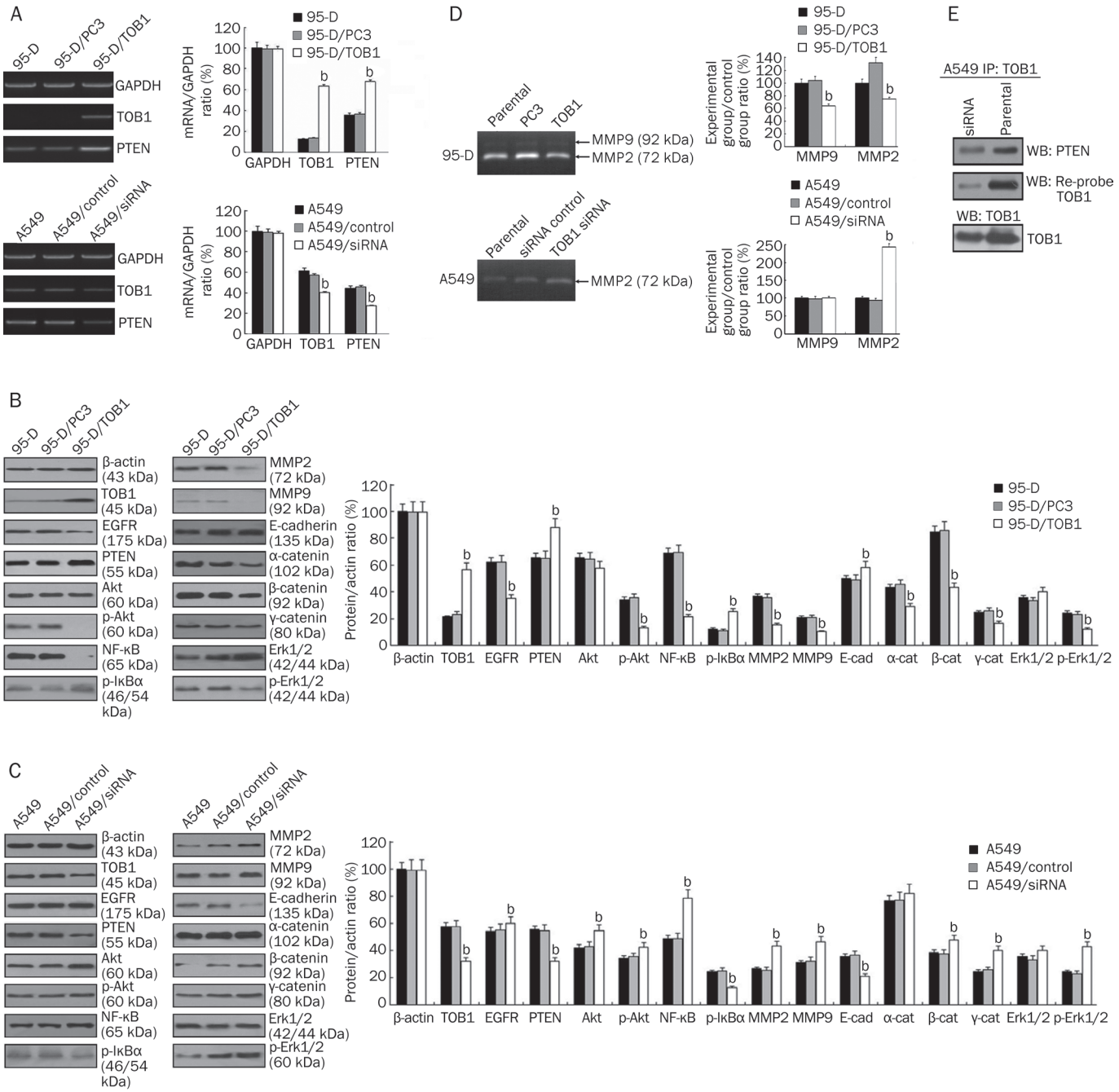

Figure 4. TOB1 is involved in the modulation of PI3K/PTEN downstream signaling pathways. (A) TOB1 regulated PTEN expression. RT-PCR assays were performed to determine the expression of PTEN mRNA in TOB1-overexpressing 95-D cells and TOB1 knockdown A549 cells. The PCR products were separated and visualized via agarose gel electrophoresis. mRNA expression was measured as fold changes in band density, with GAPDH as the loading control. $^{b}P<0.05$ *vs* the control group. (B) Whole cell lysates from 95-D/TOB1, 95-D parental cells, and vector "mock"-transfected 95-D cells were prepared, and 50 μg of proteins were resolved using SDS-PAGE, followed by immunoblotting with the indicated specific antibodies against EGFR, PTEN, TOB1, p-AKT, AKT, p-ERK1/2, ERK1/2, NF-κB, p-IκB-α, E-cadherin, α-catenin, β-catenin, and γ-catenin. (C) A549, A549/control siRNA, and A549/siRNA-TOB1 cells were harvested, and equal aliquots of the protein were subjected to a Western blot assy. The expression and activity of specific downstream factors in the PI3K/PTEN pathway were detected. The expression levels are displayed as fold changes in band density. $^{b}P<0.05$ *vs* the control group. (D) TOB1 affected activities of MMP2 and MMP9 in A549 and 95-D cells. The conditioned medium was collected and quantified, and 20 μg total protein per sample was separated by SDS-PAGE containing 500 μg/mL gelatin. After incubation, developing, and staining, the gelatinase activity of the MMPs was visualized and analyzed as band density. $^{b}P<0.05$ *vs* the control group. The representative zymograph was from three independent experiments. (E) TOB1 forms protein–protein complex with PTEN. Whole cell lysates were prepared from A549 and A549/siRNA-TOB1 cells. About 1 μg of lysate was immunoprecipitated with anti-TOB antibodies. The immunoprecipitated proteins were subsequently separated by SDS-PAGE, followed by immunoblotting with anti-PTEN antibody, and then reprobing with TOB1 antibodies.

nancies including thyroid and breast cancers[26]. In human lung cancer, in 2003, Iwanaga *et al*[15] reported reduced TOB1 expression in most of his 43 clinical specimens, but the exact biological effects of TOB1 on lung cancer carcinogenesis and progression remain unclear. In the present study, based on gain-of-function and loss-of-function principles, the roles of TOB1 in lung cancer cells have been demonstrated and TOB1-mediated downstream signaling pathways have been preliminarily explored. First, the variously decreased TOB1 mRNA and protein expression was revealed in eight lung cancer cell lines in contrast to the normal HBE cell line. These *in vitro* data confirm the findings of Iwanaga *et al*[15] that suppressed TOB1, which may be a tumor suppressor, is an important factor in human lung cancer cells.

One of the essential functions of tumor suppressors is to suppress tumor growth effectively by negatively regulating the cell cycle and/or inducing apoptosis[29-31]. The anti-proliferation activity of TOB1 in 95-D cells *in vitro* is because of increased TOB1 expression. Conversely, siRNA-mediated TOB1 downregulation in the A549 cells led to promoted growth rate, providing a supplementary confirmation for the gain-of-function experiments. The cell cycle analysis also provided evidence that TOB1 induces cell cycle arrest in lung cancer cells. Ectopic TOB1 expression in the 95-D cells caused an accumulation of cells in the G_1 and G_2/M phases and decreased the percentage of cells entering the S phase. TOB1 knockdown led to the S phase arrest of A549 cells. TOB1 overexpression results in increased cyclin B1 and decreased expression of cyclin D1, cyclin E, and CDK2. Together with the loss-of-function experiments, these results provide further evidence that the antitumor effects of TOB1 in the lung cancer cells are partly caused by its regulation of the cell cycle.

Despite cell cycle regulation and apoptosis induction, several tumor suppressors are involved in preventing tumor cells from dispersing, blocking loss of contact inhibition, and inhibiting metastasis[32–35]. We demonstrated for the first time that TOB1 overexpression significantly inhibits the ability of the highly invasive lung cancer cell line 95-D to invade through an artificial basement membrane and prevents cell migration *in vitro*. For the less invasive A549 cells, the partial knockdown of TOB1 by siRNA significantly promotes their invasiveness and migration *in vitro*.

In lung cancer, one of the well-studied pathways is EGFR and its downstream signaling cascade, which is involved in cellular proliferation, apoptosis, and metastasis[36]. The EGFR pathway has already been clinically accepted as a therapeutic target in advanced non-small cell lung cancer and other solid tumors in recent years[37]. Principle data suggest that EGFR heterodimer or homodimer formation induced by ligand binding activates the intracellular tyrosine kinase domain, consequently inducing additional downstream pathways via PLC-γ, MAPK, and PI3K, and finally affecting cell survival and metastasis through these downstream cascades[38–40]. In the current study, TOB1 overexpression reduced EGFR expression, whose phosphorylation is involved in MAP kinase signaling activation[41, 42]. Significantly decreased MAPK (ERK1/2 T185+Y187+T202+Y204) and Akt (Ser473) activity was observed in TOB1-transfected 95-D cells. Conversely, increased EGFR, MAPK, and Akt activity was observed in TOB1-knockdown A549 cells. Drastically reduced NF-κB (p65) and increased phosphorylation of IκB-α were observed in TOB1-overexpressing 95-D cells. In contrast, TOB1-siRNA promoted NF-κB expression and suppressed IκB-α phosphorylation. These results are correlated with the findings of Kojima *et al*[43] that the activation NF-κB stimulates invasion and metastasis via its regulation of MMP and cyclin D1 expression. We also found that variations in cellular TOB1 protein profoundly affect the expression of E-cadherin, α-, β-, and γ-catenin. Meanwhile, α-, β-, and γ-catenin bind to the highly conserved intracellular cytoplasmic tail of E-cadherin, and the catenin/cadherin complexes play important roles in mediating cellular adhesion[44–46]. Aside from its biological function, when not complexed with cadherins, β-catenin is an important downstream factor in the Wnt/β-catenin pathway[47, 48], which can interact with transcription factors and regulate gene transcription; thus, it is involved in the regulation of proliferation and differentiation. The negative regulation of the expression of β-catenin and the downstream factors of Wnt/β-catenin pathway by TOB1 inhibited β-catenin transcriptional activity[49]. In the 95-D/TOB1 and A549-siRNA TOB1 cells, varied MMP-2 and MMP-9 expression and activity is responsible for the degradation of extracellular matrix components, including collagen, gelatin, fibronectin, laminin, and proteoglycans[50–52]. Thus, suppression of β-catenin–regulated transcription, which induces the expression of proliferative and progressive genes such as cyclin D1 and MMPs via the PI3K/PTEN pathway, may at least mediate the anti-proliferative and anti-metastasis function of TOB1 in lung cancer cells[53, 54].

In addition, the solid protein–protein interaction between TOB1 and PTEN in human lung cancer A549 cells, aside from the expression regulation effects of TOB1 on PTEN, is shown for the first time. These results provide several clues to outline the signal cascades and specific targets of TOB1-related proliferation and metastasis regulation in lung cancer cells (Figure 5).

In conclusion, TOB1 is expressed in normal HBE cells, and the reduction of TOB1 expression is a common event in eight lung cancer cell lines. TOB1 functions as a tumor suppressor in NSCLC 95-D and A549 cells by modulating EGFR and its downstream signaling pathways through the direct or indirect interaction with the key tumor suppressor PTEN[55, 56]. However, whether the biological effects of TOB1 in lung cancer cells are triggered by its regulation on PTEN expression as a transcription factor or by its effect on PTEN phosphatase activity remain unclear. Whether TOB1 affects PTEN through other mechanisms, such as PTEN phosphorylation, ubiquitination, acetylation, or oxidation, in terms of carcinogenesis and progression is unknown. Further studies on the involvement of TOB1 in lung cancer carcinogenesis and progression are necessary; these will allow the development of more accurate theories to guide therapeutic practice.

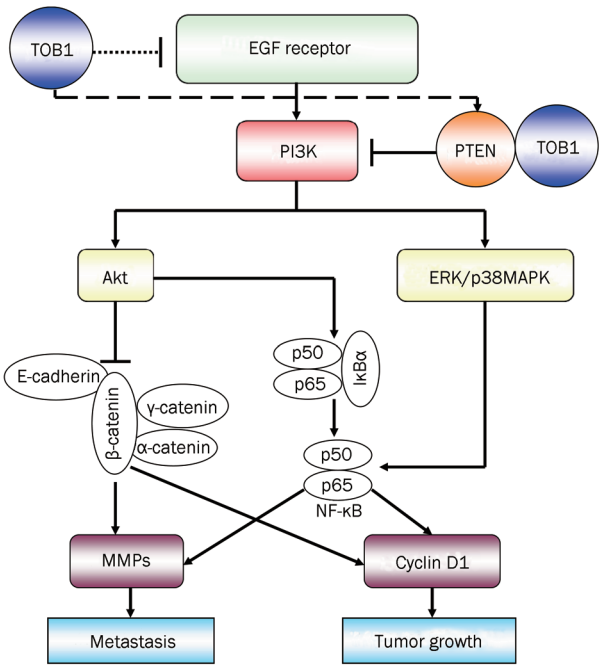

Figure 5. TOB1 was involved in regulation of tumor growth and metastasis via the PI3K/PTEN signaling pathway. The binding of EGF to the corresponding EGF receptors activates PI3K and downstream signaling pathways, including Akt and ERK/p38 MAPK, leading to the activation of NF-κB gene expression. Consequently, the expression of cyclin D1 and MMPs are increased, resulting in the promotion of lung cancer tumorigenesis and metastasis. Despite its activation of NF-κB, Akt can also inhibit β-catenin expression, which plays an important role in mediating cellular adhesion together with α- and γ-catenin/cadherin complexes. In the present study, TOB1 was identified as a negative regulator of EGFR expression, increasing the expression of PTEN, which functions as the central negative regulator of the PI3K/AKT pathway in controlling tumorigenesis and metastasis. The protein–protein interaction between TOB1 and PTEN was detected for the first time in cultured lung cancer cells; hence, TOB1 may be a regulator of PTEN activity.

Acknowledgements

This work was supported by grants from the Program for Changjiang Scholars and Innovative Research Team in University (IRT0849), the National Natural Science Foundation of China (No 81071906), the Doctoral Fund of Ministry of Education of China (K512602110), the College Nature Science Foundation of Jiangsu Province (SZ126821), and the Priority Academic Program Development of Jiangsu Higher Education Institutions.

Author contribution

Ke-kang SUN, Lin ZHAO, Jia-ying XU, and Li-li WANG performed experiments and interpreted data; Yang JIAO and Sai-jun FAN supervised all aspects of this research; and Ke-kang SUN and Yang JIAO prepared the manuscript.

References

1 Jemal A, Bray F, Center MM, Ferlay J, Ward E, Forman D. Global cancer statistics. CA Cancer J Clin 2011; 61: 69–90.
2 Inamura K, Ishikawa Y. Lung cancer progression and metastasis from the prognostic point of view. Clin Exp Metastasis 2010; 27: 389–97.
3 Mihaljevic AL, Michalski CW, Friess H, Kleeff J. Molecular mechanism of pancreatic cancer — understanding proliferation, invasion, and metastasis. Langenbecks Arch Surg 2010; 395: 295–308.
4 Hoon DS, Ferris R, Tanaka R, Chong KK, Alix-Panabieres C, Pantel K. Molecular mechanisms of metastasis. J Surg Oncol 2011; 103: 508–17.
5 Andjelkovic T, Bankovic J, Stojsic J, Milinkovic V, Podolski-Renic A, Ruzdijic S, *et al*. Coalterations of p53 and PTEN tumor suppressor genes in non-small cell lung carcinoma patients. Transl Res 2011; 157: 19–28.
6 Yoneda M, Suzuki T, Nakamura T, Ajima R, Yoshida Y, Kakuta S, *et al*. Deficiency of antiproliferative family protein Ana correlates with development of lung adenocarcinoma. Cancer Sci 2009; 100: 225–32.
7 Mukhopadhyay UK, Mooney P, Jia L, Eves R, Raptis L, Mak AS. Doubles game: Src-Stat3 versus p53-PTEN in cellular migration and invasion. Mol Cell Biol 2010; 30: 4980–95.
8 Cristofanilli M, Krishnamurthy S, Guerra L, Broglio K, Arun B, Booser DJ, *et al*. A nonreplicating adenoviral vector that contains the wild-type p53 transgene combined with chemotherapy for primary breast cancer: safety, efficacy, and biologic activity of a novel gene-therapy approach. Cancer 2006; 107: 935–44.
9 Matsuda S, Kawamura-Tsuzuku J, Ohsugi M, Yoshida M, Emi M, Nakamura Y, *et al*. Tob, a novel protein that interacts with p185erbB2, is associated with anti-proliferative activity. Oncogene 1996; 12: 705–13.
10 Winkler GS. The mammalian anti-proliferative BTG/Tob protein family. J Cell Physiol 2010; 222: 66–72.
11 Wang XM, Gao X, Zhang XH, Tu YY, Jin ML, Zhao GP, *et al*. The negative cell cycle regulator, Tob (transducer of ErbB-2), is involved in motor skill learning. Biochem Biophys Res Commun 2006; 340: 1023–7.
12 Jia S, Meng A. Tob genes in development and homeostasis. Dev Dyn 2007; 236: 913–21.
13 Mauxion F, Chen CY, Seraphin B, Shyu AB. BTG/TOB factors impact deadenylases. Trends Biochem Sci 2009; 34: 640–7.
14 Yoshida Y, Nakamura T, Komoda M, Satoh H, Suzuki T, Tsuzuku JK, *et al*. Mice lacking a transcriptional corepressor Tob are predisposed to cancer. Genes Dev 2003; 17: 1201–6.
15 Iwanaga K, Sueoka N, Sato A, Sakuragi T, Sakao Y, Tominaga M, *et al*. Alteration of expression or phosphorylation status of tob, a novel tumor suppressor gene product, is an early event in lung cancer. Cancer Lett 2003; 202: 71–9.
16 Ito Y, Suzuki T, Yoshida H, Tomoda C, Uruno T, Takamura Y, *et al*. Phosphorylation and inactivation of Tob contributes to the progression of papillary carcinoma of the thyroid. Cancer Lett 2005; 220: 237–42.
17 Yoshida Y, von Bubnoff A, Ikematsu N, Blitz IL, Tsuzuku JK, Yoshida EH, *et al*. Tob proteins enhance inhibitory Smad-receptor interactions to repress BMP signaling. Mech Dev 2003; 120: 629–37.
18 Helms MW, Kemming D, Contag CH, Pospisil H, Bartkowiak K, Wang A, *et al*. TOB1 is regulated by EGF-dependent HER2 and EGFR signaling, is highly phosphorylated, and indicates poor prognosis in node-negative breast cancer. Cancer Res 2009; 69: 5049–56.
19 Yoshida Y, Tanaka S, Umemori H, Minowa O, Usui M, Ikematsu N, *et al*. Negative regulation of BMP/Smad signaling by Tob in osteoblasts. Cell 2000; 103: 1085–97.
20 Wu QF, Liu C, Tai MH, Liu D, Lei L, Wang RT, *et al*. Knockdown of FoxM1 by siRNA interference decreases cell proliferation, induces cell

cycle arrest and inhibits cell invasion in MHCC-97H cells *in vitro*. Acta Pharmacol Sin 2010; 31: 361–6.
21 Li XL, Meng QH, Fan SJ. Adenovirus-mediated expression of UHRF1 reduces the radiosensitivity of cervical cancer HeLa cells to gamma-irradiation. Acta Pharmacol Sin 2009; 30: 458–66.
22 Jiao Y, Ge CM, Meng QH, Cao JP, Tong J, Fan SJ. Adenovirus-mediated expression of Tob1 sensitizes breast cancer cells to ionizing radiation. Acta Pharmacol Sin 2007; 28: 1628–36.
23 Jiao Y, Ge CM, Meng QH, Cao JP, Tong J, Fan SJ. Dihydroartemisinin is an inhibitor of ovarian cancer cell growth. Acta Pharmacol Sin 2007; 28: 1045–56.
24 Wu CY, Wu MS, Chiang EP, Chen YJ, Chen CJ, Chi NH, *et al*. Plasma matrix metalloproteinase-9 level is better than serum matrix metalloproteinase-9 level to predict gastric cancer evolution. Clin Cancer Res 2007; 13: 2054–60.
25 Takata F, Dohgu S, Matsumoto J, Takahashi H, Machida T, Wakigawa T, *et al*. Brain pericytes among cells constituting the blood-brain barrier are highly sensitive to tumor necrosis factor-alpha, releasing matrix metalloproteinase-9 and migrating *in vitro*. J Neuroinflammation 2011; 8: 106.
26 O'Malley S, Su H, Zhang T, Ng C, Ge H, Tang CK. TOB suppresses breast cancer tumorigenesis. Int J Cancer 2009; 125: 1805–13.
27 Yanagie H, Tanabe T, Sumimoto H, Sugiyama H, Matsuda S, Nonaka Y, *et al*. Tumor growth suppression by adenovirus-mediated introduction of a cell-growth-suppressing gene tob in a pancreatic cancer model. Biomed Pharmacother 2009; 63: 275–86.
28 Park GT, Seo EY, Lee KM, Lee DY, Yang JM. Tob is a potential marker gene for the basal layer of the epidermis and is stably expressed in human primary keratinocytes. Br J Dermatol 2006; 154: 411–8.
29 Tzachanis D, Boussiotis VA. Tob, a member of the APRO family, regulates immunological quiescence and tumor suppression. Cell Cycle 2009; 8: 1019–25.
30 Lee EY, Muller WJ. Oncogenes and tumor suppressor genes. Cold Spring Harb Perspect Biol 2010; 2: a003236.
31 Hurst DR, Welch DR. Metastasis suppressor genes at the interface between the environment and tumor cell growth. Int Rev Cell Mol Biol 2011; 286: 107–80.
32 Lin ML, Lu YC, Chung JG, Wang SG, Lin HT, Kang SE, *et al*. Down-regulation of MMP-2 through the p38 MAPK-NF-kappaB-dependent pathway by aloe-emodin leads to inhibition of nasopharyngeal carcinoma cell invasion. Mol Carcinog 2010; 49: 783–97.
33 Wang S, Cheng Z, Yang X, Deng K, Cao Y, Chen H, *et al*. Effect of wild type PTEN gene on proliferation and invasion of multiple myeloma. Int J Hematol 2010; 92: 83–94.
34 Abou Youssif T, Fahmy MA, Koumakpayi IH, Ayala F, Al Marzooqi S, Chen G, *et al*. The mammalian target of rapamycin pathway is widely activated without PTEN deletion in renal cell carcinoma metastases. Cancer 2011; 117: 290–300.
35 De Roock W, De Vriendt V, Normanno N, Ciardiello F, Tejpar S. KRAS, BRAF, PIK3CA, and PTEN mutations: implications for targeted therapies in metastatic colorectal cancer. Lancet Oncol 2011; 12: 594–603.
36 Ho-Pun-Cheung A, Assenat E, Bascoul-Mollevi C, Bibeau F, Boissière-Michot F, Cellier D, *et al*. EGFR and HER3 mRNA expression levels predict distant metastases in locally advanced rectal cancer. Int J Cancer 2011; 128: 2938–46.
37 Pennell NA, Lynch TJ Jr. Combined inhibition of the VEGFR and EGFR signaling pathways in the treatment of NSCLC. Oncologist 2009; 14: 399–411.
38 Capodanno A, Camerini A, Orlandini C, Baldini E, Resta ML, Bevilacqua G, *et al*. Dysregulated PI3K/Akt/PTEN pathway is a marker of a short disease-free survival in node-negative breast carcinoma. Hum Pathol 2009; 40: 1408–17.
39 Jin G, Kim MJ, Jeon HS, Choi JE, Kim DS, Lee EB, *et al*. PTEN mutations and relationship to EGFR, ERBB2, KRAS, and TP53 mutations in non-small cell lung cancers. Lung Cancer 2010; 69: 279–83.
40 Piguet AC, Dufour JF. PI(3)K/PTEN/AKT pathway. J Hepatol 2011; 54: 1317–9.
41 Weickhardt AJ, Tebbutt NC, Mariadason JM. Strategies for overcoming inherent and acquired resistance to EGFR inhibitors by targeting downstream effectors in the RAS/PI3K pathway. Curr Cancer Drug Targets 2010; 10: 824–33.
42 Blanco-Aparicio C, Renner O, Leal JF, Carnero A. PTEN, more than the AKT pathway. Carcinogenesis 2007; 28: 1379–86.
43 Kojima M, Morisaki T, Sasaki N, Nakano K, Mibu R, Tanaka M, *et al*. Increased nuclear factor-kB activation in human colorectal carcinoma and its correlation with tumor progression. Anticancer Res 2004; 24: 675–81.
44 Fu C, Jiang A. Generation of tolerogenic dendritic cells via the E-cadherin/beta-catenin-signaling pathway. Immunol Res 2010; 46: 72–8.
45 Lyon C, Mill C, Tsaousi A, Williams H, George S. Regulation of VSMC behavior by the cadherin-catenin complex. Front Biosci 2011; 16: 644–57.
46 Zeljko M, Pecina-Slaus N, Martic TN, Kusec V, Beros V, Tomas D. Molecular alterations of E-cadherin and beta-catenin in brain metastases. Front Biosci (Elite Ed) 2011; 3: 616–24.
47 Stein U, Arlt F, Smith J, Sack U, Herrmann P, Walther W, *et al*. Intervening in beta-catenin signaling by sulindac inhibits S100A4-dependent colon cancer metastasis. Neoplasia 2011; 13: 131–44.
48 Phillips BT, Kimble J. A new look at TCF and beta-catenin through the lens of a divergent *C elegans* Wnt pathway. Dev Cell 2009; 17: 27–34.
49 Xiong B, Rui Y, Zhang M, Shi K, Jia S, Tian T, *et al*. Tob1 controls dorsal development of zebrafish embryos by antagonizing maternal beta-catenin transcriptional activity. Dev Cell 2006; 11: 225–38.
50 Soto-Guzman A, Navarro-Tito N, Castro-Sanchez L, Martinez-Orozco R, Salazar EP. Oleic acid promotes MMP-9 secretion and invasion in breast cancer cells. Clin Exp Metastasis 2010; 27: 505–15.
51 Sato H, Takino T. Coordinate action of membrane-type matrix metalloproteinase-1 (MT1-MMP) and MMP-2 enhances pericellular proteolysis and invasion. Cancer Sci 2010; 101: 843–7.
52 Poincloux R, Lizarraga F, Chavrier P. Matrix invasion by tumour cells: a focus on MT1-MMP trafficking to invadopodia. J Cell Sci 2009; 122: 3015–24.
53 Liu W, Zhou Y, Reske SN, Shen C. PTEN mutation: many birds with one stone in tumorigenesis. Anticancer Res 2008; 28: 3613–9.
54 Jiang BH, Liu LZ. PI3K/PTEN signaling in angiogenesis and tumorigenesis. Adv Cancer Res 2009; 102: 19–65.
55 Gildea JJ, Herlevsen M, Harding MA, Gulding KM, Moskaluk CA, Frierson HF, *et al*. PTEN can inhibit *in vitro* organotypic and *in vivo* orthotopic invasion of human bladder cancer cells even in the absence of its lipid phosphatase activity. Oncogene 2004; 23: 6788–97.
56 Poon JS, Eves R, Mak AS. Both lipid- and protein-phosphatase activities of PTEN contribute to the p53-PTEN anti-invasion pathway. Cell Cycle 2010; 9: 4450–4.

Acta Pharmacologica Sinica (2012) 33: 261–270
 1671-4083/12 $32.00
www.nature.com/aps

Original Article

A novel sulfonamide agent, MPSP-001, exhibits potent activity against human cancer cells *in vitro* through disruption of microtubule

Zu-long LIU[1], Wei TIAN[2], Yong WANG[3], Shan KUANG[1], Xiao-min LUO[3], Qiang YU[1, *]

[1]*Division of Anti-Tumor Pharmacology, Shanghai Institute of Materia Medica, Chinese Academy of Sciences, Shanghai 201203, China;* [2]*The School of Life Science and Biopharmaceutics of Shenyang Pharmaceutical University, Shenyang 110016, China;* [3]*Drug Discovery and Design Center, Shanghai, Institute of Materia Medica, Chinese Academy of Sciences, Shanghai 201203, China*

Aim: To evaluate the anti-cancer effects of a new sulfonamide derivative, 2-(N-(3-chlorophenyl)-4-methoxyphenylsulfonamido)-N-hydroxypropanamide (MPSP-001).
Methods: Human cancer cell lines (HepG2, THP-1, K562, HGC-27, SKOV3, PANC-1, SW480, Kba, HeLa, A549, MDA-MB-453, and MCF-7) were examined. The cytotoxicity of MPSP-001 was evaluated using the WST-8 assay. Cell cycle distribution was examined with flow cytometry. Mitotic spindle formation was detected using immunofluorescence microscopy. Apoptosis-related proteins were examined with Western blot using specific phosphorylated protein antibodies. Competitive tubulin-binding assay was performed to test whether the compound competitively bound to the colchicine site. Molecular docking was performed to explore the possible binding conformation.
Results: MPSP-001 potently inhibited the growth of the 12 different types of human cancer cells with the IC_{50} values ranging from 1.9 to 15.7 μmol/L. The compound exerted potent inhibition on the drug-resistant Kb/VCR and MCF-7/ADR cells, as on Kba and MCF-7 cells. In HeLa, HGC-27, A549, and other cells, the compound (5 μmol/L) caused cell cycle arrest at the G_2/M phase, and subsequently induced cell apoptosis. In Hela cells, it prevented the mitotic spindle formation. Furthermore, the compound dose-dependently inhibited polymerization of tubulin *in vitro*, and directly bound to the colchicine-site of β-tubulin. Molecular docking predicted that the compound may form two hydrogen bonds to the binding pocket. The compound showed synergistic effects with colchicine and taxol in blocking mitosis of HeLa cells.
Conclusion: MPSP-001 shows a broad-spectrum of anti-tumor efficacy in vitro and represents a novel structure with anti-microtubule activity.

Keywords: MPSP-001; sulfonamide; anticancer drug; microtubules; tubulin; mitotic spindle; drug resistance; drug synergism

Acta Pharmacologica Sinica (2012) 33: 261–270; doi: 10.1038/aps.2011.156

Introduction

Cancer chemotherapy has achieved significant success in the discovery of new drugs[1]. One of the most successful classes of antitumor drugs targets microtubules, the principal components of the cytoskeleton which is important in cell division, organelle transports, cytokinesis, maintenance of cell morphology and signal transduction[2]. The essential role of microtubules in mitosis and cell division makes them and their regulatory proteins important, and perhaps the best, targets for anticancer drugs[3, 4]. There are two categories of anti-microtubule compounds used to target highly proliferating malignant cells. One is microtubule depolymerizing agents such as colchicinoids and vinca alkaloids which inhibit tubulin polymerization[5]. The other one is microtubule polymerizing agents such as taxanes and epothilones which promote or stabilize the formation of tubulin polymer[6]. The anti-microtubule agents are also classified based on their binding sites on tubulin[7]. Recent studies suggest that the inhibitory effects of these drugs are due to their interruption of microtubule dynamics rather than to alternate the microtubule polymer mass[8]. The disruption of microtubule dynamics leads to the arrest of growing cells in metaphase/anaphase, causing apoptotic or non-apoptotic cell death. Although all of the anti-microtubule agents effectively inhibit microtubule dynamics *in vitro*, their effects against different types of cancers vary *in vivo*[9]. In addition, despite the success of taxanes and vinca alkaloids to inhibit the progres-

* To whom correspondence should be addressed.
E-mail qyu@sibs.ac.cn
Received 2011-05-18 Accepted 2011-10-20

sion of some cancers in clinical use, resistance to anti-microtubule agents encounter in many tumor types, particularly after multiple cycles of therapy[10, 11]. Therefore, there has been great interest in identifying and developing novel anti-microtubule drugs.

Sulfonamides have been in clinical use for several decades. Sulfonamides have antibacterial, diuretic, antidiabetic, antithyroid, antihypertensive and antiviral activities[12]. Recently, many novel sulfonamide derivatives have shown substantial antitumor activities[13, 14]. For instance, E7070 and E7010 are regarded as breakthroughs in the discovery of new sulfonamides with strong antineoplastic abilities. E7070 belongs to a class of novel cell cycle inhibitors that block cell cycle progression at multiple points, although its target remains unclear[15–18]. E7010 reversibly binds to the colchicine-binding site of tubulin and arrests cells in the mitotic phase[19–21]. Both E7010 and E7070 display antitumor activity against rodent and human tumor xenografts and are currently undergoing phase I/II clinical trials[15, 16, 20, 22]. Another sulfonamide, HMN-214, arrests cells in G_2/M phase and exhibits antitumor activity. This antitumor activity is mediated by cytotoxicity, via inhibiting polo-like kinase, and by down-regulation of MDR1 via binding to the B-subunit of the essential transcription factor NF-Y[23–25].

Here we report our discovery of a new benzenesulfonamide, MPSP-001, and study for its ability to inhibit tumor cell growth. We found that MPSP-001 had strong antiproliferative activity against human tumor cell lines, as well as the ability to overcome drug resistance. Analysis of the function and mechanism of MPSP-001 revealed that MPSP-001 is a microtubule-destabilizing agent. It inhibits microtubule polymerization, arrests cells at early stage of mitosis and induces apoptosis. Our data suggests that MPSP-001 is a novel anti-microtubule compound. Understanding the mechanism of MPSP-001 will increase our knowledge about anti-microtubule agents and help us to design other better benzenesulfonamide drugs with anti-cancer activity.

Materials and methods

Synthesis of compound MPSP-001

MPSP-001 was synthesized through a five-step synthetic route, starting from the commercially available 4-methoxybenzenesulfonyl chloride (a) and 3-chlorobenzeneamine (b). N-(3-chlorophenyl)-4-methoxybenzenesulfonamide(c) was synthesized from a and b, and reacted with ethyl *DL*-2-bromopropionate to give methyl 2-(N-(3-chlorophenyl)-4-methoxyphenylsulfonamido) propanoate (e). After hydrolyzation, condensation, the final product was synthesized in 20% yield and characterized by ^{1}HNMR, MS, and elemental analyses. ^{1}HNMR (400 MHz, $CDCl_3$) δ=9.39 (br·s, 1H, NH), 7.63 (d, J=8.2 Hz, 2H, ArH), 7.35 (d, J=8.3 Hz, 1H, ArH), 7.25 (dd, J=8.3, 7.6 Hz, 1H, ArH), 7.12 (s, 1H, ArH), 7.04 (d, J=7.6 Hz, 1H, ArH), 6.96 (d, J=8.1 Hz, 2H, ArH), 4.79 (s, 1H, CH), 3.89 (s, 3H, OCH_3), 1.15 (d, J=6.3, 3H, CH_3) ppm. MS (ESI): *m/z*=385 $[M+H]^+$. Anal Calcd for $C_{16}H_{17}ClN_2O_5S$: C, 49.94; H, 4.45; N, 7.28; S, 8.33. Found: C, 49.90; H, 4.44; N, 7.30; S, 8.36. The purity of MPSP-001 was not less than 95% (Radiochemical Purity, HPLC).

Chemicals and antibodies

Colchicine (COL), paclitaxel (Taxol), vincristin (VCR) and Adriamycin (ADR) were purchased from Sigma Chemical Co. Antibodies were obtained from following companies: poly(ADP-ribose) polymerase (PARP) (Cell Signalling Technology); α-tubulin, horseradish peroxidase (HRP)-conjugated secondary antibody (Santa Cruz Biotechnology); and fluorescent isothiocyanate (FITC)-conjugated secondary antibody (Ancell Corporation). Medium and reagents of cell culture were acquired from Invitrogen. All other chemicals were purchased from Sigma Chemical Co.

Cell culture and reagents

Human cancer cell lines (HepG2, THP-1, K562, HGC-27, SKOV3, PANC-1, SW480, HeLa, A549, and MDA-MB-453) used in this study were procured from American Type Culture Collection. Resistant cell lines KB/VCR, MCF-7/ADR, and their parental cells were provided by Professor Jian DING from Shanghai Institute of Materia Medica, Chinese Academy of Sciences. K562, THP-1, and A549 cells were grown in RPMI -1640 medium supplemented with 10% fetal bovine serum (FBS); MCF-7, HepG2, HGC-27, SKOV3, PANC-1, SW480, HeLa, and MDA-MB-453 cells were cultured in Dulbecco's modified Eagle's medium supplemented with 10% FBS. KB and KB/VCR were grown in Minimum Essential Medium Eagle's (MEM) medium and supplemented with 10% FBS, 2 mmol/L glutamine and 1 mmol/L pyruvic acid; MCF-7/ADR cells were cultured in MEM medium and supplemented with 10% FBS, 1 mmol/L pyruvic acid and 0.01 mg/mL insulin. All resistant cell lines were incubated in the drug-free medium for 3 days before harvesting for the growth inhibition assay.

Cytotoxicity assay

In vitro growth inhibition was assessed with the WST-8 assay[26]. Exponentially growing cells were seeded into 96-well plate at a density of 3000 to 10000 cells/well (depending on the doubling time of the cell lines) and cultured overnight. Then cells were treated with various concentrations of drugs and incubated for additional 48 h. A tetrazolium salt (WST-8) was added at the last 2 h before the end of culture. After continuous incubation for 2 h, the absorbance was measured by a microplate reader at a wavelength of 450 nm. The values shown as the means and SD of at least three independent experiments performed in duplicates.

Flow cytometry analysis

The cells were harvested and washed with PBS, resuspended in 1 mL of ice-cold 75% ethanol. After being left to stand overnight, cell pellets were collected by centrifugation, resuspended in 500 μL of hypotonic buffer (0.5% Triton X-100 in PBS and 0.5 μg/mL RNase), and incubated at 37 °C for 30 min. Then 25 μL of propidium iodide solution (50 μg/mL) was added, and the mixture was allowed to stand on ice for 1 h.

Fluorescence emitted from the propidium iodide-DNA complex was quantitated after excitation of the fluorescent dye by FAC-Scan cytometry. The histogram of DNA distribution was modeled as a sum of G_1, G_2/M, S phase, and a sub-G_1 population, by using ModFitLT software.

Immunofluorescence microscopy

After culturing for 48 h on coverslips, HeLa cells were incubated with drugs at various concentrations for 16 h. Cells were then fixed. After being blocked, cells were incubated with mouse monoclonal α-tubulin antibody for 2 h at 37 °C. The secondary antibody, fluorescein (FITC)-conjugated affinity goat anti-mouse IgG (H+L), was added and incubated for 1 h. Chromosomes were stained with 1 μg/mL DAPI in PBS. After washing with PBS, the slides were mounted and sealed. Fluorescence images were captured by using Leica TCS SP2 laser confocal microscope.

Western blot analysis

Cells were lysed in the ice-cold cell lysis buffer (pH 7.6) containing 0.5 mmol/L dithiothreitol, 0.2 mmol/L EDTA, 20 mmol/L HEPES, 2.5 mmol/L $MgCl_2$, 75 mmol/L NaCl, 0.1 mmol/L Na_3VO_4, 50 mmol/L NaF, and 0.1% Triton X-100. The protease inhibitors including 1 μg/mL aprotinin, 0.5 μg/mL leupeptin, and 100 μg/mL 4-(2-aminoethyl)-benzenesulfonyl fluoride were added to the cell suspension. The cell extracts were gently rotated at 4 °C for 30 min. After centrifugation, the pellets were discarded. Equal amounts of proteins were subjected to 8%–10% SDS-PAGE. After transfered onto nitrocellulose membranes, the proteins were hybridized with various antibodies according to the instructions provided by the manufacturers.

In vitro tubulin polymerization assay

The assay was essentially performed according to Kuo *et al*[27]. Briefly, the sample (100 μL of 3 mg/mL tubulin proteins) in TP buffer (100 mmol/L PIPES, pH 6.9, 2 mmol/L $MgCl_2$, 1 mmol/L GTP, and 15% glycerol) was placed in 96-well microtiter plates in the presence of test agents. Mixtures were warmed to 37 °C and the increase in absorbance was measured at 340 nm in TECAN Genois Pro Microplate Reader and recorded every 30 s for 1 h.

Competitive tubulin-binding assay

For colchicine competitive binding assay, tubulin was co-incubated with indicated concentrations of MPSP-001 and vincristine at 37 °C for 1 h. Then colchicine was added to a final concentration of 5 μmol/L. Fluorescence was determined using a Hitachi F-2500 spectrofluorometer (Tokyo, Japan) at excitation wavelengths of 365 nm and emission wavelengths of 435 nm. Blank values (buffer alone) as background were subtracted from all samples. Then the inhibition rate (IR) was calculated as follows: IR=F/F0 where F0 is the fluorescence of the 5 μmol/L colchicine-tubulin complex, and F is the fluorescence of a given concentration of MPSP-001 or vincristine (12.5 μmol/L, 25 μmol/L, 50 μmol/L and 100 μmol/L) competition with the 5 μmol/L colchicine-tubulin complex. Vincristine, not binding in the colchicine-site of tubulin, was added as a negative control[28].

Molecular modeling

The X-ray crystal structure of α,β-tubulin complexed with N-deacetyl-N-(2-mercaptoacetyl)-colchicine (DAMA-colchicine) was obtained from the Brookhaven Protein Data Bank (entry code: 1SA0[29]) as the target structures in the molecular docking. Compounds were docked into the colchicine binding site using Autodock 4.00[30]. For each compound, 30 docking runs were performed and the conformation with the lowest binding free energy was selected as the possible binding conformation.

Analysis of drug synergism

The Combination Index (CI) was calculated to determine whether the drugs interacted synergistically, additively, or antagonistically[31]. The CI is calculated by the following equation: $CI=D_1/(Dm)_1+D_2/(Dm)_2+D_1\times D_2/[(Dm)_1\times(Dm)_2]$, in which D_1 is the concentration of a drug necessary to achieve a particular effect in the combination; $(Dm)_1$ is the concentration of the same drug that will produce the identical level of effect by itself; D_2 is the concentration of the second drug that will produce a particular effect in the combination; and $(Dm)_2$ is the concentration of the second drug, which will produce the same level of effect by itself. CI>1 indicates antagonism, CI<1 indicates synergy, and CI=1 indicates additivity[32]. Two independent experiments were performed to obtain the CI. The representative data were shown in Table 2.

Statistical analysis

Unless stated otherwise, experiments were run in triplicate and results were compared in Excel by two-tailed unpaired *t*-test. In the case of the effects analysis of MPSP-001 on the aberrant mitotic spindle, the statistical analysis of incidence rates of non-bipoles and chromosome misalignment were used to determine significance[33].

Results

MPSP-001 inhibited growth of various human tumor cells

MPSP-001 is a novel sulfonamide agent and its chemical formula is $C_{16}H_{17}ClN_2O_5S$ yielding a molecular weight of 384.83 (Figure 1). We used the WST-8 assay to evaluate the antiproliferative effect of MPSP-001 on several representative human tumor cell lines: hepatocellular carcinoma (HepG2), leukemia (THP-1 and K562), gastric carcinoma (HGC-27), ovarian carci-

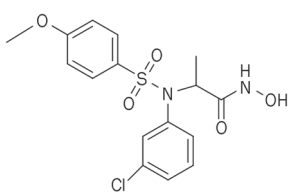

Figure 1. Chemical structure of MPSP-001.

noma (SKOV3), pancreatic carcinoma (PANC-1), colon adenocarcinoma (SW480), cervical carcinoma (KB and HeLa), lung adenocarcinoma (A549), and breast carcinoma (MDA-MB-453 and MCF-7). MPSP-001 inhibited the growth of all of the cancer cell lines that we tested with IC_{50} values ranging from 1.9 to 15.7 μmol/L (Table 1). Among the 10 solid tumor cell lines we analyzed, HeLa cell was the most sensitive cell line with an IC_{50} value about 8.1 μmol/L. We therefore used HeLa cells as a model cell in the following experiments.

Table 1. Growth inhibition of MPSP-001 against various human cancer cell lines.

Origin	Cell lines	IC_{50} (μmol/L)
Hepatocellular carcinoma	HepG2	9.1±4.2
Acute monocytic leukemia	THP-1	1.9±1.2
Chronic myelogenous leukemia	K562	6.9±3.9
Gastric carcinoma	HGC-27	15.7±2.6
Ovarian carcinoma	SKOV3	11.6±4.1
Pancreatic carcinoma	PANC-1	15.4±6.6
Colon adenocarcinoma	SW480	15.1±3.5
Cervical carcinoma	Kb[a]	8.4±2.9
Cervical carcinoma	HeLa	8.1±3.3
Lung adenocarcinoma	A549	15.0±5.8
Breast carcinoma	MDA-MB-453	14.8±4.5
Breast adenocarcinoma	MCF-7	12.4±2.7

Each value represents the mean±SD of three independent experiments.
[a]The KB cell line was originally derived from an epidermal carcinoma of the mouth but has now been shown to have HeLa characteristics.

MPSP-001 caused cell cycle arrest at the G_2/M phase and subsequently induced cell apoptosis.

We first analyzed the effects of MPSP-001 on cell cycle[34]. MPSP-001 induced a dose-dependent G_2/M arrest after 16 h of drug exposure. When exposed to 10 μmol/L MPSP-001 for 16 h, 80.11% of the cell population was blocked in G_2/M phase (Figure 2A). Similarly, MPSP-001 induced a time-dependent G_2/M arrest after different time of drug exposure. When exposed to 5 μmol/L MPSP-001 for 4, 8, 16 h, the cell population of HeLa cells in G_2/M phase was 33.74%, 46.27%, and 78.80%, respectively (Figure 2B). We further analyzed the effects of MPSP-001 on HGC-27, A549, and other cells, similar results were observed (data not shown). These data clearly indicated that MPSP-001 was a mitotic blocker.

We next analyzed the effects of MPSP-001 on cell death. The apoptosis, as indicated by the cleavage of PARP, occurred 16 h after the MPSP-001 treatment (Figure 3C).

MPSP-001 disrupted mitotic spindle in cells

Most of the anti-mitotic agents affect microtubules[35]. So the effects of MPSP-001 on microtubule structure were then examined by immuno-fluorescence microscopy using α-tubulin antibody. Normal control cells in metaphase displayed a bipolar mitotic spindle (Figure 3Ad). Cells exposed to 5 μmol/L MPSP-001 for 16 h displayed disrupted mitotic spindles and chromosome misalignment (Figure 3Ae–3Ah). Examples of spindle damage including non-bipoles (apolar metaphase, monopolar metaphase, tripolar metaphase and mutipolar metaphase) and chromosome misalignment. A typical example of a tripolar prometaphase was shown in Figure 3Af. Figure 3Ag exemplified a mutipolar metaphase. An example of bipolar metaphase with chromosome misalignment was seen in Figure 3Ah. We counted the number of cells with disrupted mitotic spindles. Among 150 randomly selected cells in the mitotic phase not treated with MPSP-001, there were 2 non-bipolar metaphase cells and 1 chromosome misalignment cell. In comparison, in the randomly selected mitotic cells treated with MPSP-001, there were 39 and 27, respectively. These data showed that the rates of mitotic spindle disruption were significantly different between the MPSP-001 exposed group and non-exposed group (Figure 3B).

To compare the effects of MPSP-001 with other mitotic blockers, we studied the morphological changes of tubulin in interphase HeLa cells after exposure to the various drugs. Cells were treated with 250 nmol/L Taxol, 100 nmol/L colchicine, 100 nmol/L vincristine, and 5 μmol/L MPSP-001 respectively for 16 h. Taxol, a microtubule-stabilizing agent, caused an increase in density of cellular microtubules (Figure 3Cb, 3Cg). In contrast, colchicine and vincristine, two microtubule depolymerizing agents, caused microtubule depolymerization with short microtubules in the cytoplasm (Figure 3Cc, 3Cd, 3Ch, 3Ci). MPSP-001 (Figure 3Ce, 3Cj) also caused similar morphological changes of microtubules to that of colchicine and vincristine, suggesting that MPSP-001 may be a microtubule depolymerizing agent.

MPSP-001 inhibited *in vitro* microtubule assembly and directly bind to colchicine-binding site on tubulin

To confirm the above observations, we investigated the effect of MPSP-001 on tubulin polymerization using an *in vitro* tubulin polymerization assay (Figure 4A). MPSP-001 inhibited polymerization of tubulin in a dose-dependent manner similar to that of colchicine and vincristine.

Two known sulfonamide agents, E7010, and HMN-214, all bind to the colchicine site of tubulin. Therefore we further assessed the ability of MPSP-001 to compete with colchicine for binding to tubulin via competitive binding assays. Because the intrinsic fluorescence of colchicine increases upon binding to tubulin[36], it was used as an index for MPSP-001 competition with colchicine in tubulin binding. As shown in Figure 4B, vincristine did not affect the binding to tubulin. However, the fluorescence of colchicine-tubulin complex was reduced in the presence of MPSP-001 in a dose-dependent manner, suggesting that MPSP-001 were competing with colchicine to bind to tubulin.

Molecular docking predicted the interaction model of MPSP-001 binding to the colchicine site of β-tubulin (Figure 4C, 4D). In the docked complex, compound MPSP-001 bound to α, β-tubulin in an extended conformation and the calculated

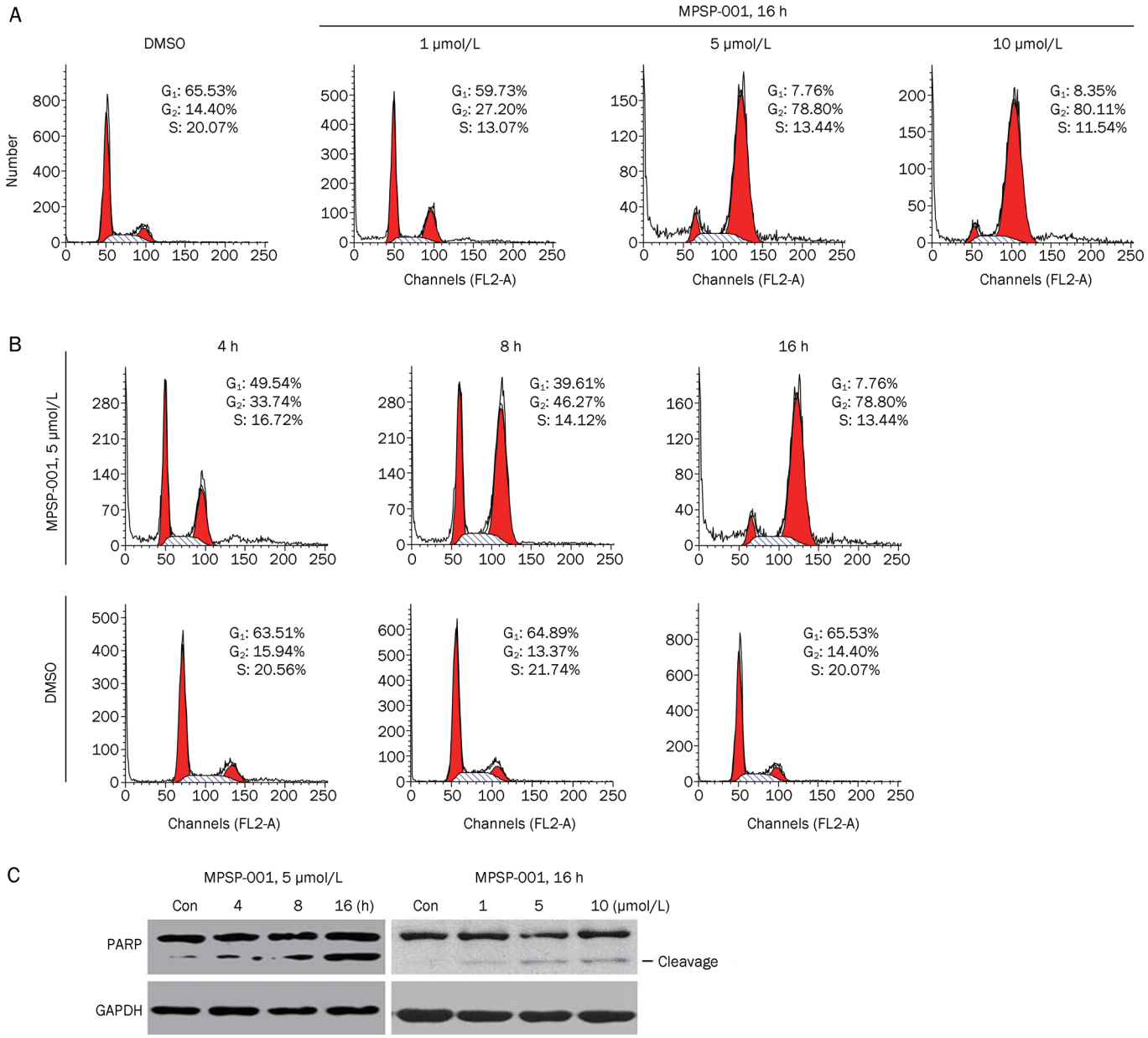

Figure 2. Effects of MPSP-001 on cell cycle distribution and cell death. (A) The concentration effects of MPSP-001 on cell cycle progression of HeLa cells. HeLa cells were treated with different concentrations of MPSP-001 for 16 h. Then, the cells were fixed and stained with PI and analyzed by flow cytometry. Percentages of cells in different phases were shown. The data are representative of three independent experiments. (B) The time effects of MPSP-001 on cell cycle progressions of HeLa cells. HeLa cells were treated with 5 μmol/L MPSP-001 for different time. The cells were then fixed and stained with PI, and analyzed by flow cytometry. Percentages of cells in different phases were shown. The data are representative of three independent experiments. (C) MPSP-001 induced apoptosis with the cleavage of PARP. The time (left panel) and concentration (right panel) effects of MPSP-001 on cell apoptosis of HeLa cells. Protein samples were separated by SDS-PAGE for immunoblot analysis using antibody against PARP and GAPDH were stained as the internal cytosolic control.

free energy of binding was -8.38 kcal/mol. The hydroxyl groups of MPSP-001 form hydrogen bonds to the residues Leu 252 and Leu 255 of the β tubulin with distances of 2.89 Å and 2.88 Å, respectively. Additionally, the phenyl ring moieties of MPSP-001 are positioned towards Val 315 and Ala 316 of the β tubulin, establishing hydrophobic contacts with the binding pocket (Figure 4C, 4D). The docking result, which has shown proper binding free energy and intermolecular interactions, shows a possible mode why MPSP-001 competes with colchicine.

MPSP-001 exhibited potent synergistic effect in combination with Taxol and colchicine

Before evaluating the interactions between MPSP-001 and

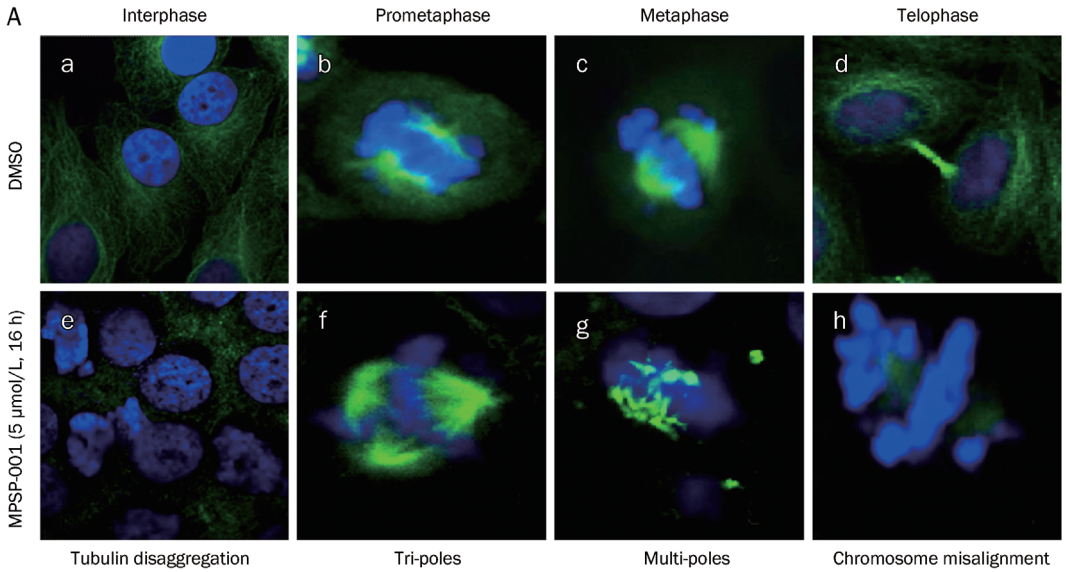

B

	DMSO	MPSP-001	*P* value
Non-bipoles	2/103 (1.94%)	39/435 (8.97%)	0.020
Chromosome misalignment	1/103 (0.97%)	27/435 (6.21%)	0.042

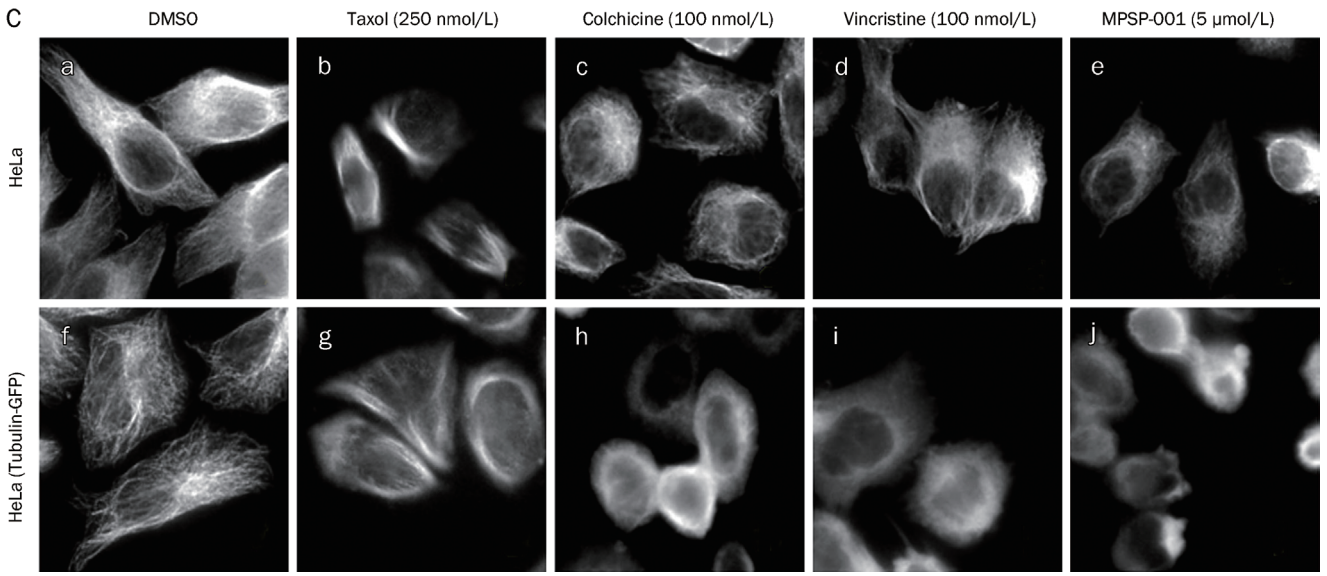

Figure 3. Effects of MPSP-001 on mitotic spindle formation and tubulin disruption. (A) Illustrations of the effects of MPSP-001 on the mitotic spindle in HeLa cells (e-h) using immuno-fluorescence microscopy technique. HeLa cells grown in log phase were treated with 5 μmol/L MPSP-001 for 16 h, followed by fixation and immunofluorescence staining for tubulin (white) and DNA (blue). Examples of a normal interphase (a), normal prometaphase (b), normal metaphase (c) and normal telophase (d) were shown. Examples of a damaged interphase (e) and various forms of abnormal mitoses include a tripolar prometaphase (f), a mutipolar metaphase (g) and an abnormal bipolar metaphase with lagging chromosomes or chromosomes not aligned to the metaphase plate (h) were shown (×600). (B) Statistical analysis of the effects of MPSP-001 on the mitotic spindles in HeLa cells. (C) Disruption of tubulin by MPSP-001, colchicine, and paclitaxel in HeLa cells and tubulin-GFP-HeLa cells (over-expression of the fusion protein of tubulin and GFP). HeLa cells and tubulin-GFP-HeLa cells grown in log phase were treated with 0.1% DMSO (a, f), 250 nmol/L Taxol (b, g), 100 nmol/L colchicine (c, h), 100 nmol/L vincristine (d, i) and 5 μmol/L MPSP-001 for 16 h, followed by fixation and immunofluorescence staining for tubulin (In Tubulin-GFP-HeLa cells, immunofluorescence staining was omitted) .Then the morphology of interphase tubulin (white) was observed (×600).

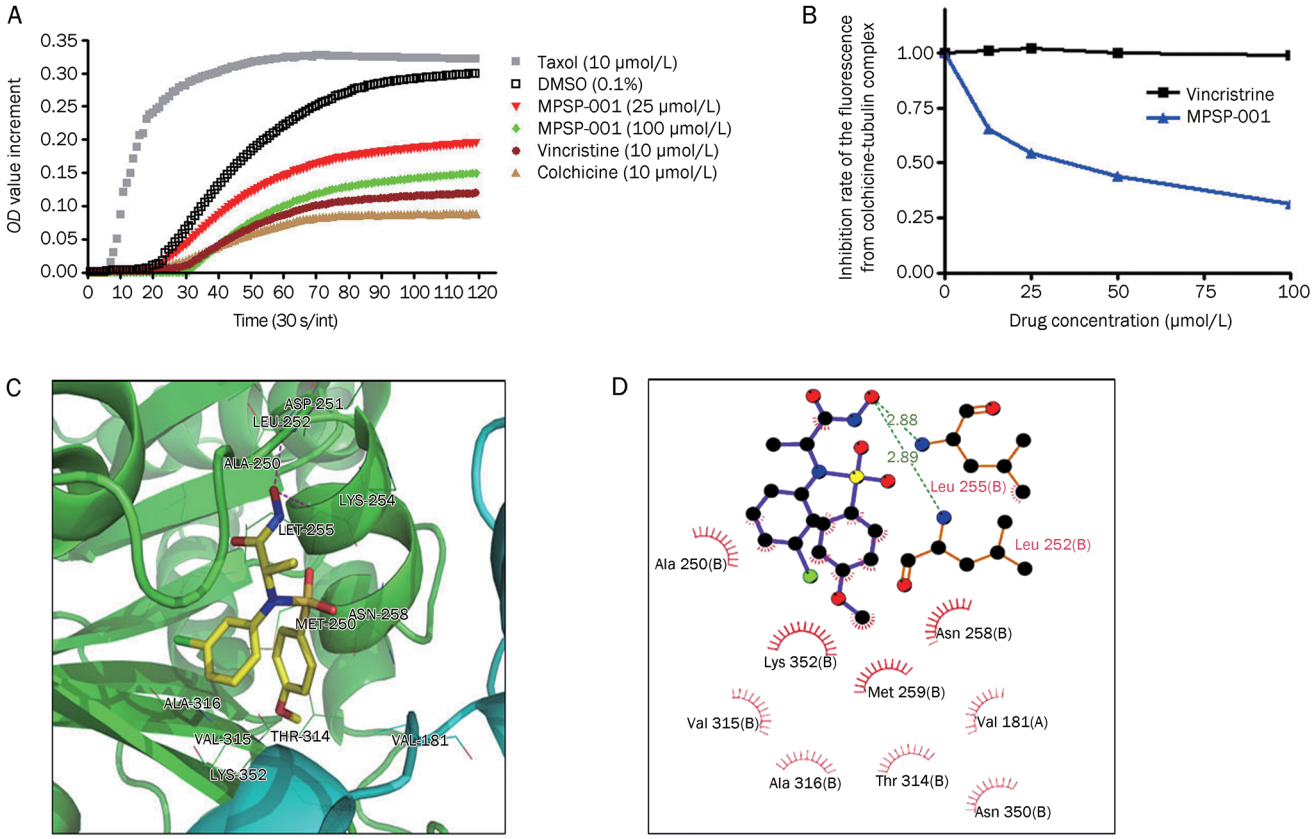

Figure 4. Effects of MPSP-001 on *in vitro* tubulin polymerization and competitive binding of colchicine site. (A) Effects of MPSP-001 (25 μmol/L, 100 μmol/L), Taxol (10 μmol/L), colchicines (10 μmol/L) and vincristine (10 μmol/L) on bovine brain tubulin polymerization were measured turbidimetrically. Changes in absorbance at 340 nm (A340) were measured and plotted as a function of time. (B) MPSP-001 binding to tubulin directly and inhibiting tubulin polymerization. Tubulin was co-incubated with indicated concentrations of VCR and MPSP-001 for 1 h, then 5 μmol/L colchicine was added. The fluorescence was measured by spectrofluorometer. All assays were repeated twice and representative data were shown. (C) Interactions between α,β-tubulin and compound MPSP-001 in the docking complex in 3D pattern. Tubulin was shown in cartoon style with the β and α subunit colored in green and cyan, respectively; compound MPSP-001 was shown in stick style; the residues within 4 Å around compound MPSP-001 were shown in line style. Magenta dashed lines denoted the potential hydrogen bonds. (D) 2D representation were drawn using LIGPLOT. Dashed lines represented hydrogen bonds and spiked residues form hydrophobic contacts with the compound.

Taxol or colchicine, we calculated the MB_{50} value for each of the compounds. It represents the concentration of compounds that render 50% of the cells to be arrested in mitosis. As shown in Figure 5A, the MB_{50} value of Taxol, colchicine and MPSP-001 were 177.7±2.7 (nmol/L), 77.8±2.8 (nmol/L), and 2.9±0.4 (μmol/L), respectively. At concentrations lower than their MB_{50} values, either colchicine (10 nmol/L)+MPSP-001 (1 μmol/L) or Taxol (25 nmol/L)+MPSP-001 (1 μmol/L) had synergism effects on arresting the Hela cells in G_2/M phase (Figure 5B). The combination index (CI) value was then calculated. The combination of colchicine with MPSP-001 against HeLa cells resulted in a CI value of 0.27. Similarly, the combination of Taxol with MPSP-001 resulted in a CI value of 0.87 (Table 2). These results demonstrated a synergy between MPSP-001 with other mitotic blockers in blocking mitosis. Moreover, we also found their synergistic effects on apoptosis

Table 2. Combination index values of COL+MPSP-001 and Taxol+MPSP-001 in HeLa cells.

Combination type	Percent of G_2/M	COL (nmol/L)		Taxol (nmol/L)		MPSP-001 (μmol/L)		CI
		D_1	$(Dm)_1$	D_1	$(Dm)_1$	D_2	$(Dm)_2$	
MPSP-001+COL	64.10%	10.00	133.32	NA	NA	1.00	5.45	0.27
MPSP-001+Taxol	41.70%	NA	NA	25.00	105.70	1.00	1.95	0.87

The CI is calculated by the following equation: $CI=D_1/(Dm)_1+D_2/(Dm)_2+D_1\times D_2/[(Dm)_1\times(Dm)_2]$. CI>1 indicates antagonism, CI<1 indicates synergy, and CI=1 indicates additivity. COL,colchicines; CI, combination index; NA, Not Applicable.

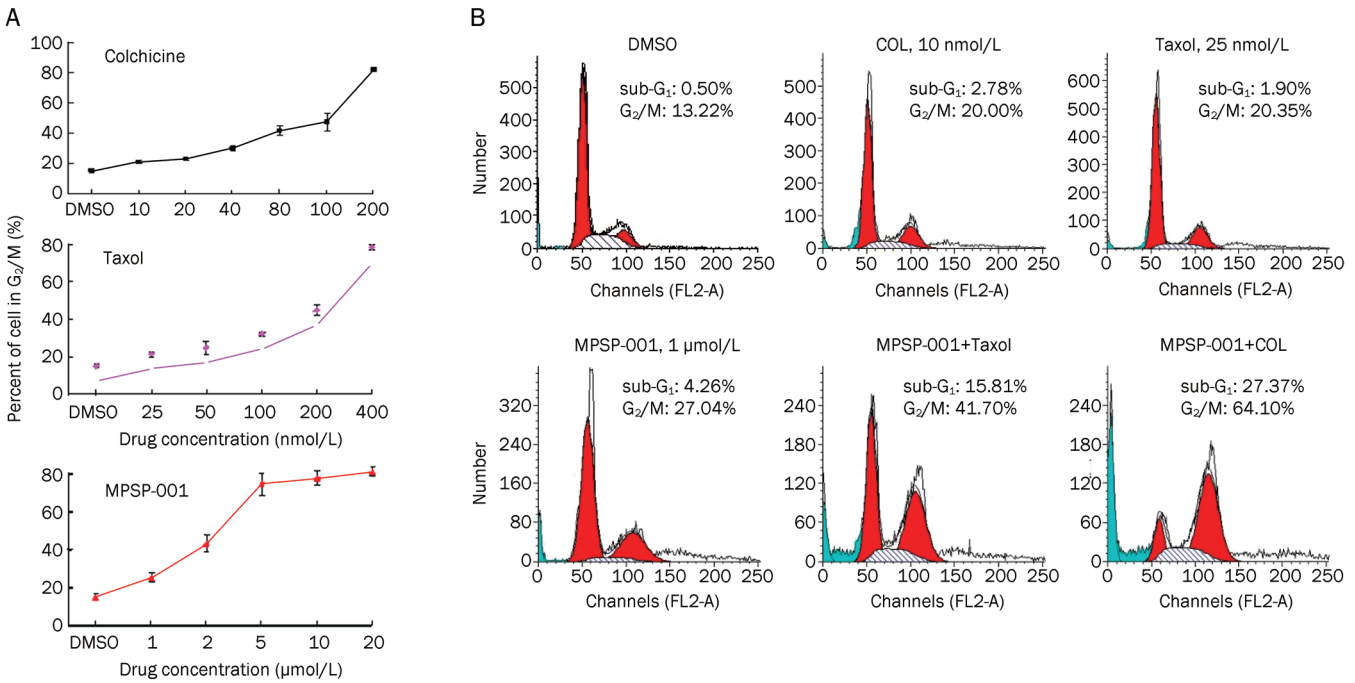

Figure 5. Synergistic effects of MPSP-001 in combination with colchicine and Taxol on blocking mitosis. (A) Flow cytometry analysis of the mitosis block effects using different concentrations of MPSP-001, colchicines and Taxol. HeLa cells were incubated with different concentrations of MPSP-001, colchicines and taxol for 16 h. Then cells were fixed and stained with PI and analyzed by flow cytometry. The G_2/M distribution values were graphed. Data are the means of triplicates±SD. (B) Flow cytometry analysis of the effects of taxol (25 nmol/L), colchicine (10 nmol/L), MPSP-001 (1 μmol/L) or the combination of Taxol+MPSP-001 and colchicines+MPSP-001 on cell cycle distribution. HeLa cells were incubated with drugs for 16 h. The cells were then fixed and stained with PI and analyzed by flow cytometry.

with an additional accumulation of sub-G_1 cells[37] (Figure 5B).

MPSP-001 exhibited potent cytotoxicity against multidrug-resistant cell lines

Multidrug resistance is a notorious nature of tumors for most naturally derived anticancer drugs[11]. To find out whether a major multidrug resistance mechanism, P-glycoprotein (P-gp) overexpression, influences the anti-cancer activity of MPSP-001, we tested the effects of MPSP-001 on two pairs of tumor cell lines with different expression levels of P-gp-overexpression, KB/VCR and MCF-7/ADR. The P-gp-overexpression cells showed high degrees of drug resistance to the control compounds VCR and ADR (RF values were 110.2 and 50.2, respectively) (Table 3). For each of these cell lines, MPSP-001 displayed equal cytotoxicity towards the multidrug resistant cells as well as the corresponding parental cells, with RF values of 1.2 and 1.9 (Table 3). These data indicated that MPSP-001' s anti-cancer activity is not affected by the P-gp pump.

Discussion

Microtubules are attractive targets for chemotherapeutic agents[2]. We report here that a novel benzenesulfonamide derivative, MPSP-001, inhibits growth of a broad-spectrum of cancer cell lines at the micromolar range (Table 1). It caused cell cycle arrest at the G_2/M phase and induced apoptosis of tumor cells. Further studies revealed that MPSP-001 disrupted

Table 3. Growth inhibition of MPSP-001 against drug-resistant cell lines.

Cell lines	Resistant type	VCR		ADR		MPSP-001	
		IC_{50} (nmol/L)	RF	IC_{50} (μmol/L)	RF	IC_{50} (μmol/L)	RF
KB	Parental	3.9±0.8	110.2	NT	NT	8.4±2.9	1.2
KB/VCR	MDR↑	429.7±18.2		NT		10.1±2.1	
MCF-7	Parental	NT	NT	1.7±0.4	50.2	12.4±2.7	1.9
MCF-7/ADR	MDR↑	NT		85.3±22.8		23.2±7.3	

All resistant cell lines were maintained in drug-free medium for 3 d before seeding for growth inhibition assay. Each value represented the mean±SD. of three independent experiments. The RF was calculated as the ratio of the IC_{50} value of the multidrug-resistant cells to that of the corresponding sensitive parental cells. VCR, vincristine; ADR, adriamycin; RF, resistant fold; NT, not tested.

mitotic spindles by inhibiting microtubule polymerization. The exact mechanism by which MPSP-001 inhibited microtubule polymerization and induced apoptosis is not completely understood. Visualization of mitotic spindle with fluorescent microscopy demonstrated that MPSP-001 caused non-bipolar mitotic spindles with chromosome misalignment. The modes of action on inhibiting microtubule polymerization and the effects on mitotic spindle formation of MPSP-001 resemble that of colchicine. We further performed *in vitro* fluorometric experiment to test whether MPSP-001 can displace colchicine from tubulin, which concluded that MPSP-001 can bind to colchicine site of tubulin. Moreover, molecular docking predicts that MPSP-001 can form two hydrogen bonds to the residues Leu252 and Leu255 of the β tubulin and establish hydrophobic contacts with the colchicine binding pocket (Figure 4C, 4D).

Drug resistance is a serious problem that restricts the use of microtubule-interfering drugs for clinical therapy[38]. MPSP-001 exerts a similar potency, regardless of the cell's MDR or MRP status (Table 3), suggesting that it is not a substrate of the efflux pumps.

Drugs often have more than one target. For exemple, another sulfonamide, HMN-214, its antitumor activity is mediated by the inhibiting of polo-like kinase and NF-Y[23–25]. S9, a novel anticancer agent, exerts its anti-proliferative activity by interfering with both PI3K-Akt-mTOR signaling and microtubule cytoskeleton[28]. Likely, the fact that MPSP-001 acted synergistically with colchicine and taxol on blocking mitosis and inducing apoptosis suggests that MPSP-001 may interact with other targets involved in spindle checkpoint or cell death.

Although its targets and mechanisms remain unclear, MPSP-001 exhibits synergistic effects with colchicine and taxol on blocking mitosis and inducing apoptosis, as well as its ability to overcome P-glycoprotein mediated multidrug resistance in taxanes and vinca alkaloids-resistant tumor cells. These results reveal its potentials in anticancer therapy.

In conclusion, our data provide compelling evidences that the novel sulfonamide-based compound, MPSP-001, has broad-spectrum anti-tumor efficacy *in vitro* by triggering tumor cell apoptosis and is effective against drug resistant tumor cells. Our study indicates that MPSP-001 is a novel microtubule depolymerizer and mitotic blocker. The in-depth studies on sulfonamides will help us to design better anti-cancer drugs.

Acknowledgements

This work was supported by the National Natural Science Foundation of China (Grant 30672481, 30771097, 90713029, and 30828018); the Shanghai Science and Technology Research Grant (08DZ1971403); the China Ministry of Science and Technology Research Grant (2008ZX10002-020); and the National Science & Technology Major Project "Key New Drug Creation and Manufacturing Program", China (Number: 2009ZX09301-001 and 2009ZX09103-064).

We thank Hai-tian QUAN, Xiu-quan MA and Yan-xin CUI for their kindly help.

Author contribution

Qiang YU and Zu-long LIU designed research; Zu-long LIU, Wei TIAN, Yong WANG, and Shan KUANG performed research; Qiang YU and Xiao-min LUO contributed reagents and analytic tools; Qiang YU and Zu-long LIU analyzed data; Zu-long LIU wrote the paper.

References

1 Urruticoechea A, Alemany R, Balart J, Villanueva A, Vinals F, Capella G. Recent advances in cancer therapy: an overview. Curr Pharm Des 2010; 16: 310.
2 Dumontet C, Jordan MA. Microtubule-binding agents: a dynamic field of cancer therapeutics. Nat Rev Drug Discov 2010; 9: 790–803.
3 Gan PP, McCarroll JA, Po'uha ST, Kamath K, Jordan MA, Kavallaris M. Microtubule dynamics, mitotic arrest, and apoptosis: drug-induced differential effects of betaIII-tubulin. Mol Cancer Ther 2010; 9: 1339–48.
4 Screpanti E, Santaguida S, Nguyen T, Silvestri R, Gussio R, Musacchio A, *et al*. A screen for kinetochore-microtubule interaction inhibitors identifies novel antitubulin compounds. PLoS One 2010; 5: e11603.
5 Kanthou C, Tozer GM. Microtubule depolymerizing vascular disrupting agents: novel therapeutic agents for oncology and other pathologies. Int J Exp Pathol 2009; 90: 284–94.
6 Bhalla KN. Microtubule-targeted anticancer agents and apoptosis. Oncogene 2003; 22: 9075–86.
7 Li CM, Lu Y, Ahn S, Narayanan R, Miller DD, Dalton JT. Competitive mass spectrometry binding assay for characterization of three binding sites of tubulin. J Mass Spectrom 2010; 45: 1160–6.
8 Liou JP, Hsu KS, Kuo CC, Chang CY, Chang JY. A novel oral indoline-sulfonamide agent, N-[1-(4-methoxybenzenesulfonyl)-2,3-dihydro-1H-indol-7-yl]-isonicotinamide (J30), exhibits potent activity against human cancer cells *in vitro* and *in vivo* through the disruption of microtubule. J Pharmacol Exp Ther 2007; 323: 398–405.
9 Wall ME, Wani MC. Camptothecin and taxol: from discovery to clinic. J Ethnopharmacol 1996; 51: 239–53; discussion 53–4.
10 Dumontet C, Sikic BI. Mechanisms of action of and resistance to antitubulin agents: microtubule dynamics, drug transport, and cell death. J Clin Oncol 1999; 17: 1061–70.
11 Gottesman MM. Mechanisms of cancer drug resistance. Annu Rev Med 2002; 53: 615–27.
12 Hansch C. Comparative QSAR of the sulfonamide function. Farmaco 2003; 58: 625–9.
13 Crespo R, de Bravo MG, Colinas PA, Bravo RD. *In vitro* antitumor activity of N-glycosyl sulfonamides. Bioorg Med Chem Lett 2010; 20: 6469–71.
14 Owa T, Yoshino H, Okauchi T, Yoshimatsu K, Ozawa Y, Sugi NH, *et al*. Discovery of novel antitumor sulfonamides targeting G1 phase of the cell cycle. J Med Chem 1999; 42: 3789–99.
15 Yamada Y, Yamamoto N, Shimoyama T, Horiike A, Fujisaka Y, Takayama K, *et al*. Phase I pharmacokinetic and pharmacogenomic study of E7070 administered once every 21 days. Cancer Sci 2005; 96: 721–8.
16 Smyth JF, Aamdal S, Awada A, Dittrich C, Caponigro F, Schoffski P, *et al*. Phase II study of E7070 in patients with metastatic melanoma. Ann Oncol 2005; 16: 158–61.
17 Baur M, Gneist M, Owa T, Dittrich C. Clinical complete long-term remission of a patient with metastatic malignant melanoma under therapy with indisulam (E7070). Melanoma Res 2007; 17: 329–31.
18 Ozawa Y, Sugi NH, Nagasu T, Owa T, Watanabe T, Koyanagi N, *et al*. E7070, a novel sulphonamide agent with potent antitumour activity *in*

vitro and *in vivo*. Eur J Cancer 2001; 37: 2275–82.
19 Iwamoto Y, Nishio K, Fukumoto H, Yoshimatsu K, Yamakido M, Saijo N. Preferential binding of E7010 to murine beta 3-tubulin and decreased beta 3-tubulin in E7010-resistant cell lines. Jpn J Cancer Res 1998; 89: 954–62.
20 Yamamoto K, Noda K, Yoshimura A, Fukuoka M, Furuse K, Niitani H. Phase I study of E7010. Cancer Chemother Pharmacol 1998; 42: 127–34.
21 Yoshimatsu K, Yamaguchi A, Yoshino H, Koyanagi N, Kitoh K. Mechanism of action of E7010, an orally active sulfonamide antitumor agent: inhibition of mitosis by binding to the colchicine site of tubulin. Cancer Res 1997; 57: 3208–13.
22 Dittrich C, Dumez H, Calvert H, Hanauske A, Faber M, Wanders J, *et al*. Phase I and pharmacokinetic study of E7070, a chloroindolylsulfonamide anticancer agent, administered on a weekly schedule to patients with solid tumors. Clin Cancer Res 2003; 9: 5195–204.
23 Garland LL, Taylor C, Pilkington DL, Cohen JL, Von Hoff DD. A phase I pharmacokinetic study of HMN-214, a novel oral stilbene derivative with polo-like kinase-1-interacting properties, in patients with advanced solid tumors. Clin Cancer Res 2006; 12: 5182–9.
24 Tanaka H, Ohshima N, Ikenoya M, Komori K, Katoh F, Hidaka H. HMN-176, an active metabolite of the synthetic antitumor agent HMN-214, restores chemosensitivity to multidrug-resistant cells by targeting the transcription factor NF-Y. Cancer Res 2003; 63: 6942–7.
25 Takagi M, Honmura T, Watanabe S, Yamaguchi R, Nogawa M, Nishimura I, *et al*. *In vivo* antitumor activity of a novel sulfonamide, HMN-214, against human tumor xenografts in mice and the spectrum of cytotoxicity of its active metabolite, HMN-176. Invest New Drugs 2003; 21: 387–99.
26 Brady AJ, Kearney P, Tunney MM. Comparative evaluation of 2,3-bis [2-methyloxy-4-nitro-5-sulfophenyl]-2*H*-tetrazolium-5-carboxanilide (XTT) and 2-(2-methoxy-4-nitrophenyl)-3-(4-nitrophenyl)-5-(2,4-disulfophenyl)-2*H*-tetrazolium, monosodium salt (WST-8) rapid colorimetric assays for antimicrobial susceptibility testing of staphylococci and ESBL-producing clinical isolates. J Microbiol Methods 2007; 71: 305–11.
27 Kuo CC, Hsieh HP, Pan WY, Chen CP, Liou JP, Lee SJ, *et al*. BPR0L075, a novel synthetic indole compound with antimitotic activity in human cancer cells, exerts effective antitumoral activity *in vivo*. Cancer Res 2004; 64: 4621–8.
28 Zhang C, Yang N, Yang CH, Ding HS, Luo C, Zhang Y, *et al*. S9, a novel anticancer agent, exerts its anti-proliferative activity by interfering with both PI3K-Akt-mTOR signaling and microtubule cytoskeleton. PLoS One 2009; 4: e4881.
29 Ravelli RB, Gigant B, Curmi PA, Jourdain I, Lachkar S, Sobel A, *et al*. Insight into tubulin regulation from a complex with colchicine and a stathmin-like domain. Nature 2004; 428: 198–202.
30 Morris GM, Goodsell DS, Halliday RS, Huey R, Hart WE, Belew RK, *et al*. Automated docking using a Lamarckian genetic algorithm and an empirical binding free energy function. J Comput Chem 1998; 19: 1639–62.
31 Chou TC. Drug combination studies and their synergy quantification using the Chou-Talalay method. Cancer Res 2010; 70: 440–6.
32 Rodea-Palomares I, Petre AL, Boltes K, Leganes F, Perdigon-Melon JA, Rosal R, *et al*. Application of the combination index (CI)-isobologram equation to study the toxicological interactions of lipid regulators in two aquatic bioluminescent organisms. Water Res 2010; 44: 427–38.
33 Kodama M, Murakami M, Kodama T. Statistical analysis of the age-adjusted incidence rates of human neoplasias: changes in time and space from early 1960's to mid 1980's with special reference to the steroid criminal hypothesis of carcinogenesis. Int J Mol Med 1999; 3: 435–41.
34 Yoshida D, Hoshino S, Shimura T, Takahashi H, Teramoto A. Drug-induced apoptosis by anti-microtubule agent, estramustine phosphate on human malignant glioma cell line, U87MG; *in vitro* study. J Neuro-oncol 2000; 47: 133–40.
35 Leoni LM, Hamel E, Genini D, Shih H, Carrera CJ, Cottam HB, *et al*. Indanocine, a microtubule-binding indanone and a selective inducer of apoptosis in multidrug-resistant cancer cells. J Natl Cancer Inst 2000; 92: 217–24.
36 Bhattacharyya B, Wolff J. Promotion of fluorescence upon binding of colchicine to tubulin. Proc Natl Acad Sci U S A 1974; 71: 2627–31.
37 Darzynkiewicz Z, Juan G, Li X, Gorczyca W, Murakami T, Traganos F. Cytometry in cell necrobiology: analysis of apoptosis and accidental cell death (necrosis). Cytometry 1997; 27: 1–20.
38 Shibayama Y, Nakano K, Maeda H, Taguchi M, Ikeda R, Sugawara M, *et al*. Multidrug resistance protein 2 implicates anticancer drug-resistance to sorafenib. Biol Pharm Bull 2011; 34: 433–5.

Acta Pharmacologica Sinica (2012) 33: 271–278
 1671-4083/12 $32.00
www.nature.com/aps

Original Article

Piperonal ciprofloxacin hydrazone induces growth arrest and apoptosis of human hepatocarcinoma SMMC-7721 cells

Zhen-yu SHI[1], Yong-qiang LI[1], YU-hua KANG[2], Guo-qiang HU[3], Chao-shen HUANG-FU[1], Jin-bo DENG[1], Bin LIU[1, *]

[1]*Institute of Neurobiology, College of Nursing, He-nan University, Kaifeng 475004, China*; [2]*Huai-he Clinical College, He-nan University Kaifeng 475001, China*; [3]*Institute of Chemical Biology, He-nan University, Kaifeng 475004, China*

Aim: To investigate the cytotoxic effects of piperonal ciprofloxacin hydrazone (QNT4), a novel antibacterial fluoroquinolone derivative, against human hepatocarcinoma SMMC-7721 cells.
Methods: Human hepatocarcinoma cells (SMMC-7721), human breast adenocarcinoma cells (MCF-7) and human colon adenocarcinoma cells (HCT-8) were tested. The effects of QNT4 on cell proliferation were examined using MTT assay. Cell apoptosis was determined using Hoechst 33258 fluorescence staining, TUNEL assay and agarose gel electrophoresis. The topoisomerase II activity was measured using agarose gel electrophoresis with the DNA plasmid pBR322 as the substrate. Mitochondrial membrane potential ($\Delta\psi m$) was measured using a high content screening imaging system. Protein expression of caspase-9, caspase-8, caspase-3, p53, Bcl-2, Bax, and cytochrome *c* was detected with Western blot analysis.
Results: Treatment with QNT4 (0.625–10 μmol/L) potently inhibited the proliferation of the cancer cells in time- and dose-dependent manners (the IC_{50} value at 24 h in SMMC-7721 cells, MCF-7 cells and HCT-8 cells was 2.956±0.024, 3.710±0.027, and 3.694±0.030 μmol/L, respectively). Treatment of SMMC-7721 cells with QNT4 (0.2146, 2.964, and 4.600 μmol/L) for 24 h dose-dependently increased the percentage of apoptotic cells, elicited characteristic DNA "ladder" bands, and decreased the mitochondrial membrane potential. QNT4 dose-dependently increased topoisomerase II-mediated DNA breaks while inhibiting DNA relegation, thus keeping the DNA in fragments. Treatment of SMMC-7721 cells with QNT4 significantly increased cytochrome c in the cytosol, and decreased cytochrome c in the mitochondrial compartment. QNT4 (3–7.39 μmol/L) significantly increased the protein expression of p53, Bax, caspase-9, caspase-3, and the cleaved activated forms of caspase-9 and caspase-3 in SMMC-7721 cells. In contrast, the expression of Bcl-2 was decreased, while caspase-8 had no significant change.
Conclusion: QNT4 induced the apoptosis of SMMC-7721 cells via inhibiting topoisomerase II activity and modulating mitochondrial-dependent pathways.

Keywords: anticancer drug; fluoroquinolone; piperonal ciprofloxacin hydrazone; hepatocarcinoma cells; breast adenocarcinoma cells; colon adenocarcinoma cells; apoptosis; topoisomerase II; mitochondrial membrane potential

Acta Pharmacologica Sinica (2012) 33: 271–278; doi: 10.1038/aps.2011.158

Introduction

Antibacterial fluoroquinolone is a very important family of antibacterial drugs that are widely prescribed for the treatment of infections in humans[1]. According to the pharmacological mechanisms elucidated in numerous reports, antibacterial fluoroquinolone corrupts the activities of prokaryotic type II topoisomerase and DNA gyrase, and induces them to kill cells by generating high levels of DNA double-strand breaks. DNA gyrase modulates the topological state of the genetic material by passing an intact DNA helix through a transient double-strand break that is generated in a separate DNA segment[2]. Like bacterial cells, eukaryotic species also require a type II topoisomerase, known as topoisomerase II, for viability. Compared with the known sequences of type II topoisomerases of bacteria and mammals, the sequences around activated tyrosine residues appear to have common homology[3]. The mechanisms by which antitumor fluoroquinolones induce cell death appear to be similar to those of quinolone antibacterial agents[4]. Mammalian DNA topoisomerase II can be inhibited by fluoroquinolones, although it is 100-fold more sensitive to prokaryotic DNA gyrase. In addition, the mode of action of fluoroquinolones is similar to that of anthracycline derivatives

* To whom correspondence should be addressed.
E-mail lbgood5912@sina.com
Received 2011-04-20 Received 2011-10-28

(such as doxorubicin, amsacrine, mitoxantrone), epipodophyllotoxin derivatives (such as etoposide), and actinomycin D (a class of polypeptide antibiotics isolated from *Streptomyces*). Accordingly, antibacterial fluoroquinolones have been shown to be cytotoxic to cancer cells[5, 6], thus representing a potentially important source of new anticancer agents. Recently, the development of antitumor agents derived from antibacterial fluoroquinolones has attracted much attention due to the mechanistic similarities and sequence homologies of the targeting eukaryotic topoisomerases[7]. However, many antitumor fluoroquinolones have been modified from clinical antibacterial fluoroquinolones with regard to the nitrogen-containing ring, such as piperazine, on the 7-position and (or) the 2-position of the fluoroquinolone scaffold[8, 9]. In addition, a few modifications of the carboxylic group at the 3-position have been reported[10]. Indeed, it does not seem necessary for an antitumor fluoroquinolone to retain the carboxylic group; fluoroquinolones with a fused heterocyclic ring as an isostere of the carboxylic group showed strong anticancer activity as well as high water solubility[11]. To search for new structural modification strategies for antibacterial fluoroquinolones, we have designed and synthesized a series of fluoroquinolone derivatives by linking various hydrazine compounds to the C-3 carboxyl group of ciprofloxacin or ofloxacin and assessed their anticancer activities. Several novel ciprofloxacin derivatives displayed potent cytotoxicity against the tested cancer cell lines *in vitro*, with IC_{50} values reaching micromolar concentrations[12]. In this study, we investigated the growth inhibitory effects and the molecular mechanisms of piperonal ciprofloxacin hydrazone (QNT4) in human hepatocarcinoma SMMC-7721 cells. We found that QNT4 (1-cyclopropyl-6-fluoro-4-oxo-7-piperazin-1, 4-dihydro-quinoline-3-carboxylic acid benzo[1,3]dioxol-5-ylmethylene-hydrazide) showed potent cytotoxicity against SMMC-7721 cells with an IC_{50} value of 2.411 μmol/L.

Materials and methods

Chemicals

Piperonal ciprofloxacin hydrazone (QNT4) was synthesized at the Institute of Chemistry and Biology at Henan University. The purity was >98% by HPLC analysis. The compound was dissolved in dimethyl sulfoxide (DMSO, Solarbio Science & Technology Co, Ltd). Its structure is illustrated in Figure 1.

Cell culture and treatments

Human hepatocarcinoma cells (SMMC-7721 and Hep3B2.1-7), human breast adenocarcinoma cells (MCF-7), and human colon adenocarcinoma cells (HCT-8), obtained from the Cell Bank of the Chinese Academy of Sciences, Shanghai, were cultured in DMEM medium (Gibco BRL, USA) supplemented with 10% heat-inactivated fetal bovine serum (Sijiqing Co, Ltd, Hangzhou, China), 100 IU/mL penicillin, and 100 μg/mL streptomycin. The cells were maintained in 5% CO_2 at 37 °C. When the cells reached approximately 50%–70% confluence, they were treated with different amounts of chemicals as indicated. DMSO was used as the vehicle control.

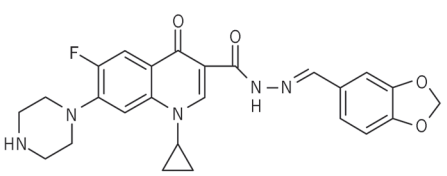

Figure 1. Structure of 1-cyclopropyl-6-fluoro-4-oxo-7-piperazin-1-yl-1,4-dihydro-quinoline-3-carboxylic acid benzo[1,3]dioxol-5-ylmethylene-hydrazide (QNT4).

MTT assay

The cells were seeded at a density of 1×10^4 cells/mL in 96-well culture plates. After 24 h, the cells were treated with the indicated concentrations of QNT4 or ciprofloxacin. Control wells consisted of cells incubated with medium only. After 24, 48, and 72 h of treatment, cells were incubated with 20 μL MTT (5 mg/mL, 3-[4,5-dimethylthiazol-2-yl]-2,5-diphenyltetrazolium bromide; Sigma, St Louis, MO, USA). After 4 h at 37 °C, the supernatant was removed, and 150 μL DMSO was added. After the blue crystals were dissolved in DMSO, the optical density (*OD*) was detected at a wavelength of 570 nm using a 96-well multiscanner autoreader (Bio-Rad, USA). The following formula was used: cell proliferation inhibited (%)=[1-(*OD* of the experimental samples/*OD* of the control)]×100. The IC_{50} is defined as the concentration at which cell proliferation is inhibited by 50%.

Hoechst 33258 staining

SMMC-7721 cells were seeded at a density of 1×10^4 cells/mL on the glass cover slides of a 35-mm chamber. After being treated with QNT4 for 24 h, the cells were washed twice with PBS and incubated with 5 μg/mL Hoechst 33258 (Sigma, St Louis, MO, USA) for 10 min at 37 °C in the dark. The cells were then washed and fixed with 4% paraformaldehyde in PBS for 5 min at 4 °C. Nuclear morphology was then examined under a fluorescent microscope (BX51, Olympus, Japan).

TUNEL assay

Cells (1×10^4 cells/mL) were seeded in growth medium on the glass cover slides of 6-well plates for overnight incubation. They were then treated with the indicated concentrations of QNT4 for 24 h. Control wells consisted of cells incubated with medium only. Next, cells were examined for apoptosis by terminal deoxynucleotidyl transferase-mediated dUTP nick-end labeling (TUNEL) assay (Promega, Madison, WI, USA), according to the manufacturer's instructions. Cells were visualized and photographed from at least five randomly chosen areas in each slide, using a fluorescent microscope (BX51, Olympus, Japan). Percent apoptosis was determined by counting the number of apoptotic cells and dividing by the total number of cells in the areas.

DNA agarose gel electrophoresis

Cells were treated with media containing different concentrations of QNT4 for 24 h and were then washed twice with PBS.

The chromosomal DNA was extracted with the Apoptotic DNA Ladder Detection Kit (Beyotime, China) according to the manufacturer's instructions. The DNA sample was incubated at 37 °C for 30 min and electrophoresed at 40 V/cm on a 1% agarose gel containing 1 mg/mL ethidium bromide. Finally, the apoptotic DNA fragments were visualized under a UV transilluminator and photographed.

Topoisomerase II-mediated supercoiled pBR322 DNA relaxation assay

DNA topoisomerase II activity was determined by the supercoiled pBR322 DNA relaxation assay[13]. The experiments were performed by incubating human topoisomerase IIα (Sigma, St Louis, MO, USA) with 1 μg supercoiled pBR322 DNA in 5 μL relaxation buffer (200 mmol/L Tris-HCl, pH 7.5, 340 mmol/L KCl, 40 mmol/L $MgCl_2$, 20 mmol/L DTT, 120 mg/L BSA, 5 mmol/L EDTA, 4 mmol/L ATP) under increasing concentrations of QNT4. In this experiment, etoposide (Sigma, St Louis, MO, USA), a known topoisomerase II poison[14], was used as a positive control. The mixture was incubated at 37 °C for 30 min and the reaction was terminated by adding 20 μL 10% SDS and 1 μL protease K (1×10^4 mg/L). Samples were subjected to electrophoresis in 1% agarose gels. DNA was then stained with 1 mg/mL ethidium bromide and photographed under a UV transilluminator.

Estimate of mitochondrial membrane potential loss

Cells were treated with media containing different concentrations of QNT4 for 24 h and were then incubated with 0.5 mg/mL of the fluorescence probe JC-1 (5,5′,6,6′-tetrachloro-l, l′,3,3′- tetraethyl-benzimidazolcarbocyanine iodide, Beyotime, China) at 37 °C for 20 min. The cells were thoroughly washed twice with buffer and incubated with 5 μg/mL Hoechst 33258 for 10 min in the dark. After two additional washes, the mitochondrial membrane potential (Δψm) was measured by a high content screening imaging system (Thermo Fisher Scientific, USA).

Western blotting assay

After treatment with different concentrations of QNT4 for 24 h, cells were lysed with ice-cold RIPA lysis buffer. Protein concentrations were determined using the Bradford method. Samples were separated by 12% SDS–PAGE under reducing conditions and transferred onto polyvinylidene fluoride (PVDF) membranes (Millipore). The membranes were blocked with 5% non-fat milk in TBST buffer (20 mmol/L Tris-HCl, 137 mmol/L NaCl, and 0.1% Tween 20, pH 8.0) for 1 h at room temperature, prior to an overnight incubation at 4 °C with specific antibodies to caspase-9, caspase-8, caspase-3, p53, Bcl-2, Bax, cytochrome *c*, or β-actin (all antibodies from Santa Cruz Biotechnology, USA). The membranes were washed and incubated with horseradish peroxidase conjugated anti-mouse IgG (Beijing ZhongShan GoldenBridge Biological Technology Co, LTD), or anti-rabbit IgG (Beyotime, China) secondary antibodies for 1 h. Once again, the membranes were washed three times with TBST, and the proteins were detected using an enhanced chemiluminescence substrate (ECL, Beyotime, China).

Cytochrome *c* release from mitochondria was evaluated by Western blotting analysis of cytosolic protein samples. Cytosolic protein fractions were prepared using the cell mitochondria isolation kit (Beyotime, China).

Statistical analyses

The data are presented as the mean±SD for the indicated number of independent experiments. Statistical significance was calculated using the *t*-test for paired samples. $P<0.05$ was regarded as significant and $P<0.01$ as highly significant.

Results

QNT4 suppressed the growth of cancer cells *in vitro*

The cytotoxicity of QNT4 against cancer cells was assessed using the MTT cell viability assay. The cells were treated with various concentrations of QNT4 for 24, 48, and 72 h, resulting in a significant decrease in cell viability in a dose- and time-dependent manner (Figure 2). Within the three cancer cell lines used in this experiment, QNT4 was most effective against SMMC-7721. As shown in Figure2A, the IC_{50} values after treatment for 24, 48, and 72 h were 2.956±0.024 μmol/L (r^2=0.9521), 3.497±0.063 μmol/L (r^2=0.8382), and 3.345±0.039 μmol/L (r^2=0.9700), respectively. For MCF-7 cells, the IC_{50} values after treatment for 24, 48, and 72 h were 3.710±0.027 μmol/L (r^2=0.8764), 3.377±0.021 μmol/L (r^2=0.9438) and 4.299±0.029 μmol/L (r^2=0.8857), respectively. For the HCT-8 cells, the IC_{50} values after treatment for 24, 48, and 72 h were 3.694±0.030 μmol/L (r^2=0.8750), 4.568±0.018 μmol/L (r^2=0.8330), and 4.318±0.025 μmol/L (r^2=0.8096), respectively. In contrast, ciprofloxacin showed weak cytotoxicity against SMMC-7721 cells (Figure 2D). The IC_{50} value at 48 h treatments was 6.860±0.194 μmol/L (r^2=0.8039).

QNT4-induced apoptosis of SMMC-7721 cells

After treatment with various concentrations of QNT4 for 24 h, marked morphological changes indicative of cell apoptosis, such as chromatin condensation and nuclear fragmentation, were clearly observed for SMMC-7721 cells following Hoechst 33258 staining (Figure 3, Table 1).

The integrity of DNA was assessed by agarose gel electrophoresis. As shown in Figure 4, 24 h incubation of SMMC-7721 cells with 2.964 μmol/L and 4.600 μmol/L QNT4 elicited characteristic DNA "ladder" bands indicative of apoptotic

Table 1. Apoptotic effects of QNT4 on SMMC-7721 cells. *n*=6. Mean±SD. [b]$P<0.05$ *vs* control. *T*=2.57.

	Total cells	Apoptotic cells	Apoptosis ratio/%
Control	352±12.1	21.42±2.6	0.6±0.1
QNT4 (2.146 μmol/L)	259.31±10.2	30.11±2.28	11.6±1.8
QNT4 (2.964 μmol/L)	212.18±8.6	42.18±3.2	19.9±2.8[b]
QNT4 (4.600 μmol/L)	160.78±2.9	53.44±6.2	33.2±3.9[b]

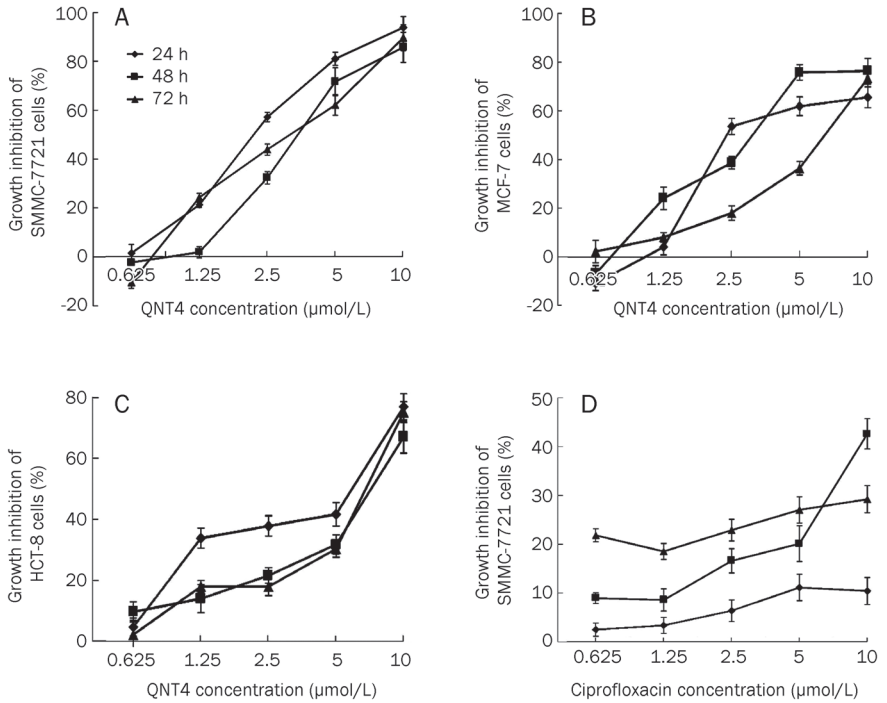

Figure 2. Dose- and time-dependent growth inhibition of the cancer cells by QNT4 or ciprofloxacin. (A) SMMC-7721 cells were treated with various concentration of QNT4. (B) MCF-7 cells were treated with various concentration of QNT4. (C) HCT-8 cells were treated with various concentration of QNT4. (D) SMMC-7721 cells were treated with various concentration of ciprofloxacin. Data represent means±SD of three independent measurements.

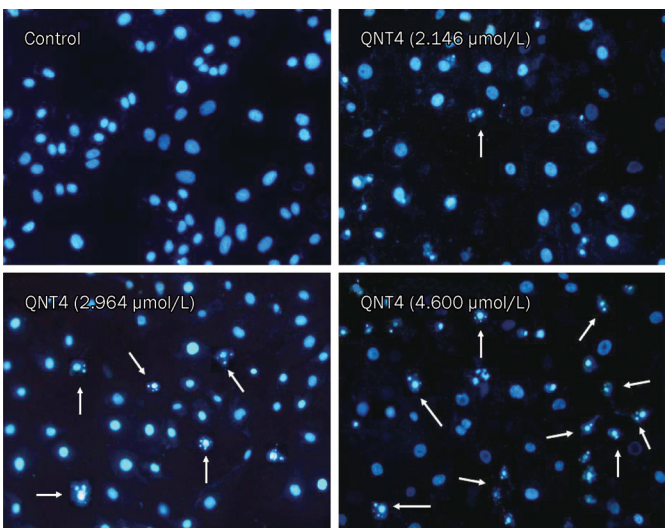

Figure 3. QNT4 induced morphological changes of SMMC-7721 cells. Cells were treated with 0, 2.146 (IC_{30} group), 2.964 (IC_{50} group), and 4.600 μmol/L (IC_{90} group) QNT4, respectively for 24 h. Morphological changes were examined by staining with Hoechst 33258, and the images were observed and photographed under a fluorescence microscope. ×400. Arrows indicate apoptotic cells.

Table 2. Apoptotic effects of QNT4 on SMMC-7721 cells. n=6. Mean±SD. $^bP<0.05$ *vs* control. T=2.46. $^cP<0.01$ *vs* control. T=3.84.

	Total cells	Apoptotic cells	Apoptosis ratio/%
Control	320.21±12.65	12.74±4.25	5.31±2.10
QNT4 (2.146 μmol/L)	256.44±12.07	33.40±5.54	19.13±4.09[b]
QNT4 (2.964 μmol/L)	180.38±15.04	37.54±8.25	28.49±2.18[c]
QNT4 (4.600 μmol/L)	109.54±11.40	45.45±6.40	45.94±4.75[c]

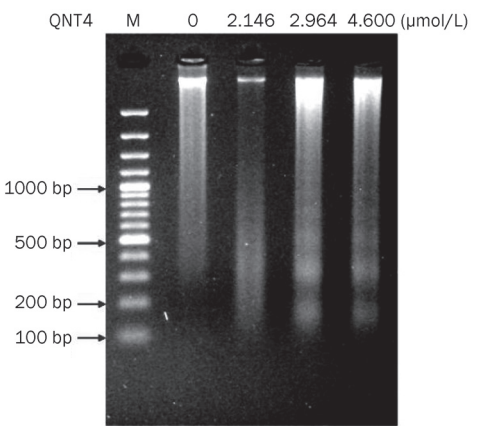

Figure 4. DNA fragmentation in SMMC-7721 cells. SMMC-7721 cells treated with 0, 2.146, 2.964, and 4.600 μmol/L QNT4, respectively for 24 h. DNA from 1×10^6 cells was electrophoresed through 1% agarose gels and stained with 0.5 μg/mL ethidium bromide. Lane M was standard marker of DNA ladder.

internucleosomal DNA fragmentation (approximately 180–200 bp).

To further investigate the role of QNT4 in apoptosis, TUNEL assay was performed. As shown in Figure 5 and Table 2, 24 h incubation with QNT4 increased the percentage of apoptotic SMMC-7721 cells in a concentration-dependent manner.

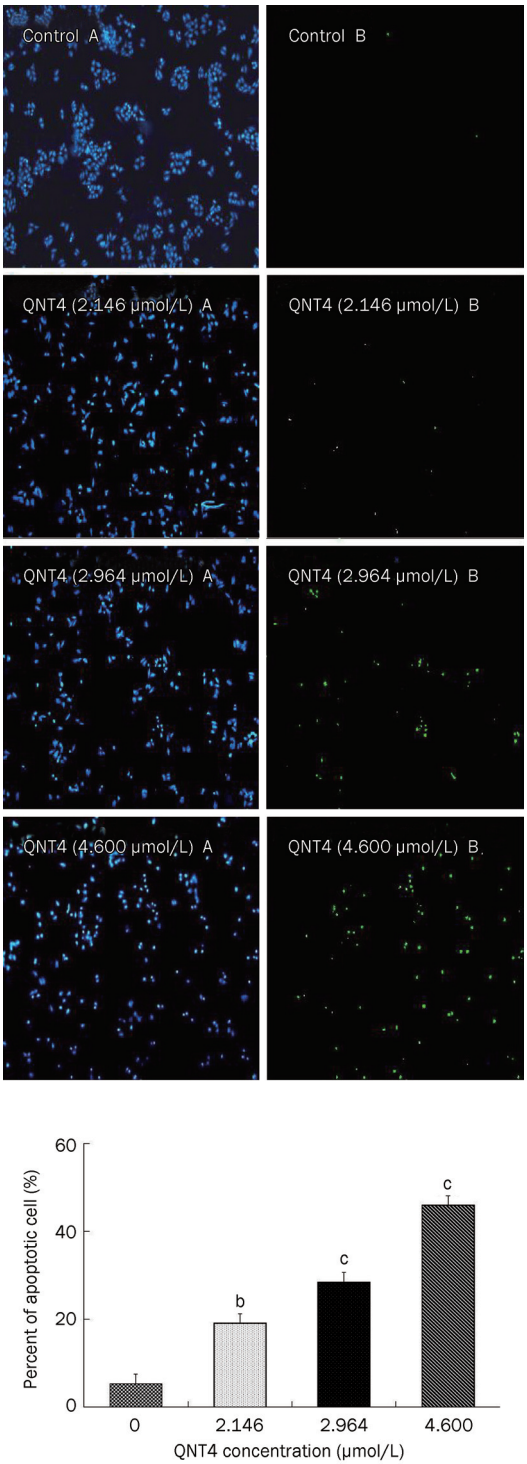

Figure 5. Induction of apoptosis in SMMC-7721 cells treated with QNT4 for 24 h was evaluated by TUNEL assay. Representative images were taken with nuclear stain (DAPI, A) and apoptosis stain (TUNEL, B). ×200. $^{b}P<0.05$, $^{c}P<0.01$ *vs* control (0 μmol/L).

The effect of QNT4 on the catalytic activities of eukaryotic topoisomerase II

In this experiment, relative double-stranded DNA cleavage/religation was determined using agarose gel electrophoresis of treated-pBR322 DNA and nontreated-pBR322 DNA (Figure 6). QNT4 decreased the amount of supercoiled DNA (Form I), while increasing nicked circular plasmid molecules (Form II) and linear molecules (Form III) in a dose-dependent manner. The effects of QNT4 on topoisomerase II-mediated DNA cleavage/religation were similar to that of etoposide. This suggests that QNT4 increased topoisomerase II-mediated DNA breaks while inhibiting DNA religation.

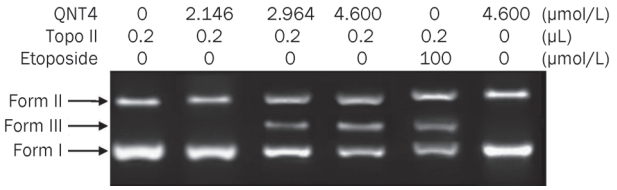

Figure 6. The inhibitory effects of QNT4 on DNA topoisomerase II activity. Human topoisomerase IIα was incubated with supercoiled pBR322 DNA in relaxation buffer under increasing concentrations of QNT4. Samples were subjected to electrophoresis in 1% agarose gels and then stained with ethidium bromide and photographed under a UV transilluminator.

The effect of QNT4 on the mitochondrial membrane potential

Mitochondrial membrane potential (Δψm) was detected with the fluorescent probe JC-1, which exists predominantly in monomeric form in cells with depolarized mitochondria and displays green fluorescence at 490 nm. In contrast, JC-1 primarily forms aggregates in cells with polarized mitochondria and shows reddish-orange fluorescence. The emission intensity ratio of the 545 nm and 595 nm peaks was used as a measure of mitochondrial depolarization; a higher ratio indicated more depolarization. QNT4 treatment of SMMC-7721 cells for 24 h resulted in green JC-1 fluorescence in a dose-dependent manner, which is consistent with a loss of Δψm (Figure 7). After treatment with QNT4 at 2.146 μmol/L, 2.964 μmol/L, and 4.600 μmol/L for 24 h, cellular Δψm decreased to (8.74±3.62)%, (39.64±4.52)%, and (46.90±3.29)%, respectively, compared to the control ($P<0.05$, $T=3.12$).

The effect of QNT4 on apoptotic protein expression in SMMC-7721 cells

To characterize the signaling pathways involved in QNT4-induced apoptosis, the expression levels of p53, Bcl-2, Bax, caspase-9, caspase-8, and caspase-3 in QNT4-treated SMMC-7721 cells were analyzed by Western blotting (Figure 8). Mitochondrial release of cytochrome *c* is a critical step in the apoptotic cascade that can activate downstream caspases. To examine whether QNT4-induced apoptosis in SMMC-7721 cells was associated with the release of cytochrome *c* from mitochondria, the levels of cytochrome *c* in both the cytosolic and mitochondrial fractions were analyzed. The results showed that there was a significant increase of cytochrome *c* in the cytosol and a decrease in the mitochondrial fraction after 24 h treatment with QNT4 (Figure 9).

As a tumor suppressor protein, p53 can induce cell apop-

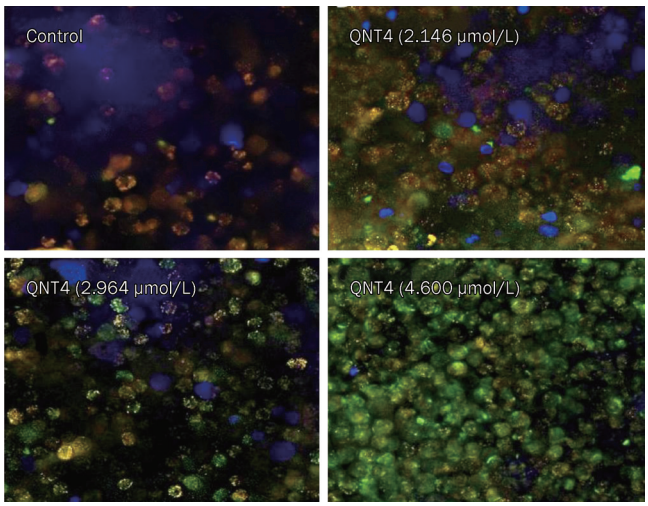

Figure 7. HCS analysis after JC-1 staining to detect changes in the mitochondrial membrane potential of SMMC-7721 cells induced by QNT4. Cells were treated with 0, 2.146 (IC_{30} group), 2.964 (IC_{50} group), and 4.600 μmol/L (IC_{90} group) QNT4, respectively for 24 h. The mitochondrial membrane potential (Δψm) was measured by high content screening image system.

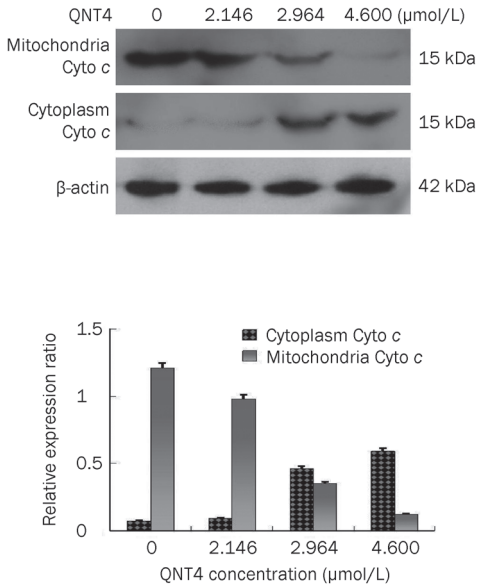

Figure 9. The effect of QNT4 on the release of cytochrome *c* from mitochondria to the cytosol were examined by Western blot analysis in SMMC-7721 cells after treatment with 0, 2.146 (IC_{30} group), 2.964 (IC_{50} group), and 4.600 μmol/L (IC_{90} group) QNT4, respectively for 24 h.

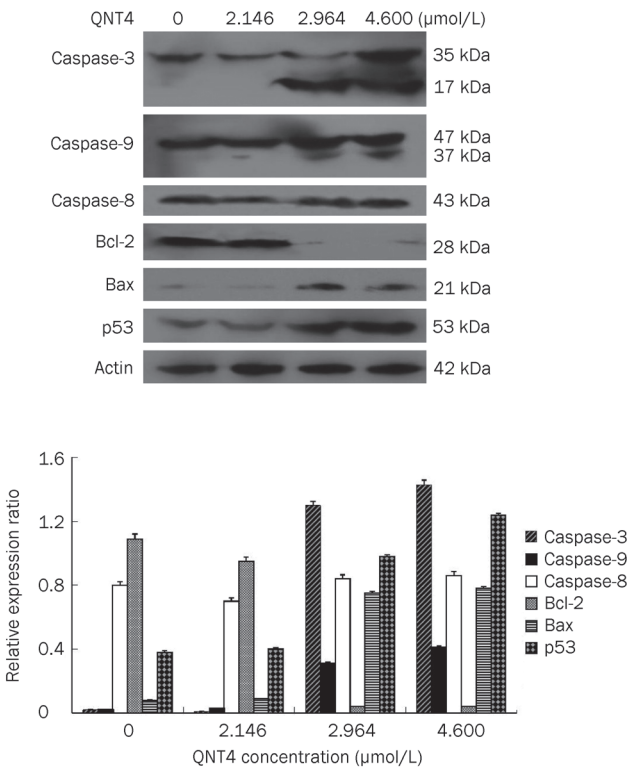

Figure 8. Protein expressions levels of caspase-9, caspase-8, caspase-3, Bcl-2, Bax, and p53 were examined by Western blot analysis in SMMC-7721 cells after treatment with 0, 2.146 (IC_{30} group), 2.964 (IC_{50} group), and 4.600 μmol/L (IC_{90} group) QNT4, respectively for 24 h.

tosis in response to stress signals, such as DNA damage. The expression of p53 protein was induced by various concentrations of QNT4 treatment. The anti-apoptotic protein Bcl-2 was also decreased, while the pro-apoptotic protein Bax was increased dramatically by QNT4 treatment. Because changes in Bax/Bcl-2 levels during the initiation of caspase signaling have been reported, caspase-9 and caspase-3 activation was examined in this study as well. Upon apoptotic stimulation, full-length caspase-9 and caspase-3 were cleaved into active fragments. QNT4 treatment (2.964 μmol/L and 4.600 μmol/L) significantly increased the cleaved, activated forms of caspase-9 and caspase-3. These results indicate that QNT4 induced apoptosis in SMMC-7721 cells through the intrinsic mitochondrial apoptotic pathway. On the other hand, QNT4 did not affect the expression of caspase-8, regardless of the treatment dose. Caspase-8 is a prominent initiator of death receptors and is activated by death receptor apoptosis stimuli. Therefore, it seems that QNT4 enhanced apoptosis through the intrinsic mitochondrial apoptosis pathway, whereas the death-receptor signaling pathway played a less important role.

Discussion

Fluoroquinolone compounds have been reported to have an inhibitory effect on cell proliferation and can induce apoptosis in carcinoma cell lines[15, 16]. In this study, MTT assays indicated that QNT4 inhibited the proliferation of human hepatocarcinoma SMMC-7721 cells in a dose- and time-dependent manner. Thus, we propose that QNT4 could be an effective candidate for therapy against malignant tumors.

Antibacterial fluoroquinolones are a class of antibacterial

agents that are commonly used to treat human and animal infections. The treatment of bacterial infection inhibits bacterial DNA gyrase by a mechanism similar to that of certain antitumor drugs against mammalian topoisomerase II[17]. Some antibacterial fluoroquinolones, such as ciprofloxacin, ofloxacin and norfloxacin, also demonstrate a slight interaction with mammalian topoisomerase II, although these antibacterials are much more selective for bacterial DNA gyrase[18]. However, a number of chemically modified antibacterial fluoroquinolone derivatives with enhanced activity against mammalian topoisomerase II have been developed. Strong inhibitory effects against eukaryotic DNA replication were demonstrated, and their structure-activity relationship have also been characterized[19]. These fluoroquinolone derivatives share a similar mechanism of action with several clinically relevant antitumor agents, such as ellipticine and etoposide. They bind to the topoisomerase II–DNA cleavage complexes, thus converting topoisomerase II into a physiological toxin that creates protein-linked DNA breaks in the genome of treated cells[20]. As shown in Figure 6, QNT4 increased topoisomerase II-mediated supercoiled pBR322 DNA breaks but inhibited topoisomerase II-mediated DNA religation. The effects of QNT4 on the topoisomerase II-mediated DNA cleavage/religation were similar to that of etoposide. These findings provide evidence that QNT4 is a poisonous inhibitor for topoisomerase II[21]. QNT4 binds the reversible complex between DNA and topoisomerase II, preventing the dissociation of the DNA–topoisomerase II complex and thereby inducing DNA damage[22, 23]. It has been reported that one of the key responses of fluoroquinolone-induced DNA damage is the expression of tumor suppressor protein p53, causing apoptosis of the treated cells[24, 25]. The results of this study showed that QNT4 induced cell apoptosis, which was accompanied by the up-regulation of p53 protein level in a dose-dependent manner, suggesting that the activation of the p53 pathway may be involved in the apoptotic process of SMMC-7721 cells.

Apoptosis may be initiated by the stimulation of death receptors located on the cell surface or through an intrinsic pathway involving the release of apoptotic signals from mitochondria[26, 27]. The cascading activation of caspases and the release of cytochrome *c* from the mitochondria play key roles in apoptosis, and the type of intracellular apoptotic pathways involved may be deduced from the activated initiator caspases. We specifically investigated the mitochondria-related events during apoptosis, such as the breakdown of the mitochondrial membrane, the expression of Bax and Bcl-2, and the activation of caspase 9. Members of the Bcl-2 protein family play an important role in apoptosis by regulating the release of cytochrome *c* from the mitochondria to the cytosol[28]. It has been shown that anti-apoptotic proteins, such as Bcl-2 and Bcl-XL, inhibit cytochrome *c* release whereas pro-apoptotic members, such as Bax, promote cytochrome *c* release, leading to the initiation of apoptosis. Here, we observe that QNT4 mediated an up-regulation of Bax and down-regulation of Bcl-2 to induce apoptosis, possibly through increased caspase activity and by preventing the formation of anti-apoptotic bodies. Therefore, it is possible that QNT4 induced the opening of the mitochondrial permeability transition pore through the up-regulation of Bax, resulting in the release of cytochrome *c*[29, 30]. In fact, we observed a QNT4-induced decrease of the mitochondrial membrane potential in SMMC-7721 cells, followed by increased cytochrome *c* release from the mitochondria into the cytosol. In the mitochondrial apoptotic pathway, the release of cytochrome *c* is a critical event because cytochrome *c* forms a complex with procaspase-9 in the cytoplasm (resulting in the activation of procaspase-9), which will eventually lead to the activation of caspases 3 and the induction of apoptosis[31]. Because activated caspase 8, activated by the death receptor, is able to cleave the proapoptotic Bcl-2 family member and then trigger a distinct apoptotic pathway involving mitochondria in some fluoroquinolone compound-treated cell types, it is possible that the activation of caspase 9 in QNT4-treated SMMC-7721 cells may be due to the activation of the death receptor-caspase 8 pathway[32, 33]. We showed that the cleavage of caspase 8 was not evident in QNT4-treated cells. Therefore, it is unlikely that the activation of caspase 9 is triggered mainly by the caspase 8 pathway, although this possibility cannot be excluded in other cell types[34]. Thus, we conclude that QNT4 induces apoptosis predominantly through the mitochondrial pathway.

In summary, these data have established QNT4 as a fluoroquinolone derivative that exerts potent anticancer activity through the mechanism of eukaryotic topoisomerase II poisoning. QNT4 also inhibited the proliferation of SMMC-7721 cells through DNA damage and up-regulation of the p53 protein. In addition, QNT4 caused mitochondrial dysfunction, accompanied by an increase in Bax protein expression, a loss of the mitochondrial membrane potential, and the cytoplasmic release of cytochrome *c*. The subsequent activation of caspase cascades plays a critical role in QNT4-induced apoptosis in human hepatocarcinoma SMMC-7721 cells. Most fluoroquinolone agents can reach concentrations that are far above serum levels in solid tissues, such as the liver[33]. QNT4 may, therefore, have a potential use as a novel chemotherapeutic agent in the treatment of liver cancer, as well as other solid cancers. The use of QNT4 as a modulating agent may also be interesting in combination with anticancer drugs for future preclinical and clinical studies.

Acknowledgements

This work was supported by the National Natural Science Foundation of China (20872028 and 31070952). We are grateful to Prof Jie-xin DENG (Henan University, China) for his critical comments and English revision of the manuscript.

Author contribution

Guo-qiang HU and Bin LIU contributed to the research design; Zhen-yu SHI, Yong-qiang LI, and YU-hua KANG performed the research; Jin-bo DENG and Chao-shen HUANGFU contributed new reagents and analytical tools; Yong-qiang LI analyzed the data; Yong-qiang LI and Bin LIU wrote the manuscript.

References

1 Bolon MK. The newer fluoroquinolones. Infect Dis Clin North Am 2009; 23: 1027–51.
2 Bax BD, Chan PF, Eggleston DS, Fosberry A, Gentry DR, Gorrec F, *et al*. Type IIA topoisomerase inhibition by a new class of antibacterial agents. Nature 2010; 466: 935–40.
3 Rajabalian S, Foroumadi A, Shafiee A, Emami S. Functionalized N-(2-oxyiminoethyl) piperazinyl quinolones as new cytotoxic agents. J Pharm Pharm Sci 2007; 10: 153–8.
4 Yamashita Y, Ashizawa T, Morimoto M, Hosomi J, Nakano H. Antitumor quinolones with mammalian topoisomerase II mediated DNA cleavage activity. Cancer Res 1992; 52: 2818–22.
5 Kamat AM, DeHaven JI, Lamm DL. Quinolone antibiotics: a potential adjunct to intravesical chemotherapy for bladder cancer. Urology 1999; 54: 56–61.
6 Koziel R, Szczepanowska J, Magalska A, Piwocka K, Duszynski J, Zablocki K. Ciprofloxacin inhibits proliferation and promotes generation of aneuploidy in Jurkat cells. J Physiol Pharmacol 2010; 61: 233–9.
7 Hawtin RE, Stockett DE, Byl JA, McDowell RS, Nguyen T, Arkin MR, *et al*. Voreloxin is an anticancer quinolone derivative that intercalates DNA and poisons topoisomerase II. PLoS One 2010; 5: e10186.
8 Foroumadi A, Emami S, Rajabalian S, Badinloo M, Mohammadhosseini N, Shafiee A. N-Substituted piperazinyl quinolones as potential cytotoxic agents: structure-activity relationships study. Biomed Pharmacother 2009; 63: 16–20.
9 Chang YH, Hsu MH, Wang SH, Huang LJ, Qian K, Morris-Natschke SL, *et al*. Design and synthesis of 2-(3-benzo[b]thienyl)-6,7-methylenedioxyquinolin-4-one analogues as potent antitumor agents that inhibit tubulin assembly. J Med Chem 2009; 52: 4883–91.
10 You QD, Li ZY, Huang CH, Yang Q, Wang XJ, Guo QL, *et al*. Discovery of a novel series of quinolone and naphthyridine derivatives as potential topoisomerase I inhibitors by scaffold modification. J Med Chem 2009; 52: 5649–61.
11 Hu GQ, Wu XK, Wang X, Zhang ZQ, Xie SQ, Huang WL, *et al*. Synthesis and antitumor activity of C3 heterocyclic-substituted fluoroquinolone derivatives (I): ciprofloxacin aminothiodiazole Schiff-bases. Acta Pharm Sin 2008, 43: 1112–5.
12 Kumar D, Sundaree S, Johnson EO, Shah K. An efficient synthesis and biological study of novel indolyl-1,3,4-oxadiazoles as potent anticancer agents. Bioorg Med Chem Lett 2009; 19: 4492–4.
13 Robinson MJ, Martin BA, Gootz TD, McGuirk PR, Moynihan M, Sutcliffe JA, *et al*. Effects of quinolone derivatives on eukaryotic topoisomerase II. A novel mechanism for enhancement of enzyme-mediated DNA cleavage. J Biol Chem 1991; 266: 14585–92.
14 Pommier Y, Leo E, Zhang H, Marchand C. DNA topoisomerases and their poisoning by anticancer and antibacterial drugs. Chem Biol 2010; 17: 421–33.
15 Efthimiadou EK, Thomadaki H, Sanakis Y, Raptopoulou CP, Katsaros N, Scorilas A, *et al*. Structure and biological properties of the copper (II) complex with the quinolone antibacterial drug N-pro-pyl-norfloxacin and 2,2′-bipyridine. J Inorg Biochem 2007; 101: 64–73.
16 DoganKoruznjak J, Slade N, Zamola B, Pavelić K, Karminski-Zamola G. Synthesis, photochemical synthesis and antitumor evaluation of novel derivatives of thieno (3′,2′:4,5) thieno (2,3-c) quinolones. Chem Pharm Bull 2002; 50: 656–60.
17 Hammonds TR, Foster SR, Maxwell A. Increased sensitivity to quinolone antibacterials can be engineered in human topoisomerase II alpha by selective mutagenesis. J Mol Biol 2000; 300: 481–91.
18 Kamat AM, De Haven JI, Lamm DL. A potential adjunct to intravesical chemotherapy for bladder cancer. Urology 1999; 54: 56–61.
19 Elsea SH, Osheroff N, Nitiss JL. Cytotoxicity of quinolones toward eukaryotic cells. Identification of topoisomerase II as the primary cellular target for the quinolone CP-115, 953 in yeast. J Biol Chem 1992; 267: 13150–3.
20 Nitiss JL. Targeting DNA topoisomerase II in cancer chemotherapy. Nat Rev Cancer 2009; 9: 338–50.
21 Elsea SH, McGuirk PR, Gootz TD, Moynihan M, Osheroff N. Drug features that contribute to the activity of quinolones against mammalian topoisomerase II and cultured cells: correlation between enhancement of enzyme-mediated DNA cleavage *in vitro* and cytotoxic potential. Antimicrob Agents Chemother 1993; 37: 2179–86.
22 Yogeeswari P, Sriram D, Kavya R, Tiwari S. Synthesis and *in-vitro* cytotoxicity evaluation of gatifloxacin Mannich bases. Biomed Pharmacother 2005; 59: 501–10.
23 Hammonds TR, Foster SR, Maxwell A. Increased sensitivity to quinolone antibacterials can be engineered in human topoisomerase II alpha by selective mutagenesis . J Mol Biol 2000; 300: 481–91.
24 Sheng Z, Cao X, Peng S, Wang C, Li Q, Wang Y, *et al*. Ofloxacin induces apoptosis in microencapsulated juvenile rabbit chondrocytes by caspase-8 dependent mitochondrial pathway. Toxicol Appl Pharmacol 2008; 226: 119–27.
25 Smart DJ, Halicka HD, Traganos F, Darzynkiewicz Z, Williams GM. Ciprofloxacin induced G2 arrest and apoptosis in TK6 lymphoblastoid cells is not dependent on DNA double-strand break formation. Cancer Biol Ther 2008; 7: 113–9.
26 Andera L. Signaling activated by the death receptors of the TNFR family. Biomed Pap Med Fac Univ Palacky Olomouc Czech Repub 2009; 153: 173–80.
27 Ott M, Norberg E, Zhivotovsky B. Mitochondrial targeting of tBid/Bax: a role for the TOM complex? Cell Death Differ 2009; 16: 1075–82.
28 Xie CY, Zhu H, Lin LP, Miao ZH, Geng MY, Cai YJ, *et al*. MFTZ-1, an actinomycetes subspecies derived antitumor macrolide, functions as a novel topoisomerase II poison. Mol Cancer Ther 2007; 6: 3059–70.
29 Chen YC, Lu PH, Pan SL, Teng CM, Kuo SC, Lin TP, *et al*. Quinolone analogue inhibits tubulin polymerization and induces apoptosis via Cdk1-involved signaling pathways. Biochem Pharmacol 2007; 74: 10–9.
30 Hsu SC, Yang JS, Kuo CL, Lo C, Lin JP, Hsia TC, *et al*. Novel quinolone CHM-1 induces apoptosis and inhibits metastasis in a human osterogenic sarcoma cell line. J Orthop Res 2009; 27: 1637–44.
31 Patil JB, Kim J, Jayaprakasha GK. Berberine induces apoptosis in breast cancer cells (MCF-7) through mitochondrial-dependent pathway. Eur J Pharmacol 2010; 645: 70–8.
32 Chang YH, Yang JS, Kuo SC, Chung JG. Induction of mitotic arrest and apoptosis by a novel synthetic quinolone analogue, CWC-8, via intrinsic and extrinsic apoptotic pathways in human osteogenic sarcoma U-2 OS cells. Anticancer Res 2009; 29: 3139–48.
33 Herold C, Ocker M, Ganslmayer M, Gerauer H, Hahn EG, Schuppan D. Ciprofloxacin induces apoptosis and inhibits proliferation of human colorectal carcinoma cells. Br J Cancer 2002; 86: 443–8.
34 Wang SW, Pan SL, Huang YC, Guh JH, Chiang PC, Huang DY, *et al*. CHM-1, a novel synthetic quinolone with potent and selective antimitotic antitumor activity against human hepatocellular carcinoma *in vitro* and *in vivo*. Mol Cancer Ther 2008; 7: 350–60.

Acta Pharmacologica Sinica (2012) 33: 279–288
 1671-4083/12 $32.00
www.nature.com/aps

Original Article

In vitro and *in vivo* investigation of dexibuprofen derivatives for CNS delivery

Xuan ZHANG, Xing LIU, Tao GONG, Xun SUN, Zhi-rong ZHANG*

Key Laboratory of Drug Targeting and Drug Delivery Systems, West China School of Pharmacy, Sichuan University, Chengdu 610041, China

Aim: Dexibuprofen, the S(+)-isomer of ibuprofen, is an effective therapeutic agent for the treatment of neurodegenerative disorders. However, its clinical use is hampered by a limited brain distribution. The aim of this study was to design and synthesize brain-targeting dexibuprofen prodrugs and to evaluate their brain-targeting efficiency using biodistribution and pharmacokinetic analysis.
Methods: *In vitro* stability, biodistribution and pharmacokinetic studies were performed on male Sprague-Dawley rats. The concentrations of dexibuprofen in biosamples, including the plasma, brain, heart, liver, spleen, lung, and kidney, were measured using high pressure lipid chromatography (HPLC). The pharmacokinetic parameters of the drug in the plasma and tissues were calculated using obtained data and statistics.
Results: Five dexibuprofen prodrugs that were modified to contain ethanolamine-related structures were designed and synthesized. Their chemical structures were confirmed using ^{1}H NMR, ^{13}C NMR, IR, and HRMS. In the biodistribution study, 10 min after intravenous administration of dexibuprofen (11.70 mg/kg) and its prodrugs (the dose of each compound was equivalent to 11.70 mg/kg of dexibuprofen) in male Sprague-Dawley rats, the dexibuprofen concentrations in the brain and plasma were measured. The C_{brain}/C_{plasma} ratios of prodrugs 1, 2, 3, 4, and 5 were 17.0-, 15.7-, 7.88-, 9.31-, and 3.42-fold higher than that of dexibuprofen, respectively (P<0.01). Thus, each of the prodrugs exhibited a significantly enhanced brain distribution when compared with dexibuprofen. In the pharmacokinetic study, prodrug 1 exhibited a brain-targeting index of 11.19 {$DTI=(AUC_{brain}/AUC_{plasma})_1/(AUC_{brain}/AUC_{plasma})_{dexibuprofen}$}.
Conclusion: The ethanolamine-related structures may play an important role in transport across the brain blood barrier.

Keywords: dexibuprofen; ethanolamine; prodrugs; brain targeting

Acta Pharmacologica Sinica (2012) 33: 279–288; doi: 10.1038/aps.2011.144

Introduction

Non-steroidal anti-inflammatory drugs (NSAIDs), including ibuprofen, naproxen and flubiprofen, are widely used as neuroprotective agents in the treatment of neurodegenerative disorders[1-3]. However, the clinical application of NSAIDs is impeded by limited brain accessibility. Several *in vivo* animal studies have shown that the concentrations of ibuprofen or flurbiprofen in the brain achieved at normal plasma concentrations are only 0.9–1.5 μmol/L[4–6]. It has also been found that most NSAIDs, including naproxen, ibuprofen, flurbiprofen, ketoprofen, and indomethacin, exhibit very limited distribution in the CNS, with steady state brain/plasma concentration ratios of 0.01– 0.05[7]. Several factors account for the low CNS distribution of NSAIDs, including high plasma protein binding rates, limited passive transport and efflux transport[8, 9]. Therefore, it is critical to enhance the brain distribution of NSAIDs to achieve therapeutic concentrations at normal doses.

Over 90% of therapeutic agents are excluded from CNS by the blood brain barrier (BBB), which is composed of the tightly connected endothelial cells of brain capillaries and the surrounding astrocytes and pericytes[10, 11]. Typically, molecules that are capable of crossing the BBB by passive diffusion are small (M_r<500 Da), lipophilic and uncharged at physiological pH[12, 13]. Various facilitated or energy-dependent transporters and receptors are highly expressed at the BBB; examples of such transporters include members of the organic cation transporter (OCT) families, organic anion transporters (OATs) and multidrug resistance proteins (MRPs)[14, 15]. A number of studies aimed at enhancing the distribution of therapeutics in the brain based on carrier- and receptor-mediated transport systems have been performed[16–18]. Due to the negative charge carried by the BBB, which expresses acetylneuraminic acid on the capillary luminal membrane and heparin sulfate on

* To whom correspondence should be addressed.
E-mail zrzzl@vip.sina.com
Received 2011-06-15 Accepted 2011-09-30

the basal lamina, compounds carrying positive charges have also been designed to cross through adsorption-mediated transport[19, 20].

Although several NSAID prodrugs have been synthesized to enhance the anti-inflammation activity or reduce the gastrointestinal toxicity of their parent compounds, few studies have investigated the targeted delivery of NSAIDs to the CNS[21, 22]. In a previous study, a series of NSAID prodrugs were synthesized to enhance transport to the brain. The carboxylic groups of NSAIDs were coupled with a 1,4-dihydro-1-methylpyridine-3-carboxylate moiety[23]. The results of this study revealed that all of the prodrugs were more lipophilic than their corresponding parent compounds, suggesting that prodrugs may exhibit better brain penetration. In another study, six ibuprofen prodrugs containing a proline moiety or related structures were synthesized and evaluated[24]. The results revealed that the synthesized prodrugs possessed anti-inflammatory properties; furthermore, three of these compounds inhibited lipoxygenase.

In this study, the *S*(+)-isomer of ibuprofen, (2*S*)-2-(4-isobutylphenyl)propionic acid (dexibuprofen), was used as a model drug because it exhibits better anti-inflammatory effects and fewer side effects than ibuprofen. Ethanolamine and its related structures were chosen as modifications to dexibuprofen in the preparation of prodrugs. Although some ethanolamine derivatives of NSAIDs were synthesized to improve the anti-inflammatory activity of parent compounds and decrease gastrointestinal toxicity[25, 26], an investigation of their potential as brain targeting agents has not yet been performed. Ethanolamine is a commonly found small molecule. Ethanolamine and its related structures are not only present in endogenous substances including phospholipids (*eg*, neurotransmitters) but also in various CNS-accessible therapeutics, such as meclofenoxate, cetirizine and procaine. Containing an amino group, ethanolamine-related structures are positively charged under physiological conditions, which may allow them to interact with the negatively charged BBB. Moreover, prodrugs that are modified by ethanolamine-related structures may act as substrates of the organic cation or choline transporters that are located at the BBB. After being transported across the BBB, the prodrugs can be further hydrolyzed by esterases in the brain to release dexibuprofen.

In this study, a series of dexibuprofen prodrugs modified by ethanolamine-related structures were designed and synthesized. The active carboxyl group of dexibuprofen was coupled with ethanolamine via an ester bond to give prodrug **4**. The amino group of ethanolamine was substituted by one methyl group, two methyl groups, two ethyl groups or one acetyl group to yield prodrugs **3**, **1**, **2**, and **5**, respectively. The stability of these prodrugs in the plasma and brain homogenates of Sprague-Dawley rats was tested. Biodistribution and pharmacokinetic studies of dexibuprofen and the prodrugs were performed in male Sprague-Dawley rats to evaluate the brain-targeting efficiency of the prodrugs. The influence of their chemical structures on their transport efficiency is discussed.

Materials and methods

Materials

Dexibuprofen (99.8% purity) was purchased from the Fourth Pharmaceutical Company of Suzhou (Suzhou, China). Acetonitrile (HPLC grade) was purchased from Kemiou (Tianjin, China). Water was prepared using an Aquapro water purification system (Chongqing, China). All of the other chemicals and reagents used in this study were of analytical grade and obtained commercially. TLC (thin-layer chromatograpy) (silica gel GF254) was used to detect spots using UV radiation. The purification of intermediates and final synthesized compounds was achieved by flash chromatography on silica gel. ^{1}H-NMR and ^{13}C-NMR analyses were performed using an AMX-400 Bruker Spectrometer. Infrared (IR) spectra were obtained using a Perkin-Elmer 983 Infrared Spectrophotometer (USA). MS spectroscopy was recorded on a Waters Q-TLF Premier mass spectrometer (USA) utilizing electrospray ionization (ESI). Optical rotations were determined using a Perkin–Elmer 341 polarimeter.

Chemistry

The synthesis routes of the dexibuprofen derivatives (**1**, **2**, **3**, **4**, and **5**) are outlined in Scheme 1. Dexibuprofen chloride was prepared as described by Song *et al*[27]. In brief, dexibuprofen was treated with thionyl chloride ($SOCl_2$) at reflux for 4 h. The reaction mixture was concentrated under reduced pressure. The resulting dexibuprofen chloride was coupled with the hydroxyl group of ethanolamine-related structures via an ester bond. To generate *N*,*N*-disubstituted ethanolamine, esterification was performed in a one-step reaction by mixing commercially available *N*,*N*-dimethylaminoethanol or *N*,*N*-diethylaminoethanol with dexibuprofen chloride in anhydrous dichloromethane (CH_2Cl_2) in the presence of triethylamine (TEA) to give target prodrug **1** or **2** in high yield[26]. For aminoethanol or 2-(methylamino)ethanol, which has a free H atom at the amino group, the amino group was protected by ditertbutyldicarbonate in the first step. The obtained intermediate, either **3a** or **4a,** was then coupled with dexibuprofen chloride in the presence of TEA to give either prodrug **3b** or **4b**. Prodrug **3b** or **4b** was then deprotected by HCl in ethyl acetate to yield prodrug **3** or **4**, respectively. In the preparation of *N*-acetyl ethanolamine dexibuprofen ester, *N*-acetylethanolamine was synthesized in the first step. Ethanolamine was dissolved in dioxane with added acetyl chloride in the presence of sodium hydride (NaOH) to yield prodrug **5a**. Prodrug **5a** was then condensed with dexibuprofen chloride to yield final compound **5**.

Animals

Male Sprague-Dawley rats (200–230 g) were provided by the Laboratory Animal Center of Sichuan University (Chengdu, China). All rats were maintained under standard conditions with access to food and water *ad libitum*. All animal study procedures were approved by the Sichuan University Animal Ethical Experimentation Committee according to the require-

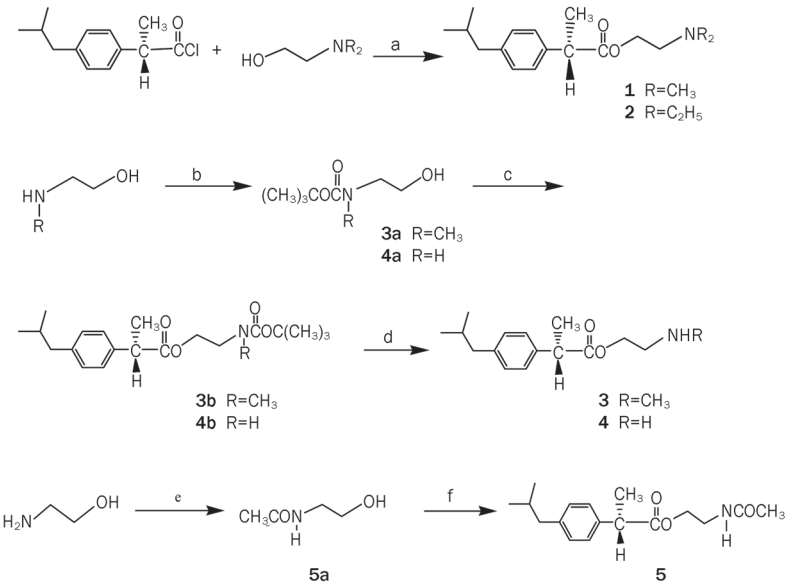

Scheme 1. Synthesis of dexibuprofen derivatives modified by ethanolamine related structures (**1**, **2**, **3**, **4**, **5**). Reagents and conditions: (a) CH_2Cl_2, TEA; (b) $(Boc)_2O$, NaOH; (c) dexibuprofen chloride, TEA; (d) EtOAc, HCl, RT; (e) CH_3COCl, NaH, dioxane; (f) dexibuprofen chloride, TEA.

ments of the National Act on the use of experimental animals (China).

In vitro stability

To determine whether ester prodrugs of dexibuprofen were hydrolyzed into free dexibuprofen in rat plasma and brain homogenates, we incubated prodrugs **1**, **2**, and **3** with the prepared cultures at 37 °C. At a specific time point, aliquots of rat plasma or brain homogenate were collected and processed. The released dexibuprofen concentrations were determined using high pressure liquid chromatography (HPLC) with a UV detector.

Rat plasma was prepared immediately before each experiment. Briefly, blood was obtained from the ocular artery and placed in a heparinized EP tube prior to centrifugation at 1110×*g* for 5 min. The resulting plasma was incubated with prodrugs without dilution. Rat brains were removed and homogenated with 0.9% sterile saline (g/mL) at a ratio of 1:2 immediately before use.

Prodrugs **1**, **2**, and **3** (2 mg each) were dissolved in a mixed solvent solution (2 mL) of ethanol, 0.9% saline and propylene glycol at a ratio of 1:2:2. The resulting solution (0.2 mL) was then added in the plasma or brain homogenates (9.8 mL), resulting in a final concentration of 20 μg/mL. The mixtures were incubated at 37 °C. Samples were prepared at predetermined time points (plasma: 0, 5, 15, 20, 25, 30, and 40 min; brain homogenates: 0, 0.5, 1, 2, 3, 4, 6, and 12 h). Aliquots of plasma (200 μL) or brain homogenate (500 μL) were withdrawn to determine the concentration of released dexibuprofen. Naproxen solution in methanol (1.266 μg/mL, 150 μL) was added immediately. A total of 1 mL or 2 mL methanol was then added to the plasma or brain homogenates, respectively, to prevent further hydrolysis of the prodrugs. The biosample processing method and chromatographic conditions are described in the following sections.

Hydrolysis half-life measurements were used to evaluate the stability of the prodrugs. These values were obtained using the formula $t_{1/2}$=0.693/K. The K values were calculated from the slope rate of the profile, which was obtained from a plot of time versus the natural logarithm of the remaining prodrug in the medium. The remaining prodrug concentration was determined by subtracting the released dexibuprofen concentration from the initial concentration of added prodrug in the medium.

Processing of biosamples

In an EP tube, an aliquot of 200 μL plasma or 500 μL tissue homogenates was mixed with naproxen solution in methanol (1.266 μg/mL, 150 μL), which was used as an internal standard. A total of 1 or 2 mL of methanol was then added to the plasma and tissue homogenates, respectively. The mixtures were then vortexed for 10 min, followed by centrifugation at 1665×*g* for 10 min. The supernatant was then transferred to an EP tube and dried at 35 °C under air flow. The residue was then ultrasonically redissolved in 150 μL of methanol for 5 min. After centrifugation at 10010×*g* for 10 min, 20 μL of the obtained supernatant was injected into an HPLC system to determine the dexibuprofen concentration.

Chromatographic conditions

An HPLC-based method was developed to determine the concentration of dexibuprofen in biosamples including plasma, brain, heart, liver, spleen, lung and kidney. The HPLC system (Waters, USA) was equipped with a Waters Delta 600 pump, a Waters 2487 Dual λ absorbance detector, a Waters 600 controller, a model 100 column heater (CBL photoelectron technology) and a 20-μL injector loop. The Kromasil C-18 column (150 mm×4.6 mm, ODS, 5 μm) was protected by a Phenomenex guard column (4 mm×3 mm, ODS). The column was eluted using a mobile-phase system containing acetonitrile/water (49/51), with 0.2% (*v*/*v*) triethylamine added. Phosphoric acid was used to adjust the pH to 2.5. The mobile

phase was then filtered and degassed by sonication before use. The flow rate used was 1.0 mL/min, and the diode-array detector was operated at 220 nm.

Naproxen was used as an internal standard. An HPLC assay for determining the concentration of dexibuprofen in different tissues was developed, including protocols for generating calibration curves and determining intra- and inter-day precision and extraction recoveries. Under the optimized HPLC conditions, the retention times of naproxen and dexibuprofen were 5.5 and 13.83 min, respectively. These values were well separated from endogenous substances and prodrugs **1**, **2**, **3**, **4**, and **5,** which had retention times of 2.730, 3.595, 2.265, 2.730, and 12.710 min, respectively (Figure 1).

Biodistribution and pharmacokinetic studies of dexibuprofen and its prodrugs in rats

To further evaluate the brain targeting efficiency of the prodrugs, a biodistribution and pharmacokinetic study was performed *in vivo*. Male Sprague-Dawley rats (200–230 g) were provided by the Laboratory Animal Center of Sichuan University. Prodrugs and dexibuprofen were injected through the caudal vein. For each sampling time point, five non-fasted male rats were treated with a single dose of either dexibuprofen (11.70 mg/kg) or prodrug **1** (15.73 mg/kg), **2** (17.34 mg/kg), **3** (14.94 mg/kg), **4** (14.15 mg/kg), or **5** (16.53 mg/kg). Each prodrug dose was equivalent to 11.70 mg/kg of dexibuprofen. Prior to administration, the compounds were dissolved in a mixed solvent containing a 1:2:2 ratio of ethanol, 0.9% saline and propylene glycol, to a final concentration of 60 mmol/L. In the biodistribution study, the rats were sacrificed 10 min after the injection of either dexibuprofen or prodrugs **1**, **2**, **3**, **4**, or **5**. For the pharmacokinetic investigations of dexibuprofen and prodrug **1**, the rats were sacrificed at 5, 10, 15, 30, 45, 60, 120, and 240 min post-dosing.

At a specific time point, the rats were bled from the ocular artery and sacrificed by cervical dislocation. Blood samples were collected and placed into heparinized EP tubes. Immediately following collection, the samples were centrifuged at 1110×*g* for 5 min. The plasma was then stored at -20 °C until assays were performed. Tissue samples, including samples from the brain, heart, liver, spleen, lung, and kidney, were removed and flushed with saline. The tissue samples were then homogenized using 0.9% saline (g/mL) at a ratio of 1:2. The homogenates were stored at -20 °C until assays were performed. Aliquots of 200 μL plasma or 500 μL tissue homogenates were processed, and the released dexibuprofen was measured as described above.

Data analysis

The pharmacokinetic parameters of dexibuprofen and the prodrugs were described as a two-compartment open model. The pharmacokinetic parameters in the plasma and tissues were calculated using Data and Statistics software pakage (DAS, Shanghai, China). The area under the curve (AUC), the maximal concentration (C_{max}) and the mean residence time (MRT_{0-t}) for the plasma, brain, heart, liver, spleen, lung and kidney were calculated separately. Statistical evaluation was performed using analysis of variance followed by a *t*-test. *P* values less than 0.01 and 0.05 were considered significant. The data shown represent mean values±SD.

The relative uptake efficiency (RE), concentration efficiency (CE) and drug targeting index (DTI) were calculated to evaluate the brain targeting efficiency of the prodrugs. The ratio of the dexibuprofen concentration in the brain compared to that in the plasma $\{(C_{brain}/C_{plasma})_{dexibuprofen}\}$ was also used to evaluate brain targeting efficiency. The values of RE, CE, and DTI are defined as follows:

$RE=(AUC)_{prodrug}/(AUC)_{dexibuprofen}$,

$CE=(C_{max})_{prodrug}/(C_{max})_{dexibuprofen}$ and

$DTI=(AUC_{brain}/AUC_{plasma})_{prodrug}/(AUC_{brain}/AUC_{plasma})_{dexibuprofen}$

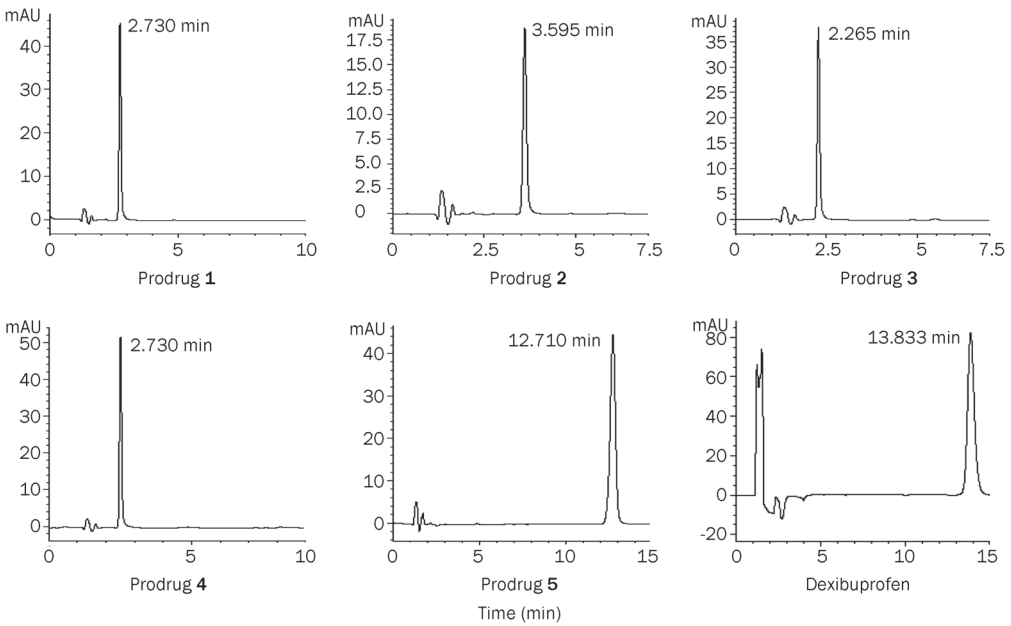

Figure 1. HPLC chromatograms of dexibuprofen and prodrugs **1**, **2**, **3**, **4**, and **5**. Compound was dissolved in methanol with concentration of 5 μg/mL.

Results

In vitro stability

The *in vitro* stability studies revealed that all of the tested dexibuprofen derivatives released dexibuprofen when incubated with rat plasma and brain homogenates (Table 1). These result suggest that compounds **1**, **2**, and **3** were rapidly hydrolyzed in rat plasma. The half-lives of compounds **1** and **2** were less than 5 min. The half-life of prodrug **3** was 11.63±1.04 min. These results imply that prodrugs **1**, **2**, and **3,** which all contain ester bonds, may be substrates of specific esterases in the plasma and are efficiently hydrolyzed. Investigation of the stability of the prodrugs in rat brain homogenates showed that compounds **1**, **2**, and **3** were cleaved by enzymes at different rates. The hydrolysis half-lives of compounds **1**, **2**, and **3** were 0.273±0.009, 1.150±0.061, and 3.712±0.174 h, respectively. The results suggested that prodrug **3** was more stable in brain homogenates than either compound **1** or **2**, which was consistent with the findings for the plasma.

Table 1. Hydrolysis half-life ($t_{1/2}$) of prodrugs **1**, **2**, **3** in rat plasma or brain homogenate at 37 ℃ (n=3).

Compound	$t_{1/2}$	
	Plasma	Brain homogenate
1	<5.0 min	0.273±0.009 h
2	<5.0 min	1.150±0.061 h
3	11.63±1.04 min	3.712±0.174 h

Biodistribution and pharmacokinetic study of dexibuprofen and prodrugs in rats

To evaluate the brain-targeting efficiency of prodrugs **1**, **2**, **3**, **4**, and **5** (Scheme 1), a biodistribution study was performed. We determined the concentrations of dexibuprofen in the plasma, brain, heart, liver, spleen, lung and kidney 10 min after intravenous administration of dexibuprofen (11.70 mg/kg) or prodrugs (at doses equivalent to 11.70 mg/kg of dexibuprofen). The concentration of dexibuprofen in the brain versus that in the plasma $(C_{brain}/C_{plasma})_{dexibuprofen}$ was used to evaluate the brain-targeting efficiency of the compounds. The concentrations of dexibuprofen in the brain and plasma 10 min after the injection of dexibuprofen or prodrug **1**, **2**, **3**, **4**, or **5** are shown in Figure 2 (n=5). Prodrugs **1**, **2**, and **3** exhibited enhanced drug concentrations in the brain in comparison with dexibuprofen (P<0.01). The $(C_{brain}/C_{plasma})_{dexibuprofen}$ ratios 10 min after administration of dexibuprofen or prodrug **1**, **2**, **3**, **4**, or **5** were 0.037±0.011, 0.626±0.091, 0.576±0.119, 0.290±0.114, 0.342±0.132, and 0.126±0.026, respectively (Figure 3; n=5). The $(C_{brain}/C_{plasma})_{dexibuprofen}$ ratios of prodrugs **1**, **2**, **3**, **4**, and **5** were 17.0-, 15.7-, 7.88-, 9.31-, and 3.42-fold higher, respectively, than that of dexibuprofen. Thus, the prodrugs exhibit good brain-targeting efficiency (P<0.01), with a relative efficiency of **1>2>4>3>5**. Among prodrugs (2*S*)-2-(4-isobutylphenyl) propionic acid 2-dimethylaminoethyl ester (prodrug **1**), exhibited the highest distribution efficiency in the brain.

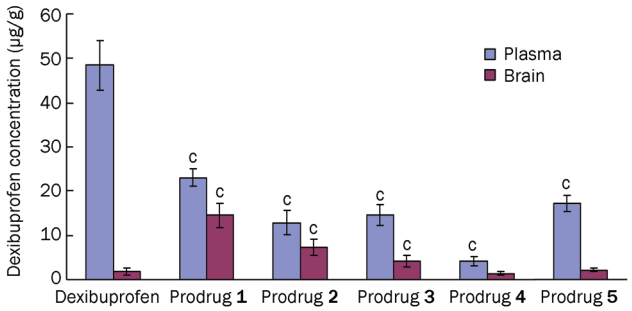

Figure 2. Dexibuprofen concentrations (μg/g) in the plasma and brain 10 min after intravenous administration of dexibuprofen (11.70 mg/kg) or prodrugs **1**, **2**, **3**, **4**, **5** (each compound was equivalent to 11.70 mg/kg of dexibuprofen) in rats. Each point represents the mean±SD of five experiments. ^cP<0.01 *vs* dexibuprofen.

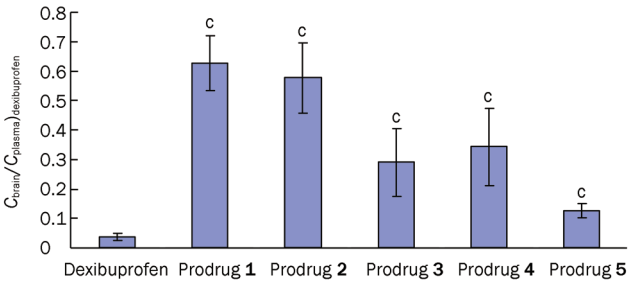

Figure 3. Comparison of $(C_{brain}/C_{plasma})_{dexibuprofen}$ ratios of dexibuprofen and prodrugs. C_{brain}, C_{plasma}: dexibuprofen concentration (μg/g) in the brain or plasma 10 min after intravenous administration of dexibuprofen (11.70 mg/kg) or prodrugs **1**, **2**, **3**, **4**, **5** (each compound was equivalent to 11.70 mg/kg of dexibuprofen) in rats. Each point represents the mean±SD of five experiments. ^cP<0.01 *vs* dexibuprofen.

We further investigated the biodistribution and pharmacokinetic parameters of dexibuprofen and prodrug **1** in Sprague-Dawley rats. The concentrations of dexibuprofen after the systemic administration of dexibuprofen (11.70 mg/kg) and prodrug **1** (15.73 mg/kg, a dose equivalent to 11.70 mg/kg of dexibuprofen) were determined and statistically analyzed. The dexibuprofen concentration profile versus time is shown in Figure 4. The C_{brain}/C_{plasma} ratio versus time is shown in Figure 5. The pharmacokinetic parameters are reported in Table 2. An evaluation of the targeting efficiency of prodrug **1** is shown in Table 3.

The results revealed that 5 min after the administration of dexibuprofen, the concentration in the plasma was initially very high, with a C_{plasma} of 64.44±14.00 μg/g (Figure 4). However, at the same time point, the concentration of dexibuprofen in the brain was only 2.81±1.16 μg/g. At different time points, the C_{brain}/C_{plasma} ratios were consistently low after the administration of dexibuprofen, never exceeding 0.05 (Figure 5). The AUC_{brain}/AUC_{plasma} ratio was only 0.025. These results indicated that the BBB was able to strongly prevent the entry of dexibuprofen into the brain. This finding is in agreement with

Table 2. Pharmacokinetic parameters (calculating from the measured dexibuprofen concentrations) in rat plasma and tissues after intravenous administration of dexibuprofen (11.70 mg/kg) or prodrug **1** (15.73 mg/kg, equivalent to 11.70 mg/kg of dexibuprofen). Each point represents the mean±SD of five experiments. $^{b}P<0.05$, $^{c}P<0.01$ *vs* dexibuprofen.

Tissue	Dexibuprofen			Prodrug **1**		
	$AUC_{0\to t}$ (μg/g·h)	C_{max} (μg/g)	MRT_{0-t} (h)	$AUC_{0\to t}$ (μg/g·h)	C_{max} (μg/g)	MRT_{0-t} (h)
Plasma	44.79±7.73	64.44±14.00	0.789±0.046	28.70±2.35^{b}	29.74±2.97^{c}	0.900±0.119
Brain	1.10±0.41	2.81±1.16	0.274±0.023	7.89±1.23^{c}	21.79±3.37^{c}	0.237±0.034
Heart	8.11±1.39	11.99±3.70	0.767±0.158	6.66±1.04	10.46±1.78	0.733±0.167
Liver	14.03±3.91	16.94±3.25	0.961±0.086	12.98±5.12	10.34±1.49^{b}	1.052±0.16
Spleen	4.01±0.62	5.60±1.27	1.128±0.357	4.12±1.12	6.24±3.15	0.591±0.096^{b}
Lung	10.60±2.10	13.19±2.56	1.220±0.072	22.07±4.84^{c}	29.03±4.41^{c}	0.853±0.037^{c}
Kidney	6.34±1.10	9.43±2.72	0.700±0.077	7.58±1.34	11.59±2.68	0.592±0.043

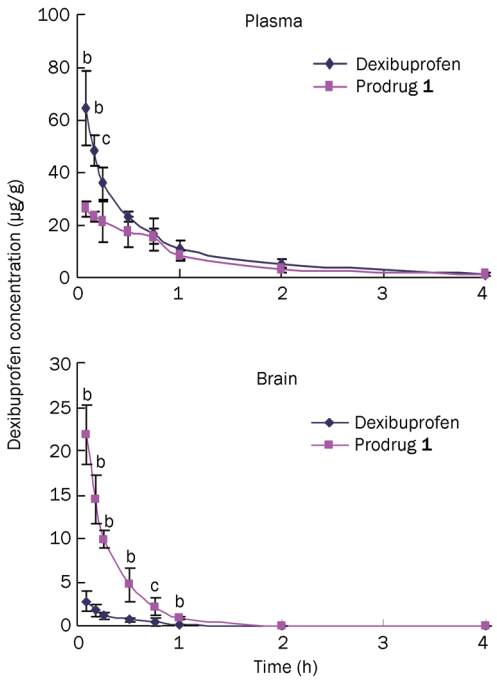

Figure 4. Dexibuprofen concentrations in the plasma and brain (μg/g) *vs* time (h) after intravenous administration of dexibuprofen (11.70 mg/kg) and prodrug **1** (15.73 mg/kg, equivalent to 11.70 mg/kg of dexibuprofen) in rats. Each point represents the mean±SD of five experiments. $^{b}P<0.05$, $^{c}P<0.01$ *vs* dexibuprofen.

Table 3. Targeting efficiency of Prodrug **1** compared with dexibuprofen after intravenous administration of dexibuprofen (11.70 mg/kg) and 1 (15.73 mg/kg, equivalent to 11.70 mg/kg of dexibuprofen) in male rats (mean±SD, n=5). $^{a}RE=(AUC)_1/(AUC)_{dexibuprofen}$. $^{b}CE=(C_{max})_1/(C_{max})_{dexibuprofen}$. $^{c}DTI=(AUC_{tissue}/AUC_{plasma})_1/(AUC_{tissue}/AUC_{plasma})_{dexibuprofen}$.

	Brain	Heart	Liver	Spleen	Lung	Kidney
RE^{a}	7.17	0.82	0.93	1.4	1.24	1.49
CE^{b}	7.75	0.87	0.61	1.11	2.20	1.23
DTI^{c}	11.19	1.28	1.44	2.18	1.94	2.32

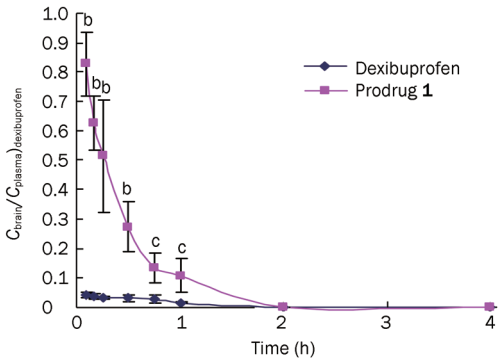

Figure 5. $(C_{brain}/C_{plasma})_{dexibuprofen}$ ratios of dexibuprofen or prodrug **1** versus time (h). C_{brain}, C_{plasma}: dexibuprofen concentration (μg/g) in the brain or plasma after intravenous administration of dexibuprofen (11.70 mg/kg) or prodrug **1** (15.73 mg/kg, equivalent to 11.70 mg/kg of dexibuprofen) in rats. Each point represents the mean±SD of five experiments. $^{b}P<0.05$, $^{c}P<0.01$ *vs* dexibuprofen.

a previous study that revealed that most NSAIDs exhibited very limited distribution in the CNS, with steady state brain/plasma concentration ratios of 0.01–0.05[7].

Compared with the administration of free dexibuprofen, the concentration of dexibuprofen in the plasma after administration of prodrug **1** was moderate. The concentration in the plasma was 29.74±2.97 μg/g 5 min after the administration of prodrug **1** (Figure 4), which was lower than that of dexibuprofen (P<0.01). With moderate concentrations in the plasma, prodrug **1** exhibited a high concentration of dexibuprofen (21.79±3.37 μg/g) in the brain 5 min after administration (Figure 4). The $(C_{brain}/C_{plasma})_{dexibuprofen}$ ratio of prodrug **1** was 0.829 at 5 min, much higher than that of dexibuprofen, which was only 0.044 (Figure 5) (P<0.01). These results revealed almost no barrier effect of the BBB in response to prodrug **1**. However, the high concentration of dexibuprofen observed decreased rapidly, with an MRT of 0.237±0.034 h, showing an active exclusion effect of the BBB toward dexibuprofen.

The AUC_{0-t} values after administration of dexibuprofen and prodrug **1** were 1.10±0.41 and 7.89±1.23 μg/g·h in the brain, respectively. The C_{max} values after the administration

of dexibuprofen and prodrug **1** were 2.81±1.16 and 21.79±3.37 μg/g in the brain, respectively (Table 2). The relative efficiency (RE=$AUC_1/AUC_{dexibuprofen}$) was 7.17, and the $(C_{max})_1/(C_{max})_{dexibuprofen}$ ratio was 7.75 in the brain (Table 3). The drug targeting index {DTI=$(AUC_{brain}/AUC_{plasma})_1/(AUC_{brain}/AUC_{plasma})_{dexibuprofen}$} was 11.19. Taken together, these data indicated a remarkable brain targeting efficiency of prodrug **1** with a marked enhancement of brain distribution, accompanied by a decreased plasma distribution. This finding supports the use of such compounds as therapeutic agents, permitting enhanced therapeutic concentrations in the brain with decreased peripheral side effects.

Discussion

In this study, ethanolamine and its related structures were coupled with dexibuprofen to generate potential brain-targeting agents. The *in vitro* stability and *in vivo* biodistribution of these compounds were investigated and biopharmacokinetic studies were performed to evaluate their brain-targeting efficiency. The results obtained were compared with that of free dexibuprofen. The influence of their chemical structures on the transport efficiency was also discussed.

In the stability study, the results showed a rapid hydrolysis of prodrugs **1**, **2**, and **3** in the plasma (Table 1). Prodrugs **1**, **2**, and **3,** which each contain ester bonds, were likely degraded by specific esterases in the plasma. Because *N,N*-dimethylaminoethanol, *N,N*-diethylaminoethanol and 2-(methylamino) ethanol have structures that are similar to that of choline, prodrugs **1**, **2**, and **3** could be substrates of plasma esterases, such as cholinesterase. These findings were in agreement with those of a previous study that showed compounds with structures similar to that of prodrug **1** undergoing very fast hydrolysis in 80% human plasma, with half-lives less than 5 min[28]. The hydrolysis profiles of the prodrugs in rat brain homogenates revealed that prodrug **3** was more stable than either prodrug **1** or **2**, suggesting that prodrugs **1** and **2** are better substrates of specific esterases in the brain than prodrug **3** and underwent hydrolysis with high efficiency to release dexibuprofen.

In our preliminary investigations, we investigated the *in vitro* stability of prodrugs **4** and **5**. The hydrolysis profiles of prodrugs **4** and **5** revealed that they were not stable and did not follow the linear kinetic equation. Therefore, we have only presented *in vitro* stability data relating to prodrugs **1**, **2**, and **3**.

In our biodistribution studies, each prodrug exhibited an enhancement relative to dexibuprofen in brain-targeting efficiency (Figure 3, $P<0.01$). As observed from the results of our HPLC studies, the lipophilicity of prodrugs **1**, **2**, **3**, **4**, and **5** are not increased when compared with dexibuprofen (Figure 1); thus, the observed enhancement of brain distribution is probably due to movement by specific transporters located at the BBB. Because ethanolamine-related structures are similar to choline and small molecular cations, the high transport efficiency of prodrugs is probably facilitated by the action of organic cations or choline transporters at the BBB. In addition, prodrugs are positively charged under physiological conditions, which may allow them to interact with the negatively charged BBB.

Among the prodrugs tested, prodrug **1**, which was prepared by coupling *N,N*-dimethylaminoethanol and dexibuprofen via an ester bond, exhibited the highest targeting efficiency. Because prodrug **1** was rapidly hydrolyzed in the rat plasma with a half-life less than 5 min, its high distribution in the brain indicated remarkable brain-transport efficiency.

During the synthesis of prodrugs **1**, **2**, **3**, **4**, and **5**, the active carboxyl group of dexibuprofen was coupled with ethanolamine-related structures via an ester bond. The present study reveals that although prodrugs have similar structures, their stability in media and brain-transport efficiency were quite different. It is interesting to note that many CNS-accessible therapeutics, such as meclofenoxate, cetirizine and procaine, contain *N,N*-dimethylaminoethanol structures. Because the structure of *N,N*-dimethylaminoethanol is very similar to choline, we hypothesize that prodrug **1** might be a substrate of the choline transporters located at the BBB. After entering the brain, prodrug **1** was hydrolyzed by esterases, resulting in the release of dexibuprofen. In addition to prodrug **1**, prodrug **2** also exhibited a high transport efficiency. The $(C_{brain}/C_{plasma})_{dexibuprofen}$ ratio of prodrug **2** was 15.7-fold higher than that of free dexibuprofen 10 min after administration (Figure 3, $P<0.01$). This result implies that the small alkyl groups disubstituted onto the amino group of ethanolamine seem to facilitate the recognition and transport of these compounds by specific transporters at the BBB.

Our results revealed that at 5 min after the administration of prodrug **1**, the $(C_{brain}/C_{plasma})_{dexibuprofen}$ ratio reached levels as high as 0.829 (Figure 5). Subsequently, the high concentration of dexibuprofen in the brain decreased rapidly. Because dexibuprofen is negatively charged at physiological pH, preventing it from passively penetrating through the BBB, the rapid efflux of dexibuprofen was probably facilitated by efflux transporters located at the BBB. A sustained-release drug delivery system for prodrug **1** designed to maintain a steady concentration of dexibuprofen in the CNS will be investigated in future studies. A more stable ester bond could also be designed to allow prodrugs to be slowly hydrolyzed by brain esterases after entering the brain.

Conclusions

In this study, we designed and synthesized a series of dexibuprofen derivatives that were modified with ethanolamine-related structures. This is the first time that ethanolamine-related structures have been utilized in the modification of compounds for brain-targeting delivery. The distribution and pharmacokinetic studies revealed that all of the prepared derivatives exhibited enhanced brain distribution compared with dexibuprofen ($P<0.01$). These results imply that ethanolamine-related structures may play an important role in transport across the BBB. The mechanism responsible for this enhancement will likely be further elucidated in the near future.

Experimental

(2*S*)-2-(4-isobutylphenyl)propionic acid 2-dimethylaminoethyl ester (1)

N,N-dimethylaminoethanol (1.30 g, 14.6 mmol) and TEA (5 mL, 36 mmol) were dissolved in anhydrous CH_2Cl_2 (15 mL). Dexibuprofen chloride (2.24 g, 10.0 mmol) was added dropwise under an ice bath. The reaction mixture was stirred continuously at room temperature for 4 h. The mixture was then extracted with CH_2Cl_2. The organic layer was combined and sequentially washed with sodium bicarbonate solution (*aq*) and water. It was then dried over anhydrous sodium sulfate and filtered. The resulting filtrate was concentrated under reduced pressure. The residue was then subjected to silica gel chromatography (dichloromethane/methanol, 20:1) to yield prodrug **1** as a colorless oil (2.32 g, 83.7%).

$[\alpha]^{20}_D$+36.3° (c 1, CH_3OH).

^{1}H-NMR ($CDCl_3$, 400 MHz): δ 7.178 (d, 2H, J=8.0 Hz, 2′-H, 6′-H), 7.059 (d, 2H, J=8.0 Hz, 3′-H, 5′-H), 4.191–4.107 (m, 2H, $CH_2C\underline{H}_2OCO$), 3.660–3.720 (m, 1H, $COC\underline{H}CH_3$), 2.503 (t, 2H, J=11.2 Hz, $NC\underline{H}_2CH_2$), 2.418 [d, 2H, J=7.2 Hz, $C\underline{H}_2CH(CH_3)_2$], 2.182 [s, 6H, $N(C\underline{H}_3)_2$], 1.850–1.783 [m, 1H, $CH_2C\underline{H}(CH_3)_2$], 1.459 (d, 3H, J=6.8 Hz, $COCHC\underline{H}_3$), 0.870 [d, 6H, J=6.4 Hz, $CH_2CH(CH_3)_2$].

IR (KBr cm^{-1}): 3089, 2955, 2869, 2821, 1735, 1513, 1460, 1160, 1067.

HRMS for $[M+H]^+$: *m/z* calculated 278.2120; found 278.2115.

(2*S*)-2-(4-isobutylphenyl)propionic acid 2-diethylaminoethyl ester (2)

N,N-diethylaminoethanol (0.88 g, 7.51 mmol) and TEA (2 mL, 14.4 mmol) were dissolved in anhydrous CH_2Cl_2 (10 mL). Dexibuprofen chloride (1.12 g, 5.0 mmol) was added dropwise under an ice bath. The reaction mixture was stirred continuously at room temperature for 2.5 h. The mixture was then extracted with CH_2Cl_2. The organic layer was combined and sequentially washed with sodium bicarbonate solution (*aq*) and water. It was then dried over anhydrous sodium sulfate and filtered. The resulting filtrate was concentrated under reduced pressure. The residue was subjected to silica gel chromatography (dichloromethane/methanol, 20:1) to yield prodrug **2** as a yellow-tinted oil (1.10 g, 72.4%).

$[\alpha]^{20}_D$+39.4° (c 1, CH_3OH).

^{1}H-NMR ($CDCl_3$, 400 MHz): δ 7.197 (d, 2H, J=8.0 Hz, 2′-H, 6′-H), 7.083 (d, 2H, J=8.0 Hz, 3′-H, 5′-H), 4.145 (t, 2H, J=6.0 Hz, $CH_2C\underline{H}_2OCO$), 3.695 (q, 1H, J=7.2 Hz, $COC\underline{H}CH_3$), 2.675 (t, 2H, J=6.0 Hz, $NC\underline{H}_2CH_2$), 2.505 [q, 4H, J=7.2 Hz, $N(C\underline{H}_2CH_3)_2$], 2.440 [d, 2H, J=6.8 Hz, $C\underline{H}_2CH(CH_3)_2$], 1.786–1.888 [m, 1H, $CH_2C\underline{H}(CH_3)_2$], 1.482 (d, 3H, J=6.8 Hz, $COCHC\underline{H}_3$), 0.976 [t, 6H, J=7.2 Hz, $(CH_2C\underline{H}_3)_2$], 0.891 [d, 6H, J=6.8 Hz, $CH_2CH(C\underline{H}_3)_2$].

IR (KBr cm^{-1}): 2967, 2872, 2808, 1736, 1513, 1461, 1380, 1164, 1069.

HRMS for $[M+H]^+$: *m/z* calcd 306.2433; found 306.2436.

N-tert-butoxycarbonyl-2-methylaminoethanol (3a)

2-(methylamino)ethanol (0.50 g, 7.0 mmol) and sodium hydroxide (0.28 g, 7.0 mmol) were dissolved in methanol (10 mL). Di-tert-butyldicarbonate (1.90 g, 8.6 mmol) was then added. The mixture was then stirred at room temperature for 5 h. The mixture was concentrated under reduced pressure, and the residue was then subjected to silica gel chromatography (dichloromethane/methanol, 20:1) to yield prodrug **3a** as a colorless oil (0.86 g, 71.1%).

^{1}H-NMR ($CDCl_3$, 400 MHz): δ 3.733 (s, 2H, $HOC\underline{H}_2CH_2$), 3.382 (s, 2H, $NC\underline{H}_2CH_2$), 2.907 (s, 3H, $CH_2NC\underline{H}_3$), 1.452 [s, 9H, $COOC(C\underline{H}_3)_3$].

(2*S*)-2-(4-isobutylphenyl)propionic acid 2-(*N*-tert-butoxycarbonyl-*N*-methylamino) ethyl ester (3b)

Prodrug **3a** (0.70 g, 4.1 mmol) was dissolved in CH_2Cl_2 (10 mL) with added TEA (1 mL, 7.2 mmol). Dexibuprofen chloride (1.10 g, 4.9 mmol) was added dropwise under an ice bath. The mixture was stirred at room temperature for 4 h. The mixture was concentrated, and the residue was subjected to silica gel chromatography (petroleum ether/ethyl acetate, 7:1) to yield prodrug **3b** as a colorless oil (1.16 g, 78.5%).

$[\alpha]^{20}_D$+16.0° (c 1, CH_3OH).

^{1}H-NMR ($CDCl_3$, 400 MHz): δ 7.186 (d, 2H, J=8.0 Hz, 2′-H, 6′-H), 7.086 (d, 2H, J=8.0 Hz, 3′-H, 5′-H), 4.165 (s, 2H, $CH_2C\underline{H}_2OCO$), 3.657–3.750 (m, 1H, $COC\underline{H}CH_3$), 3.368 (m, 2H, $NC\underline{H}_2CH_2$), 2.674–2.722 (m, 3H, $CH_2NC\underline{H}_3$), 2.438 [d, 2H, J=7.2 Hz, $C\underline{H}_2CH(CH_3)_2$], 1.799–1.875 [m, 1H, $CH_2C\underline{H}(CH_3)_2$], 1.482–1.515 (m, 3H, $COCHC\underline{H}_3$), 1.437 [s, 9H, $COOC(C\underline{H}_3)_3$], 0.879–0.901 [m, 6H, J=6.8 Hz, $CH_2CH(C\underline{H}_3)_2$].

(2*S*)-2-(4-isobutylphenyl)propionic acid 2-methylaminoethyl ester (3)

Concentrated hydrochloric acid (0.1 mL) was added to a solution of compound **3b** (1.0 g, 2.7 mmol) in ethyl acetate (10 mL). The mixture was stirred at room temperature for 14 h. The solution was then concentrated, and the residue was subjected to silica gel chromatography (dichloromethane/methanol, 10:1) to yield prodrug **3** as a white solid (0.48 g, 57.2%).

mp 103–105 °C.

$[\alpha]^{20}_D$+9.0° (c 1, CH_3OH).

^{1}H-NMR ($CDCl_3$, 400 MHz): δ 7.203 (d, 2H, J=8.0 Hz, 2′-H, 6′-H), 7.085 (d, 2H, J=8.0 Hz, 3′-H, 5′-H), 4.508–4.549 (m, 1H, $CH_2C\underline{H}_2OCO$), 4.317–4.341 (m, 1H, $CH_2C\underline{H}_2OCO$), 3.847–3.898 (m, 1H, $COC\underline{H}CH_3$), 3.053–3.146 (m, 2H, $NC\underline{H}_2CH_2$), 2.517 (s, 3H, $CH_2NC\underline{H}_3$), 2.433 [d, 2H, J=7.2 Hz, $C\underline{H}_2CH(CH_3)_2$], 1.796–1.863 [m, 1H, $CH_2C\underline{H}(CH_3)_2$], 1.508 (d, 3H, J=6.8 Hz, $COCHC\underline{H}_3$), 0.886 [d, 6H, J=6.8 Hz, $CH_2CH(C\underline{H}_3)_2$].

IR (KBr cm^{-1}): 3391, 2955, 2869, 2845, 1735, 1510, 1464, 1163, 1073.

HRMS for $[M+H]^+$: *m/z* calcd 264.1964; found 2764.1960.

N-tert-butoxycarbonyl-ethanolamine (4a)

Ethanolamine (0.60 g, 10.0 mmol) and sodium hydroxide (0.40 g, 10.0 mmol) were dissolved in water (10 mL) and dioxane (10 mL). Di-tert-butyldicarbonate (2.7 g, 12.0 mmol) was then added, and the mixture was stirred at room temperature for 3.5 h. The mixture was concentrated, and the residue was subjected to silica gel chromatography (petroleum ether/

ethyl acetate, 1:1) to yield prodrug **4a** as a colorless oil (1.54 g, 95.1%).

^{1}H-NMR ($CDCl_3$, 400 MHz): δ 3.650 (t, 2H, J=5.2 Hz, HOC$\underline{H}_2$CH_2), 3.241 (t, 2H, J=5.2 Hz, NC$\underline{H}_2$CH_2), 1.415 [s, 9H, COOC(C$\underline{H}_3$)$_3$].

(2*S*)-2-(4-isobutylphenyl)propionic acid 2-(*N*-tert-butoxycarbonyl-amino) ethyl ester (4b)

Compound **4a** (0.7 g, 4.3 mmol) was dissolved in CH_2Cl_2 (10 mL) with added TEA (1 mL, 7.2 mmol). Dexibuprofen chloride (1.44 g, 6.45 mmol) was added dropwise under an ice bath. The mixture was stirred at room temperature for 3.5 h. The mixture was then concentrated, and the residue was subjected to silica gel chromatography (petroleum ether/ethyl acetate, 10:1) to yield prodrug **4b** as a colorless oil (1.38 g, 92.1%).

$[\alpha]^{20}_D$+23.1° (c 1, CH_3OH).

^{1}H-NMR ($CDCl_3$, 400 MHz): δ 7.190 (d, 2H, J=7.6 Hz, 2′-H, 6′-H), 7.088 (d, 2H, J=7.6 Hz, 3′-H, 5′-H), 4.102 (s, 2H, $CH_2C\underline{H}_2OCO$), 3.672–3.725 (m, 1H, COC$\underline{H}$CH_3), 3.288 (s, 2H, NC$\underline{H}_2$CH_2), 2.439 [d, 2H, J=7.2 Hz, C$\underline{H}_2$CH(CH_3)$_2$], 1.793–1.891 [m, 1H, $CH_2C\underline{H}$(CH_3)$_2$], 1.478 (d, 3H, J=6.8 Hz, COCHC$\underline{H}_3$), 1.421 [s, 9H, COOC(C$\underline{H}_3$)$_3$], 0.890 [d, 6H, J=6.0 Hz, CH_2CH(C$\underline{H}_3$)$_2$].

(2*S*)-2-(4-isobutylphenyl)propionic acid 2-aminoethyl ester (4)

Concentrated hydrochloric acid (0.1 mL) was added to a solution of compound **4b** (1.0 g, 2.8 mmol) in ethyl acetate (10 mL). The mixture was stirred at room temperature for 14 h. The solution was then concentrated, and the residue was subjected to silica gel chromatography (dichloromethane/methanol, 10:1) to yield compound **4** as a white solid (0.36 g, 43.5%).

mp 117–120°C.

$[\alpha]^{20}_D$+14.0° (c 1, CH_3OH).

^{1}H-NMR (DMSO-d, 400 MHz): δ 7.214 (d, 2H, J=8.0 Hz, 2′-H, 6′-H), 7.116 (d, 2H, J=8.0 Hz, 3′-H, 5′-H), 4.278–4.335 (m, 1H, $CH_2C\underline{H}_2OCO$), 4.044–4.100 (m, 1H, $CH_2C\underline{H}_2OCO$), 3.781–3.835 (m, 1H, COC$\underline{H}$CH_3), 3.041–3.054 (m, 2H, NC$\underline{H}_2$CH_2), 2.413 [d, 2H, J=7.2 Hz, C$\underline{H}_2$CH(CH_3)$_2$], 1.770–1.837 [m, 1H, $CH_2C\underline{H}$(CH_3)$_2$], 1.408 (d, 3H, J=6.8 Hz, COCHC$\underline{H}_3$), 0.853 [d, 6H, J=6.4 Hz, CH_2CH(C$\underline{H}_3$)$_2$].

IR (KBr cm^{-1}): 3395, 2956, 2871, 1737, 1512, 1378, 1162, 1075.

HRMS for $[M+H]^+$: *m/z* calcd 250.1807; found 250.1801.

N-acetyl-2-aminoethanol (5a)

Sodium hydride (1.44 g, 60 mmol) was added at 0 °C to a stirred solution of ethanolamine (1.84 g, 30 mmol) in 20 mL dioxane, followed by the dropwise addition of acetyl chloride (1.56 g, 20 mmol). The mixture was stirred at room temperature for 2.5 h. The mixture was then extracted with CH_2Cl_2. The organic layer was combined and washed with water. It was then dried over anhydrous sodium sulfate and filtered. The filtrate was subsequently concentrated under reduced pressure. The resulting residue was subjected to silica gel chromatography (dichloromethane/methanol, 8:1) to yield compound **5a** as a colorless oil (1.27 g, 62.1%).

^{1}H-NMR ($CDCl_3$, 400 MHz): δ 1.990 (s, 3H, C$\underline{H}_3$CO), 3.326–3.390 (m, 2H, C$\underline{H}_2$NCO), 3.682 (t, 2H, C$\underline{H}_2$O)

(2*S*)-2-(4-isobutylphenyl)propionic acid 2-(acetylamino)ethyl ester (5)

Compound **5a** (0.5 g, 4.85 mmol) and TEA (2 mL, 14.4 mmol) was dissolved in anhydrous tetrahydrofuran (20 mL). Dexibuprofen chloride (1.31 g, 5.84 mmol) was added dropwise under an ice bath. The reaction mixture was then stirred continuously at room temperature for 2 h. The mixture was concentrated, and the residue was subjected to silica gel chromatography (petroleum ether/ethyl acetate, 1:1) to yield compound **5** as a colorless oil (0.94 g, 66.2%).

$[\alpha]^{20}_D$+17.8° (c 1, CH_3OH).

^{1}H-NMR ($CDCl_3$, 400 MHz): δ 7.111 (d, 2H, J=8.0 Hz, 3′-H,5′-H), 7.200 (d, 2H, J=8.4 Hz, 2′-H, 6′-H), 4.174–4.228 (m, 1H, C$\underline{H}_2$O), 4.056–4.109 (m, 1H, C$\underline{H}_2$O), 3.685–3.737 (m, 1H, COC$\underline{H}$CH_3), 3.397–3.436 (m, 2H, C$\underline{H}_2$NCO), 2.444 [d, 2H, J=7.2 Hz, C$\underline{H}_2$CH(CH_3)$_2$], 1.826–1.872 [m, 4H, C$\underline{H}_3$CO, $CH_2C\underline{H}$(CH_3)$_2$], 1.492 (d, 3H, J=7.2 Hz, COCHC$\underline{H}_3$), 0.892 [d, 6H, J=6.4 Hz, CH_2CH(C$\underline{H}_3$)$_2$].

IR (KBr cm^{-1}): 3294, 3085, 2956, 2871, 1736, 1657, 1553, 1515, 1459, 1373, 1292, 1166, 1070, 799.

HRMS for $[M+H]^+$: *m/z* calcd 292.1913; found 292.1916.

Acknowledgements

This work was supported by the National Natural Science Foundation of China (Grant No 81130060).

Author contribution

Xuan ZHANG, Zhi-rong ZHANG, Xing LIU, Tao GONG, and Xun SUN designed the research strategy; Xuan ZHANG and Xing LIU performed the research; Xuan ZHANG and Xing LIU analyzed the data; and Xuan ZHANG wrote the paper.

References

1 Patel PM, Drummond JC, Sano T, Cole DJ, Kalkman CJ, Yaksh TL. Effect of ibuprofen on regional eicosanoid production and neuronal injury after forebrain ischemia in rats. Brain Res 1993; 614: 315–24.

2 Szekely CA, Thorne JE, Zandi PP, Messias E, Breitner JC, Goodman SN. Nonsteroidal anti-inflammatory drugs for the prevention of Alzheimer's disease: a systematic review. Neuroepidemiology 2004; 23: 159–69.

3 Silakova JM, Hewett JA, Hewett SJ. Naproxen reduces excitotoxic neurodegeneration *in vivo* with an extended therapeutic window. J Pharmacol Exp Ther 2004; 309: 1060–6.

4 Bannwarth B, Lapicque F, Pehourcq F, Gillet P, Schaeverbeke T, Laborde C, *et al*. Stereoselective disposition of ibuprofen enantiomers in human cerebrospinal fluid. Br J Clin Pharmacol 1995; 40: 266–9.

5 Mannila A, Rautio J, Lehtonen M, Jarvinen T, Savolainen J. Inefficient central nervous system delivery limits the use of ibuprofen in neurodegenerative diseases. Eur J Pharm Sci 2005; 24: 101–5.

6 Matoga M, Pehourcq F, Lagrange F, Tramu G, Bannwarth B. Influence of molecular lipophilicity on the diffusion of arylpropionate non-steroidal anti-inflammatory drugs into the cerebrospinal fluid. Arzneimittel-forschung 1999; 49: 477–82.

7 Eriksen JL, Sagi SA, Smith TE, Weggen S, Das P, McLendon DC, *et al*. NSAIDs and enantiomers of flurbiprofen target gamma-secretase and lower Abeta 42 *in vivo*. J Clin Invest 2003; 112: 440–9.

8 Brune K, Neubert A. Pharmacokinetic and pharmacodynamic aspects of the ideal COX-2 inhibitor: a pharmacologist's perspective. Clin Exp Rheumatol 2001; 19: S51–7.
9 Rainsford KD, Schweitzer A, Brune K. Autoradiographic and biochemical observations on the distribution of non-steroid anti-inflammatory drugs. Arch Int Pharmacodyn Ther 1981; 250: 180–94.
10 Golden PL, Pollack GM. Blood-brain barrier efflux transport. J Pharm Sci 2003; 92: 1739–53.
11 Neuwelt EA. Mechanisms of disease: the blood-brain barrier. Neurosurgery 2004; 54: 131–40.
12 Habgood MD, Begley DJ, Abbott NJ. Determinants of passive drug entry into the central nervous system. Cell Mol Neurobiol 2000; 20: 231–53.
13 Clark DE. In silico prediction of blood-brain barrier permeation. Drug Discov Today 2003; 8: 927–33.
14 Lee G, Dallas S, Hong M, Bendayan R. Drug transporters in the central nervous system: brain barriers and brain parenchyma considerations. Pharmacol Rev 2001; 53: 569–96.
15 Kusuhara H, Sugiyama Y. Active efflux across the blood-brain barrier: role of the solute carrier family. NeuroRx 2005; 2: 73–85.
16 Smith QR. Carrier-mediated transport to enhance drug delivery to brain. International Congress Series 2005; 1277: 63–74.
17 Kurihara A, Deguchi Y, Pardridge WM. Epidermal growth factor radiopharmaceuticals: ^{111}In *chelation*, conjugation to a blood-brain barrier delivery vector via a biotin-polyethylene linker, pharmacokinetics, and *in vivo* imaging of experimental brain tumors. Bioconjugate Chem 1999; 10: 502–11.
18 Friden PM, Walus LR, Musso GF. Anti-transferrin receptor antibody and antibody drug conjugates cross the blood brain barrier. Proc Natl Acad Sci U S A 1991; 88: 4771–5.
19 Pardridge WM, Kumagai AK, Eisenberg JB. Chimeric peptides as a vehicle for peptide pharmaceutical delivery through the blood-brain barrier. Biochem Biophys Res Commun 1987; 146: 307–13.
20 Kang YS, Pardridge L. Brain delivery of biotin bound to a conjugate of neutral avidin and cationized human albumin. Pharm Res 1994; 11: 1257–64.
21 Khan MSY, Akhter M. Synthesis, pharmacological activity and hydrolytic behavior of glyceride prodrugs of ibuprofen. Eur J Med Chem 2005; 40: 371–6.
22 Zhao XG, Tao XY, Wei DZ, Song QX. Pharmacological activity and hydrolysis behavior of novel ibuprofen glucopyranoside conjugates. Eur J Med Chem 2006; 41: 1352–8.
23 Perioli L, Ambrogi V, Bernardini C, Grandolini G, Ricci M, Giovagnoli S, *et al*. Potential prodrugs of non-steroidal anti-inflammatory agents for targeted drug delivery to the CNS. Eur J Med Chem 2004; 39: 715–27.
24 Siskou IC, Rekka EA, Kourounakis AP, Chrysselis MC, Tsiakitzis K, Kourounakis PN. Design and study of some novel ibuprofen derivatives with potential nootropic and neuroprotective properties. Bioorgan Med Chem 2007; 15: 951–61.
25 Shanbhag V, Crider AM, Gokhale R, Harpalani A, Dick RM. Prodrug and amide prodrugs of ibuprofen and naproxen: synthesis, anti-inflammatory activity, and gastrointestinal toxicity. J Pharm Sci 1992; 81: 149–54.
26 Halen PK, Chagti KK, Giridhar R, Yadav MR. Combining anticholinergic and anti-inflammatory activities into a single moiety: a novel approach to reduce gastrointestinal toxicity of ibuprofen and ketoprofen. Chem Biol Drug Des 2007; 70: 450–5.
27 Song N, Li YX, Sun X, Qu F. Synthesis of (±)ibuprofen sugar derivative. Acta Pharm Sin 2004; 39: 105–9.
28 Mork N, Bundgaard H. Stereoselective enzymatic hydrolysis of various ester prodrugs of ibuprofen and flurbiprofen in human plasma. Pharm Res 1992; 9: 492–6.